UV photopolymerised biosynthetic PVA hydrogels with tailored permselectivity for cell immunoisolation

Author:
Nafea, Eman Habib Mohamed Abdel Hamid

Publication Date:
2012

DOI:
https://doi.org/10.26190/unsworks/2458

UV Photopolymerised Biosynthetic PVA Hydrogels with Tailored Permselectivity for Cell Immunoisolation

by

Eman Habib Mohamed Abdel Hamid Nafea

A Thesis submitted for the Degree of Doctor of Philosophy

Graduate School of Biomedical Engineering

University of New South Wales

November 2012

COPYRIGHT STATEMENT

AUTHENTICITY STATEMENT

ORIGINALITY STATEMENT

‘I hereby declare that this submission is my own work and to the best of my knowledge it contains no materials previously published or written by another person, or substantial proportions of material which have been accepted for the award of any other degree or diploma at UNSW or any other educational institution, except where due acknowledgement is made in the thesis. Any contribution made to the research by others, with whom I have worked at UNSW or elsewhere, is explicitly acknowledged in the thesis. I also declare that the intellectual content of this thesis is the product of my own work, except to the extent that assistance from others in the project's design and conception or in style, presentation and linguistic expression is acknowledged.’

Signed Eman Nafea

Date 4/04/2013

Abstract

Cell immunoisolation systems are fast becoming a favourable approach to cure various challenging diseases and disorders such as type I diabetes. Although the addition of biological molecules to cell immunoisolation devices can significantly enhance their performance by supporting cell viability and function, little is known about their effects on the immunoisolating membrane properties especially its permselectivity.

Therefore, this research focused on examining the effect of combining biological molecules with a synthetic polymer on the permeability of hydrogels, with a specific emphasis on encapsulation of insulin producing cells for treatment of diabetes. The research aimed at achieving an optimum balance between a controlled permselectivity and cell survival support. It was hypothesised that covalent incorporation of small amounts of model extracellular matrix (ECM) molecules, heparin and gelatin, would support cell viability without compromising the controlled permselectivity and physico-mechanical properties of the base PVA network.

Varying the number of functional groups per PVA backbone successfully controlled the PVA permeability and physico-mechanical properties. A suitable degree of permselectivity was achieved by the highly crosslinked hydrogels. Covalent incorporation of heparin and gelatin at low percentage was successfully achieved without interfering with either their biofunctionalities or the base PVA properties, including its permselectivity. Moreover, the incorporated ECM analogues supported the viability and metabolic activity of pancreatic β-cell lines encapsulated for two weeks.

Consequently, biosynthetic hydrogels composed of permselective PVA base material and a small amount of biological molecules show promise as immunoisolating materials for cell-based therapy.

Acknowledgements

First of all I wish to express my sincere gratitude to my father **Habib Nafea** whose dream was to see this PhD thesis a reality. His belief in my abilities and endless encouragement has been always the shining light of my journey. To him I dedicate this thesis. I would like also to dedicate this thesis to the souls of my beloved uncles **Prof. Adel Nassra** and **Prof. Yehia El-Gohary,** both of whom inspired me throughout my academic studies and research, as they did for thousands of their students. May their souls rest in peace.

A heartfelt thank you goes to my wonderful mother and sister for their unconditional love and for always being there when I needed them most. Many thanks go to my dear parents in law who kept encouraging me all the way.

Words fail me to express my appreciation to my husband **Mohamed Abdalla** whose dedication, love and persistent confidence in me have taken the load off my shoulders. He deserves far more credit than I can ever give him. Without his support, this thesis would not have been possible. All my love goes to my children **Ayah** and **Adam**, whose cheery smiles always inspired me to continue establishing a better future for them.

I would like to thank my supervisor **Dr. Penny Martens** for her thoughtful comments, insightful observations and careful editorial suggestions, from which this thesis has benefited. Special thanks go to my co-supervisor **Prof. Laura Poole-Warren** for her great support, guidance and fruitful discussions along the way.

Collective acknowledgments are also owed to my colleagues in the Graduate School of Biomedical Engineering for their sincere help and support. Special thanks go to the hydrogel group members: **Khoon Lim, Cara Yong, Jenny Cheng, Yogambha Ramaswamy, Helene Alves, Andy Marson and Rylie Green** for their help, advice and willingness to share their bright thoughts with me.

Finally, I would like to thank everybody who was important to the successful completion of this thesis, including all those who could not be named individually.

This Research was kindly supported by the Australian Research Council (ARC) Discovery Project Grant (DP0986447) and the Australian Postgraduate Award (APA) for 2009.

List of Publications

Peer Reviewed Journals

- **E. Nafea**, L. Poole-Warren, P. Martens, Immunoisolating semi-permeable membranes for cell encapsulation: Focus on hydrogels**,** J.Control. Release 154:110-122 (2011) - Review Article.

Conference Papers

- **E. Nafea**, L. Poole-Warren, P. Martens, Structural and functional characterization of biosynthetic PVA-gelatin hydrogels designed for cell based therapy, IFMBE Proceedings, Vol 39. World Congress on Medical Physics and Biomedical Engineering, May 26-31, 2012, Beijing, China

Conference Presentations

- **E. Nafea,** L.A. Poole-Warren, P. Martens (July 2012) "Biosynthetic hydrogels for pancreatic beta cell immunoisolation", 3rd International NanoMedicine Conference, Sydney, Australia (Oral presentation)
- P. Martens, J. Cheng, C.Young, **E.Nafea**, L.A. Poole-Warren (July 2012) "Encapsulation of Pancreatic Cells for Tissue Engineering", 3rd International NanoMedicine Conference, Sydney, Australia (Invited oral presentation)
- **E. Nafea,** L.A. Poole-Warren, P. Martens (June 2012) "UV photopolymerized biosynthetic hydrogels for cell immunoisolation", 9th World Biomaterials Congress, Chengdu, China (Oral & Poster presentation) - Received best poster award in "Leverage of hydrogels for cell encapsulation in tissue engineering applications", sponsored by Biomaterials journal

- **E. Nafea,** L.A. Poole-Warren, P. Martens (May 2012) "Structural and functional characterization of biosynthetic PVA-gelatin hydrogels designed for cell based therapy", World Congress on Medical Physics & Biomedical Engineering, Beijing, China (Oral presentation)
- **E. Nafea,** L.A. Poole-Warren, P. Martens, (Apr 2011) "Poly (vinyl alcohol)-heparin hydrogels for cell Immunoisolation", 21st Annual Conference of the Australasian Society for Biomaterials and Tissue Engineering (ASBTE), Queenstown, New Zealand (Oral presentation)
- P. Martens, C. Young, **E. Nafea**, J. Cheng, L. A. Poole-Warren. (Feb 2011) "Characterisation of a poly (vinyl alcohol) hydrogel cell encapsulation system," 32nd Australasian Polymer Symposium, Coffs Harbour, Australia (Oral presentation)
- P. Martens, C. Young, **E. Nafea**, J. Cheng, L. A. Poole-Warren. (Feb 2011) "Development and characterisation of a hydrogel cell encapsulation system," 4th Indo-Australian Meeting on Biomaterials, Tissue Engineering and Drug Delivery, Anand, India (Invited oral presentation)
- **E. Nafea**, L.A. Poole-Warren, P. Martens. (2010**) "**Permeability of UV photocrosslinked poly (vinyl alcohol) hydrogels designed for cell Immunoisolation", 20th Annual Conference of the Australasian Society for Biomaterials and Tissue Engineering (ASBTE), Brisbane, Australia (Oral presentation)

Table of Contents

Originality Statement
Abstract i
Acknowledgements iii
List of Publications v
Table of Contents vii
List of Figures x
List of tables xiii

Chapter 1 Introduction 1
1.1 Research Motive 2
1.2 Overall Aim and Hypothesis 5
1.3 Thesis objectives 5

Chapter 2 Literature Review 7
2.1 Introduction 8
2.2 Immunoisolation approaches 11
2.2.1 Intravascular devices 11
2.2.2 Extravascular devices 12
2.2.2.1 Extravascular macrodevices 13
2.2.2.2 Extravascular microcapsules 13
2.2.3 Conformal coating 14
2.3 Semi-permeable membranes for cell immunoisolation 15
2.3.1 Membrane materials 16
2.3.1.1 Hydrogels 16
2.3.1.2 Thermoplastic polymers 16
2.3.1.3 Non-Polymeric materials 17
2.3.2 Membrane requirements 18
2.3.2.1 Biocompatibility and biostability 19
2.3.2.2 Mechanical stability 19
2.3.2.3 Permselectivity and mass transport 21
2.3.2.4 Membrane morphology 22
2.4 Hydrogels in cell encapsulation 23
2.4.1 Natural, synthetic and biosynthetic hydrogels 23
2.4.2 Mechanisms of hydrogel formation 26
2.4.3 Permeability and its importance in a successful hydrogel membrane 28
2.4.3.1 Mesh size determination in nanoporous hydrogels 31
2.4.3.2 Experimental measurement of hydrogel permeability 37
2.4.3.3 Structure-permeability relationship in hydrogels 40
2.5 Modulation of hydrogel membrane permeability for immunoisolation 42
2.5.1 Factors controlling membrane permeability 43
2.5.1.1 The backbone chemistry of polymeric materials 43
2.5.1.2 The physical properties of hydrogels 45
2.5.1.3 The crosslinking density of hydrogels 45
2.5.1.4 Incorporation of extracellular matrix 50

2.6 Summary 51

Chapter 3 Synthetic UV photopolymerised PVA hydrogels with variable functional group densities 53

3.1 Introduction 54
3.2 Materials and Methods 60
3.2.1 Materials 60
3.2.2 Material Characterisation 60
3.2.3 Physico-Mechanical Characterisation of Hydrogels 62
3.2.4 Permeability Performance of Hydrogels 65
3.2.5 Statistical Analysis 67
3.3 Results 67
3.3.1 Material Characterisation and Hydrogel Formation 67
3.3.2 Physico-Mechanical Characterisation of Hydrogels 70
3.3.3 Permeability Performance of Hydrogels 74
3.4 Discussion 78
3.5 Conclusion 86

Chapter 4 Covalent incorporation of ECM analogues into PVA hydrogels and the resulting effects on permeability 88

4.1 Introduction 89
4.2 Materials and Methods 94
4.2.1 Materials 94
4.2.2 Material Characterisation 95
4.2.2.1 Synthesis of Methacrylated Macromers 95
4.2.2.2 Nuclear magnetic resonance (NMR) Characterisation of Methacrylated Macromers 97
4.2.2.3 Hydrogel Formation 97
4.2.3 Physico-Mechanical Characterisation of Hydrogels 98
4.2.4 Permeability Performance of Hydrogels 102
4.2.5 Statistical Analysis 102
4.3 Results 103
4.3.1 Macromer Synthesis and Characterisation 103
4.3.2 Physico-Mechanical Characterisation of Hydrogels 105
4.3.3 Permeability Performance of Hydrogels 111
4.4 Discussion 114
4.5 Conclusion 118

Chapter 5 PVA hydrogels with mixed ECM analogues: Structural and bioactivity characterisation 119

5.1 Introduction 120
5.2 Materials and Methods 123
5.2.1 Materials 123
5.2.2 Material Fabrication 123
5.2.3 Physico-Mechanical Characterisation of Hydrogels 124
5.2.4 Permeability Performance of Hydrogels 126
5.2.5 Bioactivity of Hydrogels 126
5.2.6 Statistical Analysis 128
5.3 Results 128

5.3.1 Physico-Mechanical Characterisation of Hydrogels 128
5.3.2 Permeability Performance of Hydrogels 133
5.3.3 Hydrogel Bioactivity 136
5.4 Discussion 143
5.5 Conclusion 148

Chapter 6 Functional evaluation of biosynthetic PVA hydrogels: Understanding the balance between permselectivity and cell survival **150**
6.1 Introduction 151
6.2 Materials and Methods 155
6.2.1 Materials 155
6.2.2 Hydrogel Formation 155
6.2.3 Insulin Diffusion within the Hydrogels 155
6.2.4 Cell Studies 156
6.2.5 Assessment of Cell Behaviour in Hydrogels 158
6.2.6 Statistical Analysis 159
6.3 Results 160
6.3.1 Insulin Diffusion within Hydrogels 160
6.3.2 Cell Studies 163
6.4 Discussion 170
6.5 Conclusion 178

Chapter 7 Conclusions and Future Recommendations **179**
7.1 Introduction 180
7.2 Thesis Conclusions 181
7.3 Recommendations for Future Research 184
7.3.1 Incorporating ECM molecules specific for cell function to prolong the effective encapsulation period 184
7.3.2 Further strategies to combat incomplete immunoprotection 185
7.4 Thesis Outcomes 188
References **189**

List of Figures

Figure		Page
2.1	Conventional and novel encapsulation devices used for cell immunoisolation. (Dotted line represents the semi-permeable membrane)	11
2.2	Requirements of a semi-permeable membrane for immunoisolation of encapsulated cells	22
2.3	Schematic representation of PVA backbone structure	24
2.4	Schematic representation of UV free radical polymerisation reaction	28
2.5	Schematic representation of part of a hydrogel network showing the macromolecular mesh (ζ) and the distance between two crosslinks, which is the number average molecular weight between crosslinks ($\overline{Mc}$)	31
2.6	States of water in hydrogels and their freezing points	32
2.7	Schematic representation of a two compartment diffusion cell. Arrows represent the direction of water flow	38
2.8	Illustration of intra-chain cyclisation (A) and inter-chain entanglement (B) that can occur during crosslinking of hydrogels	47
3.1	A schematic representation of divinyl (A) and multivinyl (B) macromers. The solid lines represent the polymer backbone and the diamond shapes represent the attached vinyl residues	55
3.2	Schematic representation of PVA methacrylation via ICEMA reaction	61
3.3	^{1}H NMR of PVA-methacrylate with 7 FG/c in D2O. Integration values of the peaks are shown. Inset at the top: schematic numbering for the attached methacrylate group and the PVA backbone	68
3.4	% Sol fraction released from PVA hydrogels (7 FG/c) at different UV curing times (min)	70
3.5	The compressive modulus of PVA hydrogels after incubation in PBS (pH 7.4) for 24 hrs and 7 days	72
3.6	Theoretical average number of molecular weight between crosslinks ($\overline{Mc}$) values versus experimental values from (A) equilibrium swelling theory and (B) rubber elasticity theory	73
3.7	Diffusion coefficient values of FITC-BSA and FITC-IgG through PVA hydrogels (* $P < 0.05$)	76
3.8	Diffusion coefficient values of BSA (A) and IgG (B) through PVA hydrogels compared to those of dextrans with approximately similar Stokes radii	77
4.1	Schematic representation of heparin methacrylation via GMA reaction. A=transesterification, B= ring opening	95
4.2	Schematic representation of gelatin methacrylation via reaction with methacrylic anhydride	96
4.3	^{1}H NMR of heparin-methacrylate with 3 FG/c in D_2O. Integration values of the peaks are shown at the bottom. Inset at the top: represents the attached methacrylates group to the heparin. Arrow points at the protons detected by ^{1}H NMR	104
4.4	^{1}H NMR of gelatin-methacrylate in D_2O showing the region of aromatic peaks and methacrylates protons used for the calculations. Integration values of the peaks are shown at the bottom. Inset at the top:	105

	represents the attached methacrylates group to the gelatin. Arrow points at the protons detected by ^{1}H NMR	
4.5	The compressive modulus of PVA and PVA:heparin hydrogels after incubation in PBS (pH 7.4) for 7 days	108
4.6	The compressive modulus of PVA and PVA:gelatin hydrogels after incubation in PBS (pH 7.4) for 7 days	108
4.7	% Release values of unbound heparin from PVA:heparin (19:1) hydrogels after incubation in PBS (pH 7.4) for 7 days	109
4.8	% Release values of unbound gelatin from PVA:gelatin (19:1) and gelatin (20%) hydrogels after incubation in PBS (pH 7.4) for 7 days	110
4.9	Diffusion coefficients of BSA-FITC through PVA, PVA:heparin, PVA:gelatin and gelatin hydrogels	113
4.10	Diffusion coefficients of IgG-FITC through PVA, PVA:heparin, PVA:gelatin and gelatin hydrogels	113
5.1	Heparin-MA standard curve via DMMB assay with and without the presence of gelatin at 120µg/ml	130
5.2	Gelatin-MA standard curve via Micro-BCA assay with and without the presence of heparin at 120µg/ml	130
5.3	% Release values of unbound heparin from PVA:heparin (19.5:0.5) and PVA:ECM Mix (19:1) hydrogels after incubation in PBS (pH 7.4) for 7 days	131
5.4	% Release values of unbound gelatin from PVA:gelatin (19.5:0.5) and PVA:ECM Mix (19:1) hydrogels after incubation in PBS (pH 7.4) for 7 days	132
5.5	The compressive moduli of PVA 20%, PVA:heparin (19.5:0.5), PVA:gelatin (19.5:0.5) and PVA:ECM Mix (19:1) hydrogels after incubation in PBS (pH 7.4) for 7 days	133
5.6	Diffusion coefficients of FITC-BSA through PVA 20%, PVA, PVA:heparin (19.5:0.5), PVA:gelatin (19.5:0.5) and PVA:ECM Mix (19:1)	135
5.7	Diffusion coefficients of FITC-IgG through PVA, through PVA 20%, PVA, PVA:heparin (19.5:0.5), PVA:gelatin (19.5:0.5) and PVA:ECM Mix (19:1)	135
5.8	Absorbance of MTS at 490nm for BaF3 cells seeded on PVA and PVA co-hydrogels containing heparin. Negative controls are cells in media only and in media supplemented with heparin or FGF2. In the positive control the cells are exposed to a mixture of both heparin and FGF2. All hydrogels were tested with FGF2	137
5.9	Absorbance of MTS at 490nm for BaF3 cells seeded on PVA 20% and PVA:gelatin hydrogels (19.5:0.5). Negative controls are cells in media only and in media supplemented with heparin or FGF2. In the positive control the cells are exposed to a mixture of both heparin and FGF2. Hydrogels were tested with FGF2 (n=1, Mean of 3 hydrogels ± SD)	138
5.10	Fluorescent images (10 x) of Live/Dead double stained L929 seeded on hydrogel surfaces for 3 days. Different compositions of hydrogels examined are (A) gelatin 20%, (B) PVA 20%, (C) PVA:gelatin, (D) PVA:heparin and (E) PVA:ECM Mix (Scale bar = 100 µm)	140
5.11	Number of attached L929 cells on PVA 20%, PVA:heparin (19.5:0.5),	141

	PVA:gelatin (19.5:0.5), PVA:ECM Mix and gelatin 20% hydrogels	
5.12	Fluorescent images (50 x) of Rh-Phalloidin and DAPI stained L929 seeded on hydrogel surfaces for 3 days. Different compositions of hydrogels examined are (A) Gelatin 20%, (B) PVA 20%, (C) PVA:gelatin, (D) PVA:heparin and (E) PVA:ECM Mix (Scale bar = 20 μm)	142
6.1	Cumulative % release profiles of insulin from pure PVA hydrogels at 37 °C over 140 min study period. Lines were drawn to guide the eye	161
6.2	Cumulative % release profiles of insulin from PVA:heparin hydrogels at 37 °C over 140 min study period. Lines were drawn to guide the eye	162
6.3	Cumulative % release profiles of insulin from PVA:gelatin hydrogels at 37 °C over 140 min study period. Lines were drawn to guide the eye	162
6.4	Cumulative % release profiles of insulin from PVA:ECM Mix hydrogels at 37 °C over 140 min study period. Lines were drawn to guide the eye	163
6.5	Cell growth inhibition profile of L929 fibroblasts in unmodified PVA and macromers with 7 and 20 FG/c compared to media only (null)	164
6.6	Fluorescent images (10x) of Live/Dead stained MIN6 cells encapsulated in PVA 7 FG/c hydrogels for 1 and 4 days. Cell controls grown on TCP are added for comparison (Scale bar = 100 μm)	165
6.7	Fluorescent images (10 x) of Live/Dead stained MIN6 cells encapsulated in PVA 7 FG/c hydrogels for 7 and 14 days. Cell controls grown on TCP are added for comparison (Scale bar = 100 μm)	166
6.8	% Live cell area coverage calculated from fluorescent images of control MIN6 cells cultured on TCP and cells encapsulated in PVA 7 FG/c PVA 20%, PVA:heparin (19.5:0.5), PVA:gelatin (19.5:0.5) and PVA:ECM Mix (19:1) hydrogels with 7 FG/c	167
6.9	Production of ATP from control MIN6 cells and cells encapsulated in PVA 20%, PVA:heparin (19.5:0.5), PVA:gelatin (19.5:0.5) and PVA:ECM Mix (19:1) hydrogels with 7 FG/c PVA	168
6.10	Production of ATP from control MIN6 cells and cells encapsulated in PVA 20%, PVA, PVA:heparin (19.5:0.5), PVA:gelatin (19.5:0.5) and PVA:ECM Mix (19:1) hydrogels with 20 FG/c	169
6.11	Insulin secretion from MIN6 cells in response to high and low glucose at different time points for both (A) PVA:heparin hydrogels and (B) unencapsulated cells after 14 days of cell culture. Values of insulin released were normalised to total insulin content (n=1, mean ± SEM of 3 different samples)	170

List of Tables

Table		Page
2.1	Examples of encapsulated cells targeting various diseases, showing their immunoisolating membrane materials and device configurations	10
2.2	Examples of different sites for transplantation of cell encapsulation devices	12
3.1	Examples of network characteristics and macromolecular permeability/release of non-degradable divinyl and multivinyl hydrogels	57
3.2	Molecular weights and Stokes radii (SR) of solutes used in the permeation studies	66
3.3	Theoretical MA FG/c versus experimental values measured using ^{1}H NMR	68
3.4	Sol fraction and volumetric swelling ratio of PVA hydrogels after 24 hours incubation in PBS	71
3.5	Comparison of the parameters of PVA hydrogels derived from both the equilibrium swelling and the rubber elasticity theories	73
3.6	Permeability parameters of dextrans in PVA hydrogels and their diffusivities in water	74
3.7	Partition coefficients, diffusivity in water for BSA and IgG proteins and their % of DW in all PVA FG/c hydrogels	75
3.8	Permeability parameters of various immunoisolating membranes compared to fabricated PVA hydrogels (20 FG/c)	83
3.9	Three-dimensional structural shapes of dextran, BSA and IgG	86
4.1	Network characteristics and release behaviour of ECM-based hydrogels for various biomedical applications	90
4.2	Sol fraction, volumetric swelling ratio, average mesh size and crosslinking density of PVA, co-hydrogels and gelatin hydrogels after 24 hours incubation in PBS calculated from the Peppas-Merrill equation	106
4.3	Average equilibrium heparin and gelatin composition (%) in the co-hydrogels after 7 days of incubation in PBS	111
4.4	Partition coefficient values of both BSA and IgG proteins with different hydrogels compositions: PVA:heparin (19:1), PVA:gelatin (19:1) and gelatin (20%)	112
5.1	Sol fraction, volumetric swelling ratio, average mesh size and crosslinking density of different compositions of PVA hydrogels after 24 hours incubation in PBS calculated from the Peppas-Merrill equation	129
5.2	Average equilibrium heparin and gelatin composition (%) in the different co-hydrogels at 7 and 20 FG/c after 7 days of incubation	132
5.3	Partition coefficient values of both BSA and IgG proteins with different hydrogels compositions: PVA:heparin (19.5:0.5), PVA:gelatin (19.5:0.5) and PVA:ECM Mix (19:1)	134
6.1	Partition and diffusion coefficient values of insulin with different hydrogels compositions: PVA (20%), PVA:heparin (19.5:0.5), PVA:gelatin (19.5:0.5) and PVA: ECM Mix (19:1)	160
6.2	Time to 100% insulin release showing the effect of functional group density and different hydrogel compositions	163

Chapter 1

Introduction

1.1 Research Motive

Cell therapies provide a biological solution for the treatment of a range of diseases such as Parkinson's, hypoparathyroidism and diabetes. However in many instances, encapsulation of cells is required to protect them from the host immune system and to provide appropriate support for sustained viability and function. Most encapsulation systems have focused on alginate and other hydrogels and semi-permeable membranes based on one polymer [1-3]. The focus of this thesis is on understanding the impact of combining more than one natural polymer with a synthetic polymer on the permeability of hydrogels with a specific emphasis on encapsulation of insulin producing cells for treatment of diabetes.

Type I diabetes results from autoimmune destruction of insulin-producing beta cells of the pancreas and is one of the most common life-long autoimmune diseases, with a high incidence in childhood. The incidence rate is expected to increase by 3% annually worldwide. In Australia, approximately 1825 people are diagnosed with type 1 diabetes every year [4]. The current treatment of type I diabetes is through exogenous insulin given by daily injections, insulin pumps or inhalation. However, these approaches necessitate multiple daily doses and frequent monitoring and have issues with compliance. In addition, the aggressive management with insulin does not prevent the development of secondary chronic complications such as nephropathy, retinopathy and neuropathy [5, 6].

The gold standard for curing type I diabetes is by providing continuous *in situ* insulin supply to the body in response to varying physiological glucose levels such as by pancreatic transplantation. Although transplantation of whole pancreas appears to be the ideal solution to restore the physiological levels of insulin, this approach has many obstacles due to donor shortage, surgical complications and the need for life-long

immunosuppressant medications. In contrast to pancreas transplantation, transplantation of pancreatic islet cells requires minimal surgical intervention with the possibility of avoiding immunosuppressant therapies using methodologies such as immunoisolation [7]. Consequently, cell-based therapy has emerged as a promising approach to replace whole organ transplantation in different diseases and disorders. In type I diabetes, transplantation of functioning β cells or islets in the form of either allografts or xenografts has been proposed to restore the normal function of the pancreas in diabetic patients.

In order for the transplanted cells to achieve successful therapeutic function, they need to be protected from the surrounding host environment after *in vivo* implantation, which is the concept underlying immunoisolation. Immunoisolation can be achieved by encapsulating cells within selectively permeable membranes. The encapsulating membrane material must prevent access of harmful components of the host immune system such as immune cells and antibodies, while allowing for diffusion of nutrients, waste products and therapeutic factors secreted by the cells. Apart from its immunoisolation requirements, the encapsulating material must also support cell survival and functionality while maintaining its physico-mechanical properties throughout the required implantation period.

Hydrogels, a class of hydrophilic polymeric materials capable of swelling in water, have shown potential as membrane materials in the cell encapsulation field. Owing to their high water content at equilibrium and viscoelasticity, hydrogels resemble natural biological tissues and have been widely used in different biomedical applications. Most research in cell encapsulation has focused on either natural or synthetic hydrogels.

Natural hydrogels, depending on their origin and composition, often have biological properties that promote cellular interactions. However, their structural complexity and source variability make it difficult to precisely control their network

characteristics. Conversely, synthetic hydrogels are advantageous in their consistent structural composition and ease of manipulating their physical and chemical characteristics depending on the target application. However, their lack of biological signals does not encourage their sole use in cell encapsulation where enhanced cell survival and function are required. Despite the extensive research and some preclinical and clinical trials for implanting encapsulated cells using either natural or synthetic hydrogels, many results remain inconsistent because of the limited ability of hydrogels to maintain cell survival and function over extended periods of time [8]. Therefore, bridging the gap between natural and synthetic hydrogels via biosynthetic hydrogels is believed to be an ideal approach for cell encapsulation, where both controlled physico-mechanical properties and specific biological signals are included. Thus, biosynthetic hydrogel encapsulation systems could offer optimal support for cell viability and functionality over the implantation time period.

One key to a successful cell encapsulation device using synthetic hydrogels is the incorporation of biological molecules such as extracellular matrix (ECM) components, to serve as a biofunctional microenvironment for the encapsulated cells [9]. In recent studies, although cell survival does appear to be enhanced in the short term [10, 11], the influence of adding biological/ECM components into synthetic hydrogels on the permeability as well as the physical and mechanical properties of the hydrogel have had little attention.

Moreover, despite the findings that natural ECM modulates the permeability of different molecules *in vivo* [12], the effect of adding ECM components on the permselectivity of immunoisolating systems has not yet been investigated. Therefore, the current thesis focused on studying the effect of incorporated ECM analogues on the permeability performance of permselective synthetic hydrogels in addition to examining

the physico-mechanical characteristics and the effectiveness of the final biosynthetic hydrogels in cell encapsulation.

1.2 Overall Aim and Hypothesis

The overall aim of the thesis was to fabricate biosynthetic hydrogel systems with mesh sizes and physico-mechanical properties specifically tailored for cell immunoisolation together with the chemical incorporation of biological signals by adding model extracellular matrix (ECM) molecules. It was hypothesised that covalent binding of small amounts of ECM analogues would not interfere with the controlled permselectivity and physico-mechanical properties of the base PVA network while supporting cell viability in the hydrogel.

1.3 Thesis objectives

The current thesis aimed at achieving an optimum balance between controlled permselectivity and cell survival support within PVA based hydrogels through the following specific aims:

1. Tailor the mesh size of UV photocrosslinked PVA hydrogels through systematic variation in the functional group density and study the impact of these changes on the physical characteristics and macromolecular permeability
2. Covalently bind a low percentage of heparin and gelatin into a PVA network without interfering with the biofunctionalities of the natural polymers or the base PVA network characteristics
3. Support the viability of model pancreatic β cells encapsulated in biosynthetic hydrogels as well as facilitating the release of their therapeutic products

The literature on cell encapsulation technology and the essential requirements for developing immunoisolating membrane material is reviewed in Chapter 2. Previous researchers' attempts in modulating hydrogels permeability for cell encapsulation purposes were covered, identifying the needs for investigating permeability in biosynthetic hydrogels with ECM mimicry.

Chapter 2

Literature Review[1]

[1] **The current literature review is modified in part from:**
Nafea, E. H., Marson, A., Poole-Warren, L.A. and Martens P.J. (2011) "Immunoisolating semi-permeable membranes for cell encapsulation: Focus on hydrogels." J Control Release 154(2): 110-122. ~ 90% of the article was written by the first author, Eman Nafea.

Elsevier publisher allows authors to use their published articles in theses

2.1 Introduction

The transplantation of therapeutic cells is fast becoming a promising approach for the treatment of various diseases and disorders that cannot be cured or treated using technologies currently available. This powerful technique allows for the local and controlled delivery of therapeutic products to specific physiological sites in order to restore lost function due to disease or degeneration. Possible targets of this approach include disorders of the endocrine system (diabetes, hypoparathyroidism) [13] and central nervous system (Parkinson's and Alzheimer's) [14-17], as well as conditions such as heart disease [18], and cancer [19-22] (Table 1).

Immunoisolation aims to protect transplanted cells from the host immune response, and was initially attempted in 1933 by Bisceglie who successfully replaced the endogenous pancreas of rats with human insulinoma cells [23]. The cells were enclosed in a membranous sac and implanted into the abdominal cavity to study the effects of lack of vascularisation on the survival of the tissues.

The concept of immunoisolation was developed experimentally in 1943 by Algire who demonstrated that graft viability could be prolonged by encapsulating tissues from the same species (allogenic) and different species (xenogenic) in diffusion chambers before transplantation [24, 25]. The term "artificial cells" was introduced 20 years later by Chang in 1960s, to describe the technique of encapsulating cells for immunoprotection [8, 26]. Since then, numerous studies have highlighted that the encapsulating membrane material must serve two vital functions. First, it must allow the inward diffusion of nutrients to allow cellular survival whilst simultaneously facilitating the outward diffusion of both waste products and potentially therapeutic factors produced and secreted by the cells. Secondly, the membrane must act as a protective barrier between the cells and harmful

components of the humoral immune system such as antibodies and cytokines. A major benefit of the cell encapsulation system is therefore not only the promotion of cell survival but also prevention of host rejection of the transplanted cells, thus eliminating the need for chronic immunosuppression.

Cell immunoisolation represents a major advance in transplant therapy as it removes constraints associated with cell sourcing, making either allogenic or xenogenic cells viable alternatives to the limited supply of autologous donor tissues currently available [27, 28]. However, this approach still has limitations, especially in maintaining an optimal balance between the permselectivity of the encapsulation device and cell survival. This chapter will review the different membrane materials that have been investigated as outlined in Table 2.1, and the progress made in the development of devices from the mass transport perspective, highlighting the problems and solutions investigated to date regarding their immunoisolating requirements. The chapter will focus on hydrogels, the most common polymers used in cell encapsulation, and discuss the advantages of these materials as well as the challenges in modifying their immunoisolation and permeability performance. Finally, research attempts to enhance cell survival within hydrogels will be reviewed while highlighting the unresolved issues from the permeability perspectives.

Table 2.1: Examples of encapsulated cells targeting various diseases, showing their immunoisolating membrane materials and device configurations.

Encapsulated cells	Targeted disease	Encapsulation device	Membrane material	Ref
Pancreatic islets	Diabetes	Conformal coating	Tannic acid /poly (vinylpyrrolidone)	[29]
			Nanothin-PEG	[30]
			PVA/PEG	[31]
			Polyion complex	[32]
			Chitosan/alginate/ chondroitin sulphate	[33]
		Macrocapsule	PEG	[34, 35]
			Chondrocyte cell sheet	[36]
			Agarose	[37]
			Polysulphone	[38]
			PVA	[39]
			PVA/PAA	[40]
			Polyurethane	[41, 42]
		Microcapsule	Alginate	[43-45]
			Alginate/PEG	[46]
			Biodritin (alginate/chondroitin sulphate)	[47]
			Agarose	[48, 49]
			Cellulose sulphate	[50]
Parathyroid	hypoparathyroidism	Microcapsule	alginate	[51]
PC12 cell line	CNS/Parkinson's	Macrocapsule	Polyurethane	[52]
293 cell line	CNS/Glioma	Microcapsule	Alginate	[53]
BHK cell line	CNS/Huntington's	Macrocapsule	PAN-PVC	[54]
			Alginate	
BHK cell line	CNS/Amyotrophic lateral sclerosis	Macrocapsule	Poly-ether-sulphone	[55]
293 cell line	Pancreas cancer	Microcapsule	Cellulose sulphate	[56, 57]
G8P2B5 hybridoma cells	Retroviral neurodegeneration	Microcapsule	Cellulose sulphate	[58]
J558/TNF-α	Cancer	Microcapsule	Alginate	[21]
HEK 293	Cancer	Microcapsule	Alginate	[59]
CYP2B1	Cancer	Microcapsule	Agarose	[60]
Hepatocytes	Liver failure	Macrocapsule	PEG	[61]
			polyacrylonitrile-sodium methallylsulphonate	[62]
		Microcapsule	Poly-l-lysine	[63]
			Polyelectrolyte copolymer/modified collagen	[64]
			Alginate-chitosan	[65]
Mesenchymal stem cells	Myocardial infarction	Microcapsule	Alginate	[66]

Abbreviations: **PEG**: poly (ethylene glycol), **PVA**: poly (vinyl alcohol), **PAA**: poly (acrylic acid), **PAN-PVC**: poly (acrylonitrile vinyl chloride).

2.2 Immunoisolation approaches

Different configurations of immunoprotecting membranes have been developed for the purpose of cell immunoisolation. These include conventional intravascular chambers, extravascular macrodevices and microcapsules as illustrated in the schematic in Figure 2.1. Conformal coating techniques have also recently been explored with the aim of reducing the size of implantation devices [67-70] (Figure 2.1).

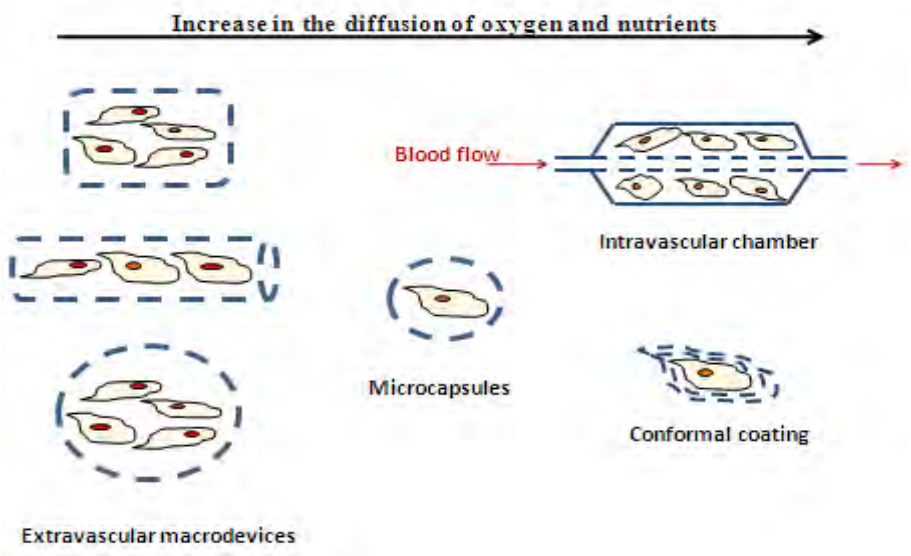

Figure 2.1: Conventional and novel encapsulation devices used for cell immunoisolation. (Dotted line represents the semi-permeable membrane)

2.2.1 Intravascular devices

Until the 1990s, intravascular chambers were commonly used for cell immunoisolation [6]. This type of chamber is composed of a tubular membrane which is connected directly to the host vascular system through its lumen following implantation by vascular anastomoses [7]. This type of device provided close contact of encapsulated cells with the host blood supply, which ensured good transportation of oxygen and nutrients. However several problems were identified, including surgical complications and post

operative thrombosis which are major obstacles in the development of these devices [6, 9, 71]. Consequently, other vascular devices have been explored.

2.2.2 Extravascular devices

In contrast to intravascular devices, extravascular devices are not directly connected to the host vasculature; however they rely on the presence of blood vessels in their surrounding environment to ensure the viability of encapsulated cells after implantation [72]. Extravascular devices can be categorised into two different types: extravascular macrodevices and extravascular microcapsules. These devices are designed to be implanted with minimal surgical procedure into different sites, depending on their size and targeted application (Table 2.2) and they are not associated with the surgical risks described for the intravascular chambers.

Table 2.2: Examples of different sites for transplantation of cell encapsulation devices

Site of transplantation	Targeted disease	Device	Ref
Peritoneal cavity	Diabetes	Macrocapsule	[37]
		Microcapsules	[73, 74]
Portal vein	Diabetes	Conformal coating	[30]
Renal capsule	Liver failure	Macrocapsule	[62]
		Microcapsules	[44]
Brain	Parkinson's	Macrocapsule	[52]
Intrathecal space	CNS/Amyotrophic lateral sclerosis	Macrocapsule	[55]
Intra-tumor	Cancer	Microcapsule	[21]
Intra-arterial	Pancreas cancer	Microcapsule	[56]
Spleen	Liver failure	Microcapsule	[63]
Subcutaneous	Retroviral neurodegeneration	Microcapsule	[58]

2.2.2.1 Extravascular macrodevices

Extravascular macrodevices, in which large groups of cells are encapsulated, include macrocapsules, planar membranes and hollow fibers (Figure 2.1). These devices have the advantage of being easily retrievable from the site of implantation in case of post operative complications. However, several associated limitations have been identified such as cell necrosis due to the large surface area-to-volume ratio of the device and consequently the limited diffusion of oxygen and nutrients. Mechanical failure and poor biocompatibility of these macrodevices have also been reported [6, 7].

2.2.2.2 Extravascular microcapsules

Extravascular microcapsules designed to encapsulate single or small groups of cells within their spherical configuration, typically have diameters less than 1mm [27, 75, 76]. Due to their relatively small size, microcapsules have the advantage of promoting increased cell viability by enhancing diffusion of oxygen and nutrients across the membrane. Other advantages of these devices over macrocapsules include ease of manufacturing by various techniques, ease of implantation and good levels of mechanical stability *in vivo*. However, the major drawbacks of microcapsules are the difficulty of their retrieval post operatively and their possible self aggregation which can lead to cell necrosis and graft failure [77].

Despite the advantages of extravascular over intravascular devices, concerns regarding long-term survival and functional performance of the graft have been raised due to the lack of direct vasculature associated with encapsulated cells. Effective diffusion of oxygen and nutrients from capillaries to neighbouring cells has been reported to occur over a distance ranging 100-200 μm [78, 79]. The membrane of an extravascular device also

acts as a physical barrier between surrounding vasculature and encapsulated cells, increasing the likelihood of hypoxia, especially at the centre of the cell mass [9].

Different approaches were investigated to ensure the longevity of extravascular grafts. Pre-vascularised support constructs such as polytetrafluoroethylene (PTFE) mesh have been used as artificial cell transplantation sites to initiate angiogenesis in an attempt to prolong viability of encapsulated cells [80-82]. These artificial sites have the advantage of ease of retrieval of microcapsules when required. In addition, angiogenic factors including vascular endothelial growth factor (VEGF) have been co-encapsulated with cells or delivered at the site of transplantation to enhance cell functionality [83-85]. VEGF is known to increase vascularisation at the transplantation site and consequently facilitate the diffusion of oxygen and nutrients to encapsulated cells.

2.2.3 Conformal coating

The relatively large size of conventional microcapsules still limits potential transplantation sites due to the capsule void volume [30]. For example, microencapsulated islets are unsuitable for transplantation into the portal vein of the liver due to their large volume [30, 86]. In order to reduce the size of the capsules and consequently improve associated diffusion levels of oxygen and nutrients, recent studies on cell encapsulation have involved the conformal coating of the surface of transplanted cells with very thin layers of different materials [30]. This approach has been shown to maximize the amount of cells that can be implanted whilst minimizing the device volume [87]. Different techniques have been used to perform these conformal coatings including interfacial photopolymerisation [67], layer-by-layer polyelectrolyte deposition [68, 69], hydrophobic polymer coating [31, 86] and more recently, conformal coating with living cells [88].

Conformal coating of cells has been shown to increase mass transport above that observed with microcapsules [31]. However, current conformal coatings tested have been found to display limited stability and recent studies showed that most of these coatings dissociated from the cell surface after only a few days [86, 89]. Moreover, the mechanical stability of such very thin coatings remains undefined. Further studies are therefore required to establish whether conformal coatings are robust enough to withstand the shear forces associated with the transplantation process and those which the graft will be exposed to at the transplantation site. Only then can this system be optimised for clinical applications.

2.3 Semi-permeable membranes for cell immunoisolation

In all potential cell encapsulation devices, the rate of delivery of essential nutrients and the removal of waste metabolites out of the encapsulating device is crucial for the survival of cells. For this reason, the mass transport properties of the device are of great interest during development. Mass transport describes the transport of atoms and molecules within a physical system. Since the total surface area is inversely proportional to the size of capsule, macrocapsules have less surface area available for mass transport than microcapsules and conformal coating. Hence, microencapsulation and conformal coating are considered the preferred techniques for encapsulating cells as their surface-to-volume ratio allows better diffusion of oxygen and nutrients and thus enhanced mass transport. Alongside the appropriate conformation, careful selection of the material is considered to be a key factor for the efficiency of immunoisolating membranes, since it determines the physical, mechanical and permeability performance of the final encapsulation device.

2.3.1 Membrane materials

The materials used to develop semi-permeable membranes for cell encapsulation can be categorised as polymeric or non-polymeric. The majority of polymeric materials that have been used in cell encapsulation devices can be divided into two major categories: hydrogels or thermoplastics. Non-polymeric membranes are typically based on silicon or ceramics. Examples of these material systems are outlined in the sections below.

2.3.1.1 Hydrogels

Hydrogels are water swollen three-dimensional networks of hydrophilic homopolymers or copolymers. They have thermodynamic compatibility with water which allows them to swell in aqueous media [90]. Their insolubility and structural integrity relies on crosslinks formed between polymer chains using different chemical bonds and physical interactions [91-93]. Hydrogels were first introduced into biomedical applications in the late 1950s following the development of poly (2-hydroxyethyl methacrylate) (PHEMA) gels for soft contact lenses. Owing to their softness and high water content at equilibrium, hydrogels resemble natural biological tissues and as such they often display minimal inflammatory response. They also have easily adjustable permeability properties making them popular in the development of cell encapsulation systems. Hydrogels will be examined in more detail in section 2.4.

2.3.1.2 Thermoplastic polymers

Thermoplastic polymers consist of long, linear, water insoluble chains that can be processed into different configurations by heat melting followed by a cooling stage [94]. They are preferred in cell encapsulation systems for their chemical stability and mechanical properties which are typically greater than those of hydrogels. Thus

thermoplastics are often selected for incorporation into vascular devices and macrocapsules.

Currently, the most popular thermoplastic membrane material used for cell immunoisolation is the acrylonitrile vinyl chloride copolymer (PAN-PVC) fabricated by phase-inversion technique and mainly used in the form of hollow fibres [3, 16]. Typically tubular PAN-PVC encapsulation membranes with ~50kDa nominal MWCO are applied. It has been shown that the fabrication conditions impact greatly on the structure of thermoplastics and subsequently their diffusive properties. For example, it has been shown that the nodular architecture and the size of nodules within PAN-PVC membranes could be altered by varying the precipitation conditions during the phase separation process.

Other thermoplastics used in cell encapsulation studies to date include polyurethane, polysulphone and dialysis membranes constituting of acrylonitrile and methallyl sulphonate mixtures [38, 42, 95]. Despite their high stability, some polyacrylate thermoplastics displayed low permeability of water-soluble nutrients and subsequently limited viability of encapsulated cells, limiting their clinical potential [27]. In addition, although some commercial ultrafiltration membranes such as XM-50 PAN-PVC have the ability to fractionate macromolecules (~50 kD) during ultrafiltration (pressure-driven process), it has been demonstrated that they tend to lose their immunoisolation efficiency in a concentration-driven process such as diffusion [96].

2.3.1.3 Non-Polymeric materials

The broad pore size distribution of current polymeric membranes could prevent complete blockage of harmful immune system components. To overcome this problem, non-polymeric membrane materials have recently been developed in the immunoisolation

field. Non-polymeric membranes, such as silicon and ceramics, have the potential to allow for better control of pore size uniformity, even in the nanometre range.

Recently, silicon nanopore membranes have been fabricated using a top-down microfabrication technique for immunoisolation of islets**.** These silicon nanopore membranes are 5 μm thick with 1% porosity and a straight pore path, which allows size selectivity [97]**.** Porous titanium dioxide/titanium (TiO_2/Ti) composite membranes have also been developed using a dip-coating method. It was found that their porous structure and associated permeability could be controlled by changing the sintering temperature [98]. Bio-ceramics have recently been introduced into the bone cell transplantation field by Liu et al. [99]. These membranes showed good stability and high levels of mechanical strength. Their topology and crystalline structure could be controlled by modifying the type of inorganic particles originally used in their manufacture and the sintering temperature, resulting in average pore sizes of 0.5 μm. This pore size was considered ideal based on previous reports which recommended pore diameters less than 1 μm for optimum immunoisolation [99, 100].

Despite the advantage of non-polymeric materials in controlling the pore size distribution, complicated and harsh conditions of fabrication could restrict their further development as cell encapsulation devices. Moreover, their fabrication techniques are restricted to macrocapsule devices mostly in the form of hollow fibres, which consequently limits the choice of their transplantation sites *in vivo*.

2.3.2 Membrane requirements

In order to provide long-term protection of the cells, encapsulation membranes should be biostable, biocompatible, mechanically stable, have appropriate permeability to support the mass transport requirements, and have appropriate physical structure. These

requirements are examined in more detail in the following sections. It should be noted that membranes should also be easily manufactured and sterilised however, these requirements are not the focus of this research and have been addressed elsewhere [6, 101].

2.3.2.1 Biocompatibility and biostability

Biocompatibility, the ability of a material to perform with an appropriate host response in a specific application, is a crucial consideration in the selection of a material for the manufacture of an implant [102]. Biocompatible materials must be selected for the manufacture of semi-permeable membranes in order to ensure optimal diffusion of oxygen and nutrients. Otherwise, overgrowth of fibrous tissue upon the membrane surface would be stimulated, resulting in impaired diffusion of oxygen and nutrients and subsequent necrosis of encapsulated cells and ultimate graft failure. Biostability of the implant must also be ensured to prevent biodegradation of the membrane material *in vivo* during the required long-term functionality of the implant [6, 27].

2.3.2.2 Mechanical stability

The mechanical stability of the cell transplantation device, its ability to resist an applied force, is usually determined by the configuration and chemical structure of the semi permeable membrane. Ultimately a cell transplantation device would be expected to last for a significant period of time *in vivo*. To achieve this target, the membrane component would be required to demonstrate optimum mechanical strength including stiffness (resistance to deformation) and toughness (resistance to fracture) in order to be able to withstand forces of compression and shear stresses imposed at the implantation site [6, 8, 103]. Any bending or breakage of the membrane *in vivo*, could lead to the failure of the whole device.

In addition, membrane stiffness may influence encapsulated cell response and regeneration. Engler et al. have reported that mesenchymal stem cells were strongly affected by the elasticity of the matrix microenvironment in which they were grown which influenced their lineage specifications [104]. Regarding cell encapsulating membranes, it has been demonstrated that neural stem cell fate was influenced by the mechanical properties of encapsulating hydrogels including alginate and hyaluronic acid [105, 106].

Different membrane configurations and chemical structures have been investigated in the optimisation of membrane mechanical stability. Long hollow cylindrical thermoplastic membranes have been shown to be highly susceptible to mechanical bending, which represents a major flaw as intravascular membranes are required to withstand high arterial blood pressures without succumbing to rupture. Surrounding the membranes with mechanically durable shells is one approach which has been developed to address this problem [107]. Hydrogel-based devices are also known to be susceptible to deformation, losing their mechanical stiffness and integrity over time, and thus limiting their life expectancy. However, it has been reported that the mechanical strength can be improved and controlled by modifying their chemical structure, such as increasing the polymer concentration and crosslinking density which has been linked to a direct increase in mechanical stiffness [8, 108, 109].

Other approaches taken to improve the mechanical strength of semi-permeable membranes include the application of multiple layers, surface modifications of the membrane with strengthening polymers, membrane reinforcement with polyester meshes and decreasing the size of the device [110-113].

2.3.2.3 Permselectivity and mass transport

Membrane permselectivity is one of the important requirements in the design of cell encapsulation devices. The cell encapsulating membrane must be able to freely permit the inflow of oxygen and nutrients and the outflow of therapeutic factors, metabolites and waste products, while totally excluding harmful components of the host immune system (e.g. antibodies and cytokines) (Figure 2.2). Consequently, the viability and functionality of encapsulated cells depend on the balance obtained between the mass transport (which determines the supply of nutrients and release of therapeutics and metabolites) and the molecular weight cutoff (MWCO) of the membrane, ideally preventing access of harmful host immune components [6, 72]. MWCO values (which determine the upper size limit of solute transport across the membrane) have been widely studied as a parameter used to characterize membrane permeability in cell encapsulation devices and have been cited within the range of 50 to 150 kDa [27, 114-116]. However, these values can be misleading as diffusing macromolecules usually exhibit a range of molecular weight values, rather than defined molecular weights. Furthermore, diffusing solutes of identical molecular weights can vary dramatically in size, shape and relative charge which often affects their diffusion behaviour [6]. Hence, other quantitative parameters such as permeability and diffusion coefficients are considered more accurate for assessing membrane permeation than MWCO values.

Developing semi-permeable membranes with optimum mechanical strength balanced with good mass transport of oxygen and nutrients remains a key challenge in cell encapsulation technology, as membrane permeation is often inversely related to membrane strength. Recently, Cha et al. introduced a new strategy aiming to decouple the inversed dependency of membrane permeability on the strength of a hydrogel, inspired by the role

of glycosaminoglycans in providing rigidity to the extracellular matrix (ECM) [117].Cha et al. demonstrated that the chemical crosslinking of methacrylic alginate with poly (ethylene glycol) dimethacrylate (PEGDA) allowed them to control the gel stiffness without affecting the permeability of the membrane.

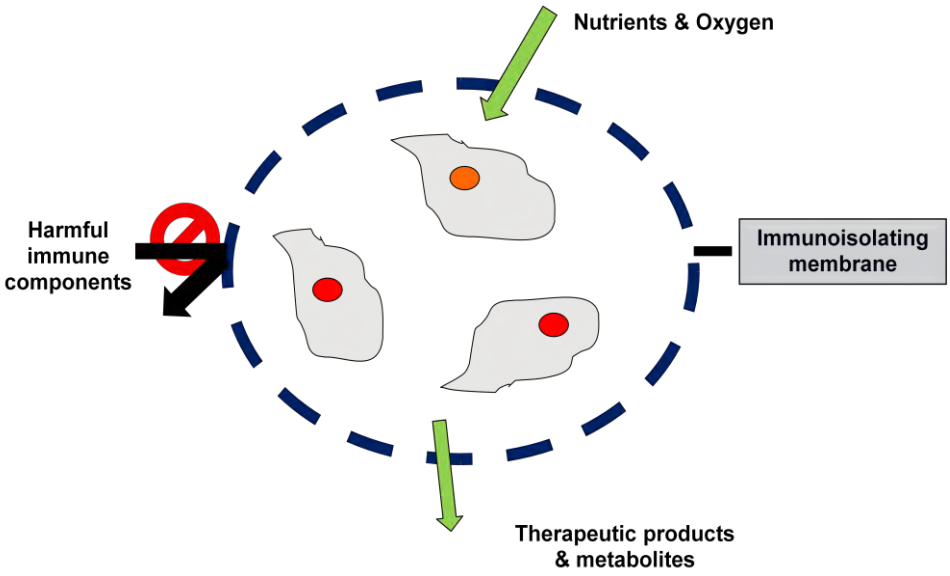

Figure 2.2: Requirements of a semi-permeable membrane for immunoisolation of encapsulated cells.

2.3.2.4 Membrane morphology

The physical structure of the capsule membrane is important both *in vitro* and *in vivo*. The specific morphology of the membrane surface is of extreme importance *in vivo* as it is highly influential on the host immune response as rough surfaces usually induce immunological and fibrotic reactions whilst this reaction is more limited with smooth surfaces [27, 101]. In addition, the uniformity of the size and shape of the encapsulating device is important as these dimensions influence other functional *in vivo* properties of the membrane including permeability and mechanical stability, as well as defining the choice of transplantation site.

2.4 Hydrogels in cell encapsulation

The above mentioned membrane requirements can be easily met using hydrogels as the membrane material. Hydrogels, with their physical similarity to many natural biological tissues, have demonstrated excellent biocompatibility in different tissue engineering applications, together with the ease of their manufacture processes and the feasibility to tailor their mechanical and permeability properties [8, 92, 118]. In particular poly (vinyl alcohol) (PVA) is an appropriate hydrogel choice due to the unique flexibility in managing its structural properties as will be further discussed in 2.4.1.

2.4.1 Natural, synthetic and biosynthetic hydrogels

The first successful application of hydrogels in cell encapsulation was achieved in 1980 when Lim and Sun developed calcium alginate microcapsules for islet cell encapsulation [119]. Since then, both synthetic and naturally derived hydrogels have been developed with varying levels of success.

Natural hydrogels

Most of the studies to date have relied on natural hydrogels such as alginate, chitosan, agarose, fibrin, hyaluronic acid and chondroitin sulphate [120-126]. Natural hydrogels are known to provide biological signals to cells *in vivo* promoting cellular proliferation and development, both of which are crucial for a successful implant [127]. However, their physical and mechanical properties are often difficult to manage compared to those of synthetic hydrogels and the presence of impurities within natural hydrogels can also compromise their biocompatibility.

Synthetic hydrogels

Synthetic hydrogels have been developed as an alternative membrane and have been shown to have consistent compositions and favourable physical and mechanical

properties which can be easily controlled. However, they lack the capacity to provide the biological signals required by cells following implantation *in vivo* which limits their utility. Examples of synthetic polymers commonly used in cell encapsulation hydrogels include polypropylene fumarate, polyethylene glycol (PEG) and poly (vinyl alcohol) (PVA) [128-130].

- ***PVA as an appropriate synthetic base material for cell encapsulation***

PVA is a hydrolytic product obtained from poly (vinyl acetate) with a wide molecular weight distribution. Depending on the degree of hydrolysis and molecular weight, the hydrophilicity and solubility of PVA can vary [131, 132]. PVA is well known for its low toxicity, hydrophilic nature, relative stability and most importantly the ease of modification of its backbone structure. A schematic representation of PVA backbone is shown in Figure 2.3.

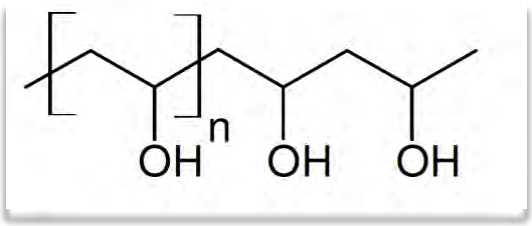

Figure 2.3: Schematic representation of PVA backbone structure.

The plethora of pendant hydroxyl groups on PVA backbone is considered a major attractant of this polymer in various biomedical applications. This high percentage of hydroxyl groups offer a great flexibility in fabricating PVA hydrogels through varying the nature and number of functional groups introduced to its backbone and also the crosslinking process whether physical or chemical. Depending on the nature of introduced functional groups, both degradable and non-degradable PVA hydrogels have been successfully fabricated for a wide variety of applications [133-136].

Different studies investigated the use of PVA hydrogels for cell encapsulation after being crosslinked using glutaraldehyde, radiation or freeze thawing methods [40, 137]. However these hydrogels are fabricated in harsh conditions that are expected to affect cell survival during encapsulation. In these systems, some attempts to control the permeability of PVA have been reported using different approaches including changing concentration of glutaraldehyde, the molecular weight of PVA and the radiation dose [137]. However, no reported studies to date have focused on the advantage of using the variable functional group density on PVA backbone in managing its permeability performance for cell immunoisolation purposes, which will be addressed in-depth in the current thesis.

Biosynthetic hydrogels

Biosynthetic hydrogels, where bioactive moieties are incorporated into synthetic networks, are becoming a convenient solution to the shortcomings of natural and synthetic hydrogels in the tissue engineering field since they combine the advantages of both natural and synthetic hydrogels. Therefore, modifications of synthetic polymers with different biological molecules have been investigated for various biomedical applications. In hydrogel membranes, PEG and PVA have been synthesised incorporating specific peptide sequences known to enhance cellular adhesion [138-140]. These modifications have been shown to dramatically change the properties of hydrogels overcoming the previous problems encountered where hydrogels failed to generate the signals required to stimulate surrounding cells. The most common peptides used to modify hydrogels are amino acid sequences derived from natural proteins, for example RGD (derived from fibronectin, laminin, or collagen), IKVAV, and YIGSR from laminin [92, 141-143]. An alternative approach involved the attachment or mixing of complete selected extracellular matrix (ECM) components, such as the proteins fibronectin, collagen and laminin with synthetic

polymers. Studies have shown that this approach can promote cell adhesion, proliferation and migration [144-146]. The copolymerisation of synthetic hydrogels with different natural glycosaminoglycans, including heparin, chondroitin sulphate and hyaluronic acid, has also been shown to support cellular growth and proliferation [147-150].

Alternatively, to regulate cellular functions, the tethering or incorporation of different growth factors has also been reported. For example, the tethering of transforming growth factor beta (TGF-β) to PEG has been reported to regulate smooth muscle function [151]. In addition, TGF-β tethered to agarose hydrogels induced chondrogenesis of bone marrow stromal cells and modulated their bioactive signaling [152].

In cell-based therapy, biosynthetic hydrogels represent the ideal approach for cell encapsulation, where controlled permselectivity and physico-mechanical properties along with specific biological signals are required. Hence, the current thesis will investigate biosynthetic PVA hydrogels as proposed immunoisolating membrane materials.

2.4.2 Mechanisms of hydrogel formation

Hydrogels can be formed by a range of different gelation mechanisms; however for cell encapsulation, the gelation process must be mild and non-cytotoxic. Depending on the type of crosslinking bonds used (covalent, ionic, or physical), hydrogels can be classified as physically or chemically crosslinked [127, 153].

Physical hydrogel networks are crosslinked mainly by molecular entanglement, and/or by secondary bonds such as ionic and hydrogen bonds or by hydrophobic interactions [153]. The most commonly used physical hydrogel in cell encapsulation is the alginate-polycation ionically crosslinked hydrogel [43, 119, 154-157]. This gelation mechanism relies on electrostatic interactions occurring between oppositely charged electrolytes, resulting in polyelectrolyte complexation or ionotropic gelation. This

technique is preferable in the field of cell encapsulation due to its simplicity and the benefits to the cells of the reaction being performed under physiological conditions. However, the reaction is reversible and can easily be disrupted by changes in pH and ionic strength or temperature [153].

Consequently, chemical hydrogels crosslinked by covalent bonds through chemical crosslinking or radical chain polymerisation are more controllable methods for hydrogel formation due to their stability afforded by covalent crosslinks, and the ability to precisely control physical properties. Although chemical crosslinking of polymeric networks using crosslinking agents such as aldehydes has been used in cell encapsulation [112, 158], the widespread application of this process has been limited due to its slow gelation rate and the cytotoxicity of the chemicals involved [109, 138, 159]. In addition, the lack of control of the uniformity of the crosslinked networks due to imperfect mixing and the diffusion of crosslinkers into the network makes it difficult to control the permeability of hydrogels made using these systems [159].

Radical chain polymerisation has become a more attractive technique for encapsulating cells, owing to its rapid polymerisation rates under physiological conditions and the ease with which the polymerisation process can be controlled [138, 159]. The reaction converts monofunctional or multifunctional vinyl monomers into a high molecular weight covalently crosslinked polymer via a chain reaction in the presence of an initiating signal (heat or light exposure) [127] where radicals are consequently generated. Different initiating stimuli have been successfully applied in cell encapsulation including thermal, redox and photoinitiating conditions [139, 140, 149, 160-162]. Specifically, UV photopolymerisation is commonly applied due to the rapid crosslinking reaction using cytocompatible photoinitiators with the feasibility of spatial and temporal control of the

polymerisation process [163-165]. Schematic representation of the UV polymerisation reaction is shown in Figure 2.4.

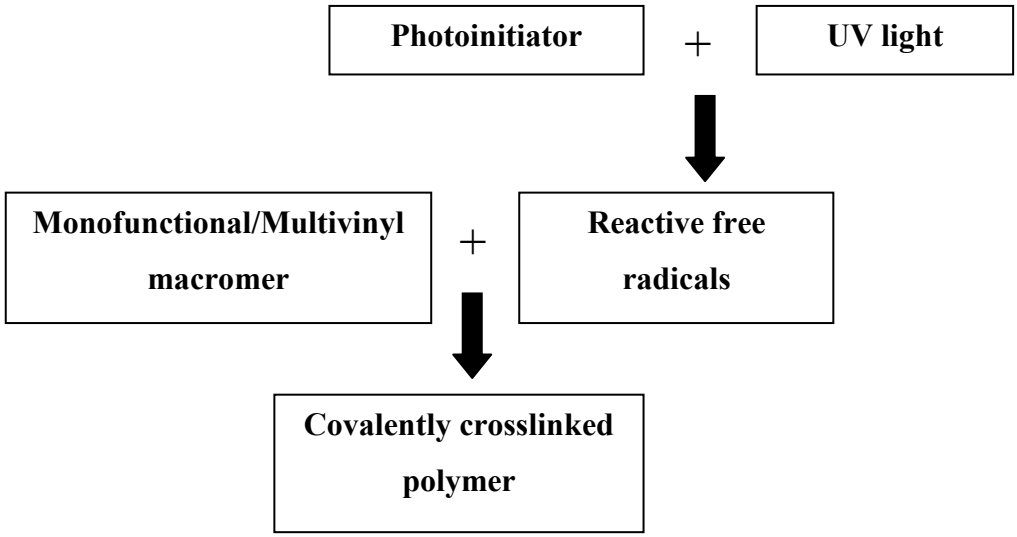

Figure 2.4: Schematic representation of UV free radical polymerisation reaction.

In the cell encapsulation field, divinyl macromers such as PEG have been widely investigated. However, multivinyl systems such as PVA are thought to be more advantageous in terms of tailoring the network characteristics of resulting hydrogels and more specifically their permselectivity. Therefore, the current thesis will investigate the ability to achieve controlled permselectivity using multivinyl PVA hydrogels fabricated by UV photopolymerisation.

2.4.3 Permeability and its importance in a successful hydrogel membrane

As described in 2.3.2.3, the optimal mass transport and permselectivity of semi-permeable immunoisolating membrane materials, including hydrogels, is crucial for a successful long lasting cell encapsulation device.

The permeability (P), describing both the transport and thermodynamic characteristics of the gel networks can be determined by equation 2.1 [153, 166]. This definition has been extracted from the equation for steady state flux of a solute across a membrane from a donor to a receptor phase [166] (Eqn 2.2). The equation was originally derived by applying Fick's first law (Eqn 2.3) to the diffusion of a species across a membrane. The law postulates an inversely proportional linear relationship between the flux of a species and the concentration gradient in one dimension (x). Considering the spherical geometry of the majority of cell encapsulating devices, where the surface area for diffusion changes as solutes diffuse radially, the differential equation for Fick's law of diffusion in a sphere (Eqn 2.4) is to be applied.

$$P = (D*K)/ L \qquad (2.1)$$

$$J = \frac{K D}{L} (C_d - C_r) \qquad (2.2)$$

$$J_x = - D \frac{dC}{dx} \qquad (2.3)$$

$$\frac{dC}{dt} = D \left\{ \frac{d^2C}{dr^2} + \frac{2}{r} \frac{dC}{dr} \right\} \qquad (2.4)$$

Where;

P: The solute permeability

D: The diffusion coefficient of diffusing solute

K: The partition coefficient of diffusing solute

L: The membrane thickness.

J: The flux of diffusing solute

C_d : The solute concentration in the donor phase

C_r : The solute concentration in the receptor phase

(dC/dx): The concentration gradient

r: Radial position

From equations 2.2 and 2.3, it is clear that any factor affecting transport properties or thermodynamic properties of a membrane will directly affect its permeability.

Solute transportation through semi-permeable membranes occurs by two main modes: 1) convective, where transport is driven by a pressure gradient across the membrane and 2) diffusive, where transport is driven by a concentration gradient across the membrane [27]. Transport of solutes through most encapsulation devices, including hydrogels, occurs by diffusion although both convective and diffusive transport can occur in intravascular devices [27, 167].

Hydrogels can be divided into three different classes in terms of solute diffusion depending on their membrane pore size [168]: macroporous hydrogels, microporous hydrogels and nanoporous hydrogels. Macroporous hydrogels have large pores > 0.1 μm through which solute transport occurs mainly by convection, whereas microporous hydrogels consist of pores ranging from 0.005-0.02 μm, which are in most cases smaller than the solute resulting in hindered diffusion. The most commonly used hydrogels in cell encapsulation are nanoporous hydrogels, which lack a true porous structure. Solute transport in nanoporous hydrogels occurs only by diffusion through spaces between macromolecular chains, known as the hydrogel mesh (Figure 2.5).

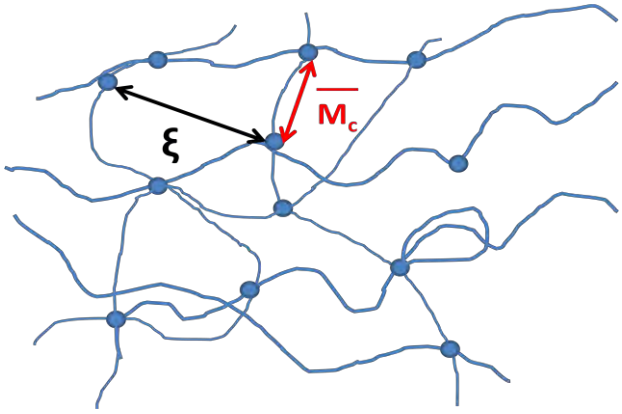

Figure 2.5: Schematic representation of part of a hydrogel network showing the macromolecular mesh (ζ) and the distance between two crosslinks, which is the number average molecular weight between crosslinks ($\overline{Mc}$).

2.4.3.1 Mesh size determination in nanoporous hydrogels

Since solute transport in nanoporous hydrogels occurs only by diffusion through the network meshes, the average mesh size becomes a key factor in determining the permeability performance. Considering that hydrogel mesh size cannot be visualised by the currently known imaging techniques, alternative approaches have been reported in literature to determine the mesh size of hydrogels, including characterisation of water states, diffusion experiments and derived theories such as the equilibrium swelling and the rubber elasticity.

Characterisation of water states in hydrogel

Different techniques have been used to estimate the mesh size via investigating the status of water in hydrogels whether bound, interfacial or bulk. These techniques include ^{1}H NMR spectroscopy, thermally stimulated depolarization (TSD) and differential scanning calorimetry (DSC) (cryoporsimetry) [153, 169, 170]. The techniques study the properties of water in hydrogel with layer-by-layer freezing out of bulk and interfacial water. Figure 2.6 classifies the different states of water in hydrogels with their freezing behaviour as reported in literature [153, 171-173].

^{1}H NMR spectroscopy measures the magnetic properties of water present in the hydrogel which varies depending on the local environment and the interaction of water with the polymer network [169]. At temperatures below 0°C, the ^{1}H NMR signal corresponds to non freezing mobile water which can be quantified. The mesh size can be then calculated by comparing ^{1}H NMR data to the thermodynamic properties of unfrozen water [174].

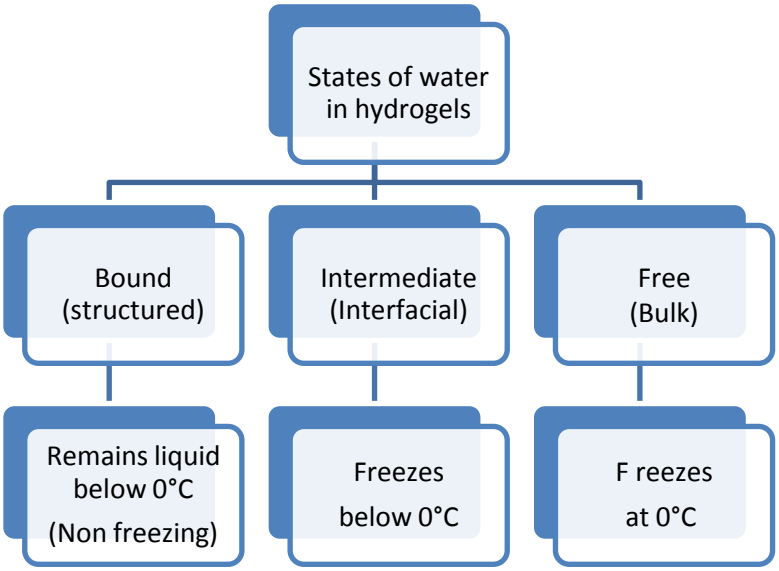

Figure 2.6: States of water in hydrogels and their freezing points.

In thermally stimulated depolarization (TSD), a broader range of temperatures is used compared to ^{1}H-NMR. TSD measures the dielectric properties of water related to relaxation of bound and mobile charges. The calculation of mesh size is then based on the relaxation energy of water dipoles, which is temperature dependent [169, 174, 175].

Differential scanning calorimetry (DSC, cryoporosimetry) has been commonly used to study the behaviour and status of water in hydrogels [173]. The amount of free and interfacial water is calculated from the enthalpies of melting or crystallization of water associated with the polymer. Hydrogel mesh size can be then calculated based on the

dependence of melting temperature (T_{mr}) and melting enthalpy (ΔH_{mr}) on crystals curvature radius (R_c) [170].

Although these techniques appear to be easily performed, the accuracy of relying on the water states in hydrogel is questionable, since the actual mesh size might be altered due to the expected widening that might occur after water freezing. In addition, the different types of water found in hydrogels remain controversial in literature.

Diffusion experiments

Another method of determining the mesh size is through a series of diffusion experiments, where the hydrodynamic radii of examined model dextrans are used in the calculation of mesh size via models modified from the free volume theory [170, 176, 177]. In the absence of solute-polymer interactions, a common model initiated by Peppas and Reinhart [178] for swollen hydrogels has been used to predict mesh size from swollen hydrogels via solute diffusion (Eqn 2.5)[179-181]. The model assumes that the probability that a solute has to diffuse through a mesh size ζ is linearly dependent on the ratio 2Rs/ζ.

$$\frac{D}{D_0} = \left(1 - \frac{2R_S}{\xi}\right) \exp\left(-Y\left(\frac{\varphi}{1-\varphi}\right)\right) \qquad (2.5)$$

Where;

D: The solute diffusion coefficient in hydrogel

D_0: The solute diffusivity in the solvent used

R_s: The radius of diffusing solute

ξ: The hydrogel mesh size

Y: the ratio of the critical volume required for a successful translational movement of the solute molecule and the average free volume per molecule of the swelling agent (can be approximated to =1)

φ : The volume fraction of polymer in hydrogel

It should be noted that this model assumes that the examined solutes have a spherical shape to calculate their hydrodynamic radius and thus it does not account for the actual shape of the diffusing solute, which might result in variations between predicted and experimental data. Such differences have been previously observed where results obtained from predicted data and experimental release study agreed only for spherical shape solutes such as lysozyme and BSA [181]. Dextran molecules due to their non-spherical conformation showed variations in the results [181]. Moreover, the estimated mesh size from this approach is dependent on the size of examined diffusing solutes, which doesn't give accurate reflection of the actual mesh size distribution but only predictable estimate since mesh sizes smaller or larger than the examined solutes might also occur in the network.

Equilibrium swelling & rubber elasticity theories

Despite the previously stated approaches, two theories remain the most commonly used for estimating hydrogel mesh size, which are the equilibrium swelling and rubber elasticity theories. They both rely on determining the number average molecular weight between crosslinks ($\overline{Mc}$) through either swelling or mechanical experiments [108, 182-186].

The equilibrium swelling theory is based on the Flory-Rehner model [187] for determining the number average molecular weight between crosslinks ($\overline{Mc}$) in neutral gels

in the absence of a solvent. The Flory-Rehner model is based mainly on two assumptions, the Gaussian distribution of the crosslinked polymer chains and the tetrafunctional arrangement of the crosslinks. In 1976, Peppas and Merrill [188] accounted for the presence of a solvent when fabricating hydrogels, where changes in the elastic potential are expected. Thus, the volume fraction density of polymer chains during crosslinking was introduced in the determination of ($\overline{Mc}$) (Eqn 2.6).

$$\frac{1}{\overline{M_c}} = \frac{2}{\overline{M_n}} - \frac{(\bar{\upsilon}/V_1)\left[\ln(1-\upsilon_{2,s})+\upsilon_{2,s}+\chi\upsilon_{2,s}^2\right]}{\upsilon_{2,r}\left[\left(\frac{\upsilon_{2,s}}{\upsilon_{2,r}}\right)^{\frac{1}{3}}-\frac{1}{2}\left(\frac{\upsilon_{2,s}}{\upsilon_{2,r}}\right)\right]} \qquad (2.6)$$

Where;

$\overline{Mn}$: Number average molecular weight in the absence of any crosslinking

$\bar{}$: The specific volume of the polymer

V_1: The molar volume of the solvent

$_{2,s}$: The equilibrium polymer volume fraction

$_{2,r}$: The polymer volume fraction after crosslinking but before swelling

χ: The polymer solvent interaction

l: Bond length

The Peppas-Merrill equation has been further adapted for the swelling of anionic and cationic hydrogels prepared in the presence of a solvent, where the ionic strength and dissociation constants for the acid and base were considered in the calculations [91, 189]. In order to predict the mesh size using the Peppas-Merrill model, equation 2.7 has been

used to estimate the end-to end distance of the unperturbed (solvent free) state $(\bar{r}_0^2)^{1/2}$ [190], from which the hydrogel mesh size (ζ) can be calculated (Eqn. 2.8) [159, 189, 190].

$$(\bar{r}_0^2)^{1/2} = l\left(\frac{2\overline{M_c}}{M_r}\right)^{\frac{1}{2}} C_n^{1/2} \quad (2.7)$$

$$\xi = \upsilon_{2,s}^{-1/3}(\bar{r}_0^2)^{1/2} \quad (2.8)$$

Where;

M_r: Molecular weight of the polymer repeating unit

C_n: The characteristic ratio of the polymer

The rubber elasticity theory is based on the resemblance of hydrogels to natural rubbers in their elastic response to applied stresses. In 1953, Flory stated the rubber elasticity theory for hydrogels (in absence of solvent) in order to characterise their structure via polymer elastic behaviour [191]. Peppas and Merrill modified this theory to account for the presence of solvent in hydrogels, where $\overline{Mc}$ could be determined from either tensile or compression testing experiments (Eqn 2.9 and 2.10) [108, 159, 192]. The mesh size is then calculated from equations 2.7 and 2.8.

$$\tau = \frac{\rho RT}{M_c}\left(1 - \frac{2M_c}{M_n}\right)\left(\alpha - \frac{1}{\alpha^2}\right)\left(\frac{\nu_{2,s}}{\nu_{2,r}}\right)^{1/3} \quad (2.9)$$

$$\frac{1}{\overline{M_c}} = \frac{2}{\overline{M_n}} + \frac{3(1-2\nu)}{2(1+\nu)\rho RT}\frac{K}{(\nu_{2,s})^{1/3}} \quad (2.10)$$

Where;

τ: Tensile stress applied to the polymer sample

K: Compressive modulus

α: Elongation ratio

ν: Poisson's ratio

ρ: Density of the polymer

R: Gas constant

T: Temperature of the gel

In addition, based on rubber elasticity theory, some reported studies used rheometric techniques where the shear modulus (G) could be measured and related to the crosslinking density (ρ_x) of highly swollen hydrogel networks (Eqn 2.11) [108, 185].

$$G = RT\,\rho_x\,Q^{-1/3} \qquad (2.11)$$

(Q: Swelling ratio determined from swelling experiments).

The network mesh size (ζ) can be then simply calculated using equation 2.12 [193].

$$\zeta = \sqrt[3]{6/\pi\rho_x N_A} \qquad (2.12)$$

(N_A: Avogadro's number)

Since both theories have assumptions in their derived equations for mesh size determination, the current thesis will compare both of them with experimental permeability results of solutes of different sizes and shapes in order to select the most reliable theory describing the mesh size in our hydrogels.

2.4.3.2 Experimental measurement of hydrogel permeability

When designing a hydrogel membrane for cell encapsulation it is essential to be able to characterise its permeability properties. A number of different methods exist for the

measurement of hydrogel permeability *in vitro*, with the method of choice being dependent upon the shape of the specific membrane being examined. Hydrogel membranes are mostly either planar membranes or microcapsules.

Planar membrane permeability

Planar membrane permeability is usually measured using a two compartment diffusion cell, consisting of two reservoirs (a receptor chamber and a donor compound) separated by the hydrogel membrane [194, 195] (Figure 2.7). The donor reservoir is filled with a solute solution of a defined concentration whilst the receiver reservoir is filled with solvent only. The concentration in one or both reservoirs is then measured as the solute permeates through the membrane. From these measurements the permeability and diffusion coefficient values, representing the permeability pattern of the membrane, can be determined. In the current thesis, a diffusion cell will be used to conduct all permeability studies on planar hydrogels.

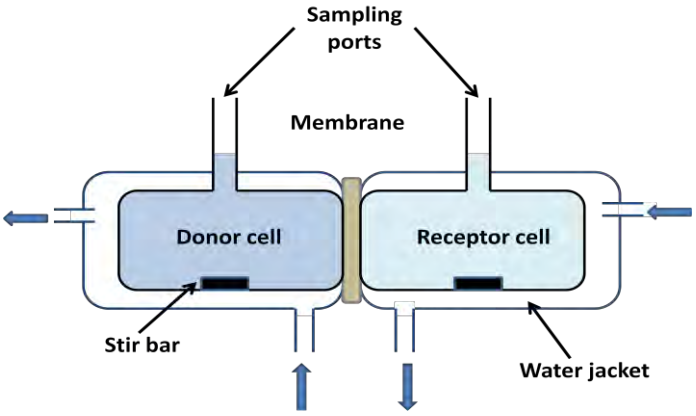

Figure 2.7: Schematic representation of a two compartment diffusion cell. Arrows represent the direction of water flow.

Microcapsule permeability

The permeability of microcapsules is generally determined by means of "uptake or release" experiments. These studies involve the microcapsule being immersed in a solvent

solution and the measurement of the change in solute concentration in the surrounding solution [110, 196, 197]. The solute concentration will increase or decrease depending on whether the solute was originally located inside or outside the capsule.

A more popular technique for measuring microcapsule permeability is inverse size exclusion chromatography (ISEC) as it provides a more comprehensive analysis of the permeability of the membrane. This technique requires a series of solutes covering a wide range of molecular sizes and allows for the evaluation of the MWCO and also the determination of the membrane pore size distribution of the capsule [114, 198, 199]. ISEC is derived from size exclusion chromatography (SEC), where solutes are partitioned between a mobile phase and a stagnant liquid phase within the pores of a packed column. When SEC is used to determine the pore size of the column packing (i.e. the pore size of microcapsules), it is called ISEC [114]. ISEC has been mainly applied using dextran standards of different molecular weights rather than proteins due to their different conformations, and possible interactions of proteins with the tested membrane.

Other methods for measuring the permeation of proteins in microcapsules have been developed exploiting specific protein-antibody interactions. Kulseng et al. [200] encapsulated magnetic monodisperse polymer particles (Dynabeads), coated with antibodies against selected radiolabeled proteins, in alginate-polylysine microcapsules. They assessed the permeability of a capsule by measuring the binding of radiolabeled proteins to the Dynabeads. Brissova et al. encapsulated another system composed of Protein A Sepharose (PAS)-antibody complex in multicomponent microcapsules [201]. The capsules were incubated with the radiolabeled proteins of interest, and the amount of protein that entered the capsule was quantified. Specific antibody techniques have several advantages: e.g. the protein of interest is specifically bound to the antibody, eliminating the

factor of protein adsorption to the capsule membrane in the permeability measurement. This technique also allows the measurement of the permeation of biologically relevant proteins at low concentrations (i.e. within the physiological range) eliminating concerns about protein self-association [201].

Selection of diffusing solutes

Most of the studies measuring membrane permeability to date have relied on standard model solutes rather than the actual solutes diffusing through the membrane after implantation *in vivo*. As previously described, permeability often depends on the size, shape and charge of the solute. In general, linear solutes diffuse faster than branched ones, while ionic solutes diffuse slower than nonionic solutes, especially when the membrane material is also charged [202, 203]. Hence, when selecting model solutes, it is preferable to select their structure, size and charge carefully in order to have approximate simulation of the *in vivo* application. The most commonly used model solutes in permeability studies are dextrans and bovine serum albumin [199, 203]. To measure the concentration of selected diffusing solutes, it is preferable to use radio- and fluorescently-labelled solutes rather than unlabeled solutes, to ensure the sensitivity and specificity of the quantitative technique [28]. In the current research, solutes of different sizes and shapes will be used including dextrans and proteins.

2.4.3.3 Structure-permeability relationship in hydrogels

Hydrogel permeability is greatly affected by the network structure. The most important characteristics of the network structure of hydrogels are the polymer volume fraction in the swollen state ($v_{2,s}$), the number average molecular weight between crosslinks ($\overline{Mc}$) (Figure 3), the network mesh size (ξ) (Figure 2.4), and the degree of crosslinking (ρ_x) [91, 92, 118, 178]. The significance of these parameters has been

examined in different models describing the structure–permeability relationship in hydrogels.

For example, the Peppas-Reinhart model describes the relationship between solute diffusion and the structural characteristics of highly swollen hydrogels [178]. The model predicts the dependence of the solute diffusion coefficient value on the solute size as well as the degree of swelling and molecular weight between the crosslinks of the network, and other structural characteristics of the polymer (Eqn 2.13).

$$\frac{Dim}{Diw} = k_1 (M_c\text{-}M_c^*/ M_n\text{-}M_c) \exp (-k_2 r_s^2/Q_m\text{-}1) \qquad (2.13)$$

Where;

D_{im} : The diffusion coefficients of the solute in the hydrogel

D_{iw}: The diffusion coefficients of the solute in water

M_c: The number average molecular weight between crosslinks

M_c*: The threshold value of Mc below which no diffusion of a particular solute can occur

M_n: The number average molecular weight of the polymer before crosslinking

r_s: The solute radius

Q_m: The equilibrium degree of swelling of the network

k_1 and k_2: Constants representing the structural parameters of the polymer/water system

This model was validated by successfully applying it to predict the diffusion of different solutes including albumin, sodium chloride, myoglobin, urea and dextran, through highly swollen cellulose and PVA-based hydrogel membranes and comparing calculated values with experimentally derived values [204, 205].

Another permeation model was developed by Dong et al., to be applied to the permeation of macromolecules through thermally reversible hydrogels [206]. The model takes into

account hydrogel porosity, tortuosity and permanent pore wall interactions, and was tested using a poly (N-isopropylacrylamide) hydrogel (Eqn 2.14).

$$\frac{Dapp}{D0} = \frac{\varepsilon}{\tau}[1-(a/r_p)]^2\,[1-2.104(a/r_p)+2.09(a/r_p)^3-0.95(a/r_p)^5] \qquad (2.14)$$

Where;

D_{app}: Apparent diffusion constant

D_0: The free solution diffusivity of the solute

ε: The porosity of the hydrogel

τ: The tortuosity of the hydrogel

r_p: The average pore radius

a: The solute radius

This model is recommended for the prediction of the permeation of both small and large sized solutes. Moreover, the estimation of mesh size of swollen hydrogels is possible using this model.

2.5 Modulation of hydrogel membrane permeability for immunoisolation

The ability to control membrane permeability is a prerequisite for the successful application of hydrogels in cell encapsulation. For that reason, different modifications of hydrogel membranes have been performed in order to optimise their permeability and control immunoisolation. The permeability of hydrogels is strongly dependent on their swelling behaviour, which in turn is highly dependent on the chemistry of the polymeric backbone material, as well as the network structure of hydrogels.

2.5.1 Factors controlling membrane permeability

2.5.1.1 The backbone chemistry of polymeric materials

Membrane permeability can be altered through modification of the chemical structure of the polymeric material. Hydrogels containing hydrophilic groups are known to swell more than those containing hydrophobic groups which collapse in the presence of water [91]. Hence, high mass transport can be achieved using hydrophilic groups in the polymeric material. For example, the hydrophilicity of PVA hydrogels could be increased by changing the percent hydrolysis of PVA polymer from 83% to 98%, resulting in a higher swelling ratio [109, 207].

Apart from changing the hydrophilicity, several studies have examined the effect of network charge on the diffusion of solutes. For example, the release of VEGF from ionically crosslinked alginate hydrogels has been modified by using different ionic crosslinkers to shield the charges of alginate and decrease the electrostatic interaction between alginate and VEGF [208, 209]**.** Schillemans et al. observed that introducing charges in dextran hydrogels influenced immobilization and ionic strength triggered release of proteins with different isoelectric points [210]. Copolymerising PVA with ionic molecules such as chondroitin sulphate and heparin has been shown to increase the swelling ratio of hydrogels [147, 148]. This behaviour was attributed to the presence of negatively charged sulphate groups on those molecules which increased the water uptake due to electrostatic repulsive forces at physiological pH.

Moreover, changing the composition of the initial monomers used and their ratios has been used as another approach in modulating the permeability of hydrogels. Gharapetian et al. succeeded in modulating hemoglobin diffusion from polyacrylate microcapsules by varying the comonomer composition and the molar ratio of monomer to

initiator during the synthesis of various polyacrylate polymers [211]. Their results showed a reduction in membrane permeability upon increasing the ratio of ionisable monomers in the comonomer composition, which was correlated to interactions between hemoglobin and ionic groups and also to the higher density of ionic bonds formed during encapsulation. Moreover, there was an inverse relationship between the diffusion rate and the molar ratio of monomer to initiator in both polyanions and polycations polymerisation, which was explained by the increase in chain entanglements and membrane tightness. In alginate based hydrogel systems, changing the ratio of glucuronic acid (G) to mannuronic acid (M) of the alginate polymer was found to be a successful method of modulating the permeability of the membrane [200, 212]. Alginate systems with high ratio of G results in a more permeable gel network than those with high ratio of M. This phenomenon was attributed to the long stiff G blocks and short flexible M blocks in high G ratio alginates [200, 213].

Thermodynamic interactions between the polymer network and the diffusing solute also affect hydrogel permeability as they influence the solute concentration within the hydrogel with respect to the outside solution. Changes in the solute concentration within the hydrogel can directly determine the presence or absence of interactions between the diffusing solute and the membrane, resulting in variable partition coefficient values. These partition coefficient values depend upon the chemical and physical characteristics of both the diffusing solute and the hydrogel, such as the polarity and the size and shape of the solutes [153].

These characteristics can lead to the formation of biospecific or electrostatic interactions between solutes and the hydrogel material, which can slow down the diffusion rates of solutes over time. This was demonstrated by Burczak et al. who observed a

progressive decrease in the permeability of high molecular weight albumin through PVA macrocapsules following long term *in vivo* implantation in the rat intraperitoneal cavity [214]. Burczak et al. showed that, over time, the protein became firmly entrapped in the hydrogel mesh causing blockage of the solute diffusion channels. It was reported that these changes in permeability were due to structural alterations in the hydrogel network resulting from physical adsorption of proteins in the intraperitoneal fluid, after long term implantation.

2.5.1.2 The physical properties of hydrogels

Apart from the backbone chemistry, physical modifications have been investigated to control the diffusion of solutes through a hydrogel membrane including the role of obstructions within the gel network, hydrodynamic friction, solvent structuring and material heterogeneity [28, 166, 215]. Solute mobility can be reduced or even hindered by obstructions within the gel often caused by the presence of impermeable, slowly moving network chains. These obstructions reduce diffusion rates by increasing the effective path length required for solute diffusion. Increased hydrodynamic friction (the resistance of fluid flow at the polymer-solvent interface) incurs a drag force on diffusing solutes and reduces the rate of their diffusion. The local viscosity of the solvent can also be increased by solvent structuring which occurs following solvent-polymer interactions and can also affect the diffusion properties of the polymer network [166, 216]. Finally, fluctuation of solute diffusion could also occur as a consequence of the extent of heterogeneity within the hydrogel network structure [28, 166].

2.5.1.3 The crosslinking density of hydrogels

The crosslinking density of hydrogels is one of the biggest determinants of network structure, and the swelling behaviour of hydrogels is known to be directly related to their

network structure. Changing the crosslinking density can have several structural implications for hydrogels, but most important for cell encapsulation is its effect on the average mesh size of the network. A decrease in the average mesh size of the network generally results in reduced swelling and subsequent restriction of the rate of solute diffusion [137, 166]. Highly crosslinked hydrogels have a tighter structure which hinders the mobility of the polymeric chains and hence decreases the swelling ratio, which limits solute mass transport through hydrogels. Different factors influence the crosslinking density including molecular weight of the polymer backbone, concentration of the polymer, functional group density, polymerisation conditions, and the addition of additives.

Molecular weight and concentration of polymeric material

In general, membrane permeability can be modified by changing the molecular weight and concentration of the polymeric material used. Significant changes in the permeability characteristics of interfacially photopolymerised PEG diacrylate hydrogels have been achieved by varying the polymer molecular weight from 2k to 20k. In this study, hydrogels prepared with low molecular weight PEG were impermeable to proteins with a size equal to or larger than 22 kDa, whereas hydrogels prepared with high molecular weight PEG were impermeable to proteins equal to or larger than 45 kDa [195]. Similar results were observed by increasing the molecular weight of the PVA backbone, where the swelling ratio of hydrogels increased due to a reduction in the crosslinking density which would consequently increase the mass transport [109].

Regarding the polymer concentration, it was observed in alginate-based systems that increasing the polymer concentration reduced diffusivity as a result of a reduction in the apparent pore size of the membrane [199, 202, 212]. In hydrogels chemically

crosslinked by radical chain polymerisation, increasing the polymer concentration often resulted in decreasing the intra-chain crosslinking (cyclisation) and an increase in the inter-chain entanglements (Figure 2.8), which lead to a decrease in the hydrogel swelling ratio [108, 109]. Burczak et al. demonstrated that increasing both the molecular weight and the concentration of PVA in PVA hydrogel membranes (prepared by chemical and radiation crosslinking methods) lead to a decrease in the number average molecular weight between crosslinks ($\overline{Mc}$) and the network mesh size (ξ), resulting in hydrogels with reduced water content and limited protein diffusion [137, 159].

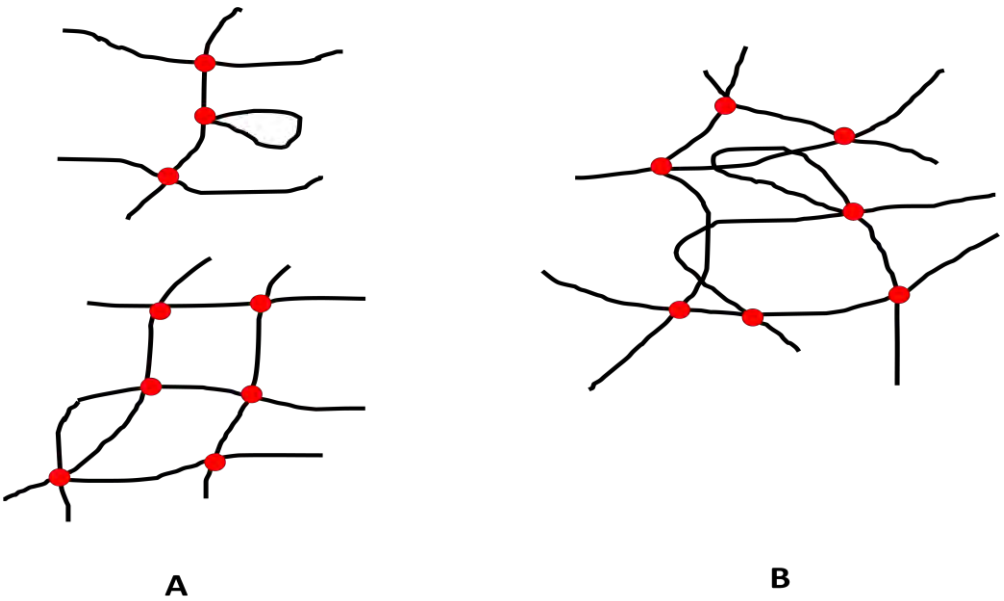

Figure 2.8: Illustration of intra-chain cyclisation (A) and inter-chain entanglement (B) that can occur during crosslinking of hydrogels

Functional group density

Increasing the number of functional groups per polymer chain usually results in an increase in the crosslinking density and a decrease in the swelling of hydrogels [109]. The functional group density can be modified by changing the number of functional groups per polymer chain or by changing the molecular weight of the polymer backbone [109]. In

multivinyl systems, where the starting polymers contain multiple pendant vinyl groups along the backbone, intramolecular cyclisation is always observed, resulting in a reduction in the crosslinking density of hydrogels [134, 217-219]. It was hypothesised that this cyclisation phenomena occurs locally because of the tendency of highly concentrated pendant vinyl groups to react together after the initiation of the radical chain reaction [134, 220]. Recently, Chong et al. tailored the permeability of poly (methacrylic acid) hydrogel capsules to different types of cargos via changing the degree of thiolation on the polymer backbone together with the number of deposited polymer layers [221]. Their system was proposed for application in microreactors. However, as previously mentioned in 2.4.1, using the variability in the functional group density as a tool for managing the permeability of PVA has not yet been deeply investigated for immunoisolation purposes and therefore this will be the focus in modulating the permeability of PVA photopolymerised hydrogels in this thesis.

Polymerisation conditions

Different factors related to the hydrogel crosslinking process have been modified in attempts to optimise hydrogel membrane permeability. These modifications include varying the contact time, the pH of the reaction and the solvent used. The effect of varying the contact time was mainly investigated in polyelectrolyte encapsulation systems. The most popular example of these systems is the alginate-poly (l-lysine) (alginate-PLL) capsule. It was found that increasing the contact time of anionic alginate beads with the cationic PLL solution above 5 minutes resulted in a significant decrease in membrane permeability [115, 116]. This finding was attributed to the increase in the number of ionic bonds between alginate and PLL and the subsequent increase of the membrane crosslinking density.

The effect of altering the pH of polymer solution has also been investigated in chitosan based systems. The permeability of chitosan-alginate microcapsules membrane decreased when chitosan solution with lower pH was used during the formation of microcapsules due to a decrease in the capsule pore size [222].

Inclusion of additives

The inclusion of additives in membrane processing has also been shown to be a convenient tool for controlling the permeability of hydrogels. However, its application is limited in cell encapsulation systems due to lack of biocompatibility and possible cytotoxic consequences of many of the additives tested. For example, sodium chloride, an ionic additive, has been investigated in polyelectrolyte systems and was found to enhance the permeability of chitosan-alginate microcapsule membrane [202]. This effect was attributed to the reduction of the effective cationic charge of chitosan and subsequent reduction in the interaction between chitosan and anionic core resulting in a decrease in the crosslinking density, strength and thickness of the membrane, which enhanced protein diffusion [202].

In addition, plasticisers have been extensively used as additives in polymeric films applied for coating pharmaceutical solid dosage forms because of their ability to control the permeability and mechanical properties of polymers by varying the mobility and flexibility of the polymer chains [223, 224]. It has been suggested that this class of additives can be used in cell encapsulation systems, specifically polyols such as polyethylene glycol, glycerol, and propylene glycol, due to their acceptable cell compatibility [202].

2.5.1.4 Incorporation of extracellular matrix

Natural extracellular matrix (ECM) is a mixture of proteins and polysaccharides which form a network within which cells reside. Recently, Lieleg and Ribbeck reviewed the selective diffusion properties of various *in vivo* biological hydrogels such as ECM, mucus and nuclear pore complexes [12]. ECM components have been found to modulate the permeability of molecules *in vivo* through different suggested mechanisms. Size exclusion has been suggested as the primary mechanism of permeability control in ECM and was demonstrated in reconstituted collagen gels *in vitro* [225, 226].

ECM-molecule interactions have also been reported in tumour ECM where hindered diffusion of large and small molecules was observed [227]. In addition, electrostatic interactions between negatively charged glycosaminoglycans such as heparan sulphate and positively charged proteins such as growth factors have been extensively studied in literature [228-230]. Moreover, enzymatic degradation of ECM components is an important process influencing matrix remodelling and shear mechanics of various organs [231-233]. This degradation could be another factor contributing to the passage of molecules through ECM matrix, since various studies investigated the effect of enzymatic degradation of biological polymers on modulating drug release for biomedical applications [234-237] .

From the reported findings on ECM permeability properties, it is hypothesised that inclusion of ECM components, whether intact or fragments, within synthetic hydrogel matrices impacts on their permeability characteristics by one or more of the abovementioned mechanisms.

In cell encapsulation systems, although there are currently growing attempts in mimicking the effects of physiological ECM by introducing variable synthetic and natural

ECM materials into synthetic polymers [9, 34, 141, 143], no reported studies to date have addressed the impact of ECM components properties on synthetic hydrogel characteristics, especially in terms of permeability. Consequently, the effect of ECM components on membrane permeability within a cell encapsulation system remains to be comprehensively investigated, which will be addressed in this thesis through *in vitro* permeability experiments.

2.6 Summary

Cell immunoisolation is a currently promising approach for successful cell-based therapy. However, several challenges in the development of immunoisolating membranes still exist, including the problem of reaching an optimum balance between the mechanical strength of the device and the mass transport properties of the membrane. Indeed, understanding and developing an encapsulation material with the appropriate balance between permselectivity of immunoisolating membrane and its ability to support cell survival represents a considerable gap in literature. The membrane material should allow for cell survival and differentiation while maintaining its physico-mechanical properties throughout the required implantation period.

Recently, research has started to focus on the incorporation of bioactive molecules and ECM components in cell encapsulating membranes. Despite successes in this approach, little is known at present regarding the effect of adding such molecules on membrane permeability and physical properties. This was the major focus of the current thesis and was addressed in the following chapters using UV photopolymerised PVA hydrogels, with tailored permeability, as a base membrane material.

First, Chapter 3 will examine the effect of a systematic increase in the functional group density of PVA polymer in determining its permselectivity. Dextrans of variable stokes radii will be examined as model solutes together with two different proteins, immunoglobulin G (IgG) and bovine serum albumin (BSA). The permeability parameters will be then compared to mesh size values estimated using two different common theories: equilibrium swelling and rubber elasticity.

The permselectivity characteristics of PVA hydrogels established in Chapter 3 will be then followed by covalent incorporation of ECM analogues into the PVA network in Chapter 4. Heparin as a glycosaminoglycan analogue and gelatin as protein-derived component of ECM will be incorporated at low percent. Their effects on the physico-mechanical characteristics and most importantly, the permeability performance of PVA will be examined

A more complex form of incorporated ECM analogues in synthetic PVA will be presented in Chapter 5, where both heparin and gelatin will be combined into the same PVA network. The effect of this combination on the ECM analogues functionalities as well as the base characteristics of PVA hydrogels will be examined.

Finally, the fabricated biosynthetic hydrogels will be assessed in Chapter 6 for their potential to improve the viability and metabolic activity of encapsulated pancreatic β cells over pure synthetic hydrogels as well as facilitating the release of their therapeutic products. These biosynthetic hydrogels in the current thesis are proposed as promising membrane materials for future islet encapsulation in curing type I diabetes

Chapter 3

Synthetic UV photopolymerised PVA hydrogels with variable functional group densities

3.1 INTRODUCTION

Modulation of the structural parameters of synthetic hydrogels allows optimisation of their permeability for different biomedical applications including drug delivery, soft and hard tissue engineering, cell encapsulation and bioartificial organs [137, 238-240]. One of the biggest determinants of the permeability and swelling behaviour of hydrogels is the crosslinking density, where modulating the crosslinking density impacts on the average mesh size which in turn influences the permeability [241]. Different factors that influence the crosslinking density have been investigated in both physically and chemically crosslinked hydrogels. These factors include molecular weight of the polymer backbone, concentration of the polymer, polymerisation conditions, inclusion of additives and functional group density [108, 109, 195, 199, 202].

The overall aim of this research was to study the impact of systematic variation in the functional group density on the physical characteristics and macromolecular permeability of UV photocrosslinked PVA hydrogels. This will provide the baseline understanding of macromolecular permeability of synthetic PVA hydrogels on which subsequent chapters will build to further understand the impact on permeability of covalent incorporation of biological molecules.

Various natural and synthetic monomers/polymers have been modified with vinyl residues in order to form chemically crosslinked hydrogels through photopolymerisation of the vinyl chemistry. The most common examples include poly (ethylene glycol) (PEG), poly (vinyl alcohol) (PVA), poly (ethylene oxide), polysaccharides, dextrans, collagen, gelatin, hyaluronic acid and heparin [123, 147, 242-247]. These polymers have been modified with different vinyl residues such as acrylic acid, methacrylic acid, methacrylamide, glycidyl acrylate and cinnamic acid [238, 248].

Vinyl-modified photocrosslinked hydrogels have been fabricated from either divinyl or multivinyl macromers. Divinyl macromers, such as PEG diacrylate macromers, result from the functionalisation of the groups located at the end of polymer backbone with vinyl residues [240]. The chain length, represented by the macromer molecular weight, usually determines the average molecular weight between crosslinks ($\overline{Mc}$). Multivinyl macromers, on the other hand, contain vinyl groups coupled to the pendant groups on the repeating units of the polymer backbone, such as the hydroxyl groups on PVA [134, 249]. Multivinyl derivatives of hydroxylated polymers such as those introduced by van Dijk-Wolthuis et al. [250] who fabricated dextran hydrogels by radical polymerisation of methacrylated dextran polymers. It was shown that the characteristics of multivinyl hydrogels, including $\overline{Mc}$ and mesh size, can be controlled by changing the crosslinking density, either through changing the molecular weight of the backbone or varying the degree of substitution. A schematic representation of a divinyl and multivinyl macromers is shown in Figure 3.1.

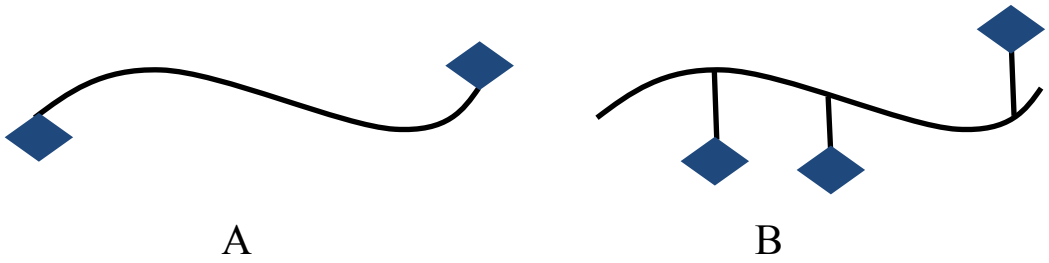

Figure 3.1: A schematic representation of divinyl (A) and multivinyl (B) macromers. The solid lines represent the polymer backbone and the diamond shapes represent the attached vinyl residues.

Although divinyl macromers such as PEG have been extensively used for various biomedical applications, multivinyl systems are thought to be more advantageous in terms of tailoring the network characteristics of the resulting hydrogels [134, 251]. Table 3.1

shows examples of non-degradable divinyl and multivinyl systems with varied hydrogel characteristics and macromolecular permeability/release behaviours. Both theoretical and experimental values of $\overline{Mc}$ are compared in table 3.1 to demonstrate the discrepancies between them. Theoretical $\overline{Mc}$ are predicted assuming 100% crosslinking efficiency of the double bonds and calculated based on the MW of the polymer and the number of FG/c. All experimental values of $\overline{Mc}$ in the table have been calculated from the equilibrium swelling theory after conducting swelling studies on the hydrogels.

Table 3.1: Examples of network characteristics and macromolecular permeability/release of non-degradable divinyl and multivinyl hydrogels.

	Polymer	FG/c	Theoretical $\overline{Mc}$ (g/mol)	Experimental $\overline{Mc}$ (g/mol)/ ζ (Å)	Permeability/ release	Ref
Divinyl	**PEG** MW 2K up to 10K % Macromer 10%	Di-MA	2K to 10 K	----------	**Release** Ovalbumin - SR 30Å Non-fickian diffusion in gels up to PEG MW 8K BSA - SR 35 Å No detectable release from any of the gels	[240]
	PEG MW 2K up to 20K % Macromer 10, 20,30%	Di-Acr	2K to 20K	$\overline{Mc}$ ~ 150 to 2 k ζ 14-70	**Permeability** BSA & IgG -restricted diffusion in all gels -D values below the detection limit	[195]
Multivinyl	**PVA** MW 70 K %Macromer 9%	MA FG/c 16-267	270- 4370	$\overline{Mc}$ 3400- 18000 ζ 70-380	**Release** BSA D = 0.65-3.02 x10^7 cm^2/s	[135]
	PVA MW 13-23 K % Macromer 20,30,50%	Acr FG/c 25	616	$\overline{Mc}$ 1155-5530	----------	[159]
	PVA MW 14 K % Macromer 10,15,20%	Acr FG/c 7	2000	$\overline{Mc}$ 762-1914 ζ 48-94	**Release** Dextran MW 20 kDa SR 33 Å D = 1.07-2.92 x10^7 cm^2/sec	[136]
	Dextran MW 16.7K % Macromer 10-50%	MA FG/100 repeat unit 4,9,18	4050 (for FG=4)	$\overline{Mc}$ 900 (for FG=4) ζ 40-100	**Release** BSA & IgG Restricted diffusion by increased FG/c	[252, 253]

Abbreviations: **MA**: Methacrylate, **Acr**: Acrylate, **FG/c**: functional groups per polymer chain, **D**: Diffusion coefficient

Discrepancies between the theoretical $\overline{Mc}$ values and those calculated experimentally were attributed to the presence of network imperfections such as intramolecular cyclisation and chain entanglements, which are common in radical chain photopolymerised systems, and are more pronounced at higher crosslinking densities [159, 252]. The release and permeability data reported in those studies demonstrated the ability to control the diffusion of macromolecules in divinyl and multivinyl systems via either changes in polymer backbone molecular weight, initial macromer concentration, functional group density or a combination of methods.

However, unexpected restriction of BSA was observed by Cruise et al. in PEG divinyl systems, where they fabricated hydrogels with a mesh size range up to 70 Å which was larger than the BSA Stokes radius, ~35 Å (Table 3.1) [195]. This observation demonstrates that the theoretical mesh size does not translate into predictable experimental behaviour. They attributed this behaviour to the crosslinked structure of PEG, where the crosslinking occurs only at the end of polymer chain, compared to multivinyl polymers where their crosslinks are distributed throughout the polymer backbone. They described each vinyl group of PEG as a node from which PEG chains originate and assumed that some of these chains do not contribute to the crosslinking process and remain unpolymerised, which explains some unexpected diffusion behaviour of macromolecules.

There are only a few reported studies to date regarding macromolecular diffusion within divinyl and multivinyl systems, and even less provide information about the correlation of diffusion to the network characteristics. Although permeability studies, as compared to release studies, provide a better understanding of the solute diffusion within hydrogel networks, there is very little reported research focusing on this area.

Therefore, this chapter focuses on the permeation of macromolecules within PVA multivinyl hydrogels of varying functional group densities. PVA was selected as the backbone polymer due to its high number of hydroxyl groups, which can be easily substituted with a range of types and amounts of functional groups [133, 147]. This flexibility is advantageous for adjusting network characteristics and consequently permeability. Therefore, the overall aim of this chapter was to tailor the permeability of PVA hydrogel via a systematic increase in the number of methacrylate functional groups introduced onto the polymer backbone. The specific aims were:

1. Understand the effect of a systematic increase in the methacrylate functional groups per PVA polymer chain (FG/c) on the swelling and mechanical properties using two common theories (equilibrium swelling and rubber elasticity)
2. Investigate the impact of PVA modifications on the permeability of solutes of different sizes and shapes

3.2 MATERIALS AND METHODS

3.2.1 Materials

Poly (vinyl alcohol) (PVA) (13-23 kDa, 98% hydrolysed) and 2-isocyanotoethylmethacrylate (ICEMA) (98% purity) were purchased from Sigma-Aldrich and used without further purification. The photoinitiator, 2-hydroxy-1-[4-(hydroxyethoxy) phenyl]-2-methyl-1-propanone (Irgacure 2959, Ciba Specialty Chemicals) was used as received. All solvents used were analytical grade including dimethyl sulfoxide (DMSO, Crown scientific), toluene (Ajax Finechem), Deuterium oxide (D_2O, Sigma-Aldrich) and Ethanol (absolute>99.5%, Sigma-Aldrich). Functionalised polymers were purified using 12 kDa molecular weight cutoff dialysis tubing (Sigma-Aldrich, Australia). Hydrogel disc moulds were made from silicone sheets (Silastic®Sheeting, reinforced medical grade silicone rubber, Dow Corning). All fluorescently labelled dextrans and proteins were purchased from Sigma-Aldrich.

3.2.2 Material Characterisation

Synthesis of PVA Methacrylate Macromers

PVA was functionalised with different number of methacrylate groups (7, 10, 14 and 20) via reaction with 2-isocyanotoethylmethacrylate (ICEMA), using a method described by Bryant et al. [148]. In details, PVA was dissolved at 60° C in dimethyl sulfoxide (DMSO) at a concentration of 10 wt% under nitrogen atmosphere. 2-ICEMA was then added to the PVA solution so that the number of moles of ICEMA was equal to that of PVA multiplied by the targeted number of methacrylate groups to be introduced to PVA chains. The reaction proceeded for 4 hours at 60° C, with stirring under nitrogen. The reaction was then stopped by precipitation in toluene. The precipitated macromer was

dissolved in distilled water and dialyzed in 12 kDa molecular weight cutoff dialysis tubing against milliQ water. The solution was then lyophilised to obtain dry macromer.

A schematic representation of the reaction is shown in Figure 3.2.

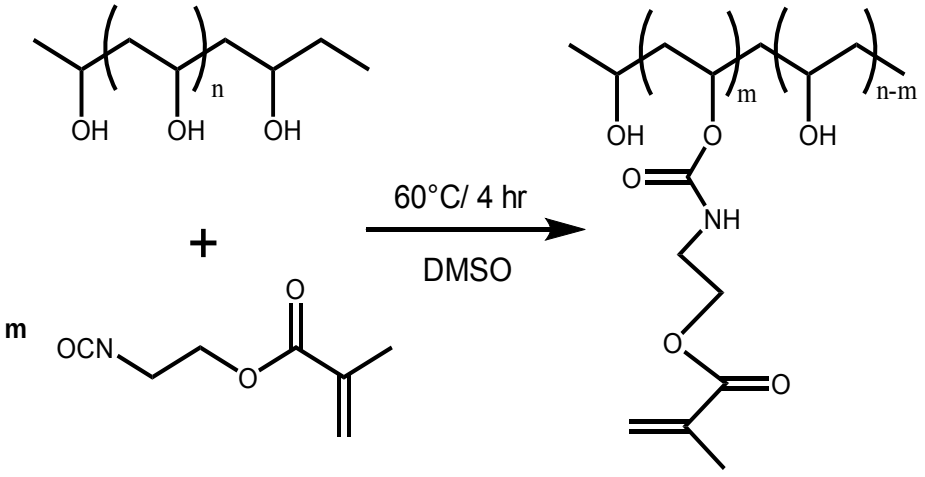

Figure 3.2: Schematic representation of PVA methacrylation via ICEMA reaction

Nuclear magnetic resonance (NMR) Characterisation of Methacrylated Macromers

The number of attached methacrylate groups was analysed using proton nuclear magnetic resonance (^{1}H NMR, 300 MHz Bruker Avance DPX-300 spectrometer). PVA macromers were dissolved in D_2O and the percent methacrylation was calculated by comparing the area under the peaks for the vinyl protons (δ = 6.1 and 5.7 ppm) to that of the PVA backbone protons (δ= 3.8-4.1 and 1.4-1.8 ppm). The number of methacrylate groups per chain was then calculated using the following formula (3.1):

$$\text{Crosslinker/chain} = \%\ \text{methacrylation} \times \frac{\text{MW polymer}}{\text{MW RU}} \qquad (3.1)$$

Where, MW is the molecular weight and RU is the repeating unit of the polymer.

Hydrogel Formation

Hydrogels were formed by radical chain polymerisation using UV light curing. PVA hydrogels were formed from 20 wt % macromers dissolved in water at 80 °C. All hydrogels were formulated with 0.05 wt % photoinitiator (Irgacure 2959). The solution was then cast into 1 mm thick molds and photopolymerised using UV light (Dymax, peaks 300-500 nm) at 30 mW/cm^2. Different photopolymerisation times from 1 to 10 min were tested to select the optimum UV exposure time required for complete photopolymerisation.

3.2.3 Physico-Mechanical Characterisation of Hydrogels

Swelling and Hydrogel Characterisation via Equilibrium Swelling Theory

The network structure of hydrogels was characterised by a swelling study followed by mass loss and mesh size analysis [109, 159]. Hydrogel discs (5 mm diameter x 1 mm thick) were weighed immediately after polymerisation (m_0). Three discs were lyophilised at t_0 to determine the actual macromer fraction. The rest of the samples were immersed in 40 ml phosphate buffer saline (PBS, pH 7.4) at 37°C. At 1 or 7 days the discs were removed, patted dry, and weighed (m_s). Dry weights (m_d) were then determined after lyophilisation of hydrogels. The initial dry weight of hydrogels (m_{id}) was calculated by equation (3.2):

$$m_{id} = m_0 \times \text{actual macromer fraction} \qquad (3.2)$$

Where: macromer fraction= m_d/m_0 at t=0

% sol fraction, which is the fraction of macromers not incorporated into the polymerisation, was extracted in the first 24 hours of swelling and calculated via equation (3.3) [159].

$$\% \text{ sol fraction} = m_{id} - m_d \,/ m_{id} \times 100 \quad (3.3)$$

Sol fraction values were used to select the UV exposure time to be used in all future studies. The volumetric swelling ratio (Q), which represents the amount of water in the gels, was then calculated from equation (3.4) [159].

$$Q = 1 + \frac{\rho_{polymer}}{\rho_{solvent}} (q\text{-}1) \quad (3.4)$$

Where;

$\rho_{polymer}$: Density of PVA macromer (1.2619 g/ml)

$\rho_{solvent}$: Density of PBS (~ 1.0 g/ml)

q: mass swelling ratio (m_s/m_d)

For the calculation of the mesh size (ξ), the average molecular weight between crosslinks ($\overline{Mc}$) was calculated using equation (3.5) developed by Peppas and Merrill [254] based on the equilibrium swelling theory and used to estimate the end-to end distance of unperturbed (solvent free) state $(\bar{r}_0^2)^{1/2}$ (Eqn 3.6) [190]. The mesh size and the crosslinking density (ρ_x) were then calculated (Eqn 3.7, 3.8) [159, 190].

$$\frac{1}{\overline{M_c}} = \frac{2}{\overline{M_n}} - \frac{(\bar{\upsilon}/V_1)\left[\ln(1-\upsilon_{2,s}) + \upsilon_{2,s} + \chi\upsilon_{2,s}^2\right]}{\upsilon_{2,r}\left[\left(\frac{\upsilon_{2,s}}{\upsilon_{2,r}}\right)^{\frac{1}{3}} - \frac{1}{2}\left(\frac{\upsilon_{2,s}}{\upsilon_{2,r}}\right)\right]} \quad (3.5)$$

$$(\bar{r}_0^2)^{1/2} = l\left(\frac{2\overline{M_c}}{M_r}\right)^{\frac{1}{2}} C_n^{1/2} \quad (3.6)$$

$$\xi = \upsilon_{2,s}^{-1/3} (\bar{r}_0^2)^{1/2} \quad (3.7)$$

$$\rho_x = \frac{1}{\bar{\upsilon}\,\overline{M_c}} \quad (3.8)$$

Where;

$\overline{Mn}$: Number average molecular weight in the absence of any crosslinking

$^{-}$: The specific volume of the polymer

V_1: The molar volume of the solvent

$_{2,s}$: The equilibrium polymer volume fraction

$_{2,r}$: The polymer volume fraction after crosslinking but before swelling

χ: The polymer solvent interaction (= 0.49 for PVA in water)

l: The bond length

M_r: Molecular weight of the repeating unit (= 44 for PVA)

C_n: The characteristic ratio (= 8.9 for PVA)

Mechanical Testing and Hydrogel Characterisation via Rubber Elasticity Theory

The mechanical properties of hydrogels were characterised using unconfined uniaxial compression testing at room temperature. Hydrogel discs (5 mm diameter x 1 mm thick) were immersed in phosphate buffer saline (PBS, pH 7.4) at 37 °C for 7 days. After 1 and 7 days, discs were removed from PBS and compressed at a strain rate of 100% strain min^{-1}, using an Instron 5543 mechanical tester. The slope of the linear regression of the stress-strain curve generated within 2-10% strain was used to calculate the compressive modulus (K). The determined compressive modulus was used to estimate the hydrogel network structure by calculating the average molecular weight between crosslinks ($\overline{Mc}$) through the rubber elasticity theory (Eqn3.9) [108, 191]. The mesh size and the crosslinking density (ρ_x) were then calculated as before (Eqn 3.7, 3.8).

$$\frac{1}{\overline{M_c}} = \frac{2}{\overline{M_n}} + \frac{3(1-2\nu)}{2(1+\nu)\rho_p RT}\frac{K}{(\nu_{2,s})^{1/3}} \qquad (3.9)$$

Where;

ν: Poisson's ratio

$\rho_{p:}$ Density of the polymer

R: Gas constant

T: The temperature of the gel

K: The compressive modulus

3.2.4 Permeability Performance of Hydrogels

Permeation Studies

The permeation studies were carried out using a side-by-side diffusion cell (Permegear, USA) at 37°C for 48 hrs. The hydrogel disc was placed between the two cells, with an effective area for permeation of 0.64 cm^2. Both cells had final volume of 3 ml. The solutes examined in the studies are shown in Table 3.2. The donor cell was filled with 0.1 mg/ml of the solute in phosphate buffer saline (PBS, pH 7.4) while the receptor cell was filled with PBS only. Both cells were stirred at a constant rate to reduce the boundary layer effect and solute aggregation. At predetermined time intervals (2, 4, 24, 28 and 48 hrs); a 100 µl sample was taken from the receptor cell and replaced with fresh PBS. After 48 hrs, the samples were analysed for fluorescence intensity using a microplate reader (Infinite® 200, Tecan). The concentrations were then calculated using a calibration curve from known solute concentrations. The solute permeability coefficient (P) was then calculated using equation (3.10) [255].

$$\ln\left(1-\frac{2C_t}{C_0}\right)=-\frac{2A}{V}\,Pt \qquad (3.10)$$

Where;

C_t: solute concentration in the receptor cell at time t

C_0: Initial solute concentration in the donor cell

A: effective area for permeation

V: cell volume

To determine P, a plot of (-V/2A) ln[1-2(ct/co)] versus time (t) was constructed with the slope representing the value of P. The values of P were then used to calculate the solute diffusion coefficient (D), using equation (3.11) [205, 255].

$$D = PL/K \tag{3.11}$$

Where;

L: equilibrium thickness of hydrogel membrane

K: Partition coefficient

Table 3.2: Molecular weights and Stokes radii (SR) of solutes used in the permeation studies

Solutes		**Average MW of solute (kDa)**	**Approximate Stokes radius of solute (Å)**
Dextrans	FITC-labelled	4	14
	Rh-labelled	20	33
	FITC-labelled	70	60
	FITC-labelled	500	145
Proteins	FITC-BSA	66	35
	FITC-IgG	150	55

Abbreviations: **FITC**: Fluorescein isothicyanate, **Rh**: Rhodamine, **BSA**: Bovine serum albumin, **IgG**: Immunoglobulin G

Partition Coefficient Determination

The partitioning of examined solutes between hydrogels and surrounding solution was determined by soaking hydrogels in solute solution of known concentration at 37°C. After reaching equilibrium (7 days), the remaining solution was analysed for fluorescence intensity using a microplate reader. The partition coefficient was calculated using the following equation (3.12) [256]:

$$K_d = \frac{C_m}{C_s} = \frac{V_{sol}\,(C_i - C_t)}{V_m\,C_t} \tag{3.12}$$

Where;

K_d: partition coefficient

C_m: concentration of solute in hydrogel

C_s: concentration of solute in solution

C_i: initial concentration of surrounding solution

C_t: solute concentration in solution at equilibrium

V_{sol}: volume of surrounding solution

V_m: volume of the hydrogel

3.2.5 Statistical Analysis

Statistical analysis of the results was conducted using general linear model (two-way ANOVA) with replication. Pairwise comparisons were also included using Tukey test. Analysis was performed with Minitab statistical software (Minitab Inc., version 15). All experiments were done with 3 replicates and the experiment was repeated 3times. Results are expressed as mean values together with their standard deviations in all tables and figures.

3.3 RESULTS

3.3.1 Material Characterisation and Hydrogel Formation

Macromers Synthesis and Characterisation

PVA was successfully functionalised with the theoretical number of methacrylate groups per chain of ~ 7, 10, 14 and 20 (± 0.2-0.3 SD) as determined by 1H-NMR (Figure 3.3 and Table 3.3). This modification allows for forming a crosslinked network by radical chain polymerisation [109, 136]. It has been previously shown that the ICEMA reaction is easily controlled with substitution efficiency ranging between 80-100% [148]. In this

study, the substitution efficiency was 95% for PVA-MA with 7 and 10 FG/c, and decreased to 90% when the substitution increased to 14 and 20 FG/c.

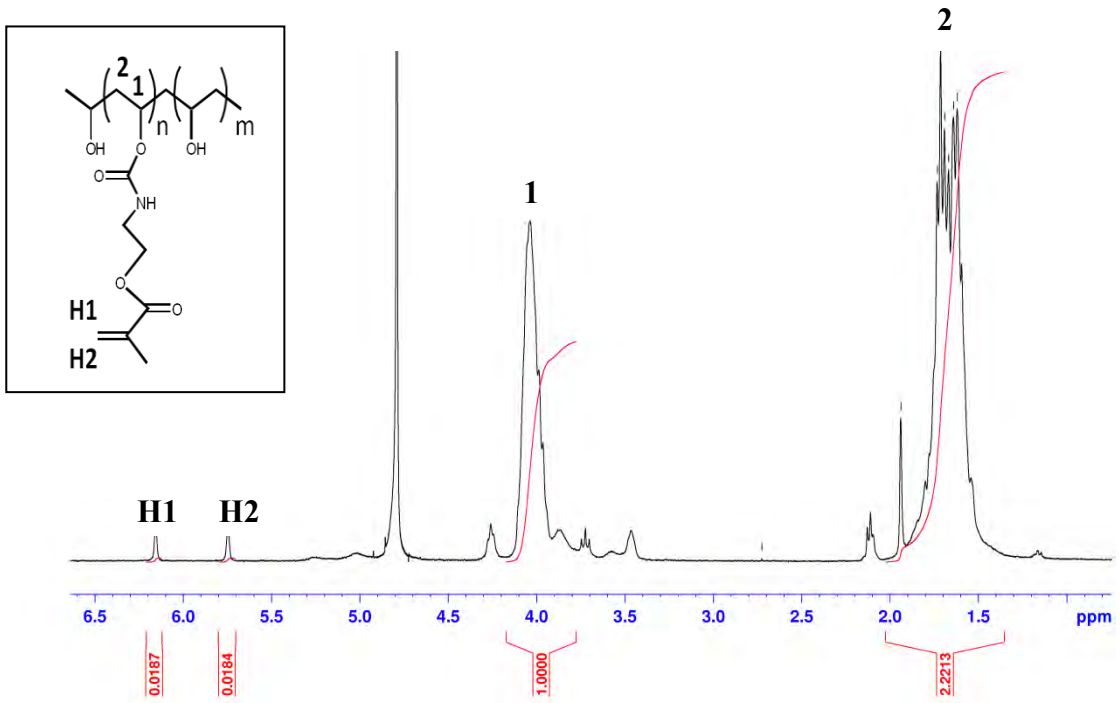

Figure 3.3: ^{1}H NMR of PVA-methacrylate with 7 FG/c in D2O. Integration values of the peaks are shown. Inset at the top: schematic numbering for the attached methacrylate group and the PVA backbone

Table 3.3: Theoretical MA FG/c versus experimental values measured using ^{1}H NMR

Theoretical MA FG/c	Experimental MA FG/c
7	6.7
10	10.3
14	13.8
20	19.8

Selection of Photopolymerisation Time

In order to select the shortest UV exposure time required for complete polymerisation of macromers, an initial swelling study for PVA hydrogels (7 FG/c) was conducted. Crosslinked hydrogels can contain a fraction of macromers that were not successfully incorporated into the final bulk hydrogel [257]. This fraction, known as the "sol fraction", is expected in these gels and has been previously observed in similar PVA hydrogels to be completely released after 24 hrs [109, 159, 258, 259]. Hence, optimal photopolymerisation time was related to the minimum % sol fraction released from hydrogels after 1 day incubation in PBS (pH 7.4). In addition, a constant % sol fraction with increased curing time indicates complete gelation.

PVA hydrogels (7 FG/c) were initially fabricated at different UV curing times (1, 3, 6 and 10 min). Figure 3.4 indicates that at different UV curing times, no significant difference was observed in % sol fraction released after 24 hrs immersion in PBS. The similarity in sol fraction values released at different UV curing times (1, 3, 6 and 10 min) proved that the quality of fabricated hydrogels was similar and consistent at all studied exposure times. In addition, the sol fraction values obtained were comparable to previously reported sol fraction percentages for PVA hydrogels in literature [136, 147, 148, 260]. However, for further hydrogel fabrication studies, 3 min UV curing time was selected to avoid the large variability in sol fraction values observed with UV curing time < 3 min (Fig 3.4).

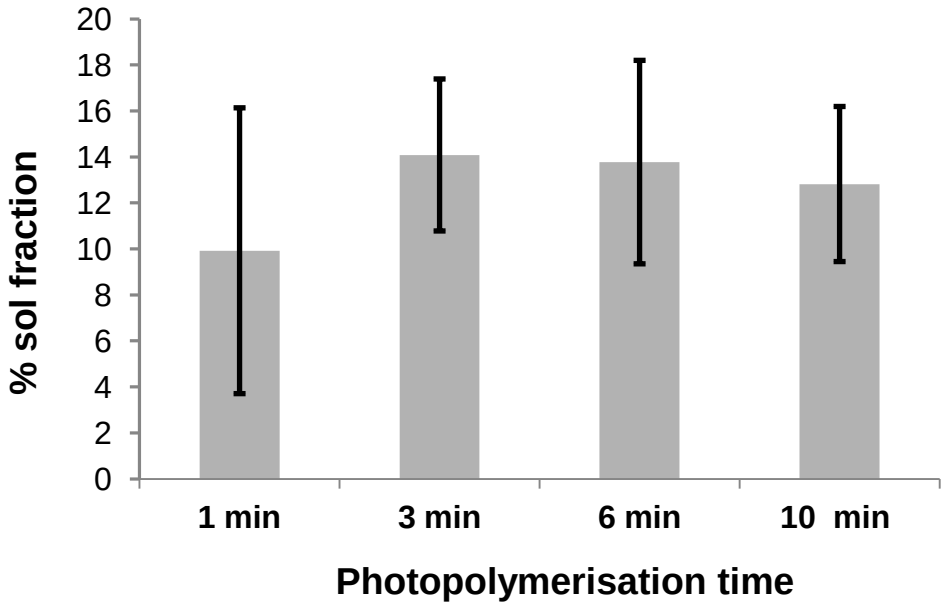

Figure 3.4: % Sol fraction released from PVA hydrogels (7 FG/c) at different UV curing times (min).

3.3.2 Physico-Mechanical Characterisation of Hydrogels

Swelling Properties and Hydrogel Characterisation via Equilibrium Swelling Theory

The effect of increasing FG/c on the swelling behaviour of hydrogels is shown in Table 3.4. As the FG/c was increased, the % sol fraction decreased ($p<0.05$). The sol fraction gives an indication of the effect of increasing the number of functional groups on the amount of polymer remaining in the hydrogel network. Lower % sol fraction values at higher FG/c is directly related to increased chain incorporation in more tightly crosslinked polymers, taking into consideration that the number of functional groups obtained from ^{1}H-NMR is an average [109].

It was observed that highly crosslinked hydrogels (14 and 20 FG/c) acquired negative % sol fraction values. This result indicates that the high number of methacrylate groups introduced resulted in the complete crosslinking of the functionalised macromers.

Although the values were expected to be zero, the negative values can be explained by either errors in measurements or the mass gain associated with the uptake of PBS salts, which are added to the final total mass after drying [109].

A significant decrease in volumetric swelling ratio (Q) was also observed when FG/c increased from 7 to 14 and 20. The Q values for all hydrogels remained constant up to 7 days of immersion in PBS.

Table 3.4: Sol fraction and volumetric swelling ratio of PVA hydrogels after 24 hours incubation in PBS.

FG/c of PVA macromers	Sol fraction (%)	Volumetric swelling ratio (Q)
7	14.08 ± 3.30	6.33 ± 0.14
10	3.68 ± 0.64	5.70 ± 0.19
14	-1.78 ± 2.27	4.44 ± 0.06
20	-4.34 ± 3.74	4.30 ± 0.13

Mechanical Properties and Hydrogel Characterisation via Rubber Elasticity Theory

All hydrogels were tested in compression to evaluate the effect of increasing FG/c on the mechanical performance of hydrogels as well as determining the mesh size of hydrogel network via the rubber elasticity theory. The compressive modulus of the 10, 14 and 20 FG/c gels were similar to each other, and the 7 FG/c gels ($p<0.05$) were significantly lower than all other gels (Fig. 3.5). Hydrogels retained their modulus up to 7 days, showing that all physico-mechanical properties of hydrogels could be determined after 24 hrs swelling study with no variations over time.

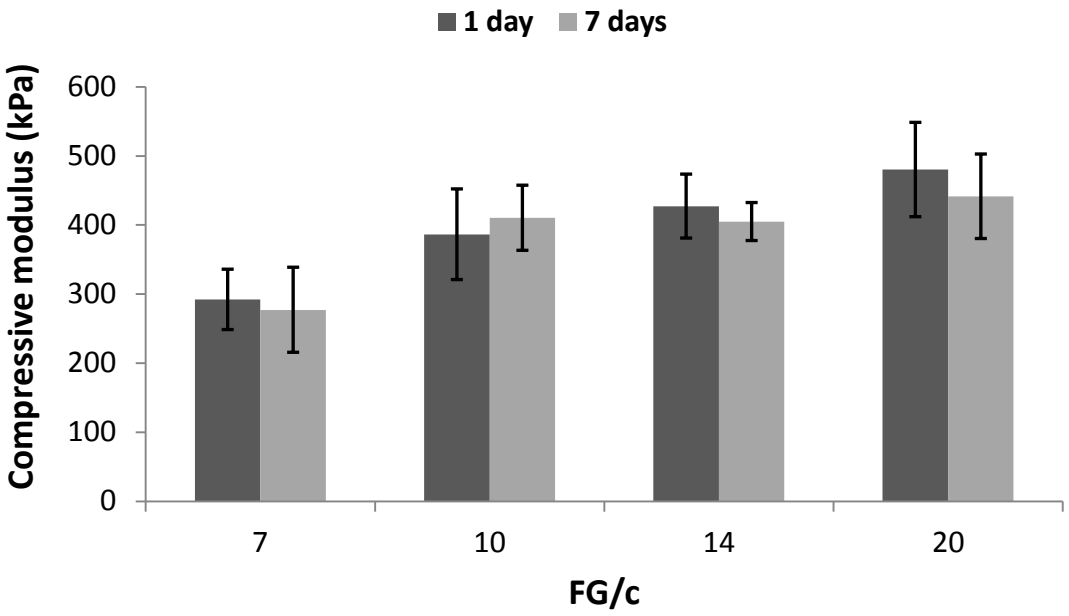

Figure 3.5: The compressive modulus of PVA hydrogels after incubation in PBS (pH 7.4) for 24 hrs and 7 days.

Table 3.5 shows the calculated values of the average molecular weight between crosslinks ($\overline{Mc}$) and the average mesh sizes (ζ) of all hydrogels through using the experimental data (Fig. 3.5 and Table 3.4) in two commonly used theories, equilibrium swelling and rubber elasticity. The experimentally calculated $\overline{Mc}$ values are also compared to theoretical values based on the number of FG/c and are presented in Figure 3.6. Overall, $\overline{Mc}$ and ζ were shown to decrease by increasing FG/c of PVA hydrogels in all methods of calculation (i.e., both theories and theoretical calculations). However, there were large differences between the values obtained from all three methods. Theoretically, increasing the FG/c should result in a significant change in the $\overline{Mc}$ (e.g., increasing from 10 to 20 FG/c should halve the $\overline{Mc}$). Neither of the two theories demonstrated this level of $\overline{Mc}$ reduction, however the equilibrium swelling calculation were much closer to the

theoretical, and did demonstrate significant changes as the FG/c increased (Fig.3.6 A). The rubber elasticity theory did not show an appreciable change in $\overline{Mc}$ values in response to increased FG/c (Fig. 3.6 B), and were also significantly higher than the theoretical values.

Table 3.5: Comparison of the parameters of PVA hydrogels derived from both the equilibrium swelling and the rubber elasticity theories

FG/c of PVA	Theoretical $\overline{Mc}$	Experimental $\overline{Mc}$ (g/mol)		Average mesh size ζ (Å)	
		Equilibrium swelling	Rubber elasticity	Equilibrium swelling	Rubber elasticity
7	2286	2726	6878	95	150
10	1600	2280	6565	83	141
14	1143	1505	6544	62	130
20	800	1448	6420	61	128

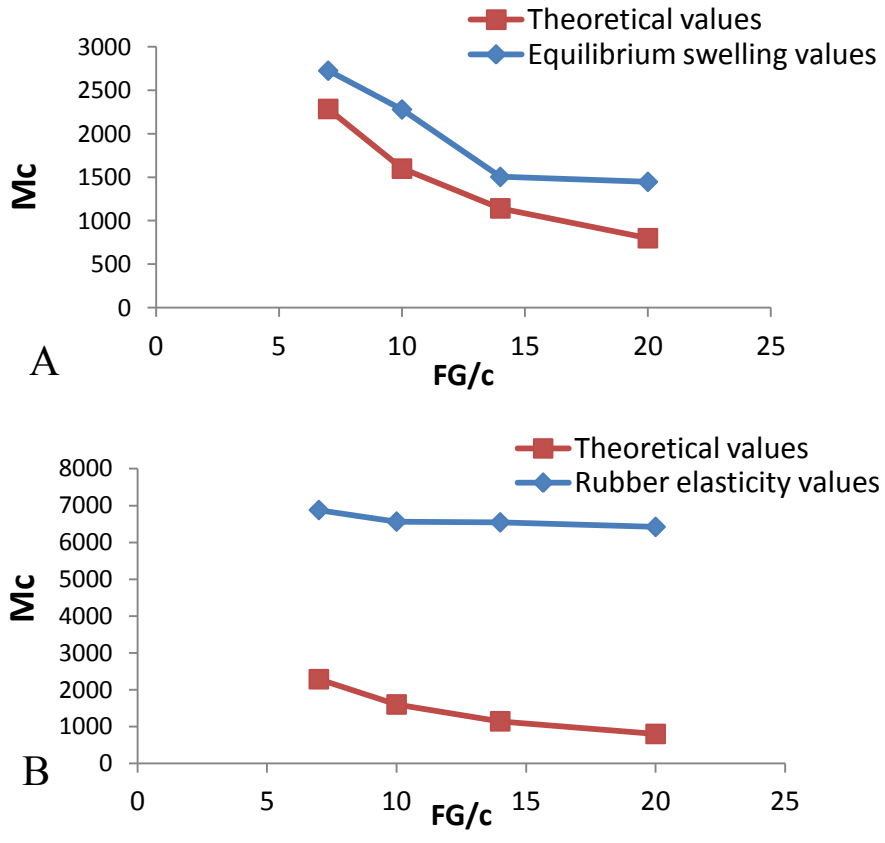

Figure 3.6: Theoretical average number of molecular weight between crosslinks ($\overline{Mc}$) values versus experimental values from (A) equilibrium swelling theory and (B) rubber elasticity theory.

3.3.3 Permeability Performance of Hydrogels

Table 3.6 shows the permeability of a range of dextrans through the different hydrogels. For all dextran/hydrogel combinations, the partition coefficient (K) values were approximately 1, and the diffusion coefficients (D) were significantly lower than their diffusivity in water (D_w), suggesting that the hydrogel network did interfere with their diffusion pathway. From calculated D values, it was observed that diffusion of large dextrans (60 and 145 Å) was limited by increasing FG/c, with complete blockage of 145 Å dextran with 14 FG/c PVA gels. On the other hand, the passage of smaller solutes (14 and 33 Å) was maintained, although a decrease in the diffusion was observed.

Table 3.6: Permeability parameters of dextrans in PVA hydrogels and their diffusivities in water.

Approximate Stokes radius of dextran (Å)	Partition coefficient K	Diffusion coefficients			Diffusivity in water D_W*10^8 (cm^2/sec) [206]
		FG/c of PVA	$D*10^8$ (cm^2/sec)	% of D_W	
14	0.98 ±0.13	7	18.79 ± 1.90	12.61± 1.27	149.00
		10	11.51 ± 0.08	7.72 ± 0.07	
		14	9.48 ± 0.51	6.36 ± 0.33	
		20	8.80 ± 1.82	5.91 ± 1.21	
33	1.03 ±0.06	7	6.46 ± 0.91	8.17 ± 1.14	79.10
		10	3.39 ± 0.28	4.28 ± 0.38	
		14	4.69 ± 0.31	5.93 ± 0.39	
		20	4.52 ± 0.87	5.71 ± 1.14	
60	0.98 ±0.13	7	0.34 ± 0.62	0.82 ± 1.94	41.20
		10	0.17 ± 0.21	0.41 ± 0.48	
		14	0.16 ± 0.08	0.39 ± 0.24	
		20	0.08 ± 0.19	0.19 ± 0.48	
145	0.98 ±0.13	7	0.10 ± 0.12	0.59 ± 0.59	17.00
		10	0.06 ± 0.09	0.35 ± 0.57	
		14	0.00 ± 0.00	0.00 ± 0.00	
		20	……	……	

The partition coefficient (K) values of both BSA and IgG were approximately 1 (Table 3.7). The D values of both proteins in all hydrogels were far below their diffusivities in water (shown from % of D_W, Table 3.6), similar to dextrans. Comparing the diffusion of BSA and IgG, it was found that increasing FG/c didn't significantly change the diffusion of BSA through PVA hydrogels ($p>0.05$) (Fig. 3.7). On the contrary, diffusion of IgG was found to be significantly limited by increasing FG/c from 7 to 20 ($p<0.05$) with no significant difference between 7, 10 and 14 FG/c ($p>0.05$).

Table 3.7: Partition coefficients, diffusivity in water for BSA and IgG proteins and their % of D_W in all PVA FG/c hydrogels.

Protein	FG/c of PVA	Partition coefficient K	% of D_W	Diffusivity in water D_W *10^8 (cm^2/sec) [195]
FITC-BSA	7	0.98±0.34	6.88 ± 0.32	90.60
	10		3.91 ± 1.51	
	14		4.84 ± 1.42	
	20		4.65 ± 0.49	
FITC-IgG	7	1.06±0.40	5.54 ± 0.29	62.50
	10		4.53 ± 0.43	
	14		3.27 ± 0.70	
	20		1.76 ± 0.14	

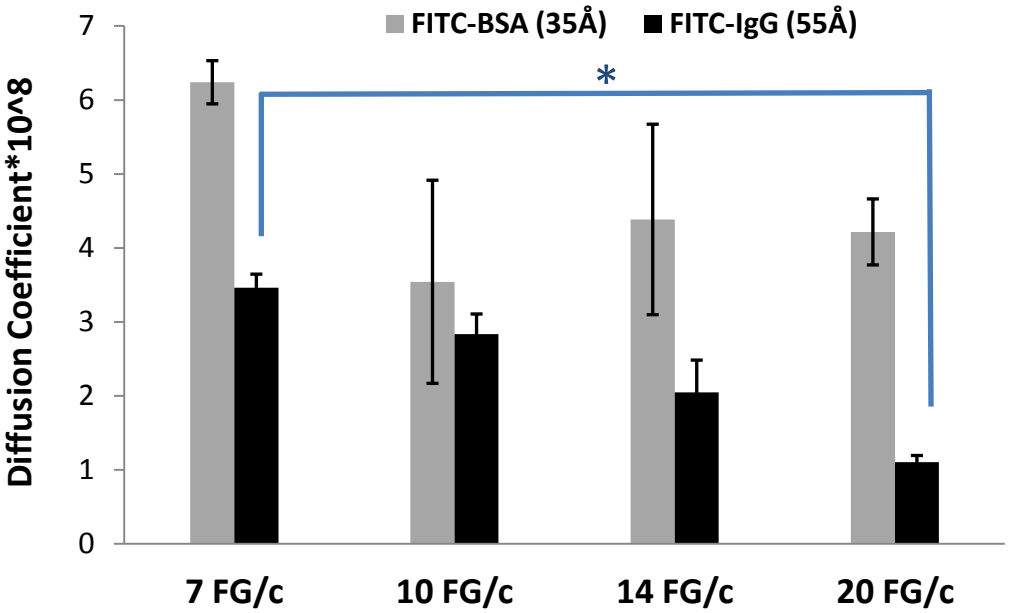

Figure 3.7: Diffusion coefficient values of FITC-BSA and FITC-IgG through PVA hydrogels (* $P < 0.05$).

A comparison of the diffusion profiles of both dextrans and proteins having equivalent Stokes radii is shown in Figure 3.8. No statistically significant difference ($p > 0.05$) was observed between the diffusion of BSA and that of its equivalent dextran (Stokes radius 33 Å). Conversely, the diffusion coefficient values of IgG were far greater than those of the corresponding dextran (Stokes radius 60 Å) ($p < 0.05$).

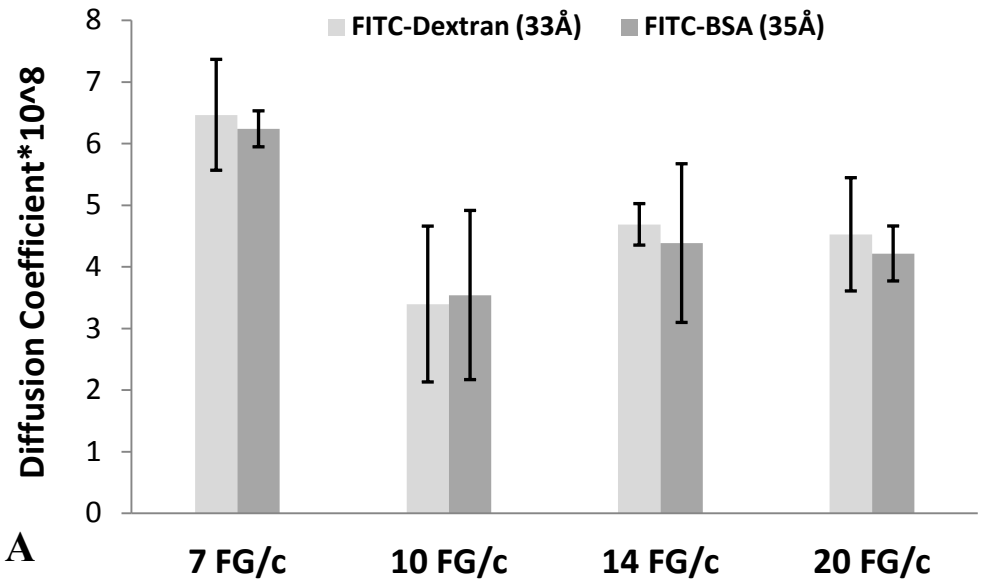

A

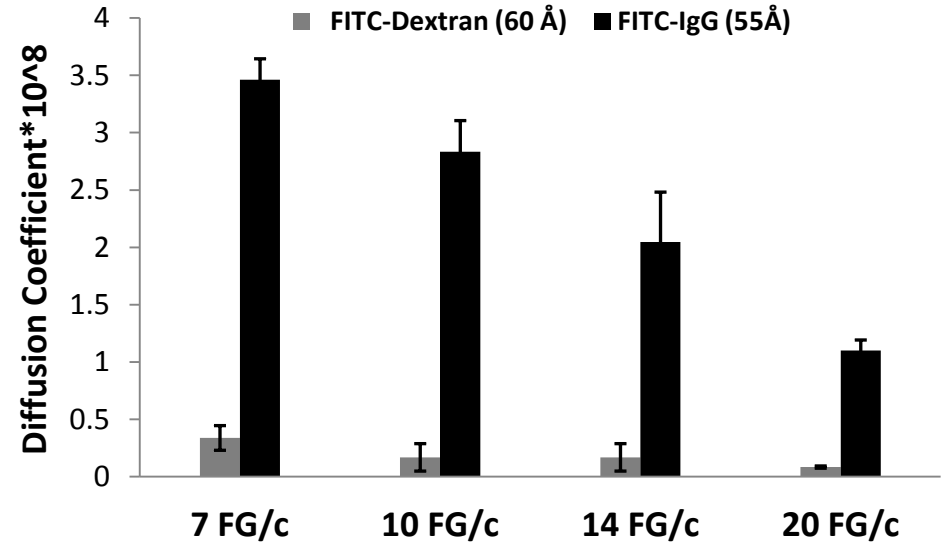

B

Figure 3.8: Diffusion coefficient values of BSA (A) and IgG (B) through PVA hydrogels compared to those of dextrans with approximately similar Stokes radii.

3.4 DISCUSSION

In this chapter, non-degradable PVA hydrogels were fabricated in which the number of functional groups per chain was increased from 7 to 20. The systematic increase in FG/c directly impacted the swelling and mechanics of the hydrogels. The physical characteristics obtained from hydrogels with different FG/c appeared to be more accurately estimated via the equilibrium swelling theory, as demonstrated by the correlation of the data to the permeability performance of solutes in a range of sizes and shapes.

Hydrogel swelling in aqueous environments influences the overall mass transport through the network. Specifically, the volume fraction of water present within the hydrogel network determines the partitioning and diffusion of solutes through the hydrogel [153]. Hence, the equilibrium swelling theory is often applied to characterise the network structure of hydrogels [136, 147]. Volumetric swelling ratio (Q) results obtained for our hydrogels compared well with previously reported findings, where a significant decrease in Q values occurred after increasing the number of functional groups per PVA chain [109].

It has been established that the swelling behaviour of hydrogels is directly related to their network structure, where increasing the number of functional group per polymer chain usually results in increasing the crosslinking density which reduces the mesh size, and subsequently decreases the swelling [109, 166]. This trend was observed in this study when increasing the FG/c from 7 up to 14 and 20. However, increasing FG/c from 14 to 20 didn't significantly change the swelling of the formed hydrogels. This finding could be due to increased intramolecular cyclisation formation at higher crosslinking densities. Cyclisation is always usually observed in multivinyl systems, where the starting polymers contain multiple pendant vinyl groups along the backbone. It was hypothesised that this cyclisation phenomena occurs more frequently in the higher FG/c gels due to the increased

local concentration of pendant vinyl groups that are attached to the same backbone polymer chain [134, 220].

Another hydrogel characteristic that was expected to be affected by the different number of FG/c was the mechanical strength. Increasing the number of crosslinks in a hydrogel network is known to increase the gel's stiffness and resistance to deformation [109]. As expected, an increase in the number of FG/c increased the compressive modulus of hydrogels. The mechanical data were directly correlated to the swelling results, where hydrogels with lower swelling showed higher modulus values. These findings are consistent with previous studies where increasing the crosslinking density resulted in reduced swelling and increased mechanical strength of hydrogels [108, 109, 148, 159, 261].

Putting the swelling and modulus results into the most commonly used theories for determination of mesh size (equilibrium swelling and rubber elasticity) demonstrated the same basic result of reduced average mesh size with increased FG/c. However, the absolute values obtained from each theory were significantly different. The difference in calculated $\overline{Mc}$ values from both theories have been previously observed in highly crosslinked networks where chain defects such as cyclisation, entanglements and free chain ends are more pronounced [184]. Although rubber elasticity theory (Eqn 3.9) accounts for the chain ends, other network imperfections were not included which explains the higher $\overline{Mc}$ and mesh size values obtained via mechanical tests and the large deviation from theoretical values. Moreover, the stress applied during mechanical testing may interfere with the network structure resulting in disentanglement of polymer chains [192, 262, 263]. Those possible modifications in the polymer network give less reliability to this method in predicting the hydrogel network structure for multivinyl systems. Due to the dissimilarities

in values from the two theories, permeability assessments of hydrogel networks were carried out to provide insight into which theory to rely on in determining the average mesh size for PVA hydrogels.

The permeability of hydrogels depends strongly on the chemistry of the polymeric material as well as the network structure of the hydrogels. In this study, the effect of increasing the number of FG/c on different solutes was investigated. Different MW dextrans were chosen to understand the effect of PVA hydrogel network characteristics on permeability in the absence of any possible interaction between the solute and PVA, which could have hindered the diffusion [255]. This lack of interaction was confirmed through the partition coefficient (K) values which were approximately 1. K values are known to be good indicator for the presence or absence of interactions between the diffusing solute and hydrogel. Low values of K (< 1), e.g. 0.1 – 0.5, indicate a repulsive force between the solute and the hydrogel matrix whereas K values >1 (reaching in some examples a range of hundreds and thousands) indicate strong hydrogel-solute interactions [203, 205, 255, 264, 265].

Comparing mesh size values derived from both theories with dextran diffusion results, it appears that mesh sizes calculated using the swelling theory relate more closely to the obtained diffusion coefficient values. The diffusion of dextran (SR=60 Å) was significantly limited by increasing the FG/c from 7 to 20, corresponding to decreased mesh size from 95 Å to 60 Å (equilibrium swelling theory) or from 150 Å to 129 Å (rubber elasticity theory) (Table 3.5). Large mesh size values from rubber elasticity theory do not correlate with the significant restrained diffusion of dextran (SR=60 Å), which should have permeated freely through both mesh sizes. Moreover, the diffusion of the largest dextran (SR=145Å) was totally blocked by 14 FG/c hydrogels having average mesh size 62 Å

(based on the swelling theory) or 130 Å (rubber elasticity theory) (Table 3.5). The complete exclusion size 145 Å appears more reasonable for a hydrogel of average mesh size 62 Å. Consequently, it was concluded that mesh size values derived from the equilibrium swelling theory are more reliable than those derived from rubber elasticity.

While dextrans are excellent model solutes due to their relative similarity with increased MW and general lack of interaction, protein permeability is crucial for the application of these hydrogels. Two proteins of different sizes, BSA (SR=35 Å) and IgG (SR =55 Å), were selected for permeability studies. For cell encapsulation applications, BSA represents a cell metabolite that would be required to diffuse out of the hydrogels, while IgG represents the smallest harmful antibody of the host immune system which needs to be excluded. Partition coefficient values were determined for both proteins and were approximately equal to 1, indicating lack of interaction with PVA polymer (Table 3.7). Similar values were observed for BSA studied in PVA hydrogels crosslinked with glutaraldehyde [204].

The diffusion of the larger protein (IgG) was restricted in all hydrogels compared to BSA and a significant decrease in D was observed by increasing FG/c from 7 to 20. This significant diffusion restriction by 20 FG/c was attributed to the similarity between the 60 Å average mesh size of 20 FG/c gels and the Stokes radius of IgG (55 Å). Conversely, the diffusion of BSA remained nearly constant in all gels due to the size of BSA (35 Å) being well below the mesh size range (~ 60-100 Å) of all hydrogels examined. These findings further substantiate the accuracy of equilibrium swelling results over those obtained from the rubber elasticity theory.

Despite the significant limitation of IgG obtained with the highly crosslinked hydrogels, complete blockage of this molecule has not been achieved by decreasing the

mesh size down to 60 Å. This diffusion, although restrained, can be explained by the average value of mesh size calculated and the difficulties in measuring the actual distribution of mesh sizes in hydrogels [136, 137]. Previous studies emphasised that highly crosslinked PVA hydrogels that would be able to completely block IgG diffusion would also restrain the free diffusion of essential nutrients to encapsulated cells [137, 266]. In addition, diffusion of IgG alone doesn't destroy encapsulated cells unless complement proteins pass through the membrane and maintain their activity to initiate cell lysis process [266-268].

Although an ideal immunoisolating membrane is expected to completely exclude the passage of complement proteins and antibodies, such a system has not yet, to our knowledge, been achieved. Hence, reported studies to date focused on the restriction of antibodies diffusion and inactivation of complement proteins. Iwata et al. demonstrated the high instability of different classes of complement proteins, with the feasibility to accelerate their inactivation through retardation of permeation or consuming their cytolytic activity using immunoisolating membranes [266]. Compared to other reported hydrogel immunoprotecting systems, PVA hydrogels with high crosslinking density showed better permselectivity to IgG (Table 3.8). Although it has been reported that poly (acrylic acid)/PVA/alginate membranes blocked IgG molecules, those membranes were fabricated under harsh thermal conditions, restricting successful cell encapsulation. On the contrary, it appears that diffusion of BSA molecule through PVA hydrogels (20 FG/c) was approximately similar to other studies (Table 3.8).

Table 3.8: Permeability parameters of various immunoisolating membranes compared to fabricated PVA hydrogels (20 FG/c)

Protein	Diffusion Coefficient D (cm^2/sec)		Ref
	PVA hydrogels (20 FG/c)	**Other hydrogel immunoisolating systems**	
IgG	**1.10 E-08**	**5.62 E-08** PVA/ PES -PVA hydrogel incorporated into microporous PES filter. -Chemical crosslinking using GA in acidic conditions.	[269]
		~ 0.2 E-08 PVA -Chemically crosslinked using GA gradient across membrane thickness -Mesh size asymmetry for higher selectivity.	[270]
		~1 E-07 PVA -Crosslinked by radiation or chemically using GA - Mesh size range: ~ 100-400 Å	[137]
		(1 E-07 range) Commercial filters/hydrogel composites -Composite of agarose hydrogel and Nuclepore filter or XM-50 ultrafiltre. -Filter range: 10.0, 2.0, 0.2, and 0.015 µm pore diameter	[96]
		Permeable (values not specified) AN Hydrogel-based hollow fibers -Anionic polyelectrolyte hydrogel from acrylonitrile copolymer formed by phase inversion -MWCO of hollow fiber system: 150-170 kDa	[62]
		Reduced permeability (values not specified) Alginate/cellulose/poly(methylene-co-guanidine) -Multicomponent microcapsule formed by polyelectrolyte complexation	[201]
		Not permeable PAA/PVA/alginate -PAA/PVA mixture crosslinked by thermal treatment under vacuum followed by coating with alginate and gelation by calcium chloride. - Pore size range: 50-100 µm -MWCO: 100 kDa	[40]

BSA/ Albumin of ~ similar MW	**4.21E-08**	**4.53 E-08** PVA/ PES -PVA hydrogel incorporated into microporous PES filter. -Chemical crosslinking using GA in acidic conditions.	[269]
		~1 E-07 PVA -Crosslinked by radiation or chemically using GA - Mesh size range: ~ 100-400 Å	[137]
		(1 E-06 to1 E-07 range) Commercial filters/hydrogel composites -Composite of agarose hydrogel and Nuclepore filter or XM-50 ultrafiltre. -Filter range: 10.0, 2.0, 0.2, 0.015 µm pore diameter	[96]
		0.8 E-09 PEG hydrogels -Photocrosslinked by UV light - Varying MW of PEG altered the hydrogel crosslinking density	[240]
		Permeable (values not specified) AN Hydrogel-based hollow fibers -Anionic polyelectrolyte hydrogel from acrylonitrile copolymer formed by phase inversion -MWCO of hollow fiber system: 150-170 kDa	[62]

Abbreviations: **PES**: Poly (ether sulphone), **GA**: Glutaraldehyde, **PEG**: Poly (ethylene glycol), **AN**: Acrylonitrile

After investigating the permeability performance of PVA hydrogels for both dextrans and proteins, the diffusion of dextrans versus proteins of comparable Stokes radii was examined. As was highlighted in Chapter 2, the molecular weight (MW) is a misleading parameter in comparing diffusing solutes through a membrane. This is due to variability in size, shape and relative charge of solutes having identical MW, which often affects their diffusion behaviour. For that reason, all studied solutes were selected based on the size represented by the Stokes radius, which was correlated to the average mesh size of fabricated hydrogels. It should be noted that these Stokes radii are theoretical values and

thus the molecule shape should be also considered. Dextrans are known for their deformable coiled shape while most proteins have compact globular structure [271, 272]. Interestingly, IgG showed significantly higher diffusion values than dextran of similar size (60Å). This result was not expected, due to the known flexibility of dextrans over proteins, especially as the partition coefficient values of both molecules were nearly the same. However, this difference in diffusion was not shown with BSA and its corresponding dextran (33 Å) (Fig.3.8).

Further studies (outside the scope of this thesis) are required to understand the difference in diffusion behaviour between different proteins and dextrans of similar Stokes radii. However, the fact that the shape of the molecules influences their diffusion is believed to be the main reason. Table 3.9 demonstrates the three dimensional structure of dextran versus both examined proteins. It has been stated that the stem of the IgG Y shape molecule, called the hinge region, allows for segmental flexibility of the antibody [273]. This flexibility could have been the reason of its unexpected diffusion through PVA hydorgels compared to dextran. On the other side, dextran molecule is a flexible coiled structure. However, it was more similar in behaviour to BSA protein, known to have compact ellipsoid shape.

Table 3.9: Three-dimensional structural shapes of dextran, BSA and IgG [274-277]

Dextran	**BSA**	**IgG**
Flexible random coil	Prolate ellipsoid	Tetramer, Y-like shape
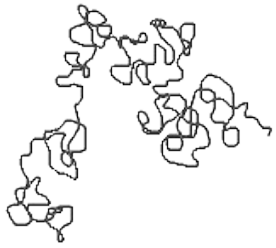	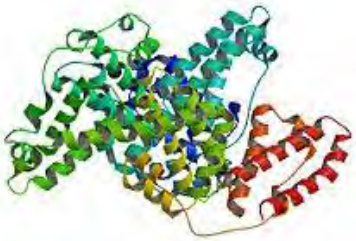	

3.5 CONCLUSION

The current chapter showed the feasibility of modifying a PVA polymer backbone with a high number of methacrylate functional groups (up to 20 FG/c) while maintaining high percent reaction efficiency. Increasing the functional group density allowed for tailoring the physical and mechanical characteristics of PVA photopolymerised hydrogels, where a range of swelling, mesh sizes and modulii were achieved. The mesh size influenced the permeability performance of PVA hydrogels, resulting in a range of diffusion coefficients for the different solutes. The permeability results highlighted the importance of considering both the size and shape when comparing diffusing solutes through membranes. Regarding hydrogel permselectivity, increasing FG/c up to 20 approached the required permselectivity, in which gels were able to significantly retard the diffusion of IgG. However, further controlling methods such as multilayered membranes are required to achieve complete exclusion of IgG. One of the most important findings of this chapter was that the permeability study proved the reliability of applying the

equilibrium swelling theory for hydrogel mesh size estimation over the rubber elasticity theory.

This chapter demonstrated that permeability can be varied by varying the functional group density on PVA backbones. This capacity to tailor permeability appears to be suitable for cell immunoisolation purposes. However, since it has also been highlighted that successful immunoisolating systems require the presence of biological cues to ensure the survival of encapsulated cells during the implantation period, what is not known is what may occur in regards to permeability when those biological molecules are added to the currently controlled system. Therefore, the following chapter will investigate the effect of biological molecule incorporation on the base PVA hydrogel in terms of physico-mechanical and permselectivity characteristics.

Chapter 4

Covalent incorporation of ECM analogues into PVA hydrogels and the resulting effects on permeability

4.1 INTRODUCTION

In the biomedical field, the ability to precisely control the network characteristics and mechanics of synthetic hydrogels has resulted in them being proposed as ideal materials to mimic the physical support of a natural extracellular matrix (ECM) network[11, 127, 278, 279]. However, synthetic hydrogels lack the biological cues that are characteristic of ECM and are essential for promoting cell function. It is now understood that successful cell encapsulation devices should incorporate ECM components to serve as a biofunctional microenvironment for the encapsulated cells [9]. Although natural ECM has been found to modulate the permeability of different molecules *in vivo* [12], the effect of adding ECM components on hydrogel permeability within a cell encapsulation system remains to be comprehensively investigated. Consequently, the current research focuses on the effect of incorporating two different ECM analogues on the PVA network characteristics and permeability.

Different ECM components have been included in hydrogels, whether alone or combined with other natural and synthetic polymers, for various biomedical applications. Table 4.1 shows examples of ECM protein and glycosaminoglycan-based hydrogels, highlighting the effect of ECM components on hydrogel physico-mechanical characteristics and release behaviour.

Table 4.1: Network characteristics and release behaviour of ECM-based hydrogels for various biomedical applications

ECM category	Hydrogel	Crosslinking method	Release behaviour	Network characteristics	Applications	Ref
Proteins	HA, dextran, CMC/Gelatin	In situ through hydrazone bonds between aldehyde modified macromers	Albumin Presence of gelatin controlled release > 3 weeks	Presence of Gelatin ↓ swelling	Controlled release of therapeutic proteins	[280]
	Gelatin	GA	bFGF Only 40% released after 1 day	……..	Sustained release of growth factors	[281]
	Gelatin	GA	bFGF Release dependant on enzymatic degradation of gelatin	……..	Angiogenesis	[282]
	Collagen-PEG	In situ gelation of solutions	……..	↑ collagen concentration ↑compressive modulus	Treatment of tissue defects	[283]
	Gelatin microgels (negatively charged)	Natural crosslinker (Genipin)	Doxorubicin Release controlled by salt concentration Rhodamine B Release controlled by pH	……..	Drug delivery carrier	[284]
	Gelatin-PVA	γ-irradiation	……..	↑gelatin concentration ↑ swelling ↓ tensile strength	3D cell culture	[285]
	PEG:Gelatin	UV crosslinking of methacrylate macromers	……..	↑gelatin concentration ↓ swelling ↑compressive modulus	3 D cell culture	[286]
	PEGylated fibrin	Thrombin exposure	TGF-β1 Release (up to 10 days) dependant on enzymatic degradation	……..	Stabilise neovascularis-ation in ischemic tissues	[287]

Glycosaminoglycans	PEG-heparin	Chemical via crosslinking hydrazide derived heparin with bis-reactive PEG	VEGF Controlled release over 3 weeks	……..	angiogenesis	[288]
	HA-heparin	Thiol-based crosslinking	BMP Heparin sustained the release for up to 28 days	……..	Bone tissue engineering	[289]
	Alginate-heparin	UV crosslinking of methacrylate macromers	BMP Heparin sustained the release for 3 weeks	Heparin ↑swelling	Sustained release of therapeutic proteins	[290]
	PEG-heparin	Michael-type addition	HGF Only 40% released after 30 days	……..	Encapsulation and cultivation of primary hepatocytes	[291]
	Gelatin-CS	Chemically crosslinked with EDC and NHS	Lysozyme ↑ CS content prolonged release time	↑ CS content ↑ swelling ↑ elastic modulus	Antibacterial release system	[292, 293]

Abbreviations: **HA**: Hyaluronic acid, **CMC**: Carboxymethyl cellulose, **GA**: Glutaraldehyde, **bFGF**: the basic form of fibroblast growth factor, **TGF-β**: transforming growth factor-β1, **VEGF**: vascular endothelial growth factor, **HGF**: Hepatocyte growth factor, **CS**: Chondroitin sulphate, **EDC**: N,N-(3-dimethylaminopropyl)-N-ethyl carbodiimide hydrochloride, **NHS**: N-hydroxysuccinimide

The previous studies have demonstrated the impact of ECM analogues on swelling and mechanics of different hydrogel systems fabricated for various biomedical applications, in addition to controlling the release of drugs or proteins, such as growth factors. The controlled release mechanisms proposed were either due to electrostatic interactions between charged ECM and released proteins (as for heparin and growth factors) or enzymatic degradation of ECM. In some of the above studies, synthetic base materials were not used and the resulting hydrogels were degradable and thus not appropriate for cell encapsulation applications that require stable membrane materials.

In addition to the abovementioned ECM effects, other studies highlighted the impact of matrix organisation on the diffusivity of molecules. In fibrous matrices such as collagen, mathematical modelling indicated that the structure and orientation of fibrous ECM, such as collagen gels, results in anisotropic diffusion of nanoparticles and macromolecules [294]. This model explained the observed hindered diffusion of macromolecules, such as IgG, by fibrous ECM present in the interstitial space of tumors [295, 296].

Despite many researchers considering the use of ECM components in hydrogels, few studies have investigated the effect of ECM analogues on the permeability performance of hydrogels, which was the focus of the current research. In this study, heparin was chosen as an analogue of ECM glycosaminoglycans and gelatin was chosen as an ECM protein analogue. Heparin, a polyglycosaminoglycan stored in the granules of mast cells, is a highly sulphated variant of heparan sulphate found on the surface of different cell types as well as in the ECM [297]. Both heparin and heparan sulphate have the same basic disaccharide building units and are biosynthesised from the same precursor N-acetyl heparosan [297, 298]. Due to this structural similarity with heparan sulphate in addition to its common availability, heparin can be used as a model of heparan sulphate in different studies.

The majority of the biological functionalities exerted by heparin are related to its protein interactions [299]. The commonly known antithrombotic property of heparin is mediated through its ability to bind antithrombin III protein via the pentasaccharide sequence present on its backbone [297, 299]. Since the discovery of this specific protein interaction in 1915, a plethora of potent anticoagulant drugs have been synthesised to treat different thrombotic disorders of the venous system [299-301]. Moreover, heparin has

attracted the attention of several research studies as a growth factor delivery vehicle or enhancer of cell behaviour due to its unique ability to sequester a wide range of ECM proteins and growth factors via heparin binding domains [147, 291, 298, 302-304]. Therefore, heparin is expected to show potential as an active biological component in cell encapsulation systems.

The other selected ECM molecule was gelatin. It is denatured collagen produced by partial acid or alkaline hydrolysis. However, gelatin retains many of the bioactive epitopes of collagen which promote cell survival, attachment, functionality and matrix remodelling. Examples of those epitopes are the classic RGD, Glycine-Proline-Y or Glycine-X-Hydroxyproline sequence, where X and Y represent various other peptides [246, 285]. Moreover, it has been reported that gelatin lacks the antigenicity characteristic of collagen, which possibly disappears after the denaturation process [305]. Another advantage of gelatin over collagen is the lack of contractility, which decreased the viability of encapsulated cells in collagen over time compared to gelatin hydrogels [306]. In addition, gelatin is soluble in water at temperatures above 37°C (while collagen is only soluble in acidic solutions), which facilitates its use for the fabrication of different scaffolds and encapsulation devices.

The attraction of gelatin for tissue engineering applications started in the 1970s and was investigated in both hard and soft tissue engineering fields [307]. To counteract the dissolution of gelatin at physiological body temperature, various chemical crosslinking methods have been applied to maintain gelatin stability *in vivo* [308] . Despite the desirable properties of gelatin, limitations have been raised regarding its mechanical strength, flexibility, and the ability to tailor its degradability and cell adhering properties [285, 286].

Hence, gelatin composites or hybrid hydrogels have been reported in literature although not widely investigated (Examples Table 4.1).

The current chapter investigates biosynthetic PVA hydrogels fabricated via incorporation of heparin and gelatin into PVA network with the following specific aims:

1. Examine the effect of heparin and gelatin on the swelling behaviour, average mesh size and mechanics of PVA based hydrogels
2. Understand the impact of heparin and gelatin on the permeability performance of PVA hydrogels to different proteins

4.2 MATERIALS AND METHODS

4.2.1 Materials

Poly (vinyl alcohol) (PVA) (13-23 kDa, 98% hydrolysed), heparin sodium salt (grade I-A, from intestinal mucosa, average MW 17-19 kDa), gelatin from porcine skin Type A (~ 300 g Bloom), glycidyl methacrylate (GMA) (97% purity), methacrylic anhydride (94% purity) and 2-isocyanotoethylmethacrylate (ICEMA) (98% purity) were purchased from Sigma-Aldrich and used without further purification. The photoinitiator, 2-hydroxy-1-[4-(hydroxyethoxy) phenyl]-2-methyl-1-propanone (Irgacure 2959, Ciba Specialty Chemicals) was used as received. All solvents used were analytical grade including dimethyl sulfoxide (DMSO, Crown scientific), toluene (Ajax Finechem), deuterium oxide (D_2O, Sigma-Aldrich) and ethanol (absolute>99.5%, Sigma-Aldrich). Functionalised polymers were purified using 12 kDa molecular weight cutoff dialysis tubing (Sigma-Aldrich, Australia). Hydrogel disc moulds were made from silicone sheets (Silastic®Sheeting, reinforced medical grade silicone rubber, Dow Corning).

4.2.2 Material Characterisation

4.2.2.1 Synthesis of Methacrylated Macromers

PVA methacrylate macromers

PVA was functionalised with an average of 7,10, 14 and 20 methacrylate FG/c via reaction with 2-isocyanotoethylmethacrylate (ICEMA), as described previously in Chapter 3.

Heparin methacrylate macromers

Heparin was functionalised with an average of 3 methacrylate FG/c via reaction with glycidyl methacrylate, as described by Nilasaroya et al. [147]. Briefly, heparin was dissolved at room temperature in PBS (pH 7.4) at a concentration of 10 wt%. GMA was then added so that the number of moles of GMA was equal to that of the heparin disaccharide repeating unit. The reaction proceeded for 14 days with stirring at room temperature. The reaction was then stopped by precipitation in acetone. The precipitated macromer was dissolved in distilled water and dialyzed in 12 kDa molecular weight cutoff dialysis tubing against milliQ water. The solution was then lyophilised to obtain dry macromer. A schematic representation of the reaction is shown in Figure 4.1[309].

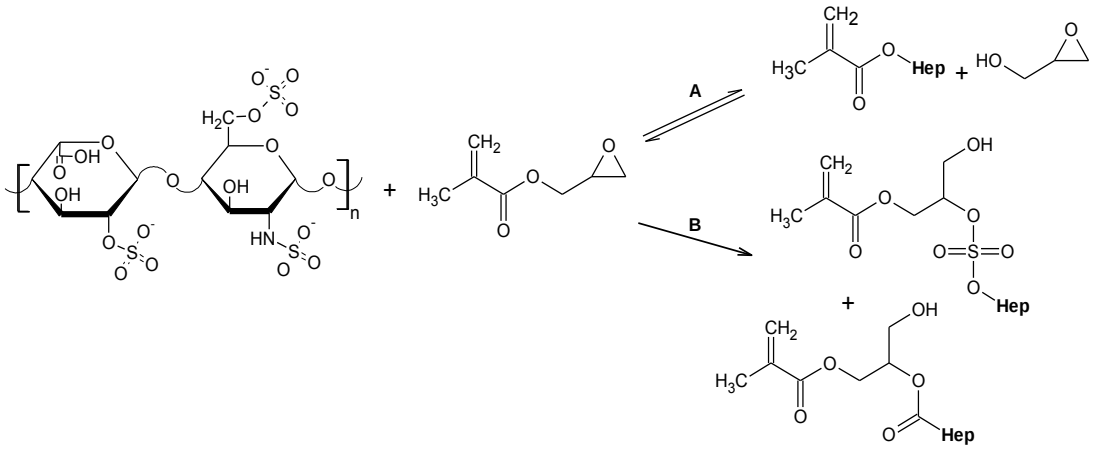

Figure 4.1: Schematic representation of heparin methacrylation via GMA reaction. A=transesterification, B= ring opening [309].

Gelatin methacrylate macromer

Gelatin from porcine skin Type A was modified with methacrylic anhydride using a method described by Van den Bulcke et al.[310]. Briefly, gelatin was dissolved in PBS (pH 7.4) at 50°C while stirring at a concentration of 10 wt%. Methacrylic anhydride was then added to the stirring mixture at 20% (w/v) at a rate of 0.5mL/min and the reaction proceeded for 1 hr at 50°C. The reaction was stopped by 5 times dilution with PBS (pH 7.4, 40°C). The mixture was dialysed in 12 kDa molecular weight cutoff dialysis tubing against milliQ water at 40°C. The solution was then lyophilised to obtain dry macromer. A schematic representation of the reaction is shown in Figure 4.2.

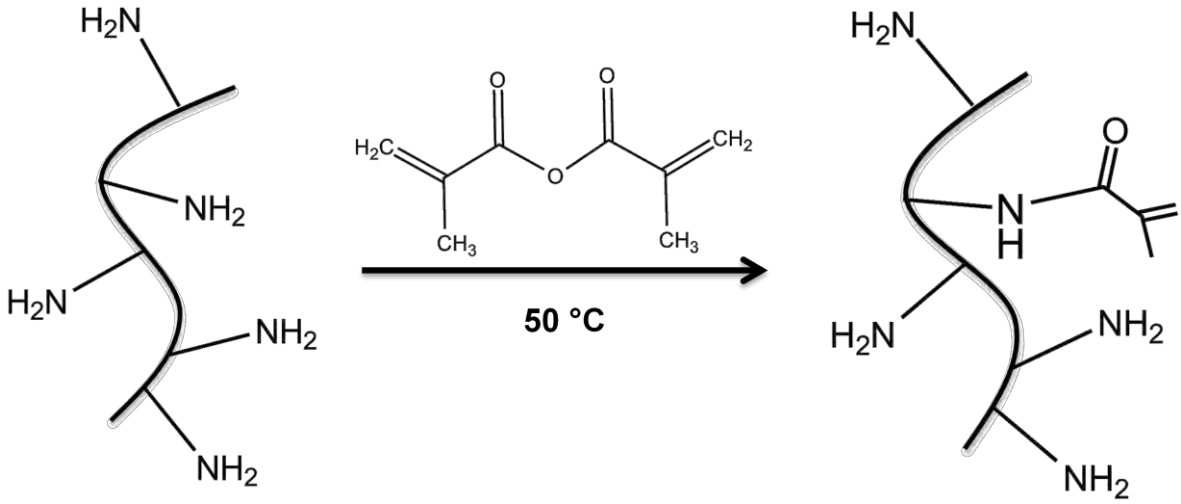

Figure 4.2: Schematic representation of gelatin methacrylation via reaction with methacrylic anhydride.

4.2.2.2 Nuclear magnetic resonance (NMR) Characterisation of Methacrylated Macromers

The number of attached methacrylate groups on the different polymers was analysed using proton nuclear magnetic resonance (^{1}H NMR, 300 MHz Bruker Avance DPX-300 spectrometer). PVA macromers were dissolved in D_2O and the percent methacrylation was calculated as discussed previously in Chapter 3. To calculate the percent methacrylation of heparin, the area under the peaks for the vinyl protons (δ = 6.1 and 5.7 ppm) was compared to the peaks representing protons 4 to 11 (δ = 3.4 and 4.6 ppm) and proton 12 (δ = 3.0 and 3.4 ppm) of the disaccharide repeating unit of heparin [147, 311].

In the case of gelatin, the percent methacrylation was determined by comparing area under the peaks for the aromatic region (δ = 7-8) with that of the vinyl protons (δ = 6.1 and 5.7 ppm). The degree of methacrylation represents the ratio of the amino groups functionalised with methacrylate to the total number of amino groups in the gelatin backbone before modification [245, 246].

4.2.2.3 Hydrogel Formation

Hydrogels were formed by radical chain polymerisation using UV light curing as previously described in Chapter 3. Hydrogels were made at 20 wt% total macromer, and were either pure PVA, pure gelatin, PVA:heparin (19:1) or PVA:gelatin (19:1). All the studies included pure PVA hydrogels (20% macromer) of various FG/c (7 to 20 FG/c) as controls. Pure gelatin hydrogels (20%) were also included to compare the behaviour of completely natural hydrogels to the proposed biosynthetic systems. Pure heparin hydrogels at 20% were too weak and difficult to handle and thus were not included.

4.2.3 Physico-Mechanical Characterisation of Hydrogels

Swelling and Network Characterisation via Equilibrium Swelling Theory

The hydrogel swelling study, followed by mass loss and mesh size analysis, was carried out as described in Chapter 3. Hydrogel discs (5 mm diameter x 1 mm thick) were immediately weighed after polymerisation (m_0). Three discs were lyophilised at t_0 to determine the actual macromer fraction. The rest of the samples were then incubated in phosphate buffer saline (PBS, pH 7.4) at 37°C. At 1, 3 or 7 days the discs were removed and weighed (m_s). Dry weights (m_d) were then determined after lyophilisation of hydrogels and the initial dry weight of hydrogels (m_{id}) was calculated. % sol fraction, the volumetric swelling ratio (Q), and average mesh size (ξ) of the different hydrogel networks were then determined using equations detailed in Chapter 3 (Eqs. 3.3-3.6). Calculations of PVA-ECM co-hydrogels included heparin and gelatin polymer parameters. The percentage of each polymer in the final hydrogel was also considered in the calculations.

$$Q = 1 + \frac{\rho_{PVA}*0.95 + \rho_{gelatin}*0.05}{\rho_{solvent}} (q-1) \qquad (4.1)$$

Where;

P_{PVA} : Density of PVA macromer (1.2619 g/ml)

$P_{gelatin}$: Density of gelatin macromer (1.369 g/ml) [312]

$\rho_{solvent}$: Density of PBS (~ 1.0 g/ml)

q: mass swelling ratio (m_s/m_d)

As detailed in Chapter 3, the average molecular weight between crosslinks ($\overline{Mc}$) was calculated using equation 4.2 developed by Peppas and Merrill [254] based on the equilibrium swelling theory and used to estimate the end-to end distance of unperturbed

(solvent free) state $(\bar{r}_0^2)^{1/2}$ (Eqn 4.3) [190]. The parameters of ECM analogues were considered in these equations. The mesh size and the crosslinking density (ρ_x) were then calculated.

$$\frac{1}{\overline{M_c}} = \frac{2}{\overline{M_n}} - \frac{(\bar{\upsilon}/V_1)\left[\ln(1-\upsilon_{2,s})+\upsilon_{2,s}+\chi\upsilon_{2,s}^2\right]}{\upsilon_{2,r}\left[\left(\frac{\upsilon_{2,s}}{\upsilon_{2,r}}\right)^{\frac{1}{3}}-\frac{1}{2}\left(\frac{\upsilon_{2,s}}{\upsilon_{2,r}}\right)\right]} \qquad (4.2)$$

$$(\bar{r}_0^2)^{1/2} = l\left(\frac{2\overline{M_c}}{M_r}\right)^{\frac{1}{2}} C_n^{1/2} \qquad (4.3)$$

Where;

$\overline{Mn}$: Number average molecular weight in the absence of any crosslinking

= $\overline{Mn}_{PVA}$* 0.95 + $\overline{Mn}_{ECM}$ * 0.05

($\overline{Mn}_{PVA}$ = 16 000, $\overline{Mn}_{heparin}$ = 18 000, $\overline{Mn}_{gelatin}$ = 100 000)

$\bar{}$: The specific volume of polymers

= $\bar{}_{PVA}$* 0.95 + $\bar{}_{ECM}$* 0.05

($\bar{}_{PVA}$ = 0.788, $\bar{}_{heparin}$ = 0.476 [313], $\bar{}_{gelatin}$= 0.73 [314])

V_1: The molar volume of the solvent

$_{2,s}$: The equilibrium polymer volume fraction

$_{2,r}$: The polymer volume fraction after crosslinking but before swelling

χ: The polymer solvent interaction (= 0.49 for both PVA and gelatin in water [315])

l: The bond length

(PVA and heparin c-c bond= 1.54 Å, gelatin peptide bond: ~ 3.6 Å [314])

M_r: Molecular weight of the repeating unit

= $M_{r\,PVA}$ * 0.95 + $M_{r\,ECM}$ * 0.05

($M_{r\,PVA}$ = 44 g/mol, $M_{r\,heparin}$ = 450 g/mol, $M_{r\,gelatin}$ = 100 g/mol [312])

C_n: The characteristic ratio

$= C_{n\,PVA} * 0.95 + C_{n\,ECM} * 0.05$ ($C_{n\,PVA}$= 8.9, $C_{n\,gelatin}$ = 5.3 [314])

In the case of pure gelatin hydrogels, different calculations were conducted for the molecular weight between crosslinks ($\overline{Mc}$) and average mesh size (ξ) as reported specifically for crosslinked gelatin hydrogel matrices [312] (Eqn 4.4,4.5)

$$\overline{Mc} = \frac{M}{X_c} \quad (4.4)$$

Where;

M: Average molecular weight of gelatin (100,000 g/mol)

X_c: Crosslinked amino groups/gelatin

$$\xi = 2\,\alpha \left(\frac{M_c}{M_r}\right)^{1/2} (2.21\ \text{Å})\, Q^{1/3} \quad (4.5)$$

Where;

α: An expansion factor (estimated at 2.0 based on previous reports of gelatin conformation)

Mechanical Characterisation

The mechanical properties of hydrogels were characterised using unconfined uniaxial compression testing at room temperature as described previously in Chapter 3. Hydrogel discs (5 mm diameter x 1 mm thick) were immersed in phosphate buffer saline (PBS, pH 7.4) at 37 °C for 7 days. After 1, 3 and 7 days, discs were removed from PBS and compressed at a strain rate of 100% strain min^{-1}, using an Instron 5543 mechanical tester. The compressive modulus was then determined.

Release of unbound heparin and gelatin from biosynthetic hydrogels

The amount of incorporated heparin and gelatin remaining in the hydrogel network was calculated by determining the percent unbound heparin and gelatin released from the hydrogels. Hydrogel discs (7 mm diameter x 1 mm thick) were immersed in 1 ml PBS, pH 7.4 at 37°C and shook for 7 days at 100 rpm. 200 µl samples were withdrawn after 1, 3 and 7 days and replaced with an identical volume of fresh PBS. Heparin concentration in the withdrawn samples was measured spectrophotometrically at λmax 535 nm after reaction with dimethylmethylene blue (DMMB) dye [316] (Sigma-Aldrich, Australia), which specifically binds to sulphated glycosaminoglycans. The amount of gelatin released was detected using a micro-BCA protein assay kit (Thermo Fisher Scientific), at λmax 562 nm. Concentrations of heparin and gelatin were then determined using calibration graphs over concentration range 0-25 µg/ml. The amount of gelatin or heparin released was then compared to the initial amount in the co-hydrogels.

Successive sampling and compensation of the release medium may result in continuous dilution of the medium, thus may lead to an apparent decrease in the percentage release particularly when the release medium is relatively small. Such an effect was corrected in the calculations using Richter et al. [309] equation (4.6):

$$C_1 = c_1 + c_1 \Delta t E \qquad (4.6)$$

Where;

C_1 = actual concentration of the released solute after correction

c_1 = uncorrected concentration of the released solute

Δt = time interval

E = rate of sample withdrawal

$c_1 \Delta t E$ = amount of drug eliminated from the solution during the interval Δt.

4.2.4 Permeability Performance of Hydrogels

Permeation studies

The permeation studies were carried out using a side-by-side diffusion cell (Permegear, USA) at 37°C for 48 hrs, as described in Chapter 3. The protein solutes examined in the studies were FITC-BSA (MW: 66 kDa, SR: 35 Å) and FITC-IgG (MW:150 kDa, SR: 55 Å). At predetermined time intervals (2, 4, 24, 28 and 48 hrs), a 100 µl sample was withdrawn from the receptor cell and replaced with fresh PBS. After 48 hrs, the samples were analysed for fluorescence intensity using a microplate reader (Infinite® 200, Tecan). The concentrations were then calculated using a calibration curve from known solute concentrations. The solute permeability coefficient (P) and diffusion coefficient (D) were calculated using equations derived in Chapter 3 (Eqs. 3.10 - 3.11).

Partition coefficient determination

The partitioning of examined proteins between hydrogels and surrounding solution was determined by soaking hydrogels in solute solution of known concentration at 37°C. After reaching equilibrium (7 days), the remaining solution was analysed for fluorescence intensity using a microplate reader. The partition coefficient was calculated as detailed in Chapter 3.

4.2.5 Statistical analysis

Statistical analysis of the results was conducted using general linear model (two-way ANOVA) with replication. Pairwise comparisons were also included using Tukey test. Analysis was performed with Minitab statistical software (Minitab Inc., version 15). All experiments were done with 3 samples and the whole experiment was repeated 3 times.

Results are expressed as mean values together with their standard deviations in all tables and figures.

4.3 RESULTS

4.3.1 Macromer Synthesis and Characterisation

Heparin was selected as an analogue of the many glycosaminoglycans present in the ECM. Heparin, together with chondroitin sulphate, has previously been functionalised with methacrylate groups through transesterification and ring opening reactions [147, 317]. 2% methacrylation of heparin (MW 17-19 kDa) was targeted to preserve its biofunctionality [147]. ^{1}H-NMR results confirmed the targeted methacrylation, which was equivalent to 3 FG/c (Fig.4.3).

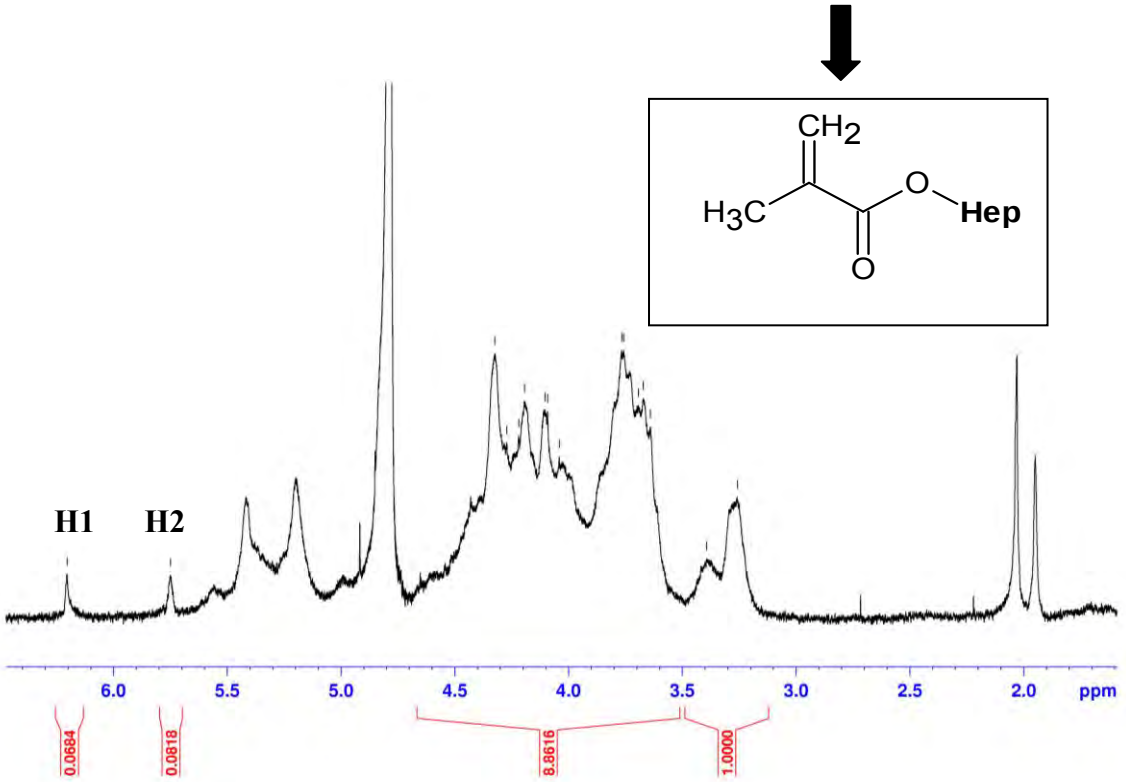

Integral of Protons 4-11	Integral of Proton 12

Figure 4.3: ^{1}H NMR of heparin-methacrylate with 3 FG/c in D_2O. Integration values of the peaks are shown at the bottom. Inset at the top: represents the attached methacrylates group to the heparin. Arrow points at the protons detected by ^{1}H NMR.

Type A gelatin was used in this study due to its abundant reactive amino groups, which improves the efficiency of methacrylation [286, 318]. Various degrees of methacrylation of gelatin have been used in the literature and were described as low, medium and high [246, 319, 320]. In this study, a "medium" degree of methacrylation was chosen, which is equivalent to ~ 50-55% methacrylation of the lysine residues in the gelatin backbone. It has been reported that this percentage of methacrylation offers optimal mechanical properties and handling for modified gelatin [246]. In addition, this modification accounts for ~ 2% methacrylation of the gelatin protein backbone (MW 100 kDa). It was hypothesised that this % functionalisation would not interfere with its

biological functionality. ^{1}H-NMR confirmed the degree of methacrylation for gelatin type A, which was equivalent to 13 methacrylates on the gelatin backbone (Fig. 4.4).

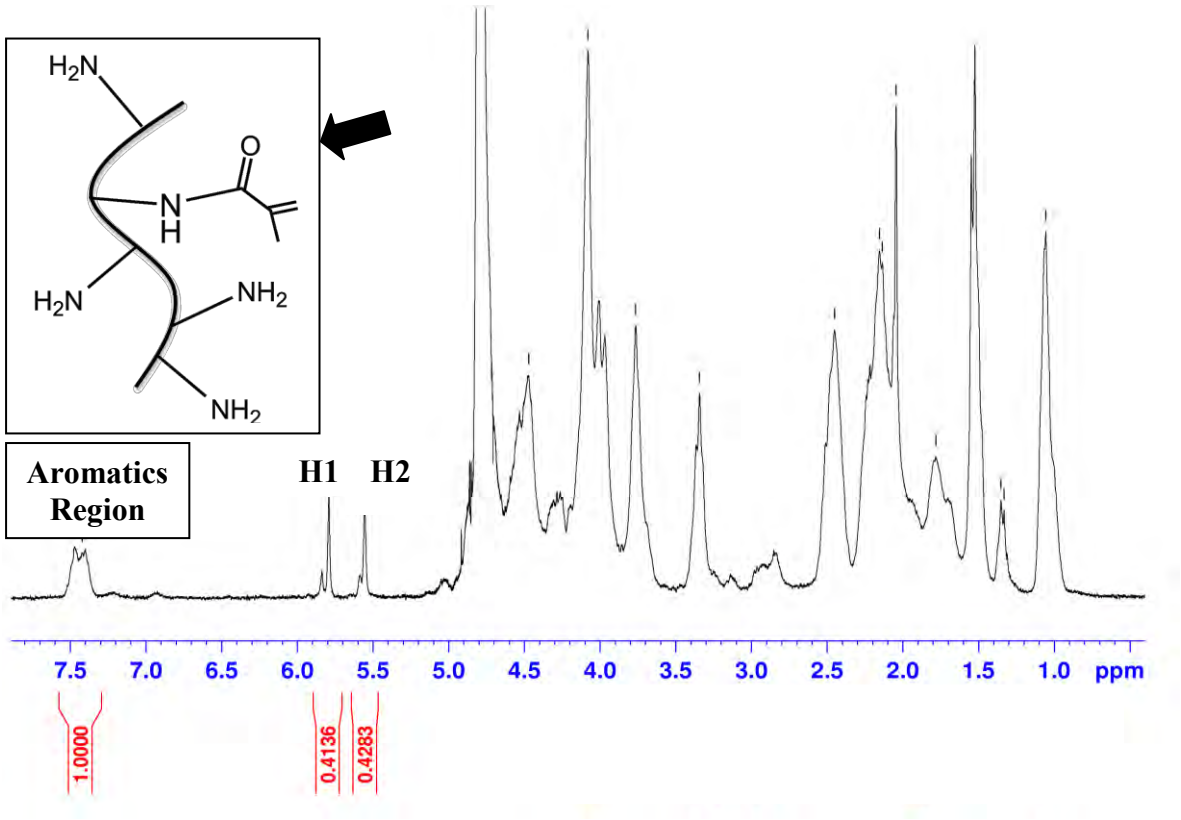

Figure 4.4: ^{1}H NMR of gelatin-methacrylate in D_2O showing the region of aromatic peaks and methacrylates protons used for the calculations. Integration values of the peaks are shown at the bottom. Inset at the top: represents the attached methacrylates group to the gelatin. Arrow points at the protons detected by ^{1}H NMR.

4.3.2 Physico-Mechanical Characterisation of Hydrogels

Swelling Properties and Network Characterisation via Equilibrium Swelling Theory

The effect of increasing FG/c on the swelling behaviour and network structure of PVA co-hydrogels is shown in Table 4.2. Pure PVA hydrogel data was previously shown in Chapter 3, but is shown again here to assist in the comparison with the co-hydrogel data. The network parameters for all hydrogels remained constant up to 7 days of immersion in

PBS. Statistical analysis showed no significant difference between the data obtained for biosynthetic hydrogels and those obtained for PVA only hydrogels. The network parameters of pure 20% gelatin hydrogels, used as natural polymer control, are also shown in Table 4.2.

Table 4.2: Sol fraction, volumetric swelling ratio, average mesh size and crosslinking density of PVA, co-hydrogels and gelatin hydrogels after 24 hours incubation in PBS.

FG/c of PVA	Hydrogel composition			Sol fraction (%)	Volumetric swelling ratio (Q)	Average mesh size* ζ (Å)	Crosslinking density ρ_x*10^4 (mol/L)
	PVA	Heparin	Gelatin				
7	20	---	---	14.08 ±3.30	6.33 ± 0.14	94.63 ± 2.20	4.68 ±0.10
	19	1	---	9.42 ± 3.13	6.56 ±0.17	97.79 ±2.46	4.46 ±0.15
	19	---	1	13.03 ±3.81	6.21 ±0.36	92.59 ±5.75	4.45 ±0.42
10	20	---	---	3.68 ±0.64	5.70 ±0.19	83.53 ± 3.50	5.88 ± 0.10
	19	1	---	11.18 ±5.76	5.46 ±0.50	79.74 ±7.71	5.99 ±0.74
	19	---	1	6.72 ±7.91	5.76 ±0.59	84.28 ±5.40	5.19 ±0.89
14	20	---	---	-1.78 ±2.27	4.44 ± 0.06	62.46 ±1.30	8.10 ± 0.30
	19	1	---	0.24 ±4.76	5.02 ±0.20	72.30 ±3.12	6.85 ±0.39
	19	---	1	1.88 ±4.94	4.97 ±0.36	72.44 ±6.14	6.30 ±0.81
20	20	---	---	-4.34 ±3.74	4.30 ± 0.13	60.74 ±1.90	8.33 ± 0.20
	19	1	---	-6.77 ±3.93	4.45 ±0.10	63.30 ±1.91	8.24 ±0.37
	19	---	1	2.56 ±8.64	4.69 ±0.18	66.23 ±3.01	7.19 ±0.46
Gelatin gels	---	---	20	1.12 ±6.10	6.07 ±0.48	139.86 ±2.65	1.65 ±0.35

*Calculated from the Peppas-Merrill equation

Mechanical Characterisation

All hydrogels were tested in compression to investigate the effect of adding biological molecules on the mechanical performance of PVA hydrogels. Since modulus values from the Instron differed from one set of experiments to another, pure PVA was tested every time with the co-hydrogel examined. As was found in Chapter 3 with the pure PVA gels, the compressive modulus increased significantly by increasing FG/c from 7 up to 20 in all PVA co-hydrogels (Fig. 4.5-4.6). No significant difference was observed in the compressive modulus values after incorporation of either heparin or gelatin in the network (Fig. 4.5-4.6). The modulus of pure 20% gelatin hydrogels was 227 kPa (±88), which was higher than PVA with 7 FG/c and lower than 10 FG/c. ANOVA statistical results of compressive modulus values for hydrogels incubated in PBS for 1, 3 and 7 days (data not shown) indicated no significant difference between days. These statistics confirm that all physico-mechanical properties of hydrogels could be determined after 24 hrs swelling study with no significant variations over time.

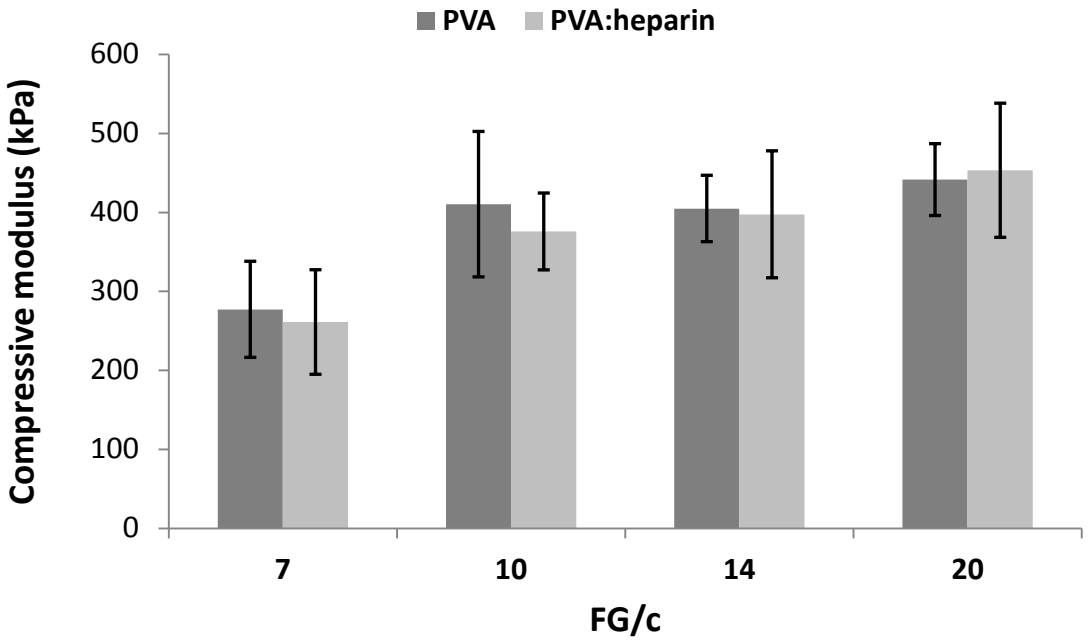

Figure 4.5: The compressive modulus of PVA and PVA:heparin hydrogels after incubation in PBS (pH 7.4) for 7 days.

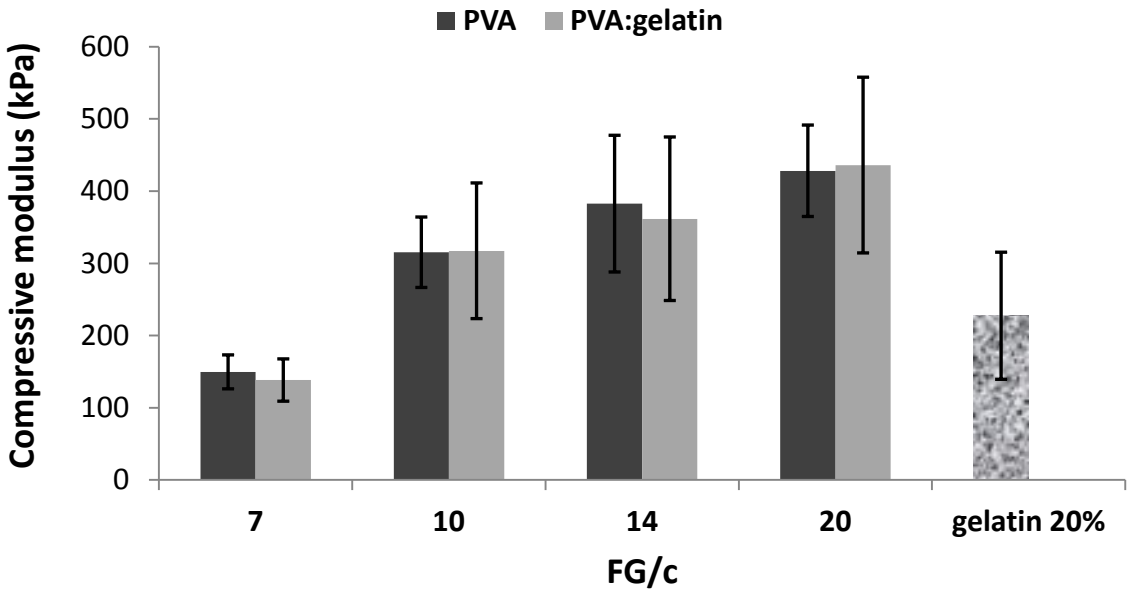

Figure 4.6: The compressive modulus of PVA and PVA:gelatin hydrogels after incubation in PBS (pH 7.4) for 7 days.

Release of unbound heparin and gelatin

The amount of heparin and gelatin that was not covalently incorporated into the PVA co-polymer network during photopolymerisation is represented in Figures 4.7 and 4.8. After incubation in PBS for 1 day, all the unbound heparin was released (~ 30-40%) and the % release was similar in all compositions tested (Fig.4.7). No significant difference was observed between day 1 and 7.

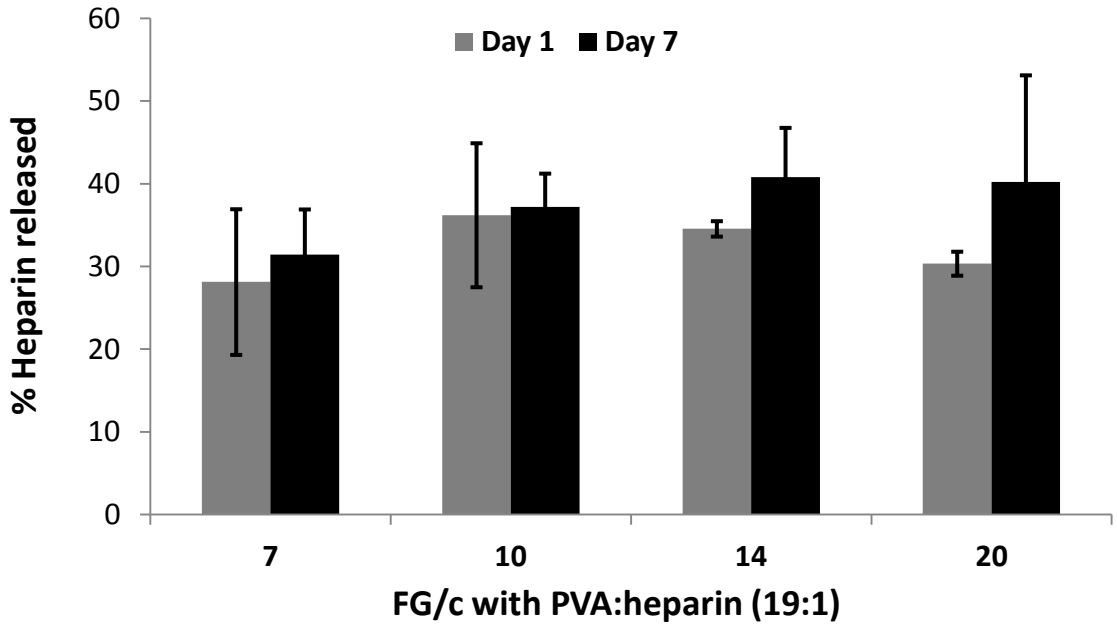

Figure 4.7: % Release values of unbound heparin from PVA:heparin (19:1) hydrogels after incubation in PBS (pH 7.4) for 7 days.

PVA:gelatin hydrogels showed maximum percent release of unbound gelatin (~ 15%) after 3 days of incubation in PBS (Fig.4.8). No significant difference was observed between day 3 and day 7 and there were no differences between samples. Pure gelatin hydrogels released their sol fraction after 1 day (~ 4-5%). This amount of release correlated well with the results obtained from the sol fraction study (1.12 % ±6.10) (Table 4.2).

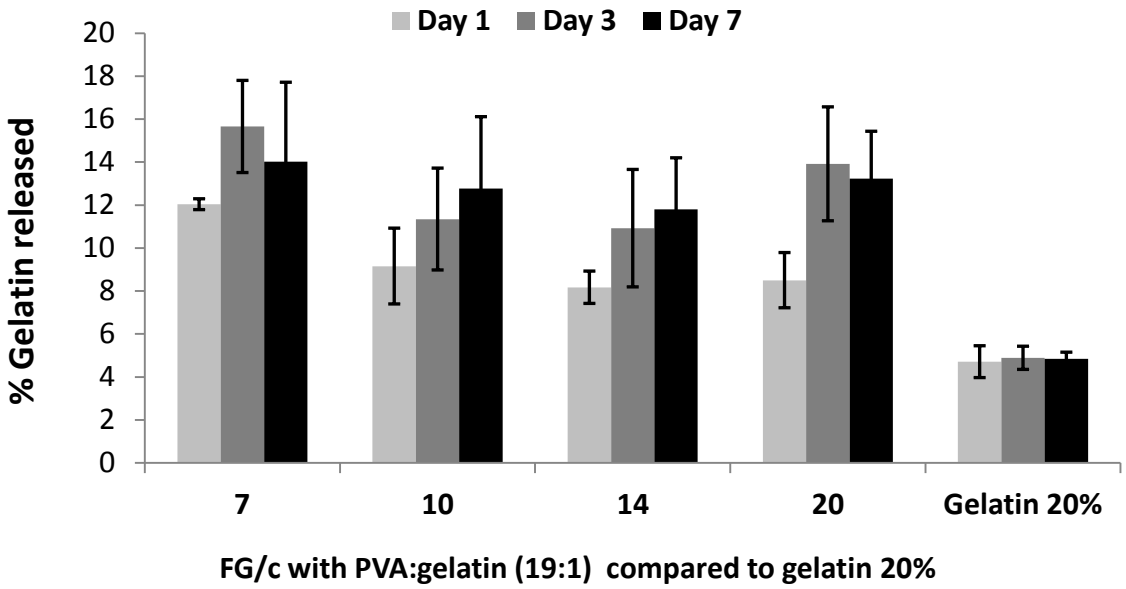

Figure 4.8: % Release values of unbound gelatin from PVA:gelatin (19:1) and gelatin (20%) hydrogels after incubation in PBS (pH 7.4) for 7 days.

Table 4.3 demonstrates the equilibrium heparin and gelatin composition in the co-hydrogels after 7 days of incubation, which were calculated based on the release values obtained. The percent of heparin and gelatin remaining in the co-hydrogels was ~ 0.6% and ~ 0.9% respectively. The actual composition of pure gelatin hydrogels after the release of sol fraction was ~ 19%.

Table 4.3: Average equilibrium heparin and gelatin composition (%) in the co-hydrogels after 7 days of incubation in PBS

FG/c	**Hydrogel composition (%)**		**Equilibrium heparin composition (%)**	**Equilibrium gelatin composition (%)**
	PVA	Heparin or gelatin		
7	19	1	0.68	0.86
10	19	1	0.63	0.87
14	19	1	0.59	0.88
20	19	1	0.60	0.87
Gelatin gels	20	.....	.....	19.03

4.3.3 Permeability Performance of Hydrogels

Possible interactions that might have occurred between examined solute proteins and incorporated ECM analogues were tested. Those interactions are represented by K values from the partition coefficient experiment and recorded in Table 4.4. K values were similar for all FG/c of PVA (data not shown), thus only values of 7 FG/c PVA co-hydrogels are shown for simplicity. Different values of K were obtained for the same solute protein with different co-hydrogel networks. Both BSA and IgG had K values <1 with co-hydrogels containing heparin whereas co-hydrogels having gelatin had higher values with K >1. K values of BSA and IgG were also examined with pure gelatin hydrogels and were higher than those obtained with all co-hydrogels (Table 4.4) with K values >1.

Table 4.4: Partition coefficient values of both BSA and IgG proteins with different hydrogels compositions: PVA:heparin (19:1), PVA:gelatin (19:1) and gelatin (20%).

Protein	Partition coefficient K		
	PVA:heparin	**PVA:gelatin**	**Gelatin 20%**
BSA	**0.93±0.11**	**1.43±0.41**	**1.81±0.74**
IgG	**0.92±0.24**	**1.37±0.55**	**2.02±0.54**

Figures 4.9 and 4.10 show the diffusion coefficients (D) of BSA and IgG through PVA co-hydrogels and pure gelatin hydrogels. It was observed that incorporation of heparin and gelatin to the PVA network at 1% did not significantly change the diffusion of either BSA or IgG through PVA hydrogels ($p>0.05$). As was shown previously in Chapter 3, diffusion of IgG was found to be significantly limited by increasing FG/c up to 20 ($p<0.05$). No significant difference was found in D values of BSA through all PVA hydrogels. The ability of pure gelatin hydrogels to permeate BSA was comparable to PVA co-hydrogels of different crosslinking densities. The diffusion of IgG was limited in pure gelatin hydrogels with D values similar to the highly crosslinked 14 FG/c PVA hydrogels.

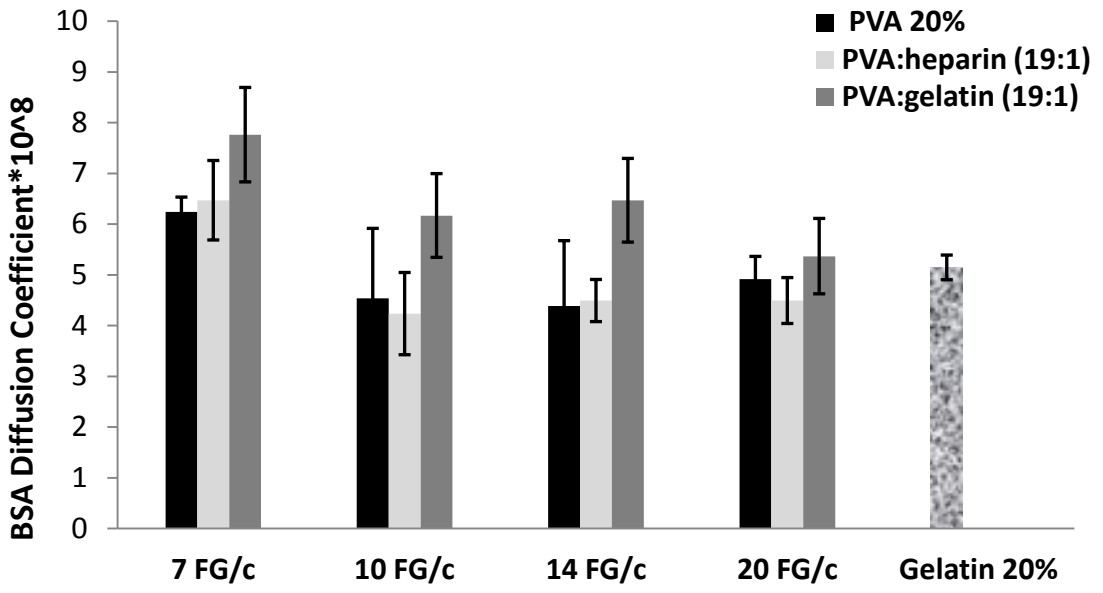

Figure 4.9: Diffusion coefficients of BSA-FITC through PVA, PVA:heparin, PVA:gelatin and gelatin hydrogels.

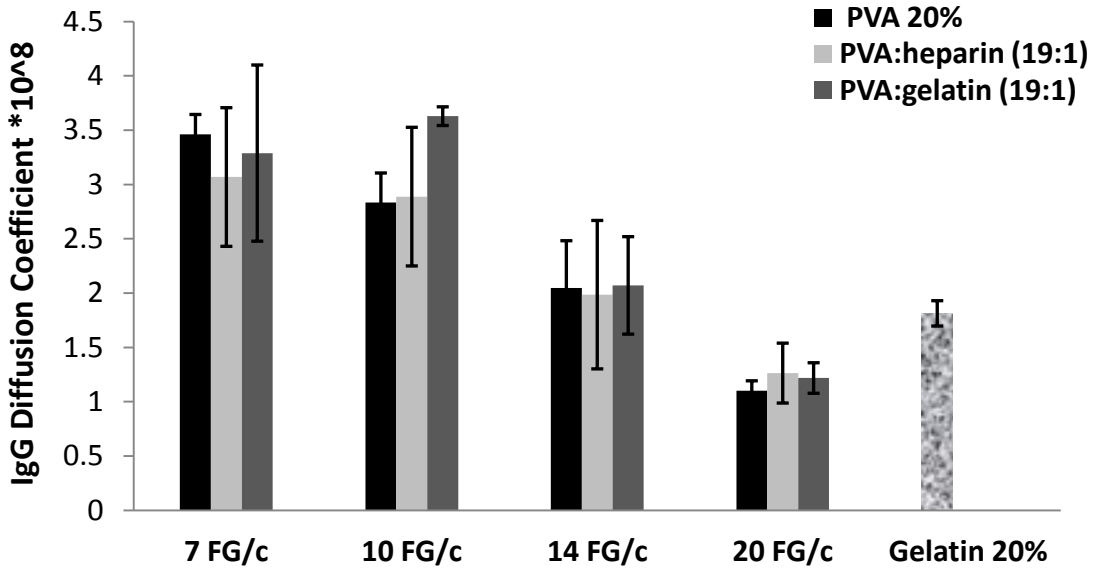

Figure 4.10: Diffusion coefficients of IgG-FITC through PVA, PVA:heparin, PVA:gelatin and gelatin hydrogels.

4.4 DISCUSSION

In the current chapter, the previously studied physico-mechanical characteristics of the base PVA hydrogels were preserved after incorporation of a small amount of heparin and gelatin into the network. More importantly, heparin and gelatin did not interfere with the expected permeability of different FG/c PVA hydrogels, which is an essential feature for determining the permselectivity capacity of these hydrogel for immunoisolation.

Covalent binding of both modified ECM analogues into the co-hydrogel was confirmed by testing the percent release of unbound ECM from the PVA network. Unbound heparin was completely released after 1 day at ~ 40% in all FG/c of PVA. The release values are lower than previous findings on PVA:heparin hydrogels formed from PVA with 3 FG/c, where the % unbound heparin released reached 50% [147]. The current results show that by increasing the FG/c of PVA from 3 to 7, the amount of incorporated heparin in the hydrogel network increased, which is hypothesised to be due to increased methacrylate crosslinkers available in the PVA network. However, heparin retention was not improved by further increasing the FG/c. Although low percent methacrylation on heparin leads to high heparin mass loss (with ~ 0.6% remaining in the gel, Table 4.3), previous studies have demonstrated that a final incorporation as low as 0.3% heparin was still sufficient to impart bioactivity to the co-hydrogels [147, 289, 321].

Pure gelatin hydrogels only had a small amount of mass loss (~ 4-5%), indicating that the selected medium degree of methacrylation was sufficient to efficiently crosslink the gelatin into the PVA co-hydrogel network via UV curing. In the PVA:gelatin hydrogels, the complete release of unbound gelatin (~ 15%) was delayed until day 3, which is most likely due to the high MW of gelatin (100 kDa) compared to that of heparin (17-19

kDa). No reported studies were found regarding testing the efficient covalent incorporation of gelatin in synthetic hydrogels.

Incorporated heparin and gelatin were then assessed for their effect on the physico-mechanical characteristics of PVA network. Swelling and mesh size analysis of co-hydrogels was conducted through the equilibrium swelling theory using the Peppas-Merrill equation, which was developed for neutral homopolymers such as PVA. Despite the anionic nature of heparin and the polyampholytic nature of gelatin, the Peppas-Merrill equation was used for mesh size calculations due to the overwhelming percentage of PVA in the final hydrogel. However, the parameters of heparin and gelatin were considered in the equation. Hickey et al. previously used the same equation for co- hydrogels of PVA and anionic poly(acrylic acid) (PAA) where PVA was the predominant polymer in the final network [255]. The network characteristics of pure gelatin hydrogels were calculated using an equation derived specifically for gelatin, taking into account the nature and conformation of this particular polymer [312].

In all tested PVA:heparin and PVA:gelatin co-hydrogels, no significant change in either the swelling or the mechanical strength was observed compared to the other co-hydrogel or to pure PVA hydrogels (Table 4.2, Fig. 4.5-4.6). This result is not unexpected, as a purposefully low amount of ECM analogues were incorporated within the network and thus it was not expected to have a large impact on the final gel properties. It has been reported that anionic polymers increase the swelling behaviour of hydrogel networks [147, 205]. However, the addition of heparin and gelatin did not impact on the final mesh size at this small percent incorporation. It has been previously reported that phase separation induced by photopolymerisation occurs with gelatin methacrylated macromers, resulting in microporous hydrogels [246, 322]. This phenomenon was not observed at these low

incorporation % and did not impact on the final structure of biosynthetic PVA hydrogel. Pure gelatin hydrogels showed swelling behaviour similar to 7 FG/c PVA hydrogels and mechanical strength ranging between 7 and 10 FG/c (Table 4.2, Fig. 4.6). Increasing the percent methacrylation of gelatin would be expected to increase the crosslinking density and the stiffness of this natural polymer. However, due to known enzymatic degradation *in vivo*, expected remodelling by encapsulated cells, and batch to batch variation, pure gelatin hydrogels were not considered as a candidate to follow on with more investigation.

Permeation of both BSA and IgG through biosynthetic hydrogels was then tested to investigate the effect of ECM analogues on the passage of proteins through PVA co-hydrogel network. From the partition coefficient values results, it was observed that incorporation of heparin shifted K values below 1 (Table 4.4), indicating that examined solute proteins were not easily distributed in the hydrogel network, which could be explained by the charge repulsion between negatively charged heparin and examined solute proteins at pH 7.4. Both BSA and IgG acquire a net negative charge at pH 7.4, which is above their isoelectric points (pI) 4.8 and 5.8-7.3 respectively [210, 323]. pI is the pH at which a molecule carries no net electrical charge. However, despite this charge repulsion, no significant difference in the diffusion of both proteins through PVA and PVA-heparin hydrogels was observed (Fig.4.9-4.10).

In the case of PVA:gelatin and pure gelatin hydrogels, the partition coefficient (K) values of both solute proteins were shifted above 1 (Table 4.4) and was more pronounced in the case of pure gelatin gels. A $K > 1$ indicates a positive interaction with the hydrogel network and could lead to hindered diffusion of solutes from the gel. This interaction could be related to the attraction between the negatively charged solute proteins and the potentially positively charged gelatin (pH 7.4). It has been reported that the isoelectric

point of gelatin ranges from 7-9 [282, 286, 319], which might have resulted in the positive charge of gelatin at pH 7.4. It should be noted that the K values observed in the current chapter were in a small range around the value 1, showing that the possible interactions occurring between the examined solutes and the hydrogel matrix might not be significantly pronounced as compared to other hydrogel systems [203, 205, 255, 264, 265].

Although K values showed possible interactions between both ECM analogues and permeating proteins, whether through electrostatic charge repulsion or attraction, the permeability performance of hydrogels was unaffected (Fig. 4.9-4.10). This result could be due to the dominant effect of mesh size over the charge interactions, especially with the low percent of ECM incorporated in the PVA hydrogel network. Conversely, the effect of interaction on the permeability was more pronounced with pure gelatin 20% hydrogels, where the diffusion coefficient values of both examined proteins were similar to the highly crosslinked 14 FG/c PVA hydrogels (mesh size ~72 Å) despite the mesh size being much larger (~140 Å). Although the mesh size calculated for gelatin hydrogels was far above that of the Stokes radii of examined proteins, the diffusion of IgG was restricted. This restriction is believed to be due to the dominant effect of charge interaction over the mesh size, related to the high percentage of natural polymer available (20%).

4.5 CONCLUSION

The incorporation of heparin and gelatin into PVA gels did not interfere with the base synthetic hydrogel characteristics previously characterised in Chapter 3, including swelling, average mesh size and mechanical strength. The interesting finding in this chapter was that despite the possible interactions between BSA and IgG proteins and the incorporated ECM analogues, the diffusion profiles were not significantly different from pure PVA hydrogel results. These findings prove that low percent incorporation of ECM analogues of different nature and charge did not impact on the base characteristics of PVA, especially its permselectivity. It was observed that the effect of mesh size was more pronounced than the charge interactions when only a low percent of ECM analogues were incorporated. Additionally, amongst the examined FG/c (7, 10, 14 and 20), pure PVA and co-hydrogels only showed significantly different characteristics at 7 and 20 FG/c. Hence, the following chapters will focus on these two FG/c as examples of low and high functional group densities.

While this chapter focused on the incorporation of a single ECM analogue, it is envisioned that an ideal cell encapsulation system will need to be more complex and include a range of ECM analogues. Therefore, in the following chapter, both heparin and gelatin will be co-polymerised with PVA to attempt to replicate the complexity of the natural ECM, where different molecules of various functionalities are assembled together in a dynamic biomolecular structure.

Chapter 5

PVA hydrogels with mixed ECM analogues: Structural and bioactivity characterisation

5.1 INTRODUCTION

The ability to incorporate a small amount of two ECM analogues, heparin and gelatin, individually into a PVA network was demonstrated in the previous chapter. While these results represent the initial steps toward mimicking incorporation of natural ECM within synthetic PVA networks, *in viv*o cellular behaviours are influenced by complex chemical and biophysical cues from the ECM microenvironment [324]. Therefore, in order to achieve complex cellular functions, presentation of multiple cues is required to simulate the natural *in vivo* cell environment within the final artificial implant [251]. Hence, the aim of the current chapter was to examine the effects on the PVA network of simultaneous covalent incorporation of two dissimilar biological molecules, heparin and gelatin within a PVA hydrogel. Presentation of two or more biological cues provides a simplified model of presentation of multifunctional ECM to cells encapsulated in a largely synthetic network.

Several approaches reported in the literature have examined presentation of multiple biological signals into hydrogel matrices by using several ECM and/or biological components. Variations to the physico-mechanical characteristics of the final co-hydrogel network have been observed compared to single component hydrogels. The most common approach is hybrid hydrogels which are composed of interpenetrating network (IPN) of biological polymers of different functionalities and structural characteristics. Shu et al. mimicked the composition and function of natural ECM via an injectable *in situ*-crosslinkable hydrogel composed of a blend of chemically modified glycosaminoglycans (GAGs) and gelatin proteins [325]. They showed that this blend possessed higher mechanical strength than each individual alone and resulted in highly swollen hydrogels (> 96% water content). It was hypothesised that the electrostatic interactions between modified GAG and gelatin macromers provided enhanced non covalent stabilisation of the

final hydrogel and possible increased crosslinking after blending all the macromers together.

IPN hydrogels from hyaluronic acid (HA) and collagen have been also fabricated [326]. The presence of collagen improved the mechanical stability of HA purportedly due to its fibrillar structure. Rowe et al. developed a collagen-fibrin IPN hydrogel seeded with vascular smooth muscle cells, which benefited from collagen characteristics [327]. They demonstrated that forming an IPN between collagen and fibrin ECM molecules exhibited a synergistic effect in terms of material moduli, where the interaction between both biological molecules yielded a final hydrogel with improved mechanical properties over the individual components alone. In addition, photocrosslinkable IPN of gelatin with silk fibroin and gellan gum were fabricated to tune the mechanical, structural and bioactive properties of the final product [320, 328]. Silk fibroin has shown to lower the swelling ratio and degradation rate while increasing the compressive modulus of the hybrid hydrogel, due to its crystalline structure.

Natural polymer blends of mixed functionalities and characteristics have also been achieved through electrostatic interactions. Marsich et al. used a binary polysaccharide mixture composed of alginate polyanion and lactose-modified chitosan polycation and demonstrated improved final scaffold structural properties and enhanced chondrocyte behaviour within the scaffold over the individual components [329]. In all of the above studies, synthetic base materials were not used in the hydrogel systems and the resulting hydrogels, as is the case with most so-called "synthetic ECM", were degradable and thus not appropriate for cell encapsulation applications that require stable support materials.

Another simple approach to introduce additional biofunctionality into hydrogels was achieved through the addition of heparin-binding proteins to thiol-functionalised

heparin-PEG gels during the gelation process [302]. Simple adsorption of fibrinogen on heparin based hydrogels enhanced cell proliferation by more than 5-fold. Similarly, Hiraoka et al. used the concept of adsorption to bind laminin-derived cell adhesive peptides to collagen under physiological conditions [141]. This combination provided an appropriate microenvironment for enhanced viability of neural cells encapsulated in collagen hydrogels.

Entrapment of several ECM molecules within synthetic hydrogels is another approach presented in the literature to enrich the biological cues in the final hydrogel matrix, albeit less common than using natural hydrogels alone. Weber et al. tested different ratios of the proteins collagen type I and IV, fibrinogen, fibronectin, laminin and vitronectin in PEG hydrogels on encapsulated MIN6 cell response [10, 146]. Overall, mixed ECM proteins had a greater effect on MIN6 viability and functionality than individual ECM components.

Recently, a combination between both glycosaminoglycans and adhesion peptides has been reported in synthetic PEG hydrogels, where chemically or photo-crosslinked heparin-PEG hydrogels have been modified by covalent attachment of RGD sequence to heparin [330, 331]. In these studies, both cell adhesive functionality and growth factor presentation have been demonstrated and expanded the biomedical applications of the synthetically-based hydrogels.

Despite the previous approaches to augment the biological signals and characteristics in hydrogels, there is a notable absence of studies examining covalent binding of multiple ECM molecules of different types (i.e. GAGs combined with proteins) within synthetic hydrogels. Moreover, little information was found in literature addressing the effect of ECM complexity on the permeability performance of hydrogels.

Consequently, this chapter aimed to investigate the combined incorporation of heparin and gelatin into PVA hydrogels through the following specific aims:

1. Understand the effects on the swelling, mechanics and permeability of hydrogels of the combination of two ECM analogues covalently incorporated into PVA hydrogel.
2. Assess the effect of combination of ECM analogues within PVA hydrogel on their respective bioactivities.

5.2 MATERIALS AND METHODS

5.2.1 Materials

All materials and solvents used for macromer synthesis and hydrogel fabrication have been mentioned in the previous Chapters 3 and 4. For cell assays, culture media were purchased from Sigma-Aldrich and supplemented with 10% fetal bovine serum (FBS, SAFC biosciences) and 1% penicillin streptomycin (PS, Sigma-Aldrich). RPMI-1640 medium was used to culture BaF3 cells while Eagle's minimum essential medium (EMEM) was used for culturing murine dermal L929 fibroblasts. Cell staining reagents including propidium iodide (PI) and calcein AM for live/dead double staining and 4',6-diamidino-2-phenylindole (DAPI) for nuclei staining were from Sigma-Aldrich. Rhodamine-phalloidin (Rh-phalloidin) was purchased from Molecular Probes, Australia.

5.2.2 Material Fabrication

Synthesis of Methacrylated Macromers

PVA was functionalised with an average of 7and 20 methacrylate FG/c via reaction with 2-isocyanotoethylmethacrylate (ICEMA), as described previously in Chapter 3. Heparin was functionalised with an average of 3 methacrylate FG/c, via reaction with

glycidyl methacrylate, as described in Chapter 4. Gelatin from porcine skin Type A was modified with 13 methacrylate FG/c via reaction with methacrylic anhydride, as detailed in Chapter 4.

Hydrogel Formation

Hydrogels were formed by radical chain polymerisation using UV light curing as previously described in Chapter 3. Chapter 4 concluded that 1% incorporation of an ECM analogue did not interfere with the controlled physico-mechanical properties of PVA hydrogels. For that reason, the final ECM percent incorporation was kept at 1% in this chapter. Instead of having only one biological component, both of the two previously investigated ECM analogues, heparin and gelatin, were mixed at an equal ratio resulting in a final PVA:heparin:gelatin composition of 19:0.5:0.5 (= PVA:ECM Mix 19:1). In all tests, this mixed composition hydrogel was compared to pure PVA hydrogels and also PVA:heparin (19.5:0.5) and PVA:gelatin (19.5:0.5) co-hydrogels. All hydrogels were investigated with two different PVA functional group densities, 7 and 20 FG/c, since significant variation was observed between these two hydrogels in all physical, mechanical and permeability characteristics in Chapter 4.

5.2.3 Physico-Mechanical Characterisation of Hydrogels

Swelling and Network Characterisation via Equilibrium Swelling Theory

A hydrogel swelling study followed by mass loss and mesh size analysis was carried out as described in Chapter 3. Hydrogel discs (5 mm diameter x 1 mm thick) were immediately weighed after polymerisation (m_0). Three discs were lyophilised at t_0 to determine the actual macromer fraction. The rest of the samples were then incubated in phosphate buffer saline (PBS, pH 7.4) at 37°C for 7 days. % sol fraction, volumetric

swelling ratio (Q), and average mesh size (ξ) of the different hydrogel networks were then determined using equations detailed previously in Chapters 3 and 4. Calculations of PVA:ECM Mix hydrogels included heparin and gelatin polymer parameters. The percentage of each polymer in the final hydrogel was also considered in the calculations.

Release of Unbound ECM Analogues from Biosynthetic Hydrogels

The amount of incorporated heparin and gelatin remaining in the hydrogel network was calculated by determining the percent unbound heparin and gelatin released from the hydrogels, as detailed in Chapter 4. Hydrogel discs (7 mm diameter x 1 mm thick) were immersed in 1 ml PBS, pH 7.4 at 37°C and shook for 7 days. Sampling time intervals were 1, 3 and 7 days. Heparin concentration in the supernatant was measured using DMMB assay while gelatin was detected using a micro-BCA protein assay. In hydrogels with both ECM analogues, both DMMB and micro-BCA protein assays were conducted on the same supernatant. For that reason, the standard curve of each assay was examined before and after the addition of fixed amount of the other ECM analogue. The fixed concentration selected was 120 μg/ml for each ECM analogue, which accounts for ~ 50% ECM analogue released (higher than any expected values as was observed previously from Chapter 4 results). The linear range for both assays was in the range from 0 to 25 μg/ml.

Mechanical Characterisation

The compressive moduli of all hydrogel compositions were determined using unconfined uniaxial compression testing, as described previously in Chapter 3 and 4. Hydrogel discs (5 mm diameter x 1 mm thick) were immersed in phosphate buffer saline (PBS, pH 7.4) at 37 °C for 7 days. Testing of hydrogels was then performed at time intervals of 1, 3 and 7 days.

5.2.4 Permeability Performance of Hydrogels

The permeation studies were carried out at 37°C for 48 hrs, as described in detail in Chapter 3. The protein solutes examined in the studies were FITC-BSA (MW: 66 kDa, SR: 35 Å) and FITC-IgG (MW: 150 kDa, SR: 55 Å). The samples were analysed for fluorescence intensity using a microplate reader (Infinite® 200, Tecan). The solute diffusion coefficient (D) was calculated using the equation derived in Chapter 3 (eq. 3.11). The partitioning of the examined proteins between the hydrogels and the surrounding solution was determined separately by soaking hydrogels in solute solution of known concentration at 37°C. After equilibrium was reached, the remaining solution was analysed for fluorescence intensity using a microplate reader. The partition coefficient was calculated as detailed in Chapter 3(Eqn 3.12).

5.2.5 Bioactivity of Hydrogels

Heparin Bioactivity

The ability of heparin to signal growth factors was examined via assessing the proliferation of mouse B lymphocytes (BaF3) in media containing FGF-2 growth factor. BaF3 cells were grown and maintained as described by Knox et al.[332]. All hydrogel compositions were fabricated under aseptic technique from sterile macromer solutions. The sol fraction was extracted from hydrogels in RPMI-1640 media for 24 hrs prior to the assay. BaF3 cells were deprived of interleukin-3 (IL-3) cytokines by incubating them in RPMI-1640 media overnight before starting the assay. Starved BaF3 cells were then seeded onto hydrogels at a cell density of 10^5 cells/ml. Negative controls were cells in RPMI-1640 media only and in media supplemented with heparin (30nM) or FGF2 (0.3nM). In the positive control, the cells were exposed to a mixture of both heparin and FGF2. All hydrogel samples were tested with 0.3 nM FGF2 in the media solution. Controls

and samples were then incubated for 72h at 37°C. Quantification of cell number was followed using MTS CellTiter 96® Aqueous One Solution Cell Proliferation Assay (Promega, Australia). The absorbance of the colorimetric reaction assay was measured at 490 nm using a 96 well microplate reader.

Gelatin Bioactivity

- **Cell Adhesion and Proliferation**

The ability of gelatin to promote cell attachment and proliferation was assessed in hydrogels. Prior to adhesion testing, the sol fraction was extracted from all hydrogel compositions. Murine dermal L929 fibroblasts were seeded on the surface of hydrogel discs at a density of $5x10^3$ cells/ml. Cell seeded hydrogels were then incubated at 37°C for 3 days in EMEM media. After 1 and 3 days in culture, attached cells stained with Live/Dead reagents (PI/Calcein AM) were visualised using a fluorescence microscope (Carl Zeiss, Sydney, Australia). Quantitative analysis of cell proliferation was performed by counting the number of attached cells using pixilated computer software (NIH ImageJ). Positive controls were pure methacrylated gelatin hydrogels (20% w/v).

- **Cell Morphology and Cytoskeleton Organisation**

The cell behaviour on the surface of hydrogels was further studied via examining the morphology and cytoskeletal organisation of L929 cells through actin filament staining. L929 cells were seeded at the same density and conditions as was used for adhesion testing. After 1 and 3 days in culture, hydrogels were fixed in 4% formaldehyde solution and rinsed with blocking solution containing 3% (w/v) BSA and 0.5% (w/v) Tween in PBS. Samples were then treated with 0.25% (w/v) Triton X to allow for permeabilisation of the cell membrane. To stain for F-action, rhodamine phalloidin (diluted 1:1000 in blocking solution) was added. Cells were then counterstained with DAPI (diluted 1:750 in

PBS) to identify the nuclei. Visualisation of cells on the surface of hydrogels was done using fluorescence microscope (Carl Zeiss, Sydney, Australia).

5.2.6 Statistical Analysis

Statistical analysis of the results was conducted using general linear model (two-way ANOVA) with replication. Pairwise comparisons were also included using Tukey test. Analysis was performed with Minitab statistical software (Minitab Inc., version 15). All experiments were done with 3 samples and the whole experiment was repeated 3 times. Results are expressed as mean values together with their standard deviations in all tables and figures.

5.3 RESULTS

5.3.1 Physico-Mechanical Properties of Hydrogels

Swelling Properties and Network Characterisation via Equilibrium Swelling Theory

Table 5.1 shows the network parameters of PVA co-hydrogels with one ECM analogue but at lower initial percent incorporation than those studied in Chapter 4. No significant difference was observed in all the examined parameters after reducing the percent incorporated of ECM analogues into PVA network. Moreover, having both heparin and gelatin molecules in the same PVA network showed similar network characteristics as determined for pure PVA hydrogels of low and high FG/c.

Table 5.1: Sol fraction, volumetric swelling ratio, average mesh size and crosslinking density of different compositions of PVA hydrogels after 24 hours incubation in PBS.

FG/c of PVA	Hydrogel composition			Sol fraction (%)	Volumetric swelling ratio (Q)	Average mesh size* ζ (Å)	Crosslinking density ρ_x*10^4 (mol/L)
	PVA	Heparin	Gelatin				
7	20	---	---	14.08 ± 3.30	6.33 ± 0.10	94.63 ± 2.20	4.68 ± 0.10
	19.5	0.5	---	14.64 ± 3.06	6.28 ± 0.39	93.67± 5.91	4.75 ± 0.44
	19.5	---	0.5	14.63 ± 6.33	6.30 ± 0.36	94.16±5.52	4.58±0.34
	19	0.5	0.5	11.25 ± 5.35	6.19 ± 0.50	92.49 ± 7.60	4.72 ± 0.56
20	20	---	---	-4.34 ± 3.7	4.3 ± 0.1	60.74 ± 1.9	8.33 ± 0.2
	19.5	0.5	---	1.13 ± 2.26	4.23 ± 0.26	60.09 ± 4.64	8.91 ± 1.03
	19.5	---	0.5	-1.05±3.36	4.50±0.39	63.66±3.33	8.12±1.23
	19	0.5	0.5	0.91±6.11	4.62±0.20	65.20±3.60	7.96±0.67

*Calculated from the Peppas-Merrill equation.

Release of Unbound ECM Analogues

The covalent incorporation of both ECM analogues in PVA network was assessed via quantifying the release of unbound ECM analogues from the final hydrogel. Heparin is well known for providing binding sites to different proteins present in the natural ECM environment [298, 302]. Therefore heparin would be expected to interact with the gelatin when both were present in the same hydrogel network. For that reason, ensuring effective incorporation of both molecules in the final hydrogel was essential. The DMMB assay is specific for glycosaminoglycans and was used to quantify the heparin release, whereas a BCA assay specific for proteins was used to quantify the gelatin release.

The standard curves of both DMMB and Micro-BCA assays are shown in Figures 5.1 and 5.2. Each curve demonstrates the absorbance values before and after the addition of the other ECM analogue. It was observed that neither of the mixed ECM analogues

interfered with the absorbance values of the other one. Hence, both assays could be used on the same release sample without interference from the other incorporated ECM analogue Therefore, the standard curves for DMMB and Micro-BCA assays were conducted as usual for PVA co-hydrogels incorporating one or mixed ECM analogues.

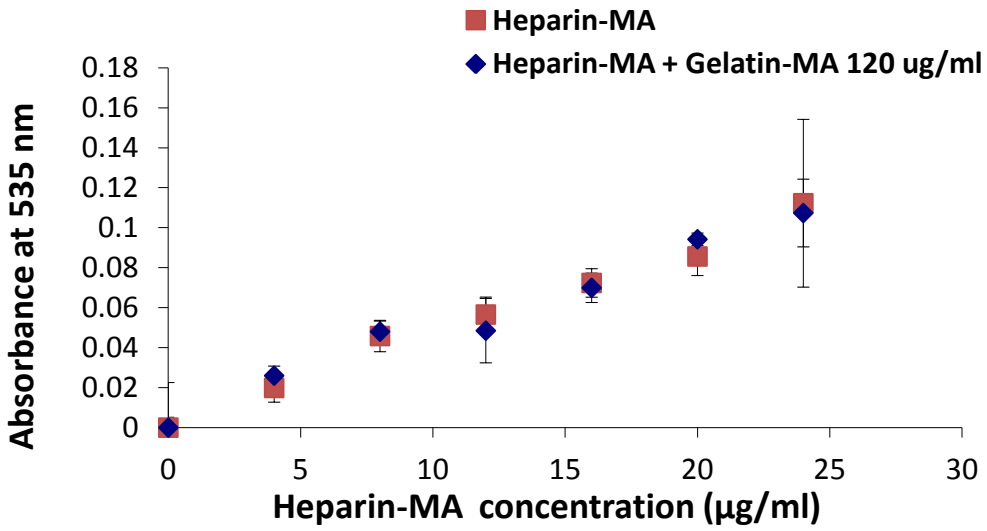

Figure 5.1: Heparin-MA standard curve via DMMB assay with and without the presence of gelatin at 120µg/ml.

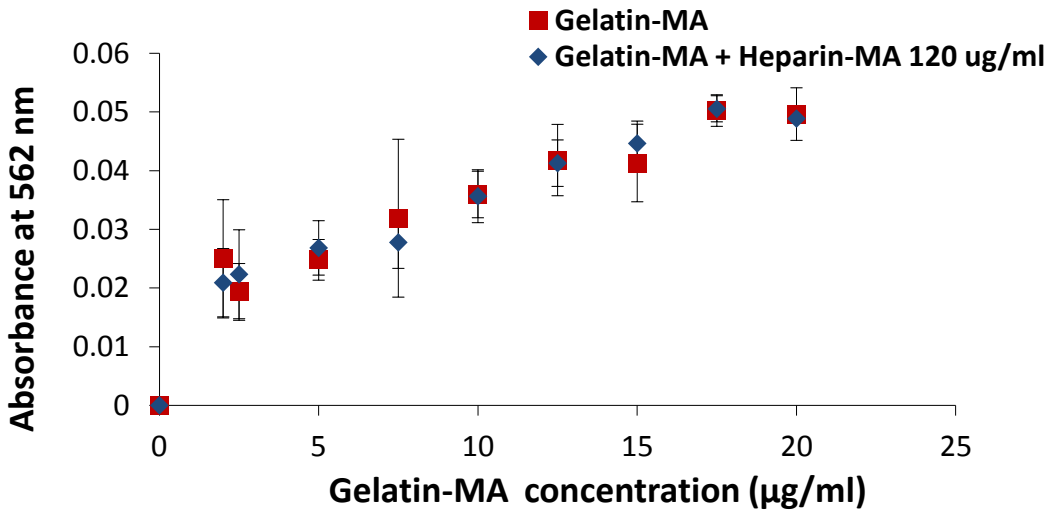

Figure 5.2: Gelatin-MA standard curve via Micro-BCA assay with and without the presence of heparin at 120µg/ml.

The amount of heparin and gelatin that was not covalently bound to the PVA network during photopolymerisation was then determined (Fig. 5.3 and 5.4). After incubation in PBS for 1 day, all the unbound heparin was released at ~ 30-35%. No significant difference was observed between day 1 and 7, or between 7 and 20 FG/c PVA. In addition, % heparin released was similar in all compositions tested with no significant difference between PVA compositions with only heparin and those mixed with gelatin (Fig.5.3).

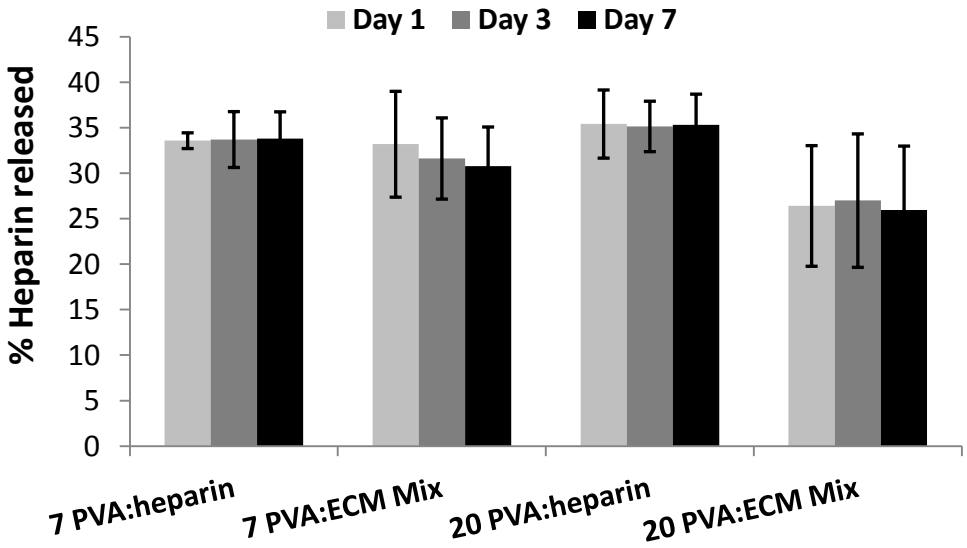

Figure 5.3: % Release values of unbound heparin from PVA:heparin (19.5:0.5) and PVA:ECM Mix (19:1) hydrogels after incubation in PBS (pH 7.4) for 7 days.

PVA:gelatin hydrogels showed maximum percent release of unbound gelatin (~ 25%) after 3 days of incubation in PBS (Fig.5.4). No significant difference was observed between day 3 and day 7 incubation results, or between 7 and 20 FG/c PVA. As observed with heparin, % gelatin released was not affected by the addition of a second biological molecule (Fig.5.4).

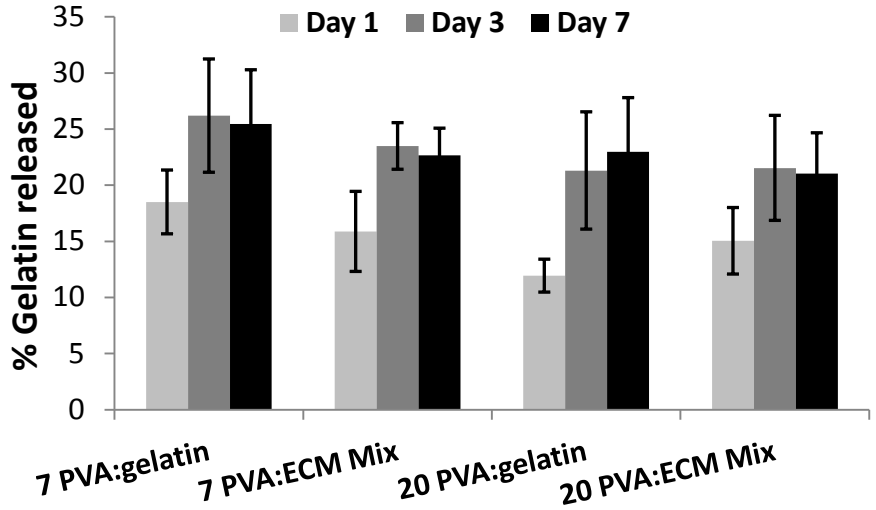

Figure 5.4: % Release values of unbound gelatin from PVA:gelatin (19.5:0.5) and PVA:ECM Mix (19:1) hydrogels after incubation in PBS (pH 7.4) for 7 days.

Table 5.2 demonstrates the equilibrium heparin and gelatin composition in all different co-hydrogels after 7 days of incubation, which were calculated based on the release values obtained. In both 7 and 20 FG/c co-hydrogels, the percent of heparin and gelatin remaining was ~ 0.3% and ~ 0.4% respectively.

Table 5.2: Average equilibrium heparin and gelatin composition (%) in the different co-hydrogels at 7 and 20 FG/c after 7 days of incubation in PBS

FG/c	Hydrogel composition (%)			Equilibrium heparin composition (%)	Equilibrium gelatin composition (%)
	PVA	Heparin	Gelatin		
7	19.5	0.5	…..	0.33	…..
	19.5	…..	0.5	…..	0.37
	19	0.5	0.5	0.35	0.39
20	19.5	0.5	…..	0.32	…..
	19.5	…..	0.5	…..	0.38
	19	0.5	0.5	0.37	0.39

Mechanical Characterisation

The effect of mixing both ECM analogues on the mechanical performance of PVA hydrogels was investigated. Mixing both ECM analogues did not interfere with the hydrogel stiffness when compared to pure PVA and PVA co-hydrogels with one ECM analogue (Fig.5.5). No significant difference was observed as a function of time (data not shown). Therefore, only the data after 7 days of incubation in PBS are shown in Figure 5.5

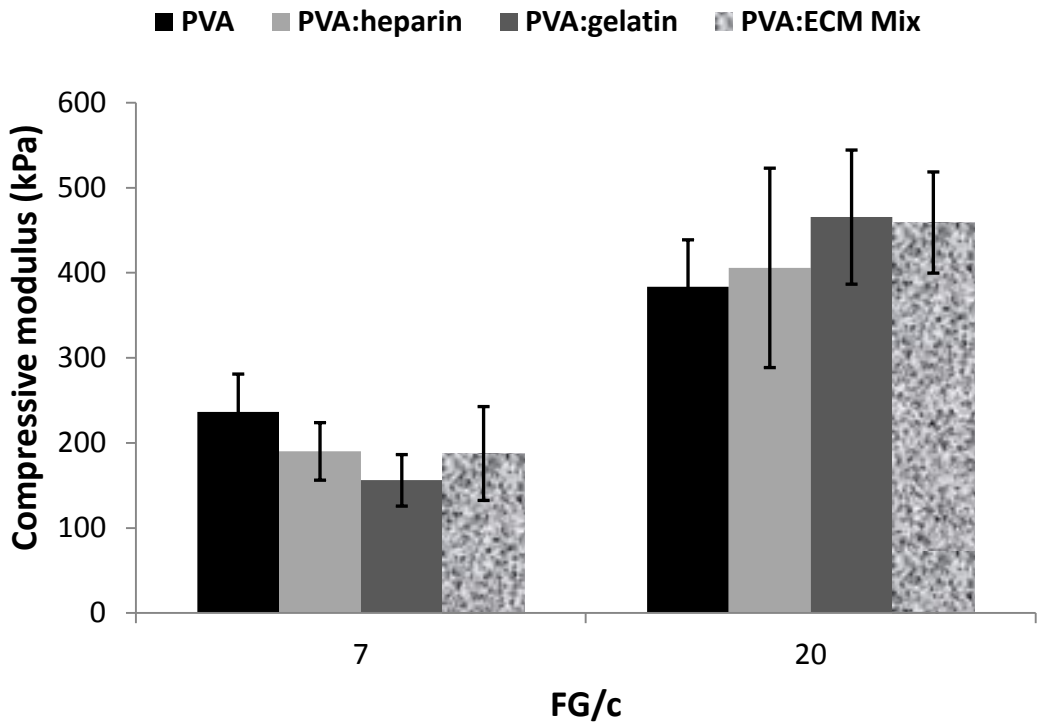

Figure 5.5: The compressive moduli of PVA 20%, PVA:heparin (19.5:0.5), PVA:gelatin (19.5:0.5) and PVA:ECM Mix (19:1) hydrogels after incubation in PBS (pH 7.4) for 7 days.

5.3.2 Permeability Performance of Hydrogels

Partition coefficient values (K) which reflect any possible interactions between examined proteins and different hydrogels compositions are presented in Table 5.3. K values examined for PVA hydrogels with only one ECM analogue (0.5%) were similar to

previously determined values (Chapter 4). K values for PVA:ECM Mix hydrogels were between the values determined for PVA:heparin and PVA:gelatin hydrogels (Table 5.3)

Table 5.3: Partition coefficient values of both BSA and IgG proteins with different hydrogels compositions: PVA:heparin (19.5:0.5), PVA:gelatin (19.5:0.5) and PVA:ECM Mix (19:1).

Protein	**Partition coefficient K**		
	PVA:heparin	**PVA:gelatin**	**PVA:ECM Mix**
BSA	0.94 ± 0.13	1.46 ± 0.30	1.24±0.11
IgG	0.93 ± 0.12	1.40 ± 0.35	1.12±0.15

The diffusion coefficient values of both BSA and IgG proteins are shown in Figures 5.6 and 5.7, respectively. There were no statistical differences between any of the samples studied. Additionally, the diffusion coefficient for the 0.5% ECM analogue/PVA gels was similar to that for the 1% ECM Mix/PVA gels.

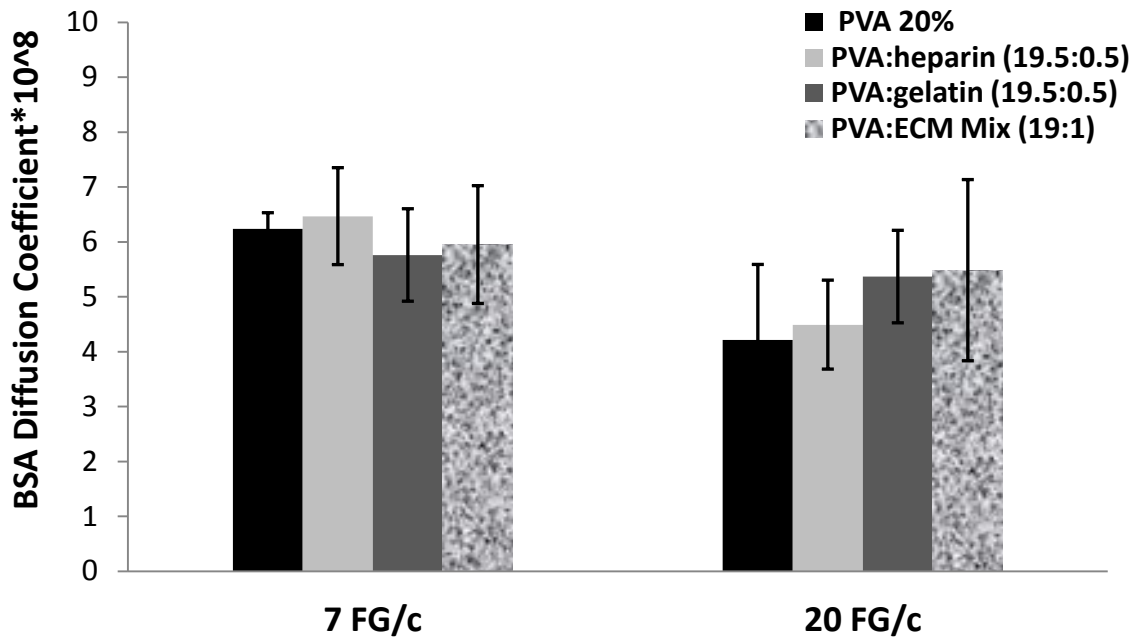

Figure 5.6: Diffusion coefficients of FITC-BSA through PVA 20%, PVA:heparin (19.5:0.5), PVA:gelatin (19.5:0.5) and PVA:ECM Mix (19:1).

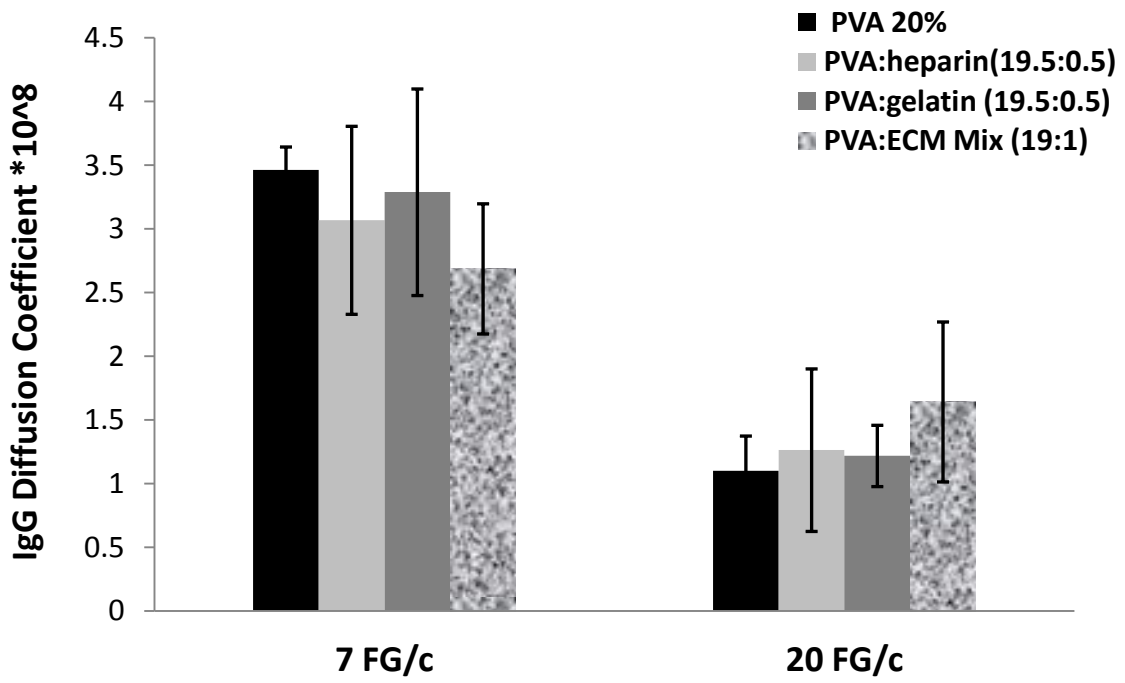

Figure 5.7: Diffusion coefficients of FITC-IgG through PVA 20%, PVA:heparin (19.5:0.5), PVA:gelatin (19.5:0.5) and PVA:ECM Mix (19:1)

5.3.3 Hydrogel Bioactivity

Heparin bioactivity

The results in the previous sections demonstrated that heparin, after being mixed with gelatin, was still retained in the same co-hydrogel matrix. However, the effect of this combination on its bioactivity needed to be assessed. Therefore, the ability of heparin to signal FGF-2 to cells having FGF receptors was tested using BaF3 cells. Proliferation of BaF3 cells reflects their ability to bind to FGF-2 presented by heparin.

Figure 5.8 shows the proliferation of BaF3 cells on pure PVA, PVA:heparin and PVA:ECM Mix hydrogels. The proliferation of cells is represented by the absorbance values of the MTS reagent. In pure PVA gels no increased cell proliferation was observed. However, in all heparin containing gels, cell proliferation was significantly higher than negative controls.

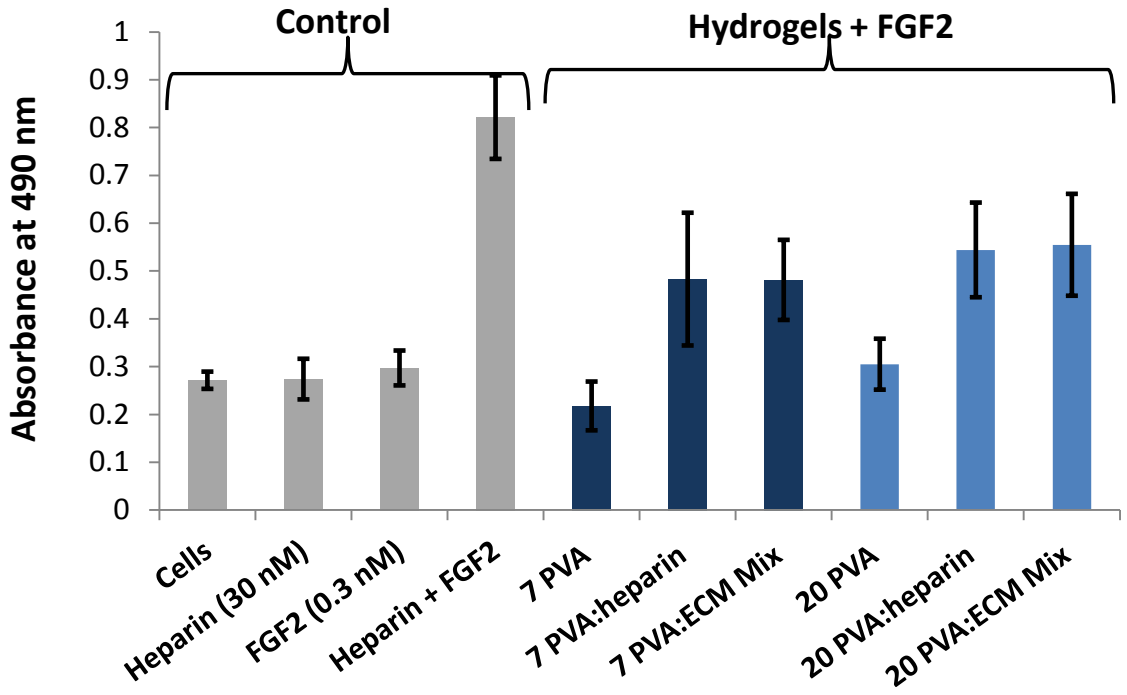

Figure 5.8: Absorbance of MTS at 490nm for BaF3 cells seeded on PVA and PVA co-hydrogels containing heparin. Negative controls are cells in media only and in media supplemented with heparin or FGF2. In the positive control the cells are exposed to a mixture of both heparin and FGF2. All hydrogels were tested with FGF2.

The effect of gelatin on BaF3 proliferation was also tested and represented in Figure 5.9. Similar to results obtained for pure PVA, PVA:gelatin hydrogels did not impact on BaF3 cell proliferation and showed MTS absorbance values comparable to negative controls used.

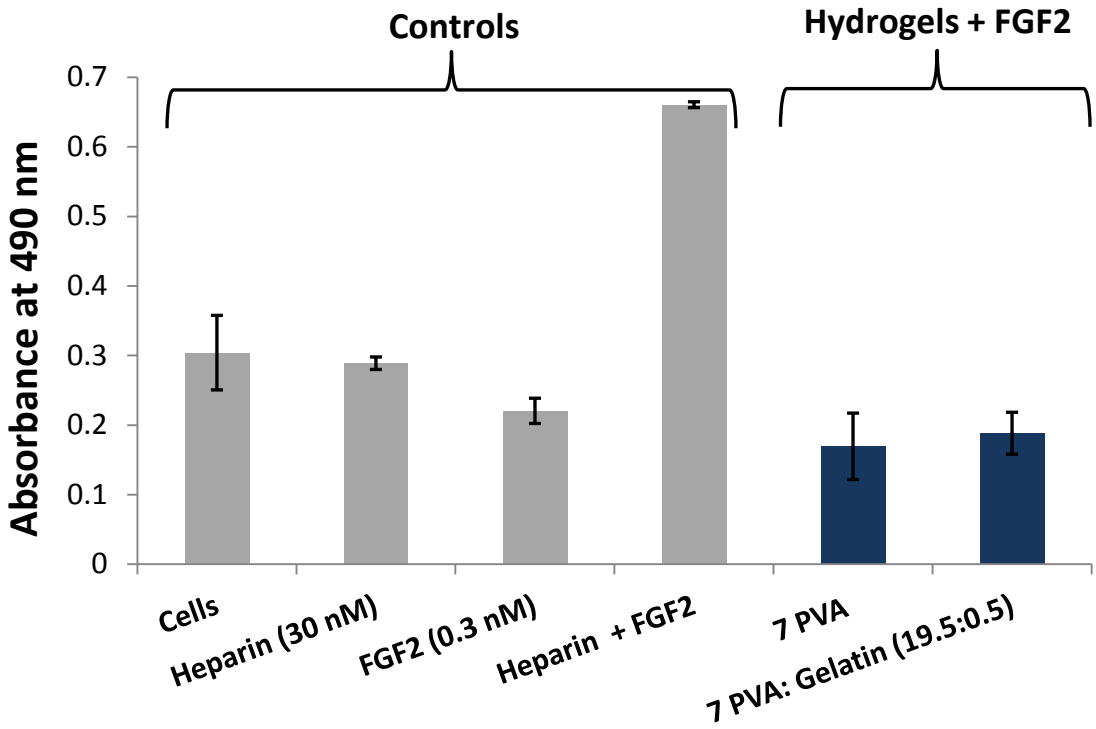

Figure 5.9: Absorbance of MTS at 490nm for BaF3 cells seeded on PVA 20% and PVA:gelatin hydrogels (19.5:0.5). Negative controls are cells in media only and in media supplemented with heparin or FGF2. In the positive control the cells are exposed to a mixture of both heparin and FGF2. Hydrogels were tested with FGF2 (n=1, Mean of 3 hydrogels ± SD).

Gelatin bioactivity

Similar to heparin, the bioactivity of gelatin in co-hydrogels with mixed ECM analogues needed to be assessed after the confirmation of gelatin retention. Therefore, the adhesive property of gelatin was tested using L929 cells that are expected to adhere and spread only onto surfaces bearing cell adhesive sequences.

Fluorescent images of live L929 cells (stained green) seeded onto the surface of different hydrogel compositions over 3 days in culture are shown in Figure 5.10. Both 7 and 20 FG/c gels demonstrated the same cell behaviour on their surfaces. Therefore, the results of only the 7 FG/c gels are presented below. All co-hydrogels containing gelatin supported L929 cell adhesion and spreading, with similar morphology to cells on pure gelatin hydrogels. Quantitative assessment of the fluorescent cell images is represented in Figure 5.11. Equivalent cell numbers were observed on hydrogel compositions containing 0.5% gelatin whether alone or mixed with heparin and on positive control hydrogels composed of 20% gelatin macromer. PVA and PVA:heparin hydrogels showed poor cell attachment at all time points.

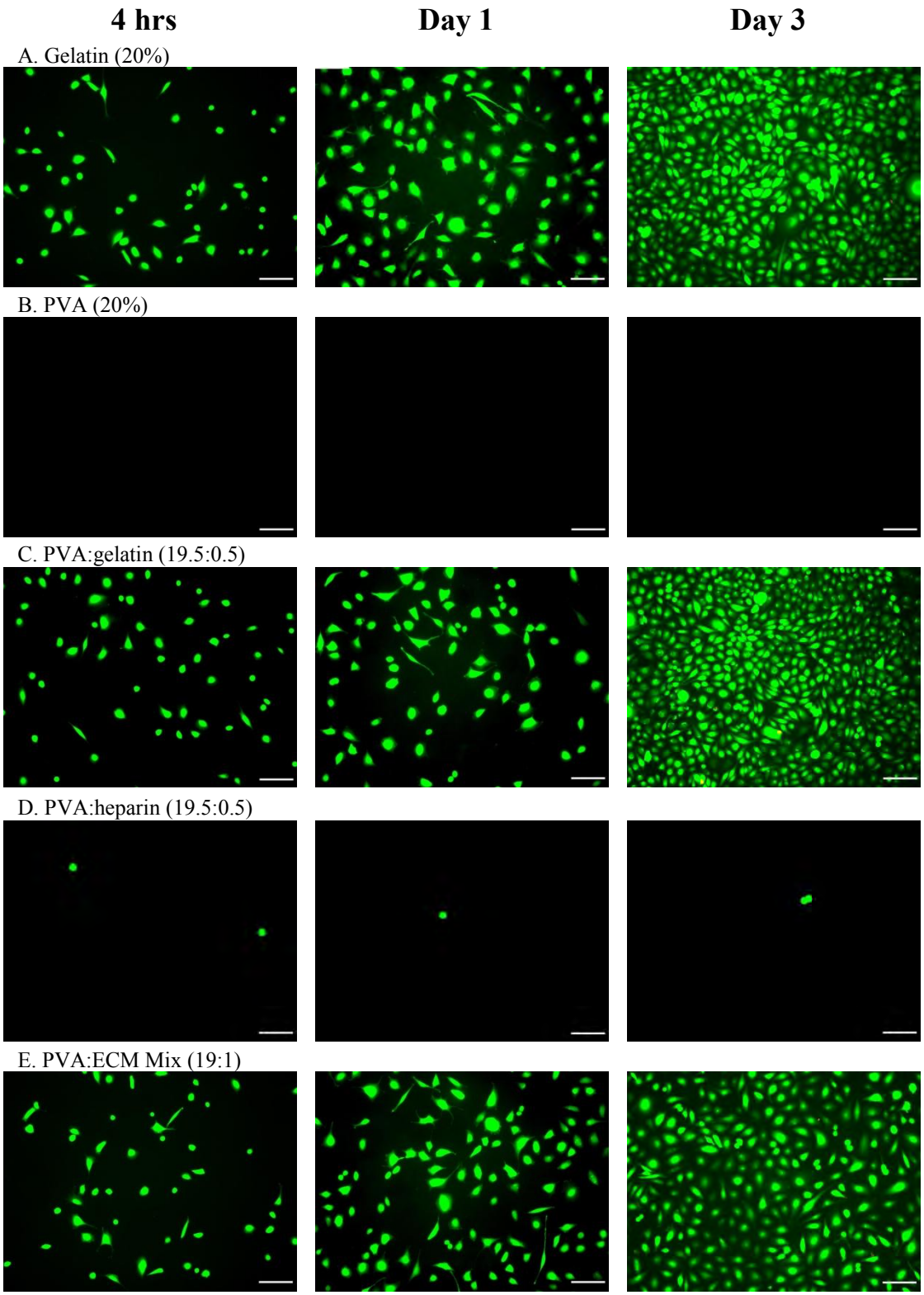

Figure 5.10: Fluorescent images (10 x) of Live/Dead double stained L929 seeded on hydrogel surfaces for 3 days. Different compositions of hydrogels examined are (A) gelatin 20%, (B) PVA 20%, (C) PVA:gelatin, (D) PVA:heparin and (E) PVA:ECM Mix (Scale bar = 100 μm).

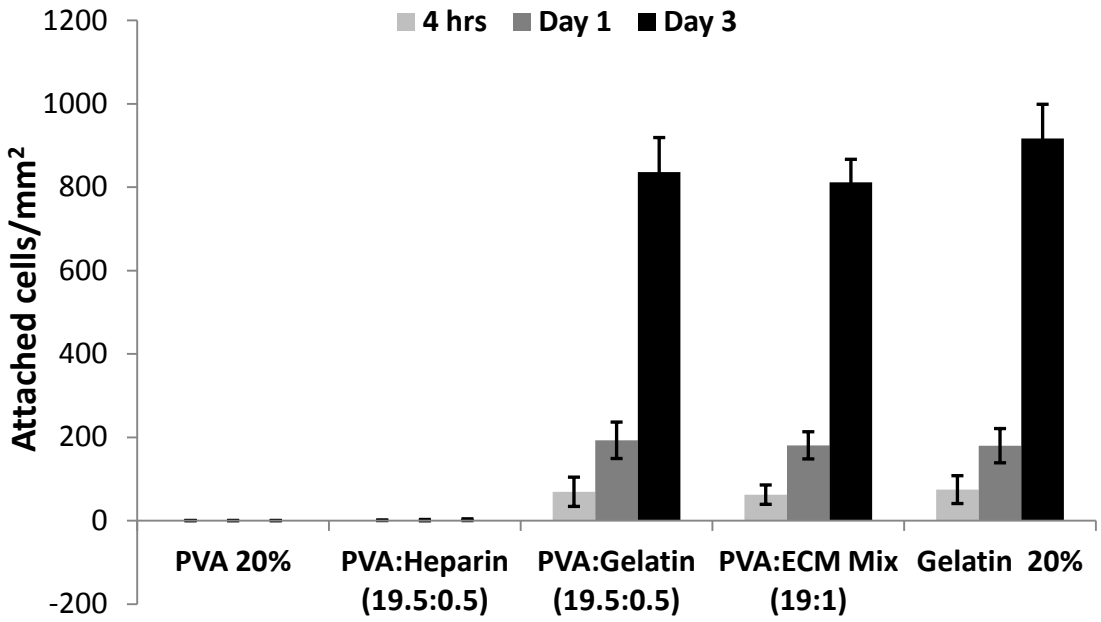

Figure 5.11: Number of attached L929 cells on PVA 20%, PVA:heparin (19.5:0.5), PVA:gelatin (19.5:0.5), PVA:ECM Mix and gelatin 20% hydrogels.

Rh-Phalloidin staining allowed for demonstrating the cytoskeletal organisation of L929 cells attached onto hydrogel surfaces via visualisation of actin filaments (Fig. 5.12). Cells adhered onto hydrogel surfaces containing gelatin were well spread, with well defined actin stress microfilaments forming a cytoplasmic network (stained red) (Fig. 5.12 A, C and E). Comparing the positive control, pure gelatin hydrogels, and PVA co-hydrogels with gelatin or gelatin mixed with heparin, no difference was detected in cell spreading or actin filaments organisation. No cells were observed on pure PVA hydrogel surfaces (Fig. 5.12 B). PVA:heparin hydrogels did not help with cell spreading on their surfaces and the small number of attached cells acquired very poorly organised actin fibers (Fig. 5.12 D).

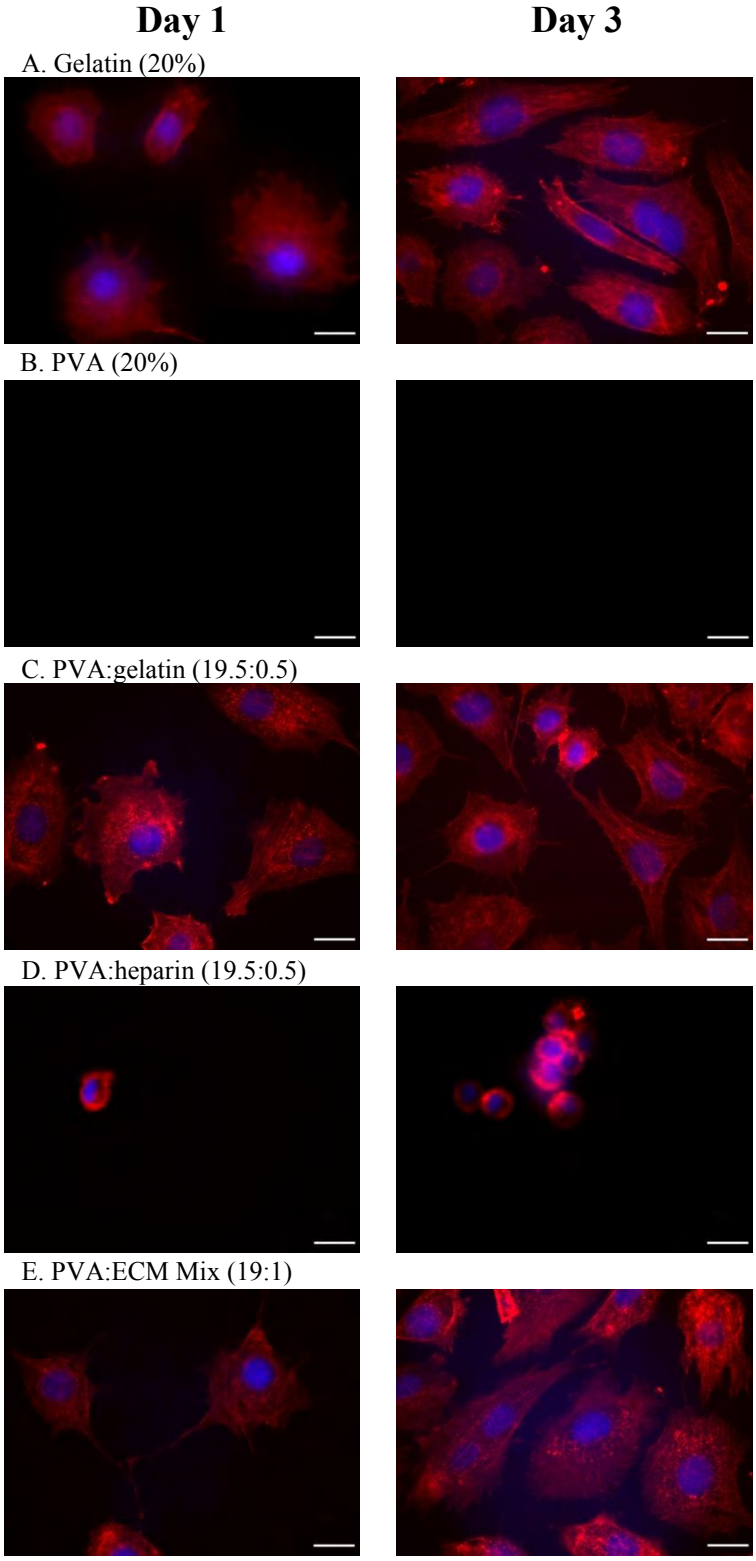

Figure 5.12: Fluorescent images (50 x) of Rh-Phalloidin and DAPI stained L929 seeded on hydrogel surfaces for 3 days. Different compositions of hydrogels examined are (A) Gelatin 20%, (B) PVA 20%, (C) PVA:gelatin, (D) PVA:heparin and (E) PVA:ECM Mix (Scale bar = 20 μm).

5.4 DISCUSSION

The current studies demonstrated the feasibility of combining more than one covalently bound ECM analogue into a PVA network while maintaining their respective biofunctionality. This combination of ECM analogues represents small scale mimicry of the diversity present in natural ECM *in vivo*. Moreover, the characteristics of the base PVA network in terms of physico-mechanical properties and permselectivity were not disrupted since both biological molecules were incorporated at small percentages.

Regarding the retention of both ECM analogues in the network, it was observed that having both ECM analogues mixed together did not interfere with their final incorporated percent in PVA network, as compared to co-hydrogels with separate ECM analogues (Fig 5.3-5.4). These results demonstrate the successful incorporation of more than one biological molecule within PVA hydrogel network. Based on the heparin nature and its ability to bind different proteins, physical binding between heparin and gelatin polymer chain would be expected after combining both polymers in one network. However, this combination did not interfere with the photocrosslinking process or the retention of both biological molecules in the final hydrogel. A recent study by Oliviero et al. reported only a minimal release of covalently bound heparin after 24 hrs in PEG hydrogel scaffolds immobilised with RGD sequences [330]. However, it was observed that heparin augmented the swelling properties of the scaffold, which was attributed to the anionic nature of heparin (as discussed in Chapter 4) as well as the possible effect of heparin interfering with the efficiency of crosslinking process. The study didn't discuss the effect of time on the release of heparin, and did not mention the effect of RGD sequence on the physical characteristics of the final scaffold or the incorporation of heparin. Despite the high percent release of both heparin and gelatin (~ 30%), they both retained their

biofunctionalities in the final co-hydrogels at final compositions of ~ 0.3-0.4%, which will be detailed below.

From the swelling and mechanical results obtained in this chapter, no significant changes were observed when comparing hydrogels with mixed ECM analogues to the ones with individual components (Table 5.1 and Fig.5.5). However, different studies combining more than one biological molecule have previously demonstrated synergistic physico-mechanical effects in the final hydrogel [320, 325-328] . As opposed to these studies in the literature where the combined biological molecules were mostly present as interpenetrating networks (IPN), both ECM analogues in this chapter were incorporated into a synthetic PVA network at very low percent (0.5%). Hence, this small percent incorporation did not show any of the previously reported possible enhanced characteristics.

Similar to the physico-mechanical characteristics findings, the permeability performance of hydrogels with mixed ECM analogues did not significantly differ from PVA alone or PVA with one ECM component (Fig. 5.6-5.7). In addition and as discussed in Chapter 4, no obvious significant interactions were observed between the examined proteins and the PVA:ECM Mix hydrogels (Table 5.3). This finding demonstrates that the ECM combination introduced into the PVA hydrogels did not interfere with its permselectivity. It has been previously shown that the diffusion of therapeutic macromolecules is controlled by the complexity of the ECM matrix, as well as on the size and structural shape of the diffusing molecules [333]. However, few studies have been reported addressing the effect of incorporating different ECM molecules into hydrogel matrices with regards to mass transport and solute diffusion. Previous work has studied the interaction and diffusion of the cationic lysozyme protein within chemically crosslinked gelatin-chondroitin sulphate hydrogels [292, 334]. Chondritin sulphate, similar to heparin

used in the current study, is another example of a GAG known for its anionic nature related to the presence of sulphate group. The combination of chondroitin sulphate with gelatin gels was found to significantly increase the lysozyme loading capacity of the gel and to prolong the release of the cationic protein due to the electrostatic interaction between the positive charges on lysozyme and negative charges chondroitin sulphate. Again, the effect of charge interactions was pronounced in this reported study due to the high percentage of biological molecules used compared to the current study.

In the current study, the proliferation of BaF3 cells on PVA:heparin hydrogels indicated that heparin retained its unique ability to sequester growth factors and present them to the cells at an actual percent incorporation less than 0.5% (~0.3%, Table 5.2). PVA hydrogels with gelatin were also tested for BaF3 proliferation and confirmed the absence of an effect on BaF3 cells, since no information was reported regarding the impact of gelatin on BaF3 cell proliferation (Fig. 5.9). Previous studies demonstrated that both methacrylated heparin and gelatin maintained their known biofunctionality after chemical modification [147, 246, 286, 335]. Heparin has been conjugated to various natural and synthetic hydrogels in order to regulate the release of growth factors or enhanced cell proliferation for various biomedical applications [336-340]. Most heparin containing hydrogels utilised large amounts of heparin, and the concentrations required remain controversial [289, 321, 341]. High concentrations may result in harmful anticoagulant side effects that could be exerted *in vivo* and the possibility of delaying the release of growth factors beyond the physiological required time. In terms of hydrogel formation, high amount of heparin may also interfere with the crosslinking process resulting in less stable hydrogels. In addition, the anionic nature of heparin is expected to be more pronounced at high percent incorporation, and thus might alter the diffusivity of proteins in a non-specific

way. Therefore, Bahkta et al. covalently bound small amounts of heparin (0.3% w/w) to a hyaluronan polymer backbone using thiol-based chemistry [289]. They demonstrated that the small percent of heparin incorporated sustained the release of bone morphogenic protein (BMP-2) and prolonged its osteogenic activity for up to 28 days. Pike et al. also have shown that the addition of less than 1% heparin to a hyaluronic acid-based hydrogel prolonged the release of VEGF and bFGF from the gel for several weeks [321]. In addition, Nilasaroya et al. found that modified heparin retained its bioactivity when incorporated into PVA hydrogels fabricated via photochemical crosslinking, at incorporation as low as 0.5% [147, 335].

In addition to the functions of heparin in sequestering growth factors, the current research demonstrated that incorporation of gelatin did confer adhesive functionality. ECM-derived molecules, such as collagen, gelatin and peptide sequences including RGD, have been commonly used to introduce adhesive properties and specific cell interactions to many natural and synthetic hydrogels, resulting in improved cell viability and functionality [286, 342-348]. The ECM proteins were usually present as a major constituent of the hydrogel matrix, affecting both functional and physical characteristics.

The combined biofunctionality of both heparin and gelatin in this study was examined at an initial percent incorporation into PVA as low as 0.5 % of each ECM analogue. Previous studies demonstrated dual functionalities exerted in systems containing both adhesive molecules and glycosaminoglycans. Recently, PEG functionalised with RGD peptide sequences was crosslinked with methacrylated heparin (PEG:heparin, 5:1) via UV irradiation to fabricate 3D porous hydrogels through a foaming process [330]. The scaffold controlled the delivery of vascular endothelial growth factor (VEGF) for 21 days. In addition, the RGD sequence supported the attachment and spreading of endothelial cells

on the surface of hydrogels. The mixed molecule scaffold was suggested as a potential system to recruit endothelial cells for studying angiogenesis as a function of VEGF release. Another group modified a photocrosslinked alginate-heparin hydrogel with RGD peptides to introduce cell adhesive functionality to the hydrogel [290]. Their results revealed that RGD peptides did not interfere with the growth factor delivery ability of the covalently bound heparin. The previous examples demonstrated that RGD sequences did not interfere with the ability of heparin to regulate the release of growth factors. However, when intact gelatin molecule was incorporated at relatively high percent, it was found to impact on the functionality of heparin. This observation was reported by Peattie et al. in hyaluronic acid-based hydrogels incorporating 0.3% w/w heparin [341]. Introduction of gelatin at 50% was found to accelerate the release of growth factors, which was attributed to the lower molecular weight of gelatin relative to long-chain HA.

In the current study, despite the null effect of gelatin on BaF3 cell proliferation, it supplemented PVA and PVA:heparin hydrogels with additional bioadhesive functionality, as observed from the live/dead and Rh-phalloidin stained L929 fluorescent images (Fig 5.10 and 5.12). Incorporation of gelatin allowed L929 fibroblasts to attach and proliferate with similar spindle-shape morphology and spreading behaviour on PVA:gelatin and PVA:ECM Mix as compared to the positive control of pure methacrylated gelatin hydrogels 20% (Fig. 5.10-5.12). This positive control was selected based on the known adhesive functionality of gelatin after methacrylation, as previously reported [246]. PVA is known to lack the ability to adhere cells on its surface due to its hydrophilic nature which prevent the adsorption of cell adhesion proteins. This was also shown in the current results, as hardly very few cells could be observed on the surface of PVA hydrogels at any time point (Fig. 5.10 C). In case of PVA:heparin hydrogels, only a few cells were observed on

the surface with rounded morphology and poorly organised filament structure, demonstrating its inability to support appropriate cell adhesion and proliferation. Similar results have been reported with other GAG molecules such as hyaluronic acid and chondroitin sulphate [325]. Consequently, it can be concluded that heparin, although unable to support cell adherence, did not interfere with the bioadhesive property of gelatin when mixed together in the same hydrogel network.

5.5 CONCLUSION

It was demonstrated that both heparin and gelatin could be incorporated as a mixture into PVA network with approximate 30% loss after photopolymerisation. Although both ECM analogues have different structural properties and possible interactions have been reported between them, their presence together did not interfere with the hydrogel characteristics (e.g. swelling, mechanics and permeability performance). These findings together with those from chapter 4, further prove that the biosynthetic system is controlled via the base PVA polymer and not the incorporated ECM components. However, the ECM analogues were able to supplement PVA hydrogels with biological functionality from two different classes of molecules, i.e., GAGs and proteins. Most importantly, both biofunctionalities were maintained in mixture at percent incorporation as low as 0.3-0.4% for each individual ECM analogue.

Since the dual functionalities of PVA co-hydrogels have been demonstrated in this chapter without disrupting the base permselectivity, the ability of such a system to enhance the survival of encapsulated cells needed to be assessed. The multi-component hydrogel is proposed to be used as a bioactive immunoisolating membrane for cell based therapy.

Accordingly, chapter 6 will examine the application of PVA co-hydrogels for cell encapsulation at two different functional group densities 7 and 20 FG/c.

Chapter 6

Functional evaluation of biosynthetic PVA hydrogels: Understanding the balance between permselectivity and cell survival

6.1 INTRODUCTION

Thus far, it has been shown that by systematically increasing the functional group density on the PVA backbone, the permeability performance of PVA based hydrogels could be tailored for immunoisolation purposes, and that biological functionality could be imparted to those gels through the co-incorporation of small amounts of heparin and gelatin. The current chapter aims to investigate the suitability of these UV photocrosslinked biosynthetic PVA hydrogels as a potential material for cell encapsulation by understanding the balance between hydrogel permselectivity and pancreatic cell survival.

This chapter focuses on encapsulation of a model pancreatic β-cell line (MIN6) and insulin release *in vitro*. The two commonly studied synthetic polymers for pancreatic cell encapsulation are PEG and PVA. Burczak et al. fabricated crosslinked PVA hydrogels via chemical and radiation crosslinking with tailored permeability to different proteins including glucose, insulin, BSA and proteins [137]. Their system, however, used harsh crosslinking conditions which might affect the long term survival of encapsulated cells. Qi et al. initiated the islet-sheet macroencapsulation technique using PVA hydrogels via the freeze/thawing method that has recently shown promising results in islet allotransplantation and cryopreservation [129, 349, 350]. However, the physical characteristics, including the permeability performance, of this system have not been investigated. It is believed that tailoring the permeability through a freeze/thawing technique would negatively impact on the cell encapsulation process.

From the reviewed PVA encapsulation systems to date, UV photopolymerised PVA hydrogels have not been widely investigated for pancreatic cell encapsulation. However, this system has proven potential for cell applications where photopolymerisation is

performed under physiological and cytocompatible conditions [147, 259, 309]. Only one study reported by Iwata et al. [351] was found to successfully encapsulate pancreatic islets in a photocrosslinkable PVA bearing styrlpyridinium group (PVA-SbQ). The study showed the ability of encapsulated islets to maintain viability and ability of insulin secretion over 6 weeks post implantation in the peritoneal cavity. However, no details were reported regarding the network characteristics or permeability performance of the hydrogel system.

Several reported immunoisolating membranes highlighted the insulin permeability as an indication of good mass transport of the proposed systems for islet encapsulation. Burczak et al. studied the permeation of different proteins through PVA hydrogels crosslinked by glutaraldehyde or radiation and demonstrated that increasing hydrogel water content enhanced the diffusion of small molecules such as glucose and insulin [112, 137].

Kurian et al. fabricated a tricomponent PEG/polypentamethylcyclopentasiloxane (PD5)/polydimethylsiloxane (PDMS) hydrogel membranes for the purpose of immunoisolation via macroencapsulation [352]. They enhanced the permeability of insulin by increasing the molecular weight (MW) of the hydrophilic PEG domain, where P increased from 3.1 x 10^{-8} to 4.8 x10^{-7} when PEG MW increased from 4600 to 20,000 g/mol respectively. Insulin permeability was directly related to hydrophilicity of the composite due to the water solubility of insulin. The same concept of increasing hydrophilicity was also used in a precision-synthesised amphiphilic co-network (APCN) membranes recently developed as a bioartificial pancreas [267]. The rate of insulin diffusion was increased via increasing the molecular weight of the hydrophilic segment (Poly N, N-dimethyl acrylamide, PDMAA) between two crosslinking sites.

Despite the essential role of permselectivity to the success of a cell encapsulating device, few studies have discussed the challenging balance between permselectivity and pancreatic cell survival in hydrogel systems. Cruise et al. reported attenuation of insulin secretion from islets encapsulated in PEG hydrogels with high macromer concentration (25%), while higher rates of insulin secretion were observed in low macromer concentration hydrogels (10-13%) [353]. Weber et al. also demonstrated that islets encapsulated in PEG hydrogels had a delayed release of insulin within the first hour of a glucose challenging test, which was directly related to an increase in PEG macromer molecular weight [240]. Therefore, in the current study, the effect of increased functional group density in PVA networks on the performance of encapsulated functioning β-cells was investigated via studying the insulin diffusion.

As it was previously highlighted that purely synthetic hydrogels are unable to maintain the viability of encapsulated cells due to lack of biological signals, various efforts in islet encapsulation have focused on supplying the synthetic network with natural matrix functionalities via incorporation of ECM components that are specific to pancreatic islets. Intact ECM proteins, such as collagen type IV and laminin were entrapped in PEG hydrogels and were shown to enhance viability and functionality of encapsulated β-cells over ~28 days [10, 34]. In addition, the covalent incorporation of peptide sequences in PEG gels improved the viability and insulin secretion of β-cells compared to pure PEG hydrogels, although to a lower extent than intact ECM proteins [34, 143, 146]. However, the use of short peptide sequences was questioned recently, as the full replication of a natural ECM environment is difficult in peptide-based systems [354]. Alternatively, the current study focuses on providing biological cues to encapsulated cells by the covalent coupling of ECM analogues within a PVA hydrogel network.

Despite the previous studies emphasising the importance of adding ECM components in islet encapsulation devices, little is known regarding the interaction of ECM components, such as GAGs and proteins, with the insulin released from the cells and how ECM components can influence insulin diffusion within cell encapsulating hydrogel systems. The binding affinity of heparin to insulin has been recently reported after demonstrating the ability of heparin to suppress insulin aggregation [355, 356]. It has been also suggested that since heparin is commonly known of its binding affinity to insulin-like growth factors [357], parts of its backbone chain would also possess binding domains for insulin [355]. Earlier, insulin has shown to bind different ECM proteins including collagen, fibronectin, vitronectin and laminin [358]. The strongest affinity of insulin to these proteins has been observed with collagen type V. Hence, similar behaviour of insulin with gelatin protein is expected in the current study. Therefore, the effect of incorporated heparin and gelatin on insulin release and diffusion within hydrogels will be examined.

This chapter investigates the capability of multi-component biosynthetic hydrogels to support the viability of encapsulated cells and the release of their therapeutic products through the following specific aims:

1. Examine the permeability of β-cell therapeutic product, insulin, within the multi-component biosynthetic hydrogels with low and high crosslinking densities.
2. Assess the viability and metabolic activity of β-cells encapsulated in the biosynthetic hydrogels with separate and mixed ECM analogues

6.2 MATERIALS AND METHODS

6.2.1 Materials

All materials and solvents used for macromer synthesis and hydrogel fabrication have been mentioned in the previous Chapters 3, 4 and 5. For cell culture, Eagle's minimum essential media (EMEM), used for murine L929 fibroblasts culture, and Dulbecco's minimum essential media (DMEM), used for MIN6 insulinoma culture, were purchased from Sigma-Aldrich and supplemented with 10% fetal bovine serum (FBS, SAFC biosciences), 1% penicillin streptomycin (PS, Sigma-Aldrich). DMEM media was additionally supplemented with 1% L-Glutamine (Invitrogen Australia). Propidium iodide (PI) and calcein AM for Live/Dead double staining and adenosine 5′-triphosphate disodium salt solution (ATP) were purchased from Sigma-Aldrich. CellTiter-Glo® Luminescent Cell Viability Assay was from Promega Australia. Ultra Sensitive Mouse Insulin ELISA kit was used as per the protocol provided from Crystal Chem Inc, USA.

6.2.2 Hydrogel Formation

Hydrogels were fabricated using UV light curing as previously described in Chapter 3. All hydrogels were made at 20 wt% total macromer, and were either pure PVA, PVA:heparin (19.5:0.5), PVA:gelatin (19.5:0.5) or PVA:ECM Mix (19:1).

6.2.3 Insulin Diffusion within the Hydrogels

Insulin Permeation Studies and Partition Coefficient Determination

Permeation studies were carried out for all hydrogels with 7 and 20 FG/c at 37°C for 48 hrs. The study was conducted at the same conditions used in the previous chapters in order to allow for comparison between diffusion of insulin and larger BSA and IgG proteins. The solute examined was FITC-Insulin (MW: 5808 g/mol, SR: 11.9 Å). The samples were analysed for fluorescence intensity using a microplate reader (Infinite® 200,

Tecan). The solute diffusion coefficient (D) and partition coefficient (K) were determined as detailed in Chapter 3

In vitro Release of Insulin

Although insulin diffusion can be ensured from the permeability study, the time required for complete release of insulin from cells encapsulated in hydrogels needed to be investigated. A GSIS test, where the cells were exposed to different levels of glucose for a specified period of time, is the most common method of measuring insulin secretion from cells. However, the GSIS is normally just done on cells in solution and therefore it was important to examine the effect of hydrogel materials on the release of insulin by using an *in vitro* release study. Insulin release from thin hydrogels (8mm diameter x 0.5mm thick) was studied over a short time period (140 min) with a loading concentration of 0.1 mg/ml. Hydrogels loaded with fluorescently labelled insulin were immersed in 1 ml PBS as a release medium and shook at 37°C. The release was continued for a period of 140 min. 100 µl of the release medium was withdrawn every 20 min and replaced with an identical volume of fresh PBS. The withdrawn samples were analysed for fluorescence intensity using a microplate reader.

6.2.4 Cell Studies

Cell Growth Inhibition Testing of PVA Macromers

Solutions of prepared macromers and unmodified PVA in PBS (4 mg/ml) were filter sterilised and diluted to a concentration of 1mg/ml with EMEM containing 10% FBS and 1% PS. Murine L929 fibroblasts were seeded onto 35 mm^2 culture dishes at a concentration of 5 x 10^4 cells/ml. Cells were then incubated at 37°C in 5% CO_2 humidified atmosphere for 24 hours. The media was then discarded and solutions of samples or controls were added. A negative control (media only) and a positive control (7.5% ethanol)

were used for comparison. After incubation for 48 hours, cells were detached from the dishes by trypsinisation and their numbers counted by a cell viability analyser (Vi-Cell XR, Beckman Coulter). Cell growth inhibition was then calculated as a percentage compared to the negative control using the following equation:

$$\text{Cell growth inhibition (\%)} = 1 - \frac{\text{number of cells in test sample}}{\text{number of cells in media}}$$

MIN6 Cell Encapsulation

MIN6 insulinoma cells[2] were cultured in DMEM media with high glucose content. At 80% confluence, cells were trypsinised and dispersed in sterile DPBS prior to macroencapsulation. All macromer solutions were prepared in sterile DPBS and mixed with the cell suspension, giving a final cell concentration of 10^7 cells/ml. Sterile photoinitiator (I2929) was then added at 0.05 wt% and followed by UV curing of the cell-macromer mixture at 30 mW/cm^2 for 3 min. All cell encapsulating hydrogels were made at 20 wt% total macromer, and were either pure PVA, PVA:heparin (19.5:0.5), PVA:gelatin (19.5:0.5) or PVA:ECM Mix (19:1). Hydrogel discs were fabricated using thin sterile moulds (0.5mm thick, 8mm diameter). Unencapsulated cells were used as control in every experiment and cultured at 10^5 cells/ml using tissue culture plates (TCP). Hydrogels and cell controls were incubated in DMEM media (37°C, 5% CO_2) for 14 days and replaced with fresh media every 2 days. Cell controls and hydrogel samples were characterised at different time points: 1, 4, 7 and 14 days to assess cell behaviour within the study period.

[2] The MIN6 mouse insulinoma cell line was a kind gift from Dr Jenny Gunton (The Garvan Institute, Sydney) and permission for its use was granted by Dr Jun-ichi Miyazaki (Kumamoto University Medical School, Japan).

6.2.5 Assessment of Cell Behaviour in Hydrogels

Cell Morphology and Viable Cell Number

At predetermined time points, encapsulated cells were examined morphologically using Live/Dead cell double staining reagents (PI/Calcein AM) applied for 10 min after washing the samples with DPBS. Stained samples were then visualised using a fluorescence microscope (Carl Zeiss, Sydney, Australia). Quantitative analysis of cell proliferation was performed by determining the live cell area coverage (%) using pixilated computer software (NIH ImageJ).

Cell Metabolic activity

The ability of MIN6 cells to maintain their metabolic activity was measured using the ATP assay. CellTiter-Glo® Luminescent Cell Viability Assay is a recently developed assay to detect cell metabolic activity based on quantifying the ATP produced from metabolically active cells. The assay mixture results in cell lysis and generation of a luminescent signal proportional to the amount of ATP present. The ATP assay has proven to be a highly accurate and sensitive quantitative measure of metabolic activity, especially at low cell numbers compared to other cell quantitative techniques such as MTS and MTT [359-361]. After removal of culture media, both hydrogel samples and cell controls were allowed to react under orbital shaking conditions for 1hr with CellTiterGlo reagent diluted 1:1 in DPBS. Resulting luminescence was measured using a microplate reader. Luminescence readings were then compared to standard curve constructed using different standard ATP dilutions.

Optimisation of Static Glucose Stimulated Insulin Secretion

In order to correlate the free insulin release results with the actual insulin produced and released by MIN6 cells, an optimisation of the Glucose Stimulated Insulin Secretion

(GSIS) study was conducted for the glucose responsiveness of MIN6 cells encapsulated in co-hydrogels. This was done to determine the slowest *in vitro* insulin release rate from encapsulated cells. The glucose responsiveness of MIN6 cells encapsulated for relatively a long period was determined by static glucose stimulation at day 14. Insulin released from MIN6 cells was measured in response to varying glucose concentrations (1mM and 25mM) and normalised to total cell insulin content.

The time required for incubation with each glucose concentration was tested with the highly crosslinked PVA:heparin hydrogel samples compared to cell controls. Glucose response was assessed after 1, 1.5, 2 and 2.5 hrs incubation to select the shortest time required for maximum insulin secretion. In a typical GSIS assay, samples were incubated in low glucose DMEM solution (1mM) (200 µl for hydrogels and 1ml for cell controls). The same samples were then exposed to an equal volume of higher glucose DMEM solution (25mM) for the same amount of time. The supernatant collected after incubation with each glucose level was stored at -20°C for further insulin analysis. 1ml of acid ethanol was then added to each cell sample and the mixture stored at -20°C to allow for total insulin extraction from MIN6 cells. The insulin content of collected samples from the static glucose stimulation and acid ethanol extraction was determined by Enzyme Linked Immuno Sorbant Assay (ELISA) using the ELISA kit protocol provided by CrystalChem.

6.2.6 Statistical analysis

Statistical analysis of the results was conducted using a general linear model (two-way ANOVA) with replication. Pairwise comparisons were also included using Tukey test. Analysis was performed with Minitab statistical software (Minitab Inc., version 15). All experiments were done with 3 samples and the whole experiment was repeated 3 times.

Results of hydrogel characterisation are expressed as mean values together with their standard deviations. Since cell experiments did not follow normal distribution, Poisson distribution was considered in the analysis and thus values of standard error of the mean (SEM) were indicated as error bars in all graphs presented.

6.3 RESULTS

6.3.1 Insulin Diffusion within Hydrogels

Partition Coefficient and Permeation of Insulin

Partition coefficient values (K) of insulin with the different hydrogel compositions are presented in Table 6.1. K values were not affected by the change in the number of FG/c. All K values were approximately 1 without statistically significant differences although slightly higher values were observed with co-hydrogels. 7 FG/c showed higher diffusion of insulin compared to 20 FG/c although not significant. In addition, no significant difference was observed in the diffusion coefficient values between the different hydrogel compositions.

Table 6.1: Partition and diffusion coefficient values of insulin with different hydrogels compositions: PVA (20%), PVA:heparin (19.5:0.5), PVA:gelatin (19.5:0.5) and PVA: ECM Mix (19:1).

Composition	FG/c	Partition coefficient (K)	Diffusion coefficient (D) x 10^8 (cm^2/sec)
PVA 20%	7	1.02± 0.60	20.31± 3.67
	20		13.29 ± 1.96
PVA:heparin (19.5:0.5)	7	1.70±0.23	19.90± 4.45
	20		11.76±3.58
PVA:gelatin (19.5:0.5)	7	1.21±0.66	19.53±3.72
	20		14.90±2.83
PVA:ECM Mix (19:1)	7	1.33±0.73	17.79±2.75
	20		13.77±3.83

In vitro release of insulin

Release data obtained for insulin loaded hydrogels are shown in Figures 6.1-6.4 with the time to 100% release shown in Table 6.2. *In vitro* release was assessed in comparison to the control free insulin, which showed immediate dissolution. All hydrogels showed monophasic release profiles with 100% release attained between 1-2 hrs. Two factors appeared to influence the insulin release from hydrogels: the functional group density and the presence of ECM analogues. Although the release rate of insulin was lower from pure PVA hydrogels with 20 FG/c in the first hour of release, no difference was observed between the two functional group densities when ECM analogues were added. PVA:heparin hydrogels were observed to have the slowest insulin release rate where 100% release was reached at 2 hrs. All other hydrogels released their insulin within 80-100 min.

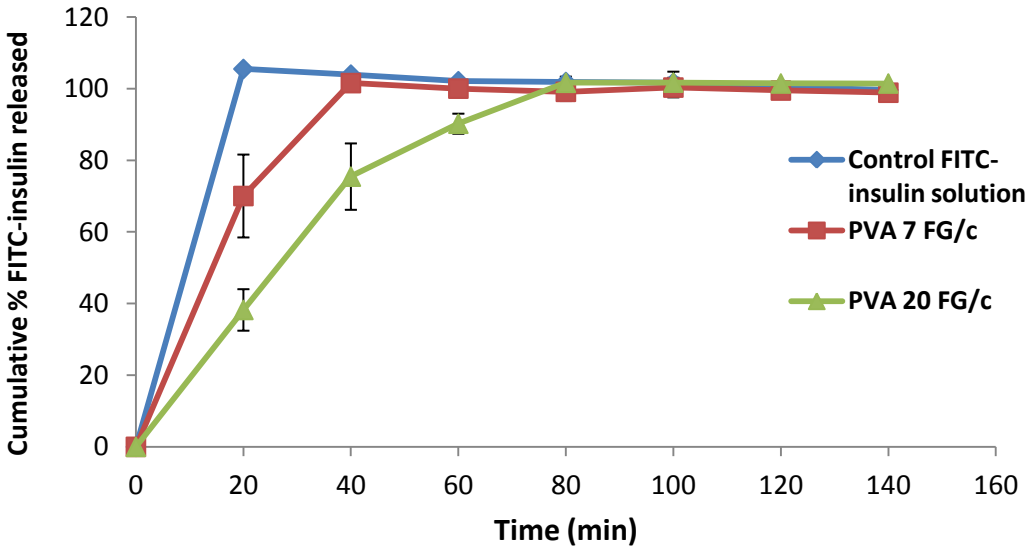

Figure 6.1: Cumulative % release profiles of insulin from pure PVA hydrogels at 37 °C over 140 min study period. Lines were drawn to guide the eye.

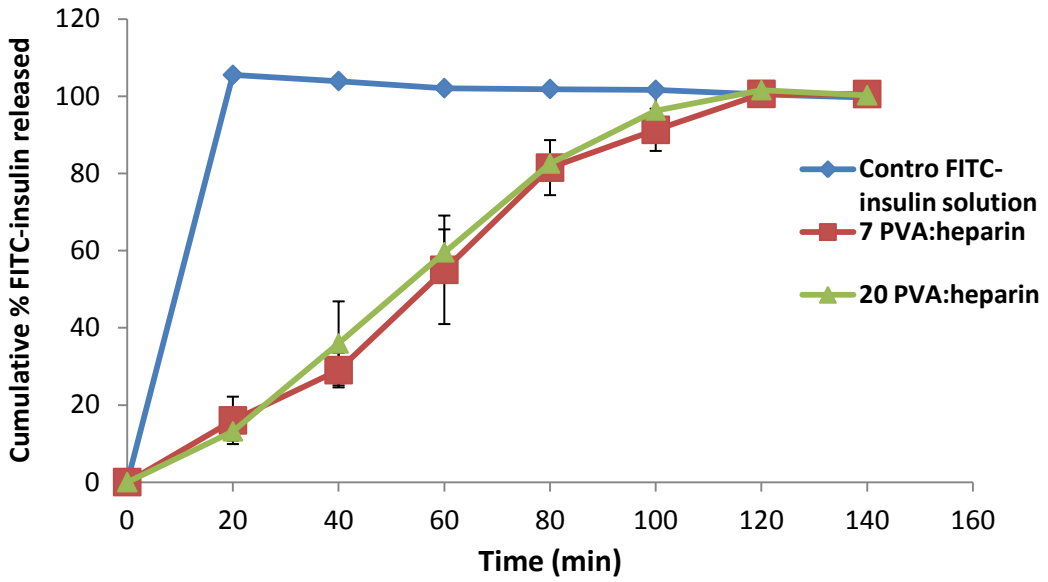

Figure 6.2.: Cumulative % release profiles of insulin from PVA:heparin hydrogels at 37 °C over 140 min study period. Lines were drawn to guide the eye.

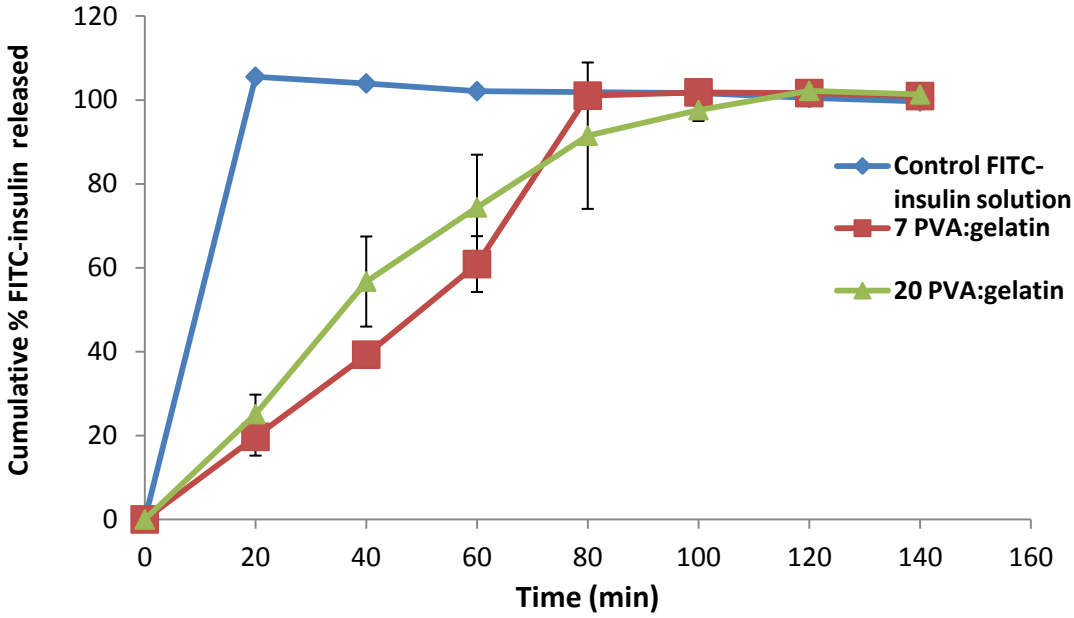

Figure 6.3: Cumulative % release profiles of insulin from PVA:gelatin hydrogels at 37 °C over 140 min study period. Lines were drawn to guide the eye.

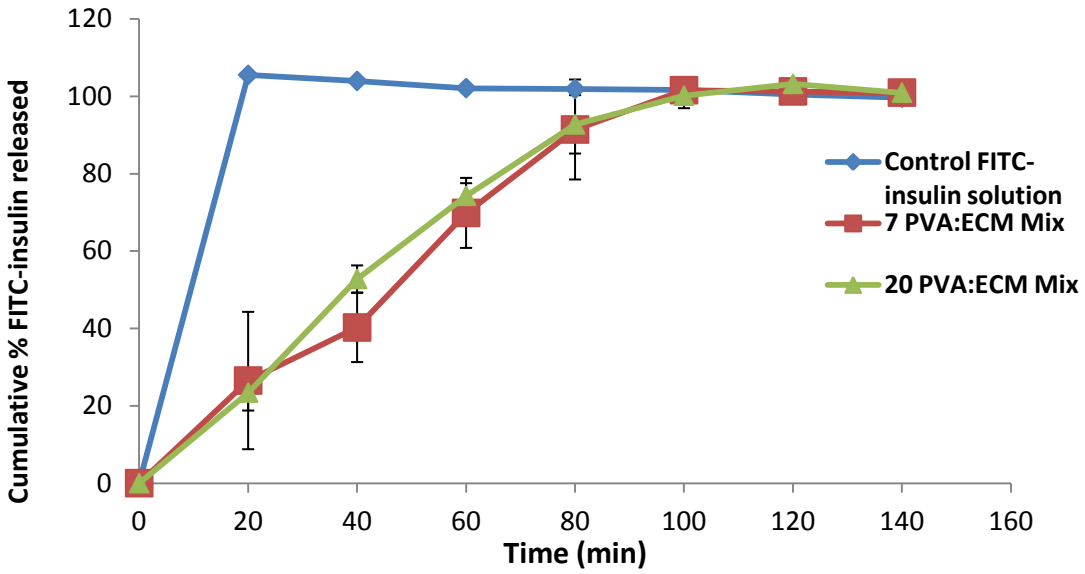

Figure 6.4: Cumulative % release profiles of insulin from PVA:ECM Mix hydrogels at 37 °C over 140 min study period. Lines were drawn to guide the eye.

Table 6.2: Time to 100% insulin release showing the effect of functional group density and different hydrogel compositions

FG/c	Hydrogel composition			Time to 100% insulin release (min)
	PVA	Heparin	Gelatin	
7	20	.....	.....	40
	19.5	0.5		120
	19.5	.....	0.5	80
	19	0.5	0.5	100
20	20	.....	.....	80
	19.5	0.5	.....	120
	19.5	.....	0.5	100
	19	0.5	0.5	100

6.3.2 Cell Studies

Cell Growth Inhibition Testing of PVA Macromers

The cell growth inhibition test investigates the effect of macromers on normal cell growth compared to negative and positive controls. Figure 6.5 shows the percent cell

growth inhibition at the end of the test period for macromers with different FG/c and unmodified PVA. Ethanol 7.5% was used as a positive control to validate the assay and showed a marked inhibition of cell growth with 89% (± 3.5). Analysis of variance showed no significant difference between unmodified PVA (precipitated and cleaned in the same way as for tested macromers) and the macromers with different FG/c ($p>0.05$)

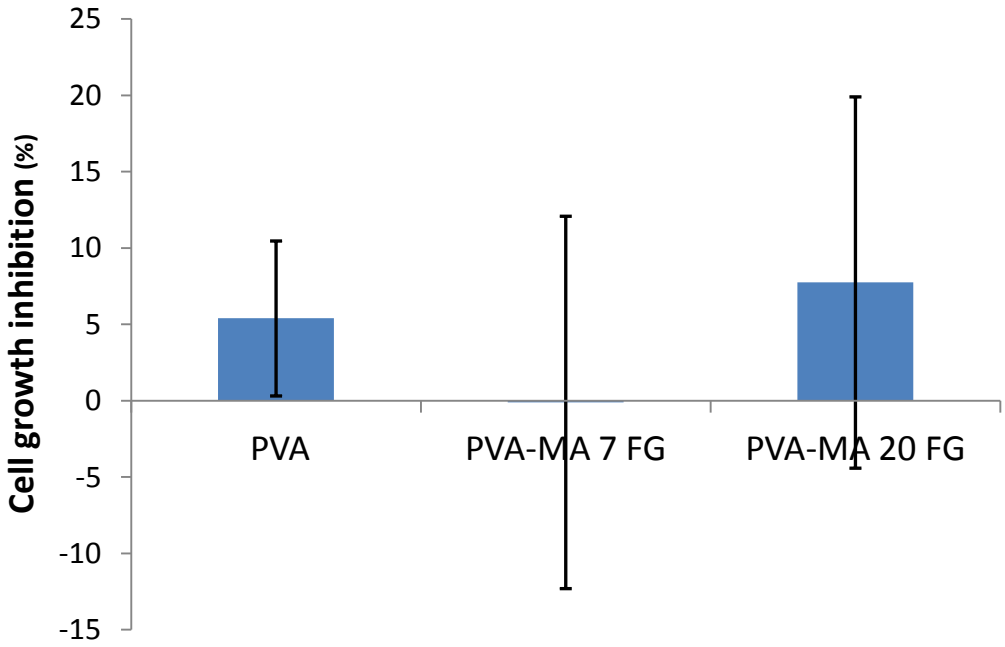

Figure 6.5: Cell growth inhibition profile of L929 fibroblasts in unmodified PVA and macromers with 7 and 20 FG/c compared to media only (null).

Viability of MIN6 cells

Fluorescent images of MIN6 cells (live cells stained green, dead cells stained red) encapsulated within different hydrogel compositions for 14 days are shown in Figures 6.6-6.7. Both 7 and 20 FG/c hydrogels indicated similar cell morphology and behaviour and thus only the results from the 7 FG/c are shown.

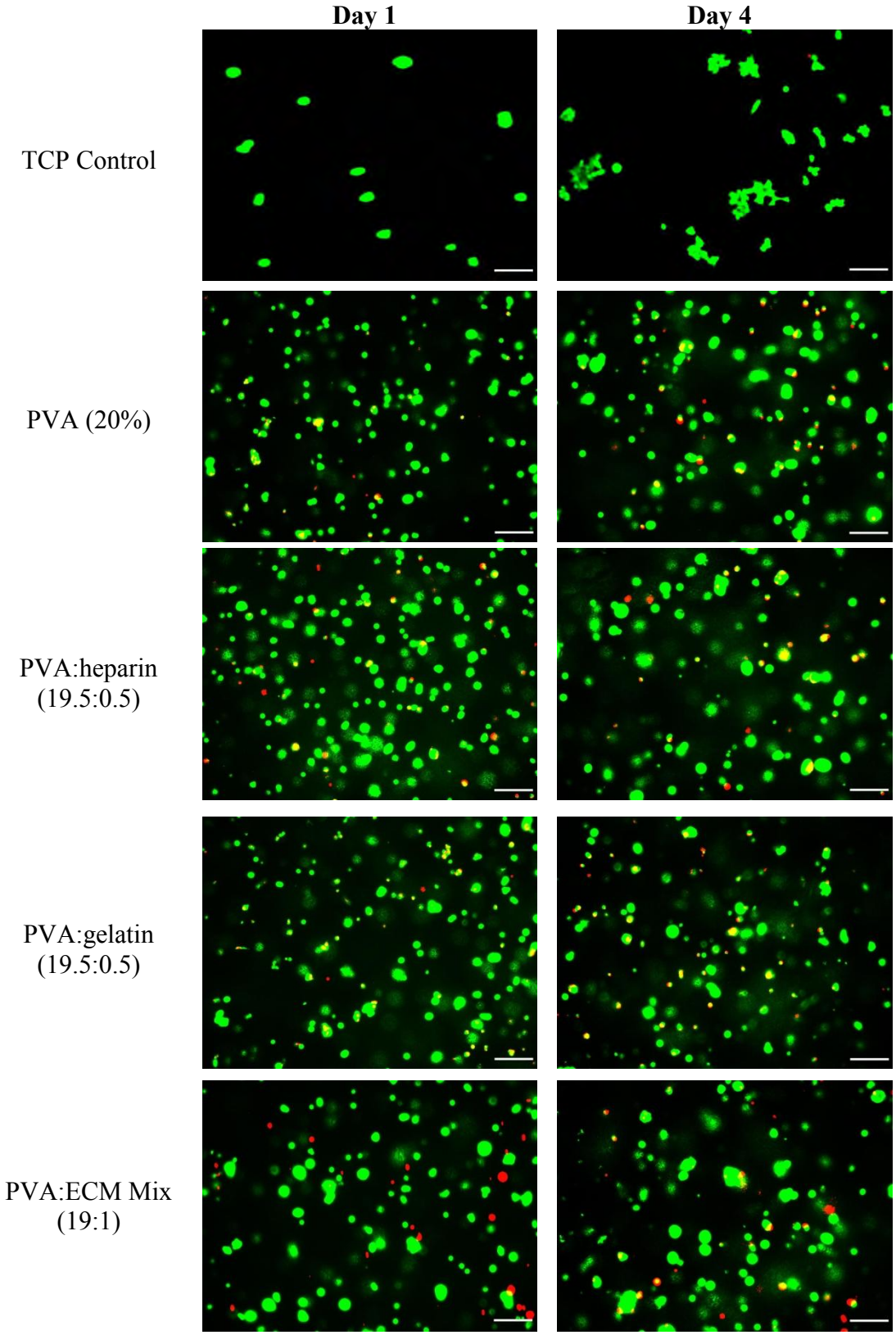

Figure 6.6: Fluorescent images (10x) of Live/Dead stained MIN6 cells encapsulated in PVA 7 FG/c hydrogels for 1 and 4 days. Cell controls grown on TCP are added for comparison (Scale bar = 100 μm).

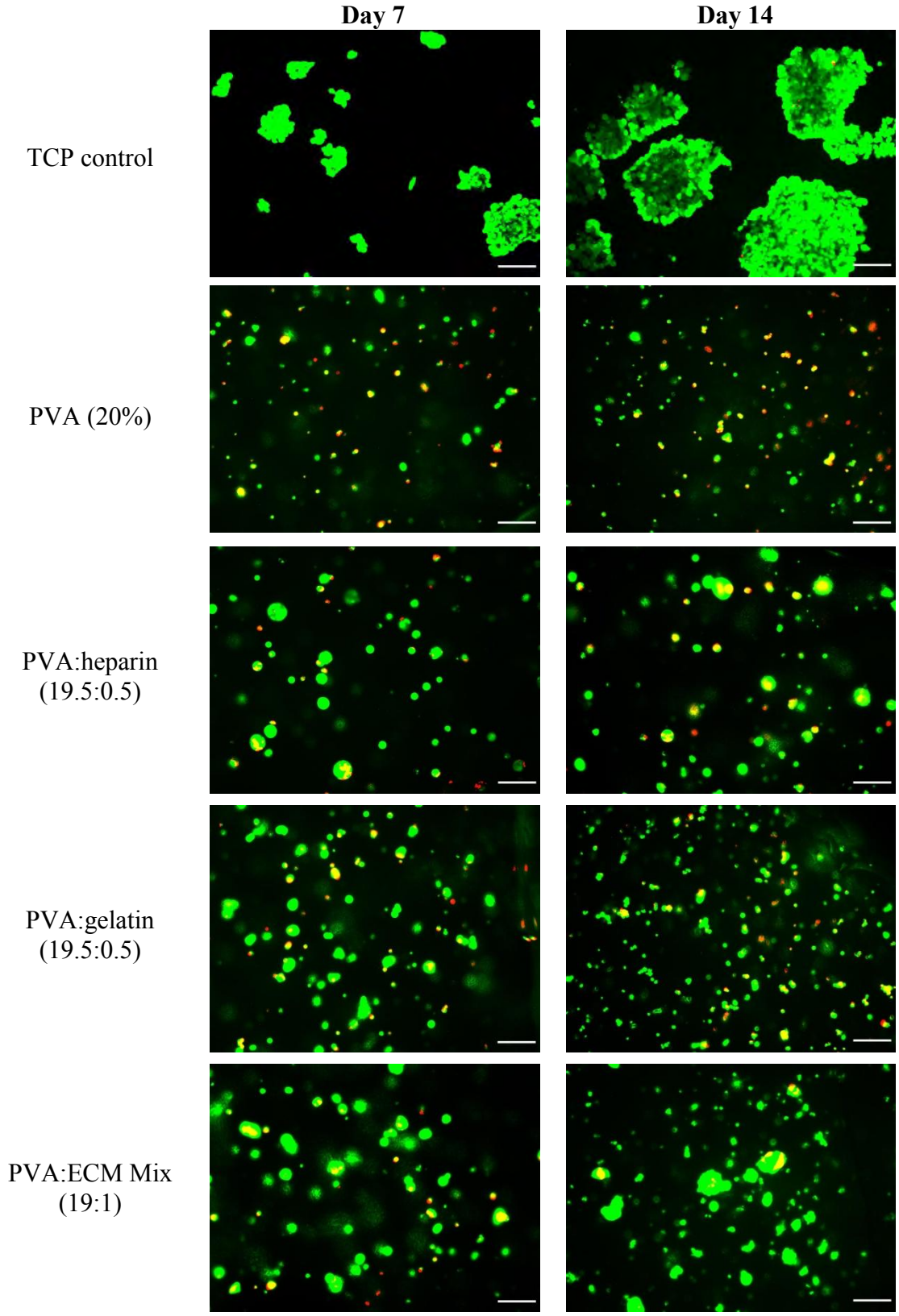

Figure 6.7: Fluorescent images (10 x) of Live/Dead stained MIN6 cells encapsulated in PVA 7 FG/c hydrogels for 7 and 14 days. Cell controls grown on TCP are added for comparison (Scale bar = 100 μm).

Quantitative assessment of the fluorescent cell images is represented in Figure 6.8. Equivalent cell coverage area was observed in all hydrogel compositions at early time points of the study (1 and 4 days). A decrease in cell area was then observed after 1 week of encapsulation in all hydrogels with a more pronounced reduction shown in pure PVA hydrogels, where elevated number of red stained cells was obvious (Fig.6.7). The higher amount of live cells observed in the co-hydrogels at later time points in culture was correlated to the formation of cell aggregates, which were not shown in pure PVA hydrogels (Fig. 6.7). These cell aggregates were comparable in their morphology to the unencapsulated cell spheroids that started to appear earlier in culture (Fig. 6.6). On the other hand, a serial increase in cell coverage area was obvious on TCP cultured with unencapsulated cells, together with increased areas of cell spheroids (Fig. 6.6-6.7), demonstrating their ability to proliferate over time in culture media.

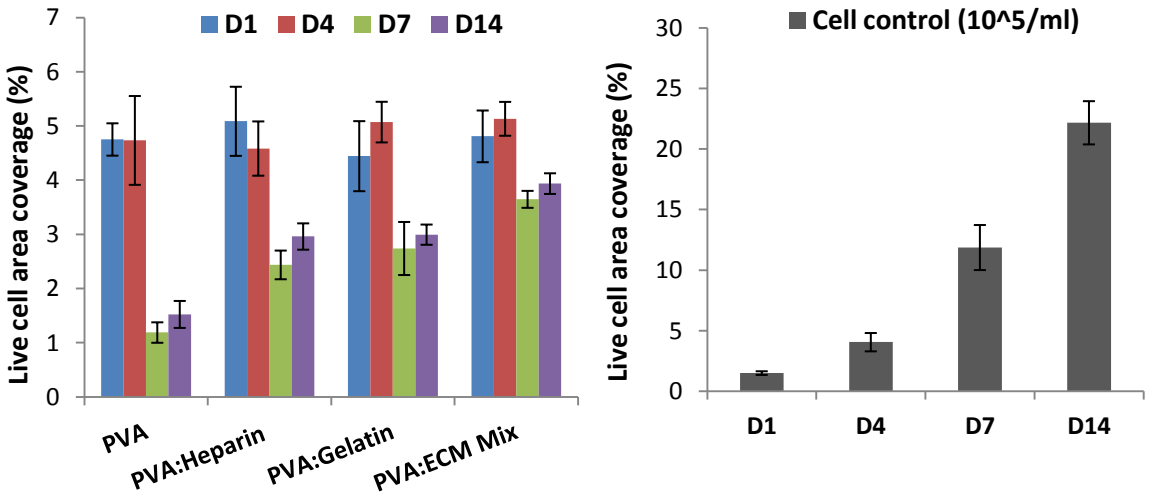

Figure 6.8: % Live cell area coverage calculated from fluorescent images of control MIN6 cells cultured on TCP and cells encapsulated in PVA 7 FG/c PVA 20%, PVA:heparin (19.5:0.5), PVA:gelatin (19.5:0.5) and PVA:ECM Mix (19:1) hydrogels with 7 FG/c.

MIN6 Cell Metabolic Activity

Figures 6.9 and 6.10 show the amount of ATP produced by encapsulated MIN6 cells which reflects their metabolic activity. It was observed despite the similarity in cell number after 1 day of encapsulation, cells in PVA only gels demonstrated lower metabolic activity than those in the co-hydrogels (Fig.6.8-6.9). All hydrogels with ECM analogues had similar metabolic activity for the first 4 days of encapsulation, and these ATP values were significantly higher than the PVA only gels. In all gels, the cell metabolic activity was significantly reduced after 2 weeks of encapsulation and no significant difference was found between the different PVA-ECM compositions.

Both 7 and 20 FG/c hydrogels showed similar results in metabolic activity over time. However, pure 20 FG/c PVA hydrogels had much lower metabolic activity of encapsulated cells compared to pure 7 FG/c PVA hydrogels. Unencapsulated MIN6 cells examined parallel to each experiment demonstrated increased ATP production over time, indicating an increase in cell number.

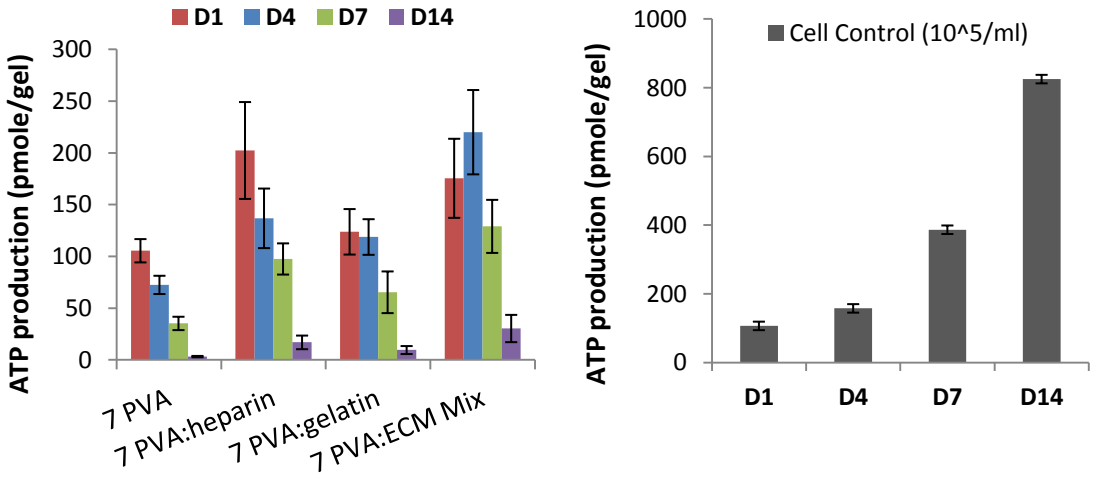

Figure 6.9: Production of ATP from control MIN6 cells and cells encapsulated in PVA 20%, PVA:heparin (19.5:0.5), PVA:gelatin (19.5:0.5) and PVA:ECM Mix (19:1) hydrogels with 7 FG/c PVA

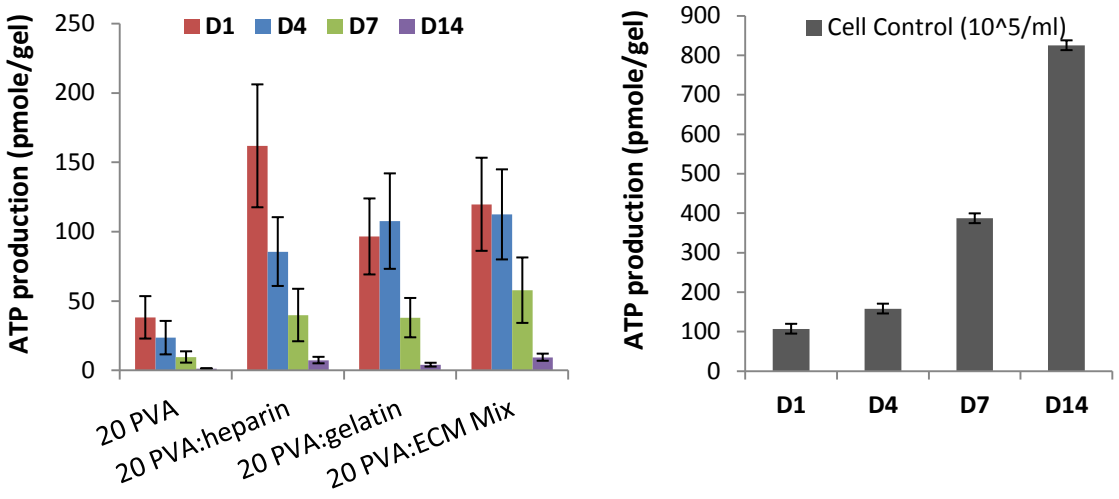

Figure 6.10: Production of ATP from control MIN6 cells and cells encapsulated in PVA 20%, PVA, PVA:heparin (19.5:0.5), PVA:gelatin (19.5:0.5) and PVA:ECM Mix (19:1) hydrogels with 20 FG/c

Optimisation of GSIS Assay

GSIS assay of PVA:heparin co-hydrogels was performed at different exposure time points to both low and high glucose levels and is shown in Figure 6.11. No significant difference was observed between 1 and 2 hrs incubation period in terms of insulin content and responsiveness to glucose. Increasing exposure time up to 2.5 hours resulted in loss of cell responsiveness to glucose in hydrogel samples, although increased insulin secretion was observed. Unencapsulated MIN6 cells showed normal glucose responsiveness at all time points with increased insulin content observed at 2.5 hrs.

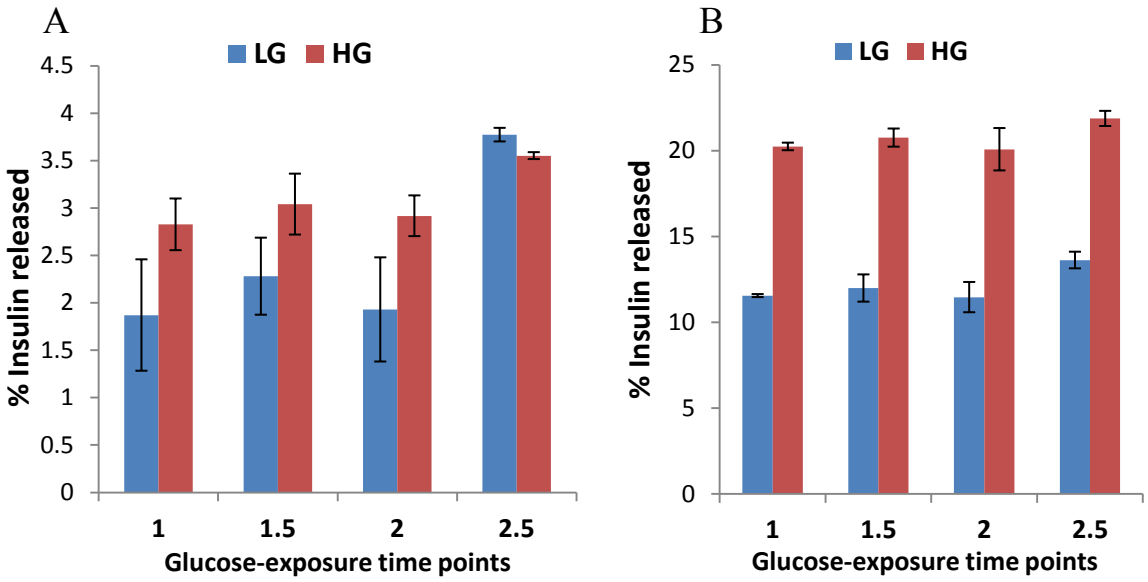

PVA:heparin hydrogels

Unencapsulated cells

Figure 6.11: Insulin secretion from MIN6 cells in response to high and low glucose at different time points for both (A) PVA:heparin hydrogels and (B) unencapsulated cells after 14 days of cell culture. Values of insulin released were normalised to total insulin content (n=1, mean ± SEM of 3 different samples).

6.4 DISCUSSION

The current research demonstrated the ability of permselective biosynthetic PVA based hydrogels to completely release cell specific therapeutic products while supporting cell survival compared to pure synthetic hydrogels.

The gels' ability to release the therapeutic product (insulin) was confirmed in all fabricated hydrogels. The permeability studies demonstrated high diffusion of insulin in all hydrogels compared to previously examined BSA and IgG. In addition, a rapid rate of insulin release

was confirmed by *in vitro* release studies with influences of the functional group density and type of ECM analogue being observed.

The high insulin diffusion coefficient values obtained in this study ($Dx10^8$~14-20 cm^2/sec), compared to lower values obtained with BSA ($Dx10^8$~ 4.5- 7 cm^2/sec) and IgG ($Dx10^8$ ~ 1-3 cm^2/sec) in Chapter 5, demonstrated the rapid diffusivity of insulin through all examined hydrogels (Figure 6.2). However, the partition coefficient values of co-hydrogels were slightly higher than those of pure PVA hydrogels (Table 6.1). Specifically, heparin co-hydrogels had the highest K values which could be due to the higher affinity of insulin to bind to heparin compared to gelatin. Although diffusion of insulin from highly crosslinked 20 FG/c hydrogels was lower than those with 7 FG/c, diffusion coefficient values were still high enough to demonstrate the rapid permeability of such molecule within the examined PVA network.

Similar insulin diffusion coefficient values to those obtained in the current study with PVA hydrogels of 7 FG/c have been demonstrated in PVA hydrogels crosslinked chemically or via radiation. It was found that the diffusion of small molecules such as glucose and insulin could be enhanced by increasing the mesh size and water content through varying the crosslinker concentration or the radiation dose [112, 137].

Another group enhanced the permeability of insulin through PVA casted membranes by the addition of polyethylene glycol as a pore former [362]. This technique improved the permeability coefficient (P) of insulin from 1.45 $x10^{-6}$ to 4.15 x 10^{-6} cm/sec, while preventing the passage of large molecules. Those improved values are approximately similar to the permeability coefficient values obtained for hydrogels in this chapter with 7 FG/c (~ 4 x 10^{-6} to 5 x 10^{-6} cm/sec). Lower insulin permeability values have been reported in literature using tricomponent PEG/polypentamethylcyclopentasiloxane

(PD5)/polydimethylsiloxane (PDMS) hydrogel as immunoisolating membrane materials, where their maximum P values (4.8×10^{-7}) were far below any of the obtained values from the currently examined hydrogels [352].

Many reported GSIS studies from hydrogels have mentioned a specified stimulation time of 45 min to 1 hr [129, 240, 353, 363]. However, heparin and gelatin ECM analogues have not been previously reported with insulin secretion studies and had slightly higher K values than pure PVA hydrogels. Therefore, a release experiment was conducted with the same hydrogel dimensions used for cell encapsulation. Thin hydrogel dimensions were selected for cell encapsulation studies in order to reduce the distance between encapsulated cells and the surroundings. This short distance would allow for faster diffusion of oxygen and nutrients to the cells trying to avoid the likelihood of hypoxia in thicker hydrogels, especially at the centre of the cell mass [78, 364].

Although the insulin release rate of higher crosslinked (20 FG/c) PVA only hydrogels was shown to be slower than those with 7 FG/c, 100% release of insulin was achieved after ~ 1 hr from both (Figure 6.3). Similar findings were observed by Weber et al. in PEG hydrogels, where increasing the crosslinking density reduced the release rate of insulin within the 1 hr stimulation period of GSIS test from encapsulated islets [240]. The total insulin released at 1 hr was however the same in all different crosslinking densities examined. They assumed that reducing the thickness of the gel barrier and consequently the diffusion distance, counteracted the delay observed in insulin release by highly crosslinked samples.

In all PVA co-hydrogels with different ECM incorporated, no difference was observed between both PVA functional group densities examined, with the release of insulin observed to be completed after 100-120 min (Figure 6.6). No reported studies to

date have discussed the effect of ECM or biological components on insulin diffusion within hydrogels although the binding affinity of insulin to GAGs and proteins has been previously reported [355, 356, 358]. Since partition coefficient experiments showed higher K values in co-hydrogels although not statistically significant, it could be possible that this delay was related to temporary binding of insulin onto ECM analogues, which dominated over the effect of crosslinking difference in the release study. Based on the K values and the time to 100% insulin release (Tables 6.1-6.2), it appears that the binding affinity of insulin to heparin was higher than with gelatin resulting in prolonging the time for complete insulin release from the gels up to 2 hrs.

Since the slowest release rate of insulin was observed from PVA:heparin hydrogels with 100% release achieved after 2 hrs, a GSIS study was conducted using this hydrogel composition at different glucose stimulation times starting from 1hr up to 2.5 hrs. The study aimed at identifying the shortest glucose stimulation time showing maximum insulin release and relative cell response to different glucose concentrations. An ELISA assay showed similar insulin release content and glucose response over a 2 hr period from the co-hydrogels, indicating that ECM analogues did not interfere with the short stimulation time reported so far in literature, which is 1 hr (Figure 6.11). The difference observed between GSIS and *in vitro* release results could be due to the difference in the assays used for insulin measurements and also the nature of insulin assessed. The insulin used for the release experiments was free insulin from a bovine source and was fluorescently tagged with FITC while the GSIS assay determined insulin secreted directly from the MIN6 cell line.

After confirming the ability of all fabricated hydrogels to efficiently release insulin in a short time period, the suitability of these materials for encapsulating therapeutic β-cells

was investigated. Before the actual encapsulation process, PVA macromers (7 & 20 FG/c) were tested for their cytocompatibility, as cells will be in contact with macromers (modified polymer solutions) prior to the formation of hydrogels. The cell growth inhibition test investigated the effect of macromer exposure on the normal cell growth and hence it gives an indication on the degree of material cytotoxicity. Previous studies have investigated the cytotoxicity of acrylate and methacrylate groups used in biomedical materials with variable results shown depending on the backbone polymer, dose applied and cell type tested [365-370]. The toxicity of methacrylates was found to be lower than that of acrylate-based materials [368].

The current results indicated that increasing the methacrylate group density on PVA macromers up to 20 FG/c did not affect the normal cell growth and were comparable to unmodified PVA. Similar findings were observed previously with degradable acrylated PVA macromers, where the effect of functional group density was found to be insignificant [207]. Other studies on PVA hydrogels also showed the insignificant cytotoxic effect of methacrylate functional group added onto PVA by using either direct cytotoxicity tests such as an MTT assay or indirect tests such as the cell growth inhibition assay used in the current chapter [258, 259].

In the current study, a model pancreatic β-cell line (MIN6) was used, as it is a well known model for primary islets in the study of β-cell function [371]. The survival of MIN6 cells in PVA synthetic and biosynthetic hydrogels of both PVA functional group densities (7 & 20 FG/c) was monitored for 14 days in culture. In both 7 and 20 FG/c hydrogels, no difference was observed in the behaviour of cells encapsulated in terms of morphology and metabolic activity. Similar findings were reported by Weber et al. in PEG hydrogels fabricated with variable number average molecular weight of PEG core

($\overline{Mn}$ ranged from 2,000 up to 10,000 g/mol) [240]. The increase in the final crosslinking density of PEG hydrogels was found not to interfere with the viability of encapsulated islets for 14 days culture period. Cruise et al. also demonstrated similar percent viability of islets encapsulated in PEG diacrylate hydrogels after increasing PEG macromer concentration and molecular weight [353]. A slight increase in viability, although significant, was observed in the lowest crosslinking density diacrylate hydrogels studied (10% PEG 20K) as compared to unencapsulated control islets for the first week of culture.

Despite the difference in cell density, the behaviour and metabolic activity of both encapsulated and unencapsulated cells could be compared over 2 weeks in culture. Both microscopic and metabolic activity results demonstrated the ability of unencapsulated cells to proliferate over time. This was shown by the distinctly formed large cell spheroids which started to aggregate from day 4 in control MIN6 cells on TCP, and also the increased metabolic activity by time which reflects the increase in cell number. Conversely, encapsulated MIN6 cells showed significant reduction in cell viability in pure PVA hydrogels, which was more pronounced over time. This was demonstrated by the elevated number of red stained cells from Live/Dead assay and the reduction in live cell coverage area which was obvious by day 7 of encapsulation. In addition, there was a significant reduction in ATP production from the cells, which was observed after the first day of encapsulation.

On the other hand, incorporated ECM analogues showed significant enhancement of the viability of encapsulated cells in both 7 and 20 FG/c PVA hydrogels. Small cell aggregates were observed after 7 days in PVA hydrogels with heparin, gelatin or mixture of both (Figure 6.7). It has been previously reported that pancreatic β-cells depend mainly on cell-cell contact for their survival, where a close proximity between cells was found to

be essential for the survival and function of the individual β-cells [11, 35, 372]. In addition, it was found that a minimum loading density of 10^7 cells⁄mL was necessary to maintain the survival of encapsulated β-cells in synthetic hydrogels [11]. However, PVA only hydrogels were unable to meet such goal at the recommended cell density. It is believed that other than the physical cell to cell contact, cell-cell communication cues are mandatory to maintain the viability of encapsulated cell [11]. It is hypothesised the small spheroids formed in the current PVA co-hydrogels were a result of cell to cell communication signals provided only by ECM analogues.

It has been demonstrated that gelatin, as well as other cell adhesive proteins and peptides, not only enhances cellular adhesion but also cell viability, function and matrix remodelling in hydrogels through signalling pathways between encapsulated cells and their external microenvironment [141, 246, 285, 286, 319, 373]. However, the effect of gelatin, as denatured product of collagen, hasn't been yet reported on either β-cells or primary islets.

Recently, Takahashi et al. and Ziolkowski et al. reported the discovery of high level of heparan sulphate (HS) expression within mouse islets, and correlated the loss of HS after cell isolation with immediate cell death [374, 375]. Ziolkowski et al. succeeded in identifying the crucial role of HS molecules for islet cell survival, where it preserves their resistance to harmful reactive oxygen species (ROS) [374]. This finding suggests an additional protective effect of heparin molecule on encapsulated cells. Since generation of free radicals is expected during radical chain photopolymerisation, those radicals might induce some cell damage at the start of the encapsulation process [376]. This damage was more pronounced in PVA only hydrogels that showed an immediate drop in their cell metabolic activity after 1 day of encapsulation. Thus, the ROS scavenging property

discovered with HS would explain the currently observed results with heparin, where cells survived the radical-mediated photopolymerisation process compared to purely synthetic PVA hydrogels.

In the current study, one of the aims was to investigate the effect of ECM mixture on β-cell response compared to individually incorporated ECM analogues. All results revealed no significant difference obtained for cell viability between the different co-hydrogels examined. Previous studies in the literature demonstrated some synergistic effects on β-cell viability and functionality by combining different ECM proteins or specific peptides in synthetic hydrogels. PEG Hydrogels containing both collagen type IV and laminin were found to enhance islet insulin secretion over single component co-hydrogels, specifically with higher ratios used of laminin relative to collagen IV [10, 146]. Also, laminin-derived IKVAV peptide showed superior effect on β-cell viability when combined with glucagon-like peptide 1 (GLP-1) compared to PEG-only, PEG/IKVAV, and PEG/GLP-1 gels [376]. In the current study, although the enhanced effect of the addition of either heparin or gelatin was demonstrated, no synergistic effects were observed when they were mixed at equal incorporation ratios. Thus, further changes of the ratios applied might show different results. However, it can be concluded that only 0.5% ECM incorporation in PVA network provided equivalent enhancement effect of cell viability as compared to 1 % total ECM incorporation.

6.5 CONCLUSION

The current study demonstrated the ability of highly crosslinked PVA biosynthetic hydrogels to maintain the diffusion of insulin through their network. Insulin diffusion is considered a key limiting factor for the normal functionality of encapsulated β-cells. In addition, cytotoxicity results revealed that increased FG/c did not impair normal cell growth, proving the suitability of developed macromers for cell encapsulation. This was proven by the successful encapsulation of sensitive pancreatic cells into PVA hydrogels after UV photopolymerisation.

Incorporation of both heparin and gelatin in PVA hydrogels significantly enhanced the viability of encapsulated cells compared to pure PVA hydrogels in both 7 and 20 FG/c. Although cell survival continued to decrease over time, the current results introduced heparin and gelatin as candidate ECM analogues to promote the survival of pancreatic β-cells in hydrogel matrices. The results did not show any additional effect upon mixing both ECM analogues, however it was concluded that a percent incorporation of ECM analogues (whether individual or mixed) as small as 0.5% was sufficient to improve viability of encapsulated cells. This finding further supports the hypothesis that only a small percentage of ECM is required in synthetic hydrogels to induce effective biofunctionality. Consequently, this chapter demonstrated that biosynthetic PVA hydrogels with controlled permselectivity supported the viability of pancreatic β-cells over two weeks of encapsulation compared to pure synthetic hydrogels. Subsequently, both heparin and gelatin molecules are suggested as potential ECM components to be considered in future islet encapsulation devices.

Chapter 7

Conclusions
and Future Recommendations

7.1 Introduction

In cell based therapy, immunoisolation has emerged as a promising approach capable of overcoming host rejection and attack following cell transplantation and thus has the potential to remove constraints associated with cell sourcing. Despite extensive research in the field of cell encapsulation, several challenges in the development of an ideal immunoisolating membrane still exist. One of the major unsolved problems is obtaining an optimum balance between stable permselectivity and physico-mechanical characteristics of the encapsulating membrane material and its ability to maintain cell survival over the implantation period.

Therefore, this thesis addressed this challenge through a systematic study of biosynthetic hydrogels which aimed to understand the impact on permeability, a critical physical property of immunoisolation membranes, of adding biological polymers to the synthetic base material. The major research aim was to achieve a balance between a controlled permselectivity and cell survival support via covalent incorporation of model ECM molecules, heparin and gelatin, into a synthetic PVA network specifically tailored for immunoisolation. It was hypothesised that the covalent incorporation of a small amount of ECM analogues would support cell viability within the biosynthetic hydrogel without compromising the controlled permselectivity and physico-mechanical properties of the base PVA network.

7.2 Thesis Conclusions

Overall, the current thesis demonstrated the ability to control the permselectivity of PVA multivinyl hydrogels through a systematic increase in the functional group density. These modifications of the polymer backbone impacted directly on the swelling and mechanical properties that proved to be stable over the study period. More importantly, all PVA hydrogel characteristics, especially macromolecular permeability, were not disrupted after the covalent incorporation of small amounts of ECM analogues, whether singularly or combined. The supplementation of PVA with biological cues proved to improve the viability of encapsulated cells without interfering with the *in vitro* release of their therapeutic product.

In order to provide the baseline understanding of macromolecular permeability of synthetic PVA hydrogels on which the whole thesis was built, a systematic variation in the methacrylates functional group density on the PVA backbone was studied from 7 up to 20 FG/c. These modifications allowed for controlling the network average mesh sizes in a range from ~ 95 Å down to ~ 60 Å. This range of mesh sizes influenced both the swelling and compressive modulus of the hydrogels, which were shown to be stable after the release of sol fraction (24 hrs post photopolymerisation). Most importantly, the tailored mesh sizes resulted in a consistent degree of permselectivity for PVA hydrogels to solutes of different shapes and sizes. This permselectivity has been proven by permeability studies of dextran models having various molecular weights and also protein solutes including insulin, bovine serum albumin (BSA) and immunoglobulin G (IgG).

For cell immunoisolation applications, large antibodies are required to be blocked out of the encapsulation device while permitting the passage of nutrients and cell

metabolites. PVA hydrogels with highly crosslinked networks (20 FG/c) showed a significant retardation of IgG with diffusion values lower that other immunoisolation membranes reported so far in literature. In addition, insulin and BSA were able to pass through the hydrogels, which was important for maintaining the passage of nutrients required for cell survival within the membrane material.

To ensure an enhanced viability of cells encapsulated within the permselective hydrogel network, biological signals were introduced to the synthetic PVA gels using two different ECM analogues: heparin and gelatin. A low percent incorporation of ECM analogues did not to interfere with the base PVA network characteristics, where the controlled hydrogel mesh sizes, swelling and compressive modulii remained unchanged after incorporation of both heparin and gelatin. Interestingly, despite the nature and charge of these ECM analogues, their presence within the hydrogel network did not impact on the permselectivity of PVA to different examined proteins. Although some interactions appeared to be possibly occurring between the co-hydrogels and different permeating proteins, the effect of hydrogel mesh size dominated and resulted in similar diffusion results within the final co-hydrogels compared to pure synthetic PVA hydrogels.

Additionally, the combination of both heparin and gelatin within a PVA network has proven to be stable over time without compromising the PVA base characteristics including its permselectivity. Most importantly, this combination of ECM analogues supplemented PVA with the dual functionalities of promoting cellular adhesion and sequestering growth factors essential for cellular proliferation.

After the successful fabrication of permselective biosynthetic hydrogels with demonstrated ECM biofunctionalities, it was important to assess the efficacy of these hydrogels in cell encapsulation. First, the ability of highly crosslinked PVA biosynthetic

hydrogels to maintain the diffusion of insulin through their network was demonstrated. Insulin diffusion is considered a key limiting factor for the normal functionality of encapsulated β-cells. This was followed by conducting a cell growth inhibition study which proved the cytocompatibility of highly methacrylated macromers to be used for cell encapsulation.

Encapsulation of therapeutic cells within hydrogels was then performed with a model pancreatic β-cell line (MIN6). The viability and metabolic activity of encapsulated cells were monitored for 14 days post encapsulation. Covalently incorporated heparin and gelatin significantly enhanced the survival and metabolic function of encapsulated MIN6 cells in highly crosslinked hydrogels, which was not shown with pure synthetic ones. Moreover, it has been demonstrated that as low as 0.5% incorporation of ECM analogues was sufficient to improve encapsulated cell viability. Although the metabolic activity of cells encapsulated in biosynthetic hydrogels started to drop with time, heparin and gelatin showed positive effects in improving cell survival for at least 7 days in tightly crosslinked hydrogel networks. Since both heparin and gelatin have not been yet reported for their bioactive effects with MIN6 or islet cells, the current research results demonstrated their potential to be considered in future islet encapsulation devices.

In conclusion, this thesis demonstrated an achievable way to tailor the permselectivity of PVA hydrogels while improving their performance in terms of cell support through the addition of biological molecules. However, other challenges need to be addressed in the future to improve this proposed biosynthetic hydrogel material for efficient cell immunoisolation, in terms of prolonging the effective encapsulation period and broadening the permselectivity capacity.

7.3 Recommendations for Future Research

7.3.1 Incorporating ECM molecules specific for cell function to prolong the effective encapsulation period

This research succeeded in improving the viability of encapsulated cells within highly crosslinked permselective hydrogels for 14 days. However, in addition to the currently proposed ECM analogues, other biological molecules are proposed to be examined in the future in order to prolong the effective encapsulation period for more than two weeks. Although the current thesis did not investigate in-depth the insulin secretory function of MIN6 cells encapsulated in the different hydrogel compositions, it is believed that the ECM effect on cell viability and metabolic activity would reflect their ability to function properly and secrete insulin, which needs to be examined in the future. Heparin and gelatin showed promise in improving MIN6 cell viability and metabolic activity within the hydrogel matrix, however it would be interesting to investigate the effect of more specific ECM molecules to this particular type of cells.

Adhesive molecules such as integrins and cadherins have been previously reported to influence insulin secretion in islets and could be incorporated into PVA gels [377-379]. It has been observed that amongst the known islet ECM proteins, both laminin and fibronectin facilitated the highest levels of islet and β-cells insulin secretion and response to glucose [143, 146, 380, 381]. In addition, when ECM mixed components were applied, mixtures having laminin or its peptide derivatives in a high ratio showed superior effect on improving pancreatic cell viability and insulin secretion [10, 146]. It is thus advised to further investigate the possibility of covalent binding of these molecules within biosynthetic hydrogels and their impact on prolonging cell survival and functionality.

Another important consideration is the ratio of combined ECM molecules within the PVA network. Previous studies have shown that β cells demonstrated different behaviour with the same incorporated ECM mixture at variable ratios. Therefore, it is suggested to expand this knowledge by studying the optimum ratio of each of individual ECM molecules selected to be combined within one hydrogel network. In the current study, heparin and gelatin were combined at equal percentage and did not show any synergistic effects over the individual components. However, alternating the ratio of each of them together with more specific ECM molecules is expected to show various impacts on both cell metabolic activity and insulin secretion.

7.3.2. Further strategies to combat incomplete immunoprotection

The attempts in this thesis to control biosynthetic hydrogel permeability were effective in restricting the entry of large antibodies, however toxic factors with sizes similar to and smaller than therapeutic proteins would still be able to diffuse through the membrane. Nitric oxide (NO) and cytokines are examples of small factors which can exert toxic effects on encapsulated cells. Previous trials have successfully prevented the inward diffusion of some cytokines such as IL-1β and TNF-α by increasing the contact time between alginate and poly-lysine in the formation of alginate-PLL capsules [382, 383]. However, passage of smaller nitric oxide molecules could not be prevented without impairing the diffusion of therapeutic proteins. Other means of protection small size toxic factors have been investigated and can be combined to the currently proposed biosynthetic hydrogels in this thesis to broaden their permselectivity.

- **Co-encapsulation of immunosuppressive cells**

The technique of encapsulating immunosuppressive cells together with the therapeutic cells within a membrane has shown promising results in prolonging the

immunoisolation of transplanted encapsulating devices. For example, the co-encapsulation of immunosuppressive autologous erythrocytes within alginate beads has been found to provide protection against macrophage-mediated lysis of islet cells by releasing hemoglobin molecules which scavenged NO radicals and hence increased islet viability [384]. Recently, Doyle et al. studied the immunoprotective properties of primary Sertoli cells found in testes and identified their role in suppressing the inflammation triggered by specific cytokines, slowing of leukocyte migration and inhibition of complement activation and membrane-associated cell lysis [385]. Co-encapsulation of Sertoli enriched testicular cell fractions in alginate microcapsules was shown to down regulate the apoptosis of xenografted islets by T-lymphocytes [386].

- **Inhibition of complement activity**

It has been reported that destruction of xenogeneic cells occurs by the activation of complement by antigen-antibody complexes on the transplanted cell surface. The small size of complement proteins allows them to penetrate through most encapsulating semi-permeable membranes. It is proposed that the retardation of their permeation for a certain period of time will destroy their lytic activity due to the known high instability of some complement proteins such as C_1, C_2 and C_5. Moreover, specific polymer-complement interactions have been proven to prevent the cytolytic complement activities [266]. Iwata et al. demonstrated that the incorporation of poly(styrene sulphonic acid) polymer in agarose microcapsules protected xenogeneic islets from the effects of complement activity by interfering with the activation pathways of the complement system through polyion complex formation with cationic factors C1q and H [266, 387].

- **Cytokine suppressive molecules**

Other approaches to increase membrane immunoprotection have investigated the use of a range of immunosuppressive molecules such as inhibitors of cytokines as well as the use of molecules which promote T-cell apoptosis. Ketoprofen, a non steroidal anti-inflammatory drug, was found to be a selective inhibitor of IL-8 which is involved in inflammatory and immune reactions [388, 389]. It was consequently proposed that incorporating ketoprofen into encapsulating devices may improve the life-span of cells [390].

Conjugation of immunosuppressive molecules to hydrogels has been developed to provide local immunosuppression and prolong the functionality of encapsulated cell grafts. Su et al. succeeded in maintaining the viability of encapsulated islets in the presence of a combination of cytokines by the covalent binding of FEWTPGWYQPY-NH2, an inhibitory peptide for cell surface IL-1 receptor, to a PEG hydrogel [373]. Furthermore, Lin et al. succeeded in prolonging the survival and function of encapsulated PC12 cells and mouse islets by encapsulating them in WP9QY-functionalized TNFα-antagonizing PEG hydrogels [391]. The autoimmune response against encapsulated cells has also been reduced by targeting the T-cells of the host. It was shown that the conjugation of anti-Fas monoclonal antibodies to the surface of PEG hydrogels was associated with the enhanced apoptosis of Fas-sensitive T-cells which thus inhibited the autoimmune response against encapsulated cells [392].

7.4 Thesis Outcomes

The current research addressed the problem of achieving an optimum balance between membrane permselectivity and supporting the viability of encapsulated cells. Throughout the research the following major outcomes have been generated:

a. The permselectivity of synthetic PVA hydrogels was manipulated through introducing a high number of functional groups per polymer backbone

b. The reliability of applying the equilibrium swelling theory for hydrogel mesh size estimation over the rubber elasticity theory was proved through permeability studies

c. Two different model ECM molecules, heparin and gelatin, were covalently incorporated into synthetic PVA network at low percentage without interfering with the base physico-mechanical characteristics and permselectivity

d. A simplified form of multifunctional natural ECM was replicated into synthetic hydrogels after combining heparin and gelatin together while maintaining their biofunctionalities in the PVA network

e. Encapsulated cell viability was significantly enhanced in highly crosslinked hydrogels after incorporation of ECM analogues

References

1. Lamb, M., et al., *Function and viability of human islets encapsulated in alginate sheets: In vitro and in vivo culture.* Transplant Proc, 2011. **43**(9): p. 3265-3266.
2. Reza, A.T. and S.B. Nicoll, *Characterization of novel photocrosslinked carboxymethylcellulose hydrogels for encapsulation of nucleus pulposus cells.* Acta Biomater, 2010. **6**(1): p. 179-186.
3. Tresco, P.A., et al., *Ethanol treatment alters the ultrastructure and permeability of PAN-PVC hollow fiber cell encapsulation membranes.* J Membr Sci, 2002. **195**(1): p. 51-64.
4. JDRF. *Fact Sheets: Type 1 Diabetes Facts*. 2011; Available from: http://www.jdrf.org/index.cfm?page_id=102585.
5. Clayton, H.A., R.F. James, and N.J. London, *Islet microencapsulation: a review.* Acta Diabetol, 1993. **30**(4): p. 181-9.
6. Lacik, I., *Polymer chemistry in diabetes treatment by encapsulated islets of Langerhans: Review to 2006.* Aust J Chem, 2006. **59**(8): p. 508-524.
7. De Vos, P., et al., *Advances and barriers in mammalian cell encapsulation for treatment of diabetes.* Immunol Endocr Metabol Agents in Med Chem, 2006. **6**(2): p. 139-153.
8. Schmidt, J.J., J. Rowley, and H.J. Kong, *Hydrogels used for cell-based drug delivery.* J Biomed Mater Res A, 2008. **87**(4): p. 1113-22.
9. Beck, J., et al., *Islet encapsulation: strategies to enhance islet cell functions.* Tissue Eng, 2007. **13**(3): p. 589-99.
10. Weber, L.M., K.N. Hayda, and K.S. Anseth, *Cell-matrix interactions improve beta-cell survival and insulin secretion in three-dimensional culture.* Tissue Eng Part A, 2008. **14**(12): p. 1959-68.
11. Lin, C.C. and K.S. Anseth, *Cell-cell communication mimicry with poly(ethylene glycol) hydrogels for enhancing β-cell function.* PNAS, 2011. **108**(16): p. 6380-6385.
12. Lieleg, O. and K. Ribbeck, *Biological hydrogels as selective diffusion barriers.* Trends Cell Biol, 2011. **21**(9): p. 543-51.
13. Lee, M.K. and Y.H. Bae, *Cell transplantation for endocrine disorders.* Adv Drug Deliv Rev, 2000. **42**(1-2): p. 103-20.
14. Emerich, D.F. and S.R. Winn, *Immunoisolation cell therapy for CNS diseases.* Crit Rev Ther Drug Carrier Syst, 2001. **18**(3): p. 265-298.
15. Emerich, D. and H.C. Salzberg, *Update on immunoisolation cell therapy for CNS diseases.* Cell Transplant, 2001. **10**(1): p. 3-24.
16. Sagen, J., et al., *Transplants of immunologically isolated xenogeneic chromaffin cells provide a long-term source of pain-reducing neuroactive substances.* J Neurosci, 1993. **13**(6): p. 2415-23.
17. Portero, A., et al., *Cell encapsulation for the treatment of central nervous system disorders.* Rev Neuro, 2010. **50**(7): p. 409-419.
18. Wollert, K.C. and H. Drexler, *Cell-based therapy for heart failure.* Curr Opin Cardiol, 2006. **21**(3): p. 234-239.
19. Visted, T., R. Bjerkvig, and P.O. Enger, *Cell encapsulation technology as a therapeutic strategy for CNS malignancies.* Neuro Oncol, 2001. **3**(3): p. 201-10.

20. Visted, T. and M. Lund-Johansen, *Progress and challenges for cell encapsulation in brain tumour therapy.* Expert Opin Biol Ther, 2003. **3**(4): p. 551-61.
21. Hao, S., et al., *A novel approach to tumor suppression using microencapsulated engineered J558/TNF-alpha cells.* Exp Oncol, 2005. **27**(1): p. 56-60.
22. Salmons, B., et al., *Encapsulated cells to focus the metabolic activation of anticancer drugs.* Curr Opin Mol Ther, 2010. **12**(4): p. 450-60.
23. Bisceglie, V., *Über die antineoplastische Immunität - I. Mitteilung. Heterologe Einpflanzung von Tumoren in Hühnerembryonen.* Ztschr Krebsforsch, 1934. **40**(1): p. 122-140.
24. Algire, G.H., *Microscopic studies of the early growth of a transplantable melanoma of the mouse, using the transparent chamber technique.* J the Natl Cancer Inst, 1943. **4**: p. 13-20.
25. Algire, G.H., *An adaptation of the transparent chamber technique to the mouse.* J Natl Cancer Inst, 1943. **4**: p. 1-11.
26. Chang, T.M., *Semipermeable Microcapsules.* Science, 1964. **146**(3643): p. 524-5.
27. Li, R.H., *Materials for immunoisolated cell transplantation.* Adv Drug Delivery Rev, 1998. **33**(1-2): p. 87-109.
28. De Vos, P., et al., *Multiscale requirements for bioencapsulation in medicine and biotechnology.* Biomaterials, 2009. **30**(13): p. 2559-2570.
29. Kozlovskaya, V., et al., *Ultrathin polymeric coatings based on hydrogen-bonded polyphenol for protection of pancreatic islet cells.* Adv Funct Mater, 2012. **22**(16): p. 3389-3398.
30. Wilson, J.T., W. Cui, and E.L. Chaikof, *Layer-by-layer assembly of a conformal nanothin PEG coating for intraportal islet transplantation.* Nano Letters, 2008. **8**(7): p. 1940-1948.
31. Teramura, Y., Y. Kaneda, and H. Iwata, *Islet-encapsulation in ultra-thin layer-by-layer membranes of poly(vinyl alcohol) anchored to poly(ethylene glycol)-lipids in the cell membrane.* Biomaterials, 2007. **28**(32): p. 4818-25.
32. Miura, S., Y. Teramura, and H. Iwata, *Encapsulation of islets with ultra-thin polyion complex membrane through poly(ethylene glycol)-phospholipids anchored to cell membrane.* Biomaterials, 2006. **27**(34): p. 5828-35.
33. Zhi, Z.L., et al., *Polysaccharide multilayer nanoencapsulation of insulin-producing beta-cells grown as pseudoislets for potential cellular delivery of insulin.* Biomacromolecules, 2010. **11**(3): p. 610-616.
34. Weber, L.M., C.Y. Cheung, and K.S. Anseth, *Multifunctional pancreatic islet encapsulation barriers achieved via multilayer PEG hydrogels.* Cell Transplant, 2008. **16**(10): p. 1049-57.
35. Weber, L.M., et al., *PEG-based hydrogels as an in vitro encapsulation platform for testing controlled beta-cell microenvironments.* Acta Biomater, 2006. **2**(1): p. 1-8.
36. Lee, J.I., et al., *A newly developed immunoisolated bioartificial pancreas with cell sheet engineering.* Cell Transplant, 2008. **17**(1-2): p. 51-9.
37. Gazda, L.S., et al., *Encapsulation of porcine islets permits extended culture time and insulin independence in spontaneously diabetic BB rats.* Cell Transplant, 2007. **16**(6): p. 609-20.
38. Silva, A.I. and M. Mateus, *Development of a polysulfone hollow fiber vascular bio-artificial pancreas device for in vitro studies.* J Biotechnol, 2009. **139**(3): p. 236-49.

39. Qi, Z., et al., *The in vivo performance of polyvinyl alcohol macro-encapsulated islets.* Biomaterials, 2010. **31**(14): p. 4026-4031.
40. Lelli, L., et al., *Preparation and Characterization of Permselective, Biocompatible Membranes for the Macroencapsulation of Pancreatic-Islets.* Journal of Materials Science-Materials in Medicine, 1994. **5**(12): p. 887-890.
41. George, S., et al., *Nonporous polyurethane membranes as islet immunoisolation matrices--biocompatibility studies.* J Biomater Appl, 2002. **16**(4): p. 327-40.
42. Kadam, S.S., et al., *Reversal of experimental diabetes in mice by transplantation of neo-islets generated from human amnion-derived mesenchymal stromal cells using immuno-isolatory macrocapsules.* Cytotherapy, 2010. **12**(8): p. 982-991.
43. Mazzitelli, S., et al., *Production and characterization of alginate microcapsules produced by a vibrational encapsulation device.* J Biomater Appl, 2008. **23**(2): p. 123-45.
44. Dufrane, D., et al., *Six-month survival of microencapsulated pig islets and alginate biocompatibility in primates: proof of concept.* Transplantation, 2006. **81**(9): p. 1345-53.
45. Strand, B.L., et al., *Alginate-polylysine-alginate microcapsules: effect of size reduction on capsule properties.* J Microencapsul, 2002. **19**(5): p. 615-30.
46. Hall, K.K., K.M. GattÃ¡s-Asfura, and C.L. Stabler, *Microencapsulation of islets within alginate/poly(ethylene glycol) gels cross-linked via Staudinger ligation.* Acta Biomater, 2011. **7**(2): p. 614-624.
47. Campos-Lisboa, A.C., et al., *Biodritin microencapsulated human islets of Langerhans and their potential for type 1 diabetes mellitus therapy.* Transplant Proc, 2008. **40**(2): p. 433-5.
48. Kobayashi, T., et al., *Survival of microencapsulated islets at 400 days posttransplantation in the omental pouch of NOD mice.* Cell Transplant, 2006. **15**(4): p. 359-65.
49. Agudelo, C.A., Y. Teramura, and H. Iwata, *Cryopreserved agarose-encapsulated islets as bioartificial pancreas: a feasibility study.* Transplantation, 2009. **87**(1): p. 29-34.
50. Schaffellner, S., et al., *Porcine islet cells microencapsulated in sodium cellulose sulfate.* Transplant Proc, 2005. **37**(1): p. 248-52.
51. Picariello, L., et al., *Microencapsulation of human parathyroid cells: an "in vitro" study.* J Surg Res, 2001. **96**(1): p. 81-9.
52. Kim, Y.T., et al., *A cell encapsulation device for studying soluble factor release from cells transplanted in the rat brain.* J Control Release, 2005. **102**(1): p. 101-11.
53. Read, T.A., et al., *Local endostatin treatment of gliomas administered by microencapsulated producer cells.* Nat Biotechnol, 2001. **19**(1): p. 29-34.
54. Emerich, D.F., et al., *Protective effect of encapsulated cells producing neurotrophic factor CNTF in a monkey model of Huntington's disease.* Nature, 1997. **386**(6623): p. 395-9.
55. Aebischer, P., et al., *Intrathecal delivery of CNTF using encapsulated genetically modified xenogeneic cells in amyotrophic lateral sclerosis patients.* Nat Med, 1996. **2**(6): p. 696-9.
56. Lohr, M., et al., *Cell therapy using microencapsulated 293 cells transfected with a gene construct expressing CYP2B1, an ifosfamide converting enzyme, instilled intra-arterially in patients with advanced-stage pancreatic carcinoma: a phase I/II study.* J Mol Med, 1999. **77**(4): p. 393-8.

57. Dautzenberg, H., et al., *Development of cellulose sulfate-based polyelectrolyte complex microcapsules for medical applications.* Ann N Y Acad Sci, 1999. **875**: p. 46-63.
58. Pelegrin, M., et al., *Immunotherapy of a viral disease by in vivo production of therapeutic monoclonal antibodies.* Hum Gene Ther, 2000. **11**(10): p. 1407-15.
59. Visted, T., et al., *Prospects for delivery of recombinant angiostatin by cell-encapsulation therapy.* Hum Gene Ther, 2003. **14**(15): p. 1429-40.
60. Sakai, S., et al., *Small agarose microcapsules with cell-enclosing hollow core for cell therapy: transplantation of Ifosfamide-activating cells to the mice with preestablished subcutaneous tumor.* Cell Transplant, 2009. **18**(8): p. 933-9.
61. Underhill, G.H., et al., *Assessment of hepatocellular function within PEG hydrogels.* Biomaterials, 2007. **28**(2): p. 256-70.
62. Honiger, J., et al., *Permeability and biocompatibility of a new hydrogel used for encapsulation of hepatocytes.* Biomaterials, 1995. **16**(10): p. 753-9.
63. Aoki, T., et al., *A novel method of cryopreservation of rat and human hepatocytes by using encapsulation technique and possible use for cell transplantation.* Cell Transplant, 2005. **14**(9): p. 609-20.
64. Quek, C.H., et al., *Photo-crosslinkable microcapsules formed by polyelectrolyte copolymer and modified collagen for rat hepatocyte encapsulation.* Biomaterials, 2004. **25**(17): p. 3531-40.
65. Haque, T., et al., *In vitro study of alginate-chitosan microcapsules: an alternative to liver cell transplants for the treatment of liver failure.* Biotechnol Lett, 2005. **27**(5): p. 317-22.
66. Yu, J., et al., *The use of human mesenchymal stem cells encapsulated in RGD modified alginate microspheres in the repair of myocardial infarction in the rat.* Biomaterials, 2010. **31**(27): p. 7012-7020.
67. Desmangles, A.I., O. Jordan, and F. Marquis-Weible, *Interfacial photopolymerization of beta-cell clusters: approaches to reduce coating thickness using ionic and lipophilic dyes.* Biotechnol Bioeng, 2001. **72**(6): p. 634-41.
68. Krol, S., et al., *Multilayer nanoencapsulation. New approach for immune protection of human pancreatic islets.* Nano Lett, 2006. **6**(9): p. 1933-9.
69. Veerabadran, N.G., et al., *Nanoencapsulation of stem cells within polyelectrolyte multilayer shells.* Macromol Biosci, 2007. **7**(7): p. 877-882.
70. Zhi, Z.L., et al., *Nano-scale encapsulation enhances allograft survival and function of islets transplanted in a mouse model of diabetes.* Diabetologia, 2012. **55**(4): p. 1081-90.
71. de Vos, P. and P. Marchetti, *Encapsulation of pancreatic islets for transplantation in diabetes: the untouchable islets.* Trends Mol Med, 2002. **8**(8): p. 363-6.
72. Uludag, H., P. De Vos, and P.A. Tresco, *Technology of mammalian cell encapsulation.* Adv Drug Deliv Rev, 2000. **42**(1-2): p. 29-64.
73. Iwata, H., et al., *Strategy for developing microbeads applicable to islet xenotransplantation into a spontaneous diabetic NOD mouse.* J Biomed Mater Res, 1994. **28**(10): p. 1201-7.
74. Schneider, S., et al., *Long-term graft function of adult rat and human islets encapsulated in novel alginate-based microcapsules after transplantation in immunocompetent diabetic mice.* Diabetes, 2005. **54**(3): p. 687-693.
75. Kizilel, S., M. Garfinkel, and E. Opara, *The bioartificial pancreas: progress and challenges.* Diabetes Technol Ther, 2005. **7**(6): p. 968-85.

76. Ma, Y., et al., *Study of the effect of membrane thickness on microcapsule strength, permeability, and cell proliferation.* J Biomed Mater Res A, 2012.
77. Lum, Z.P., et al., *Xenografts of rat islets into diabetic mice. An evaluation of new smaller capsules.* Transplantation, 1992. **53**(6): p. 1180-3.
78. Wilson, J.T. and E.L. Chaikof, *Challenges and emerging technologies in the immunoisolation of cells and tissues.* Adv Drug Delivery Rev, 2008. **60**(2): p. 124-145.
79. Cushing, M.C. and K.S. Anseth, *Hydrogel cell cultures.* Science, 2007. **316**(5828): p. 1133-1134.
80. De Vos, P., et al., *Efficacy of a prevascularized expanded polytetrafluoroethylene solid support system as a transplantation site for pancreatic islets.* Transplantation, 1997. **63**(6): p. 824-830.
81. Hussey, A.J., et al., *Seeding of pancreatic islets into prevascularized tissue engineering chambers.* Tissue Eng Part A, 2009. **15**(12): p. 3823-33.
82. Lembert, N., et al., *Encapsulation of islets in rough surface, hydroxymethylated polysulfone capillaries stimulates VEGF release and promotes vascularization after transplantation.* Cell Transplant, 2005. **14**(2-3): p. 97-108.
83. Trivedi, N., et al., *Improved vascularization of planar membrane diffusion devices following continuous infusion of vascular endothelial growth factor.* Cell Transplant, 2000. **9**(1): p. 115-124.
84. Sigrist, S., et al., *Influence of VEGF on the viability of encapsulated pancreatic rat islets after transplantation in diabetic mice.* Cell Transplant, 2003. **12**(6): p. 627-35.
85. Moon, J.J., et al., *Biomimetic hydrogels with pro-angiogenic properties.* Biomaterials, 2010. **31**(14): p. 3840-7.
86. Teramura, Y. and H. Iwata, *Bioartificial pancreas microencapsulation and conformal coating of islet of Langerhans.* Adv Drug Deliv Rev, 2010. **62**(7-8): p. 827-40.
87. Sefton, M.V., et al., *Making microencapsulation work: conformal coating, immobilization gels and in vivo performance.* J Control Release, 2000. **65**(1-2): p. 173-86.
88. Teramura, Y. and H. Iwata, *Islet encapsulation with living cells for improvement of biocompatibility.* Biomaterials, 2009. **30**(12): p. 2270-5.
89. Teramura, Y., et al., *Behavior of synthetic polymers immobilized on a cell membrane.* Biomaterials, 2008. **29**(10): p. 1345-1355.
90. Peppas, N.A. and A.G. Mikos, *Preparation methods and structure of hydrogels*, in *Hydrogels in Med and Pharm*, N. Peppas, Editor. 1986, CRC Press. p. 1-26.
91. Peppas, N.A., et al., *Hydrogels in pharmaceutical formulations.* Eur J Pharm Biopharm, 2000. **50**(1): p. 27-46.
92. Drury, J.L. and D.J. Mooney, *Hydrogels for tissue engineering: scaffold design variables and applications.* Biomaterials, 2003. **24**(24): p. 4337-51.
93. Peppas, N.A., et al., *Physicochemical foundations and structural design of hydrogels in medicine and biology.* Annu Rev Biomed Eng, 2000. **2**: p. 9-29.
94. Ernst, L.J., et al., *Polymer materials characterization, modeling and application*, in *Micro- and opto-electronic materials and structures*, E. Suhir, C. Wong, and Y.C. Lee, Editors. 2006, Springer. p. 3-34.

95. Kessler, L., et al., *Influence of corona surface treatment on the properties of an artificial membrane used for Langerhans islets encapsulation: permeability and biocompatibility studies.* Biomaterials, 1995. **16**(3): p. 185-91.
96. Iwata, H., N. Morikawa, and Y. Ikada, *Permeability of filters used for immunoisolation.* Tissue Eng, 1996. **2**(4): p. 289-298.
97. Smith, C., et al., *Diffusion characteristics of microfabricated silicon nanopore membranes as immunoisolation membranes for use in cellular therapeutics.* Diabetes Tech Therapeut, 2005. **7**(1): p. 151-162.
98. Minjing, Z., et al., *Preparation of porous TiO2/Ti composite membrane for immunoisolation.* Appl Surf Sci, 2008. **255**(5 PART 1): p. 2256-2258.
99. Liu, L., et al., *Bio-ceramic hollow fiber membranes for immunoisolation and gene delivery. I: Membrane development.* J Membr Sci, 2006. **280**(1-2): p. 375-382.
100. Loudovaris, T., et al., *Destruction of xenografts but not allografts within cell impermeable membranes.* Transplant Proc, 1992. **24**(5): p. 2291-2.
101. Zimmermann, H., et al., *Hydrogel-based encapsulation of biological, functional tissue: fundamentals, technologies and applications.* Appl Phys A, 2007. **89**(4): p. 909-922.
102. Williams, D.F., *Definitions in biomaterials : proceedings of a consensus conference of the European Society for Biomaterials, Chester, England, March 3-5, 1986*. Progress in biomedical engineering 4. 1987, Amsterdam ; New York: Elsevier. vii, p.72
103. Hou, Q.P. and Y.H. Bae, *Biohybrid artificial pancreas based on macrocapsule device.* Adv Drug Deliv Rev, 1999. **35**(2-3): p. 271-287.
104. Engler, A.J., et al., *Matrix elasticity directs stem cell lineage specification.* Cell, 2006. **126**(4): p. 677-89.
105. Banerjee, A., et al., *The influence of hydrogel modulus on the proliferation and differentiation of encapsulated neural stem cells.* Biomaterials, 2009. **30**(27): p. 4695-9.
106. Seidlits, S.K., et al., *The effects of hyaluronic acid hydrogels with tunable mechanical properties on neural progenitor cell differentiation.* Biomaterials, 2010. **31**(14): p. 3930-3940.
107. Moussy, F., et al., *In vitro evaluation of a bioartificial pancreas under various hemodynamic conditions.* Artif Organs, 1989. **13**(2): p. 109-15.
108. Anseth, K.S., C.N. Bowman, and L. BrannonPeppas, *Mechanical properties of hydrogels and their experimental determination.* Biomaterials, 1996. **17**(17): p. 1647-1657.
109. Martens, P., et al., *Effect of poly(vinyl alcohol) macromer chemistry and chain interactions on hydrogel mechanical properties.* Chem Mater, 2007. **19**(10): p. 2641-2648.
110. Schneider, S., et al., *Multilayer capsules: a promising microencapsulation system for transplantation of pancreatic islets.* Biomaterials, 2001. **22**(14): p. 1961-70.
111. Calafiore, R., et al., *Transplantation of pancreatic islets contained in minimal volume microcapsules in diabetic high mammalians.* Ann N Y Acad Sci, 1999. **875**: p. 219-32.
112. Inoue, K., et al., *Experimental hybrid islet transplantation: application of polyvinyl alcohol membrane for entrapment of islets.* Pancreas, 1992. **7**(5): p. 562-8.

113. Kung, I.M., et al., *Surface modifications of alginate/poly(L-lysine) microcapsular membranes with poly(ethylene glycol) and poly(vinyl alcohol).* Biomaterials, 1995. **16**(8): p. 649-55.
114. Brissova, M., et al., *Evaluation of microcapsule permeability via inverse size exclusion chromatography.* Anal Biochem, 1996. **242**(1): p. 104-11.
115. King, G.A., et al., *Alginate-polylysine microcapsules of controlled membrane molecular weight cutoff for mammalian cell culture engineering.* Biotechnol Progr, 1987. **3**(4): p. 231-240.
116. Vandenbossche, G.M.R., et al., *The molecular weight cut-off of microcapsules is determined by the reaction between alginate and polylysine.* Biotechnol Bioeng, 1993. **42**(3): p. 381-386.
117. Cha, C., et al., *Decoupled control of stiffness and permeability with a cell-encapsulating poly(ethylene glycol) dimethacrylate hydrogel.* Biomaterials, 2010. **31**(18): p. 4864-4871.
118. Peppas, N.A., et al., *Hydrogels in biology and medicine: From molecular principles to bionanotechnology.* Adv Mater, 2006. **18**(11): p. 1345-1360.
119. Lim, F. and A.M. Sun, *Microencapsulated islets as bioartificial endocrine pancreas.* Science, 1980. **210**(4472): p. 908-10.
120. Buschmann, M.D., et al., *Chondrocytes in agarose culture synthesize a mechanically functional extracellular matrix.* J Orthop Res, 1992. **10**(6): p. 745-58.
121. Ye, Q., et al., *Fibrin gel as a three dimensional matrix in cardiovascular tissue engineering.* Eur J Cardiothorac Surg, 2000. **17**(5): p. 587-91.
122. Chung, C., et al., *Differential behavior of auricular and articular chondrocytes in hyaluronic acid hydrogels.* Tissue Eng Part A, 2008. **14**(7): p. 1121-31.
123. Li, Q., et al., *Photocrosslinkable polysaccharides based on chondroitin sulfate.* J Biomed Mater Res A, 2004. **68**(1): p. 28-33.
124. Okhamafe, A.O., et al., *Modulation of protein release from chitosan-alginate microcapsules using the pH-sensitive polymer hydroxypropyl methylcellulose acetate succinate.* J Microencapsul, 1996. **13**(5): p. 497-508.
125. Risbud, M.V. and R.R. Bhonde, *Islet immunoisolation: experience with biopolymers.* J Biomater Sci Polym Ed, 2001. **12**(11): p. 1243-52.
126. Imani, R., et al., *Preparation and characterization of agarose-gelatin blend hydrogels as a cell encapsulation matrix: An in-vitro study.* J Macromol Sci B, 2012. **51**(8): p. 1606-1616.
127. Nicodemus, G.D. and S.J. Bryant, *Cell encapsulation in biodegradable hydrogels for tissue engineering applications.* Tissue Eng Part B Rev, 2008. **14**(2): p. 149-65.
128. Behravesh, E., et al., *Synthesis of in situ cross-linkable macroporous biodegradable poly(propylene fumarate-co-ethylene glycol) hydrogels.* Biomacromolecules, 2002. **3**(2): p. 374-81.
129. Qi, M., et al., *PVA hydrogel sheet macroencapsulation for the bioartificial pancreas.* Biomaterials, 2004. **25**(27): p. 5885-92.
130. Bryant, S.J. and K.S. Anseth, *Hydrogel properties influence ECM production by chondrocytes photoencapsulated in poly(ethylene glycol) hydrogels.* J Biomed Mater Res, 2002. **59**(1): p. 63-72.
131. Lee, K.Y. and D.J. Mooney, *Hydrogels for tissue engineering.* Chem Rev, 2001. **101**(7): p. 1869-79.
132. Hamidi, M., A. Azadi, and P. Rafiei, *Hydrogel nanoparticles in drug delivery.* Adv Drug Deliv Rev, 2008. **60**(15): p. 1638-49.

133. Martens, P., T. Holland, and K.S. Anseth, *Synthesis and characterization of degradable hydrogels formed from acrylate modified poly(vinyl alcohol) macromers.* Polymer, 2002. **43**(23): p. 6093-6100.
134. Martens, P.J., S.J. Bryant, and K.S. Anseth, *Tailoring the degradation of hydrogels formed from multivinyl poly(ethylene glycol) and poly(vinyl alcohol) macromers for cartilage tissue engineering.* Biomacromolecules, 2003. **4**(2): p. 283-292.
135. Cavalieri, F., et al., *Study of gelling behavior of poly(vinyl alcohol)-methacrylate for potential utilizations in tissue replacement and drug delivery.* Biomacromolecules, 2004. **5**(6): p. 2439-46.
136. Mawad, D., R. Odell, and L.A. Poole-Warren, *Network structure and macromolecular drug release from poly(vinyl alcohol) hydrogels fabricated via two crosslinking strategies.* Int J Pharm, 2009. **366**(1-2): p. 31-7.
137. Burczak, K., et al., *Protein permeation through poly(vinyl alcohol) hydrogel membranes.* Biomaterials, 1994. **15**(3): p. 231-8.
138. Schmedlen, R.H., K.S. Masters, and J.L. West, *Photocrosslinkable polyvinyl alcohol hydrogels that can be modified with cell adhesion peptides for use in tissue engineering.* Biomaterials, 2002. **23**(22): p. 4325-32.
139. Burdick, J.A. and K.S. Anseth, *Photoencapsulation of osteoblasts in injectable RGD-modified PEG hydrogels for bone tissue engineering.* Biomaterials, 2002. **23**(22): p. 4315-23.
140. Salinas, C.N., et al., *Chondrogenic differentiation potential of human mesenchymal stem cells photoencapsulated within poly(ethylene glycol)-arginine-glycine-aspartic acid-serine thiol-methacrylate mixed-mode networks.* Tissue Eng, 2007. **13**(5): p. 1025-34.
141. Hiraoka, M., et al., *Enhanced survival of neural cells embedded in hydrogels composed of collagen and laminin-derived cell adhesive peptide.* Bioconjug Chem, 2009. **20**(5): p. 976-83.
142. Stephens-Altus, J.S., et al., *Development of bioactive photocrosslinkable fibrous hydrogels.* J Biomed Mater Res A, 2011. **98**(2): p. 167-76.
143. Weber, L.M., et al., *The effects of cell-matrix interactions on encapsulated beta-cell function within hydrogels functionalized with matrix-derived adhesive peptides.* Biomaterials, 2007. **28**(19): p. 3004-11.
144. Nuttelman, C.R., et al., *Attachment of fibronectin to poly(vinyl alcohol) hydrogels promotes NIH3T3 cell adhesion, proliferation, and migration.* J Biomed Mater Res, 2001. **57**(2): p. 217-223.
145. Zajaczkowski, M.B., et al., *Cell-matrix adhesions on poly(vinyl alcohol) hydrogels.* Tissue Eng, 2003. **9**(3): p. 525-533.
146. Weber, L.M. and K.S. Anseth, *Hydrogel encapsulation environments functionalized with extracellular matrix interactions increase islet insulin secretion.* Matrix Biol, 2008. **27**(8): p. 667-673.
147. Nilasaroya, A., et al., *Structural and functional characterisation of poly(vinyl alcohol) and heparin hydrogels.* Biomaterials, 2008. **29**(35): p. 4658-64.
148. Bryant, S.J., et al., *Synthesis and characterization of photopolymerized multifunctional hydrogels: Water-soluble poly(vinyl alcohol) and chondroitin sulfate macromers for chondrocyte encapsulation.* Macromolecules, 2004. **37**(18): p. 6726-6733.

149. Leach, J.B., et al., *Development of photocrosslinkable hyaluronic acid-polyethylene glycol-peptide composite hydrogels for soft tissue engineering.* J Biomed Mater Res A, 2004. **70**(1): p. 74-82.
150. Shah, D.N., S.M. Recktenwall-Work, and K.S. Anseth, *The effect of bioactive hydrogels on the secretion of extracellular matrix molecules by valvular interstitial cells.* Biomaterials, 2008. **29**(13): p. 2060-72.
151. Mann, B.K., R.H. Schmedlen, and J.L. West, *Tethered-TGF-beta increases extracellular matrix production of vascular smooth muscle cells.* Biomaterials, 2001. **22**(5): p. 439-44.
152. Kopesky, P.W., et al., *Controlled delivery of transforming growth factor beta1 by self-assembling peptide hydrogels induces chondrogenesis of bone marrow stromal cells and modulates Smad2/3 signaling.* Tissue Eng Part A, 2011. **17**(1-2): p. 83-92.
153. Hoffman, A.S., *Hydrogels for biomedical applications.* Adv Drug Deliv Rev, 2002. **54**(1): p. 3-12.
154. Thanos, C.G., et al., *Intraperitoneal stability of alginate-polyornithine microcapsules in rats: an FTIR and SEM analysis.* Biomaterials, 2006. **27**(19): p. 3570-9.
155. Huang, X., et al., *Microenvironment of alginate-based microcapsules for cell culture and tissue engineering.* J Biosci Bioeng, 2012. **114**(1): p. 1-8.
156. Martinez, C.J., et al., *A Microfluidic Approach to Encapsulate Living Cells in Uniform Alginate Hydrogel Microparticles.* Macromol Biosci, 2012. **12**(7): p. 946-951.
157. Yang, F., et al., *The prolonged survival of fibroblasts with forced lipid catabolism in visceral fat following encapsulation in alginate-poly-l-lysine.* Biomaterials, 2012. **33**(22): p. 5638-5649.
158. Shu, X.Z., et al., *Disulfide cross-linked hyaluronan hydrogels.* Biomacromolecules, 2002. **3**(6): p. 1304-11.
159. Martens, P. and K.S. Anseth, *Characterization of hydrogels formed from acrylate modified poly(vinyl alcohol) macromers.* Polymer, 2000. **41**(21): p. 7715-7722.
160. Temenoff, J.S., et al., *Thermally cross-linked oligo(poly(ethylene glycol) fumarate) hydrogels support osteogenic differentiation of encapsulated marrow stromal cells in vitro.* Biomacromolecules, 2004. **5**(1): p. 5-10.
161. Hong, Y., et al., *Covalently crosslinked chitosan hydrogel: properties of in vitro degradation and chondrocyte encapsulation.* Acta Biomater, 2007. **3**(1): p. 23-31.
162. Williams, C.G., et al., *In vitro chondrogenesis of bone marrow-derived mesenchymal stem cells in a photopolymerizing hydrogel.* Tissue Eng, 2003. **9**(4): p. 679-688.
163. Mironi-Harpaz, I., et al., *Photopolymerization of cell-encapsulating hydrogels: Crosslinking efficiency versus cytotoxicity.* Acta Biomater, 2012. **8**(5): p. 1838-1848.
164. Young, C.J., L.A. Poole-Warren, and P.J. Martens, *Combining submerged electrospray and UV photopolymerization for production of synthetic hydrogel microspheres for cell encapsulation.* Biotechnol Bioeng, 2012. **109**(6): p. 1561-1570.
165. Fairbanks, B.D., et al., *Photoinitiated polymerization of PEG-diacrylate with lithium phenyl-2,4,6-trimethylbenzoylphosphinate: polymerization rate and cytocompatibility.* Biomaterials, 2009. **30**(35): p. 6702-7.

166. Gehrke, S.H., et al., *Factors determining hydrogel permeability.* Ann N Y Acad Sci, 1997. **831**: p. 179-207.
167. Pillarella, M.R. and A.L. Zydney, *Theoretical analysis of the effect of convective flow on solute transport and insulin release in a hollow fiber bioartificial pancreas.* J Biomech Eng, 1990. **112**(2): p. 220-8.
168. Peppas, N.A. and S.R. Lustig, *Solute diffusion in hydrophilic network structures*, in *Hydrogels in medicine and pharmacy*, N.A. Peppas, Editor. 1986, CRC press. p. 57-83.
169. Savina, I.N., et al., *Characterization of macroporous gels*, in *Macroporous Polymers: Production Properties and Biotechnological/Biomedical applications*, B. Mattiasson, A. Kumar, and I. Galeaev, Editors. 2010, CRC Press. p. 211-230.
170. Pescosolido, L., et al., *Mesh size distribution determination of interpenetrating polymer network hydrogels.* Soft Matter, 2012. **8**(29): p. 3708-3715.
171. Zainuddin, et al., *The states, diffusion, and concentration distribution of water in radiation-formed PVA/PVP hydrogels.* Soft Mater, 2004. **2**(2-3): p. 195-212.
172. Li, W., F. Xue, and R. Cheng, *States of water in partially swollen poly(vinyl alcohol) hydrogels.* Polymer, 2005. **46**(25): p. 12026-12031.
173. Ruiz, J., A. MantecÃ³n, and V. CÃ¡diz, *States of water in poly(vinyl alcohol) derivative hydrogels.* J Polym Sci B, 2003. **41**(13): p. 1462-1467.
174. Mikhalovska, L.I., et al., *Characterisation of the nanoporous structure of collagen-glycosaminoglycan hydrogels by freezing-out of bulk and bound water.* Biomaterials, 2006. **27**(19): p. 3599-607.
175. Kyritsis, A., et al., *Water and polymer dynamics in poly(hydroxyl ethyl acrylate-co-ethyl acrylate) copolymer hydrogels.* Eur Polym J. **47**(12): p. 2391-2402.
176. Liao, H.M., et al., *Influence of hydrogel mechanical properties and mesh size on vocal fold fibroblast extracellular matrix production and phenotype.* Acta Biomaterialia, 2008. **4**(5): p. 1161-1171.
177. Browning, M.B., et al., *Compositional control of poly(ethylene glycol) hydrogel modulus independent of mesh size.* J Biomed Mater Res Part A, 2011. **98 A**(2): p. 268-273.
178. Peppas, N.A. and C.T. Reinhart, *Solute diffusion in swollen membranes. Part I. A new theory.* J Membr Sci, 1983. **15**(3): p. 275-287.
179. Grassi, M., et al., *Scleroglucan/borax/drug hydrogels: Structure characterisation by means of rheological and diffusion experiments.* Carbohyd Polym, 2009. **78**(3): p. 377-383.
180. Grassi, M., et al., *Structural characterization of calcium alginate matrices by means of mechanical and release tests.* Molecules, 2009. **14**(8): p. 3003-3017.
181. Lu, S.X. and K.S. Anseth, *Release behavior of high molecular weight solutes from poly(ethylene glycol)-based degradable networks.* Macromolecules, 2000. **33**(7): p. 2509-2515.
182. Flory, P.J. and J. Rehner, *Statistical mechanics of cross-linked polymer networks I Rubberlike elasticity.* Journal of Chemical Physics, 1943. **11**(11): p. 512-520.
183. Flory, P.J. and J. Rehner, *Statistical mechanics of cross-linked polymer networks II Swelling.* Journal of Chemical Physics, 1943. **11**(11): p. 521-526.
184. Peppas, N.A. and R.E. Benner, *Proposed Method of Intracordal Injection and Gelation of Poly (Vinyl Alcohol) Solution in Vocal Cords - Polymer Considerations.* Biomaterials, 1980. **1**(3): p. 158-162.

185. Salinas, C.N. and K.S. Anseth, *Mixed mode thiol-acrylate photopolymerizations for the synthesis of PEG-peptide hydrogels.* Macromolecules, 2008. **41**(16): p. 6019-6026.
186. Peppas, N.A. and E.W. Merrill, *Crosslinked Polyvinyl-Alcohol) Hydrogels as Swollen Elastic Networks.* Journal of Applied Polymer Science, 1977. **21**(7): p. 1763-1770.
187. Flory, P.J. and J. Rehner Jr, *Statistical mechanics of cross-linked polymer networks II. Swelling.* J Chem Phys, 1943. **11**(11): p. 521-526.
188. Peppas, N.A. and E.W. Merrill, *Polyvinyl-Alcohol) Hydrogels - Reinforcement of Radiation-Crosslinked Networks by Crystallization.* J Polym Sci Polym Chem, 1976. **14**(2): p. 441-457.
189. Slaughter, B.V., et al., *Hydrogels in regenerative medicine.* Adv Mater, 2009. **21**(32-33): p. 3307-29.
190. Canal, T. and N.A. Peppas, *Correlation between mesh size and equilibrium degree of swelling of polymeric networks.* J Biomed Mater Res, 1989. **23**(10): p. 1183-93.
191. Flory, P.J., ed. *Principles of polymer chemistry*. 1953, Cornell University Press: Ithaca, NY.
192. Peppas, N.A. and E.W. Merrill, *Crosslinked poly(vinyl alcohol) hydrogels as swollen elastic networks.* J Appl Polym Sci, 1977. **21**(7): p. 1763-1770.
193. Turco, G., et al., *Mechanical spectroscopy and relaxometry on alginate hydrogels: a comparative analysis for structural characterization and network mesh size determination.* Biomacromolecules, 2011. **12**(4): p. 1272-82.
194. Singh, T.R.R., A.D. Woolfson, and R.F. Donnelly, *Investigation of solute permeation across hydrogels composed of poly(methyl vinyl ether-co-maleic acid) and poly(ethylene glycol).* J Pharm Pharmacol, 2010. **62**(7): p. 829-837.
195. Cruise, G.M., D.S. Scharp, and J.A. Hubbell, *Characterization of permeability and network structure of interfacially photopolymerized poly(ethylene glycol) diacrylate hydrogels.* Biomaterials, 1998. **19**(14): p. 1287-94.
196. Coromili, V. and T.M. Chang, *Polydisperse dextran as a diffusing test solute to study the membrane permeability of alginate polylysine microcapsules.* Biomater Artif Cells Immobilization Biotechnol, 1993. **21**(3): p. 427-44.
197. Dembczynski, R. and T. Jankowski, *Characterisation of small molecules diffusion in hydrogel-membrane liquid-core capsules.* Biochem Eng J, 2000. **6**(1): p. 41-44.
198. Nurdin, N., et al., *Capsule permeability via polymer and protein ingress/egress.* J Appl Polym Sci, 2000. **75**(9): p. 1165-1175.
199. Dembczynski, R. and T. Jankowski, *Determination of pore diameter and molecular weight cut-off of hydrogel-membrane liquid-core capsules for immunoisolation.* J Biomater Sci Polym Ed, 2001. **12**(9): p. 1051-8.
200. Kulseng, B., et al., *Alginate polylysine microcapsules as immune barrier: permeability of cytokines and immunoglobulins over the capsule membrane.* Cell Transplant, 1997. **6**(4): p. 387-94.
201. Brissova, M., et al., *Control and measurement of permeability for design of microcapsule cell delivery system.* J Biomed Mater Res, 1998. **39**(1): p. 61-70.
202. Okhamafe, A.O. and M.F. Goosen, *Control of membrane permeability in microcapsules*, in *Fundamentals of animal cell encapsulation and immobilization*, M.F. Goosen, Editor. 1993, CRC press. p. 55-78.

203. Shin, H.S., et al., *Permeation of solutes through interpenetrating polymer network hydrogels composed of poly(vinyl alcohol) and poly(acrylic acid).* J Appl Polym Sci, 1998. **69**(3): p. 479-486.
204. Reinhart, C.T. and N.A. Peppas, *Solute diffusion in swollen membranes. Part II. Influence of crosslinking on diffusive properties.* J Membr Sci, 1984. **18**(C): p. 227-239.
205. Peppas, N.A. and S.L. Wright, *Drug diffusion and binding in ionizable interpenetrating networks from poly(vinyl alcohol) and poly(acrylic acid).* Eur J Pharm Biopharm, 1998. **46**(1): p. 15-29.
206. Dong, L.C., A.S. Hoffman, and Q. Yan, *Dextran permeation through poly(N-isopropylacrylamide) hydrogels.* J Biomater Sci Polym Ed, 1994. **5**(5): p. 473-84.
207. Mawad, D., et al., *The effect of redox polymerisation on degradation and cell responses to poly (vinyl alcohol) hydrogels.* Biomaterials, 2007. **28**(6): p. 947-55.
208. Gu, F., B. Amsden, and R. Neufeld, *Sustained delivery of vascular endothelial growth factor with alginate beads.* J Control Release, 2004. **96**(3): p. 463-72.
209. Jay, S.M. and W.M. Saltzman, *Controlled delivery of VEGF via modulation of alginate microparticle ionic crosslinking.* J Control Release, 2009. **134**(1): p. 26-34.
210. Schillemans, J.P., W.E. Hennink, and C.F. van Nostrum, *The effect of network charge on the immobilization and release of proteins from chemically crosslinked dextran hydrogels.* Eur J Pharm Biopharm, 2010. **76**(3): p. 329-335.
211. Gharapetian, H., et al., *Polyacrylate microcapsules for cell encapsulation: Effects of copolymer structure on membrane properties.* Biotechnol Bioeng, 1987. **30**(6): p. 775-9.
212. Kuo, C.K. and P.X. Ma. *Controlling diffusion of solutes through ionically crosslinked alginate hydrogels designed for tissue engineering*. in *Materials Research Society Symposium - Proceedings*. 2001.
213. Martinsen, A., G. Skjak-Braek, and O. Smidsrod, *Alginate as immobilization material: I. Correlation between chemical and physical properties of alginate gel beads.* Biotechnol Bioeng, 1989. **33**(1): p. 79-89.
214. Burczak, K., E. Gamian, and A. Kochman, *Long-term in vivo performance and biocompatibility of poly(vinyl alcohol) hydrogel macrocapsules for hybrid-type artificial pancreas.* Biomaterials, 1996. **17**(24): p. 2351-6.
215. Muhr, A.H. and J.M.V. Blanshard, *Diffusion in Gels.* Polymer, 1982. **23**(7): p. 1012-1026.
216. Brown, W. and k. Chitumbo, *Solute diffusion in hydrated polymer networks. Part 1.—Cellulose gels.* J Chem Soc , Faraday Trans 1, 1975. **71**: p. 1-11.
217. Matsumoto, A., et al., *Specific polymerization behavior of triallyl isocyanurate. Accumulation of radicals before gelation.* Polymer Journal, 2000. **32**(1): p. 79-81.
218. Salmons, B. and W.H. Gunzburg, *Therapeutic application of cell microencapsulation in cancer.* Adv Exp Med Biol, 2010. **670**: p. 92-103.
219. Matsumoto, A., et al., *Steric Control of Gelation in Monovinyl-Multivinyl Polymerization Leading to Preparation of Self-Cross-Linkable Polymer Having Pendant Vinyl Groups.* Eur Polym J, 1991. **27**(12): p. 1417-1420.
220. Martens, P., et al., *A generalized bulk-degradation model for hydrogel networks formed from multivinyl cross-linking molecules.* J Phys Chem B, 2001. **105**(22): p. 5131-5138.

221. Chong, S.F., et al., *Tuning the permeability of polymer hydrogel capsules: an investigation of cross-linking density, membrane thickness, and cross-linkers.* Langmuir, 2011. **27**(5): p. 1724-30.
222. Kim, S.K., J.H. Son, and S.H. Yu, *Encapsulated animal cell culture for the production of monoclonal antibody (MAb).* Biotechnol Bioprocess Eng, 1997. **2**(2): p. 73-76.
223. Sauer, D. and J.W. McGinity, *Influence of additives on melt viscosity, surface tension, and film formation of dry powder coatings film formation of dry powder coatings.* Drug Dev Ind Pharm, 2009. **35**(6): p. 646-654.
224. Daly, M.M., *Chitosan-alginate complex coacervate capsules: Effects of calcium chloride, plasticizers, and polyelectrolytes on mechanical stability.* Biotechnol Progr, 1988. **4**(2): p. 76-81.
225. Ramanujan, S., et al., *Diffusion and convection in collagen gels: implications for transport in the tumor interstitium.* Biophys J, 2002. **83**(3): p. 1650-60.
226. Erikson, A., et al., *Physical and chemical modifications of collagen gels: impact on diffusion.* Biopolymers, 2008. **89**(2): p. 135-43.
227. Magzoub, M., S. Jin, and A.S. Verkman, *Enhanced macromolecule diffusion deep in tumors after enzymatic digestion of extracellular matrix collagen and its associated proteoglycan decorin.* FASEB J, 2008. **22**(1): p. 276-84.
228. Liu, L., et al., *A focused sulfated glycoconjugate Ugi library for probing heparan sulfate-binding angiogenic growth factors.* Bioorg Med Chem Lett, 2012. **22**(19): p. 6190-6194.
229. Chen, F.F., et al., *Significance of heparin binding to basic residues in homologous to the amino terminus of hepatoma-derived growth factor and related proteins.* Glycobiology, 2012. **22**(5): p. 649-661.
230. Cecchi, F., et al., *Targeted Disruption of Heparan Sulfate Interaction with Hepatocyte and Vascular Endothelial Growth Factors Blocks Normal and Oncogenic Signaling.* Cancer Cell, 2012. **22**(2): p. 250-262.
231. Lee, S.I., et al., *Endoplasmic reticulum stress modulates nicotine-induced extracellular matrix degradation in human periodontal ligament cells.* J Periodontal Res, 2012. **47**(3): p. 299-308.
232. Gu, Z., V. Fonseca, and C.M. Hai, *Nicotinic acetylcholine receptor mediates nicotine-induced actin cytoskeletal remodeling and extracellular matrix degradation by vascular smooth muscle cells.* Vasc Pharmacol, 2012.
233. Jacobs, N.T., et al., *Effect of orientation and targeted extracellular matrix degradation on the shear mechanical properties of the annulus fibrosus.* J Mech Behav Biomed, 2011. **4**(8): p. 1611-1619.
234. Coviello, T., et al., *Polysaccharide hydrogels for modified release formulations.* J Control Release, 2007. **119**(1): p. 5-24.
235. Young, S., et al., *Gelatin as a delivery vehicle for the controlled release of bioactive molecules.* J Control Release, 2005. **109**(1–3): p. 256-274.
236. Yamamoto, M., Y. Ikada, and Y. Tabata, *Controlled release of growth factors based on biodegradation of gelatin hydrogel.* J Biomater Sci Polym Ed, 2001. **12**(1): p. 77-88.
237. Cheng, F., et al., *Modeling of small-molecule release from crosslinked hydrogel microspheres: effect of crosslinking and enzymatic degradation of hydrogel matrix.* Int J Pharm, 2011. **403**(1-2): p. 90-5.

238. Baroli, B., *Photopolymerization of biomaterials: Issues and potentialities in drug delivery, tissue engineering, and cell encapsulation applications.* J Chem Technol Biotechnol, 2006. **81**(4): p. 491-499.
239. Davis, K.A. and K.S. Anseth, *Controlled release from crosslinked degradable networks.* Crit Rev Ther Drug Carrier Syst, 2002. **19**(4-5): p. 385-423.
240. Weber, L.M., C.G. Lopez, and K.S. Anseth, *Effects of PEG hydrogel crosslinking density on protein diffusion and encapsulated islet survival and function.* J Biomed Mater Res A, 2009. **90**(3): p. 720-729.
241. Nafea, E.H., et al., *Immunoisolating semi-permeable membranes for cell encapsulation: Focus on hydrogels.* J Control Release, 2011. **154**(2): p. 110-122.
242. Fu, Y., et al., *3D cell entrapment in crosslinked thiolated gelatin-poly(ethylene glycol) diacrylate hydrogels.* Biomaterials, 2012. **33**(1): p. 48-58.
243. Bryant, S.J. and K.S. Anseth, *The effects of scaffold thickness on tissue engineered cartilage in photocrosslinked poly(ethylene oxide) hydrogels.* Biomaterials, 2001. **22**(6): p. 619-626.
244. Pescosolido, L., et al., *Hyaluronic Acid and Dextran-Based Semi-IPN Hydrogels as Biomaterials for Bioprinting.* Biomacromolecules, 2011. **12**(5): p. 1831-1838.
245. Brinkman, W.T., et al., *Photo-cross-linking of type I collagen gels in the presence of smooth muscle cells: Mechanical properties, cell viability, and function.* Biomacromolecules, 2003. **4**(4): p. 890-895.
246. Benton, J.A., et al., *Photocrosslinking of Gelatin Macromers to Synthesize Porous Hydrogels That Promote Valvular Interstitial Cell Function.* Tissue Engineering Part A, 2009. **15**(11): p. 3221-3230.
247. Prado, S.S., J.M. Weaver, and B.J. Love, *Gelation of photopolymerized hyaluronic acid grafted with glycidyl methacrylate.* Mater Sci Eng C, 2011. **31**(8): p. 1767-1771.
248. Baroli, B., *Hydrogels for tissue engineering and delivery of tissue-inducing substances.* J Pharm Sci, 2007. **96**(9): p. 2197-223.
249. Martens, P.J., C.N. Bowman, and K.S. Anseth, *Degradable networks formed from multi-functional poly(vinyl alcohol) macromers: Comparison of results from a generalized bulk-degradation model for polymer networks and experimental data.* Polymer, 2004. **45**(10): p. 3377-3387.
250. Van Dijk-Wolthuis, W.N.E., et al., *Synthesis, characterization, and polymerization of glycidyl methacrylate derivatized dextran.* Macromolecules, 1995. **28**(18): p. 6317-6322.
251. Deforest, C.A. and K.S. Anseth, *Advances in bioactive hydrogels to probe and direct cell fate.* Annu Rev Chem Biomol Eng. **3**: p. 421-44.
252. Hennink, W.E., et al., *Controlled release of proteins from dextran hydrogels.* J Control Release, 1996. **39**(1): p. 47-55.
253. Hennink, W.E., et al., *Dextran hydrogels for the controlled release of proteins.* J Control Release, 1997. **48**(2-3): p. 107-114.
254. Peppas, N.A. and E.W. Merrill, *Polyvinyl-Alcohol) Hydrogels - Reinforcement of Radiation-Crosslinked Networks by Crystallization.* J. Polym. Sci., Part A: Polym. Chem., 1976. **14**(2): p. 441-457.
255. Hickey, A.S. and N.A. Peppas, *Solute diffusion in poly(vinyl alcohol)/ poly(acrylic acid) composite membranes prepared by freezing/thawing techniques.* Polymer, 1997. **38**(24): p. 5931-5936.

256. Bourke, S.L., et al., *A photo-crosslinked poly(vinyl alcohol) hydrogel growth factor release vehicle for wound healing applications.* AAPS PharmSci, 2003. **5**(4): p. E33.
257. Nandi, S. and H.H. Winter, *Swelling behavior of partially cross-linked polymers: A ternary system.* Macromolecules, 2005. **38**(10): p. 4447-4455.
258. Kundu, J., et al., *Silk fibroin/poly(vinyl alcohol) photocrosslinked hydrogels for delivery of macromolecular drugs.* Acta Biomater, 2012. **8**(5): p. 1720-9.
259. Lim, K.S., et al., *The influence of silkworm species on cellular interactions with novel PVA/silk sericin hydrogels.* Macromol Biosci, 2012. **12**(3): p. 322-32.
260. Martens, P., S.J. Bryant, and K.S. Anseth, *Photopolymerization of poly(vinyl alcohol) and poly(ethylene glycol) based macromers to produce crosslinked, degradable hydrogels with controlled transport properties.* Abstracts of Papers of the American Chemical Society, 2002. **224**: p. U54-U54.
261. Ouasti, S., et al., *Network connectivity, mechanical properties and cell adhesion for hyaluronic acid/PEG hydrogels.* Biomaterials, 2011. **32**(27): p. 6456-70.
262. Ube, T., et al., *Relaxation of single polymer chain in binary molecular weight blends observed by scanning near-field optical microscopy.* Soft Matter, 2012. **8**(20): p. 5603-5611.
263. Peppas, N.A. and B.D. Barr-Howell, *Characterization of the cross-linked structure of hydrogels*, in *Hydrogels in medicine and pharmacy*, N.A. Peppas, Editor. 1986, CRC press. p. 27-56.
264. Matsuyama, H., M. Teramoto, and H. Urano, *Analysis of solute diffusion in poly(vinyl alcohol) hydrogel membrane.* J Membr Sci, 1997. **126**(1): p. 151-160.
265. He, H., X. Cao, and L.J. Lee, *Design of a novel hydrogel-based intelligent system for controlled drug release.* J Control Release, 2004. **95**(3): p. 391-402.
266. Iwata, H., Y. Murakami, and Y. Ikada, *Control of complement activities for immunoisolation*, in *Ann N Y Acad Sci*1999. p. 7-23.
267. Kang, J., et al., *Toward a bioartificial pancreas: diffusion of insulin and IgG across immunoprotective membranes with controlled hydrophilic channel diameters.* Macromol Biosci, 2010. **10**(4): p. 369-77.
268. Colton, C.K., *Implantable biohybrid artificial organs.* Cell Transplant, 1995. **4**(4): p. 415-36.
269. Baker, A.R., et al., *Evaluation of an immunoisolation membrane formed by incorporating a polyvinyl alcohol hydrogel within a microporous filter support.* Cell Transplant., 1997. **6**(6): p. 585-595.
270. Dai, W.S. and T.A. Barbari, *Hydrogel membranes with mesh size asymmetry based on the gradient crosslinking of poly(vinyl alcohol).* J Membr Sci, 1999. **156**(1): p. 67-79.
271. Venturoli, D. and B. Rippe, *Ficoll and dextran vs. globular proteins as probes for testing glomerular permselectivity: effects of molecular size, shape, charge, and deformability.* Am J Physiol Renal Physiol, 2005. **288**(4): p. F605-13.
272. Ryabov, Y., et al., *Using the experimentally determined components of the overall rotational diffusion tensor to restrain molecular shape and size in NMR structure determination of globular proteins and protein-protein complexes.* J Am Chem Soc, 2009. **131**(27): p. 9522-31.
273. Wang, W., et al., *Antibody structure, instability, and formulation.* J Pharm Sci, 2007. **96**(1): p. 1-26.

274. Granath, K.A., *Solution properties of branched dextrans.* J Colloid Sci, 1958. **13**(4): p. 308-328.
275. Polymer Science Learning Center-Department of Polymer Science-The University of Southern Mississippi. *How polymers behave in dilute solutions*. [cited 2012 15/4/2012]; Available from: http://www.pslc.ws/macrog/ps5.htm.
276. Wikipedia-The Free Encyclopedia. *Bovine serum albumin*. [cited 2012 15/04/2012]; Available from: http://en.wikipedia.org/wiki/Bovine_serum_albumin.
277. Oxford Glycobiology Institute. *Molecular Model Archive*. [cited 2012 15/04/2012]; Available from: http://www.bioch.ox.ac.uk/glycob/archive/index.html.
278. DeForest, C.A. and K.S. Anseth, *Advances in bioactive hydrogels to probe and direct cell fate.* Annu Rev Chem Biomol Eng, 2012. **3**: p. 421-44.
279. Bellamkonda, R., et al., *Hydrogel-based three-dimensional matrix for neural cells.* J Biomed Mater Res, 1995. **29**(5): p. 663-71.
280. Epstein-Barash, H., C.F. Stefanescu, and D.S. Kohane, *An in situ cross-linking hybrid hydrogel for controlled release of proteins.* Acta Biomater, 2012. **8**(5): p. 1703-1709.
281. Ikada, Y. and Y. Tabata, *Protein release from gelatin matrices.* Adv Drug Deliv Rev, 1998. **31**(3): p. 287-301.
282. Matsui, M. and Y. Tabata, *Enhanced angiogenesis by multiple release of platelet-rich plasma contents and basic fibroblast growth factor from gelatin hydrogels.* Acta Biomater, 2012. **8**(5): p. 1792-1801.
283. Sargeant, T.D., et al., *An in situ forming collagen-PEG hydrogel for tissue regeneration.* Acta Biomater, 2012. **8**(1): p. 124-132.
284. Wang, A., et al., *Fabrication of gelatin microgels by a "cast" strategy for controlled drug release.* Adv Funct Mater, 2012. **22**(13): p. 2673-2681.
285. You, S.J., et al., *Preparation and characterization of gelatin-poly(vinyl alcohol) hydrogels for three-dimensional cell culture.* J Ind Eng Chem, 2007. **13**(1): p. 116-120.
286. Hutson, C.B., et al., *Synthesis and Characterization of Tunable Poly(Ethylene Glycol): Gelatin Methacrylate Composite Hydrogels.* Tissue Eng Part A, 2011. **17**(13-14): p. 1713-1723.
287. Drinnan, C.T., et al., *Multimodal release of transforming growth factor-β1 and the BB isoform of platelet derived growth factor from PEGylated fibrin gels.* J Control Release, 2010. **147**(2): p. 180-186.
288. Tae, G., et al., *PEG-cross-linked heparin is an affinity hydrogel for sustained release of vascular endothelial growth factor.* J Biomater Sci Polym Ed, 2006. **17**(1-2): p. 187-97.
289. Bhakta, G., et al., *Hyaluronic acid-based hydrogels functionalized with heparin that support controlled release of bioactive BMP-2.* Biomaterials, 2012. **33**(26): p. 6113-6122.
290. Jeon, O., et al., *Affinity-based growth factor delivery using biodegradable, photocrosslinked heparin-alginate hydrogels.* J Control Release, 2011. **154**(3): p. 258-266.
291. Kim, M., et al., *Heparin-based hydrogel as a matrix for encapsulation and cultivation of primary hepatocytes.* Biomaterials, 2010. **31**(13): p. 3596-3603.

292. Kuijpers, A.J., et al., *In vitro and in vivo evaluation of gelatin-chondroitin sulphate hydrogels for controlled release of antibacterial proteins.* Biomaterials, 2000. **21**(17): p. 1763-72.
293. Kuijpers, A.J., et al., *In vivo and in vitro release of lysozyme from cross-linked gelatin hydrogels: a model system for the delivery of antibacterial proteins from prosthetic heart valves.* J Control Release, 2000. **67**(2-3): p. 323-36.
294. Stylianopoulos, T., et al., *Diffusion anisotropy in collagen gels and tumors: The effect of fiber network orientation.* Biophys J, 2010. **99**(10): p. 3119-3128.
295. Netti, P.A., et al., *Role of extracellular matrix assembly in interstitial transport in solid tumors.* Cancer Res, 2000. **60**(9): p. 2497-2503.
296. Pluen, A., et al., *Role of tumor-host interactions in interstitial diffusion of macromolecules: Cranial vs. subcutaneous tumors.* PNAS, 2001. **98**(8): p. 4628-4633.
297. Casu, B., *Structure and active domains of heparin*, in *Chemistry and biology of heparin and heparan sulphate*, H.G. Garg, R.J. Linhardt, and C.A. Hales, Editors. 2005, Elsevier: UK.
298. Whitelock, J.M. and R.V. Iozzo, *Heparan sulfate: a complex polymer charged with biological activity.* Chem Rev, 2005. **105**(7): p. 2745-64.
299. Casu, B., A. Naggi, and G. Torri, *Heparin-derived heparan sulfate mimics to modulate heparan sulfate-protein interaction in inflammation and cancer.* Matrix Biol, 2010. **29**(6): p. 442-452.
300. Lohrmann, J. and R.C. Becker, *New anticoagulants - The path from discovery to clinical practice.* New Engl J Med, 2008. **358**(26): p. 2827-2829.
301. Gémez-Outes, A., et al., *Discovery of anticoagulant drugs: A historical perspective.* Curr Drug Discov Tech, 2012. **9**(2): p. 83-104.
302. Tae, G., et al., *Formation of a novel heparin-based hydrogel in the presence of heparin-binding biomolecules.* Biomacromolecules, 2007. **8**(6): p. 1979-86.
303. Tsurkan, M.V., et al., *Enzymatically degradable heparin-polyethylene glycol gels with controlled mechanical properties.* Chem Commun (Camb), 2010. **46**(7): p. 1141-1143.
304. Nie, T., R.E. Akins, Jr., and K.L. Kiick, *Production of heparin-containing hydrogels for modulating cell responses.* Acta Biomater, 2009. **5**(3): p. 865-75.
305. Hu, X., et al., *Gelatin hydrogel prepared by photo-initiated polymerization and loaded with TGF-beta1 for cartilage tissue engineering.* Macromol Biosci, 2009. **9**(12): p. 1194-201.
306. Hunt, N.C. and L.M. Grover, *Cell encapsulation using biopolymer gels for regenerative medicine.* Biotechnology Letters, 2010. **32**(6): p. 733-742.
307. Dubruel, P., et al., *Porous gelatin hydrogels: 2. In vitro cell interaction study.* Biomacromolecules, 2007. **8**(2): p. 338-44.
308. Elvin, C.M., et al., *A highly elastic tissue sealant based on photopolymerised gelatin.* Biomaterials. **31**(32): p. 8323-31.
309. Nilasaroya, A., *Poly(vinyl alcohol) and heparin hydrogels:Synthesis, structure and presentation of signalling molecules for growth factor activation*, in *Graduate school of biomedical engineering*2010, Doctor of Philosophy thesis,New South wales: Australia.
310. Van Den Bulcke, A.I., et al., *Structural and rheological properties of methacrylamide modified gelatin hydrogels.* Biomacromolecules, 2000. **1**(1): p. 31-8.

311. Toida, T., et al., *Chemical microdetermination of heparin in plasma.* Anal Biochem, 1997. **251**(2): p. 219-26.
312. Mwangi, J.W. and C.M. Ofner, 3rd, *Crosslinked gelatin matrices: release of a random coil macromolecular solute.* Int J Pharm, 2004. **278**(2): p. 319-27.
313. Gohon, Y., et al., *Partial specific volume and solvent interactions of amphipol A8-35.* Anal Biochem, 2004. **334**(2): p. 318-34.
314. Deiber, J.A., et al., *Characterization of cross-linked polyampholytic gelatin hydrogels through the rubber elasticity and thermodynamic swelling theories.* Polymer, 2009. **50**(25): p. 6065-6075.
315. Bohidar, H.B., *Hydrodynamic properties of gelatin in dilute solutions.* International Journal of Biological Macromolecules, 1998. **23**(1): p. 1-6.
316. Farndale, R.W., D.J. Buttle, and A.J. Barrett, *Improved quantitation and discrimination of sulphated glycosaminoglycans by use of dimethylmethylene blue.* Biochim Biophys Acta, 1986. **883**(2): p. 173-7.
317. Li, Q., D.A. Wang, and J.H. Elisseeff, *Heterogeneous-phase reaction of glycidyl methacrylate and chondroitin sulfate: Mechanism of ring-opening-transesterification competition.* Macromolecules, 2003. **36**(7): p. 2556-2562.
318. Dreesmann, L., M. Ahlers, and B. Schlosshauer, *The pro-angiogenic characteristics of a cross-linked gelatin matrix.* Biomaterials, 2007. **28**(36): p. 5536-43.
319. Nichol, J.W., et al., *Cell-laden microengineered gelatin methacrylate hydrogels.* Biomaterials, 2010. **31**(21): p. 5536-44.
320. Xiao, W.Q., et al., *Synthesis and characterization of photocrosslinkable gelatin and silk fibroin interpenetrating polymer network hydrogels.* Acta Biomater, 2011. **7**(6): p. 2384-2393.
321. Pike, D.B., et al., *Heparin-regulated release of growth factors in vitro and angiogenic response in vivo to implanted hyaluronan hydrogels containing VEGF and bFGF.* Biomaterials, 2006. **27**(30): p. 5242-51.
322. Vlierberghe, S.V., et al., *Porous gelatin hydrogels: 1. Cryogenic formation and structure analysis.* Biomacromolecules, 2007. **8**(2): p. 331-7.
323. Jansson, E. and P. Tengvall, *Adsorption of albumin and IgG to porous and smooth titanium.* Colloids Surf B, 2004. **35**(1): p. 45-51.
324. Kim, T.G., H. Shin, and D.W. Lim, *Biomimetic scaffolds for tissue engineering.* Advanced Functional Materials. **22**(12): p. 2446-2468.
325. Shu, X.Z., et al., *Synthesis and evaluation of injectable, in situ crosslinkable synthetic extracellular matrices for tissue engineering.* J Biomed Mater Res A, 2006. **79**(4): p. 902-12.
326. Xin, X., et al., *Hyaluronic-acid-based semi-interpenetrating materials.* J Biomater Sci Polym Ed, 2004. **15**(9): p. 1223-36.
327. Rowe, S.L. and J.P. Stegemann, *Interpenetrating collagen-fibrin composite matrices with varying protein contents and ratios.* Biomacromolecules, 2006. **7**(11): p. 2942-8.
328. Shin, H., B.D. Olsen, and A. Khademhosseini, *The mechanical properties and cytotoxicity of cell-laden double-network hydrogels based on photocrosslinkable gelatin and gellan gum biomacromolecules.* Biomaterials, 2012. **33**(11): p. 3143-3152.

329. Marsich, E., et al., *Alginate/lactose-modified chitosan hydrogels: a bioactive biomaterial for chondrocyte encapsulation.* J Biomed Mater Res A, 2008. **84**(2): p. 364-76.
330. Oliviero, O., M. Ventre, and P.A. Netti, *Functional porous hydrogels to study angiogenesis under the effect of controlled release of vascular endothelial growth factor.* Acta Biomater, 2012. **8**(9): p. 3294-3301.
331. Freudenberg, U., et al., *A star-PEG-heparin hydrogel platform to aid cell replacement therapies for neurodegenerative diseases.* Biomaterials, 2009. **30**(28): p. 5049-5060.
332. Knox, S., et al., *Not all perlecans are created equal: interactions with fibroblast growth factor (FGF) 2 and FGF receptors.* J Biol Chem, 2002. **277**(17): p. 14657-65.
333. Reitan, N.K., et al., *Macromolecular diffusion in the extracellular matrix measured by fluorescence correlation spectroscopy.* J Biomed Opt, 2008. **13**(5).
334. Kuijpers, A.J., et al., *Combined gelatin-chondroitin sulfate hydrogels for controlled release of cationic antibacterial proteins.* Macromolecules, 2000. **33**(10): p. 3705-3713.
335. Nilasaroya, A., P.J. Martens, and J.M. Whitelock, *Enzymatic degradation of heparin-modified hydrogels and its effect on bioactivity.* Biomaterials, 2012. **33**(22): p. 5534-40.
336. Prokoph, S., et al., *Sustained delivery of SDF-1α from heparin-based hydrogels to attract circulating pro-angiogenic cells.* Biomaterials, 2012. **33**(19): p. 4792-4800.
337. Zieris, A., et al., *Dual independent delivery of pro-angiogenic growth factors from starPEG-heparin hydrogels.* J Control Release, 2011. **156**(1): p. 32-40.
338. Sakiyama-Elbert, S.E. and J.A. Hubbell, *Controlled release of nerve growth factor from a heparin-containing fibrin-based cell ingrowth matrix.* J Control Release, 2000. **69**(1): p. 149-58.
339. Wu, J.M., et al., *Heparin-functionalized collagen matrices with controlled release of basic fibroblast growth factor.* J Mater Sci Mater Med, 2011. **22**(1): p. 107-14.
340. Tanihara, M., et al., *Sustained release of basic fibroblast growth factor and angiogenesis in a novel covalently crosslinked gel of heparin and alginate.* J Biomed Mater Res, 2001. **56**(2): p. 216-21.
341. Peattie, R.A., et al., *Effect of gelatin on heparin regulation of cytokine release from hyaluronan-based hydrogels.* Drug Deliv, 2008. **15**(6): p. 389-97.
342. Zhu, J., et al., *Biomimetic poly(ethylene glycol)-based hydrogels as scaffolds for inducing endothelial adhesion and capillary-like network formation.* Biomacromolecules, 2012. **13**(3): p. 706-713.
343. Weiss, M.S., et al., *The impact of adhesion peptides within hydrogels on the phenotype and signaling of normal and cancerous mammary epithelial cells.* Biomaterials, 2012. **33**(13): p. 3548-3559.
344. Rafat, M., et al., *Dual functionalized PVA hydrogels that adhere endothelial cells synergistically.* Biomaterials, 2012. **33**(15): p. 3880-3886.
345. Rafat, M., et al., *Engineered endothelial cell adhesion via VCAM1 and E-selectin antibody-presenting alginate hydrogels.* Acta Biomater, 2012. **8**(7): p. 2697-2703.
346. Park, H. and K.Y. Lee, *Facile control of RGD-alginate/hyaluronate hydrogel formation for cartilage regeneration.* Carbohyd Polym, 2011. **86**(3): p. 1107-1112.
347. Song, W., et al., *Poly(vinyl alcohol)/collagen/hydroxyapatite hydrogel: Properties and in vitro cellular response.* J Biomed Mater Res A, 2012.

348. Liu, Y. and M.B. Chan-Park, *A biomimetic hydrogel based on methacrylated dextran-graft-lysine and gelatin for 3D smooth muscle cell culture.* Biomaterials, 2010. **31**(6): p. 1158-1170.
349. Qi, Z., et al., *The in vivo performance of polyvinyl alcohol macro-encapsulated islets.* Biomaterials, 2010.
350. Qi, Z., et al., *Immunoisolation effect of polyvinyl alcohol (PVA) macroencapsulated islets in type 1 diabetes therapy.* Cell Transplant, 2012. **21**(2-3): p. 525-534.
351. Iwata, H., et al., *The use of photocrosslinkable polyvinyl alcohol in the immunoisolation of pancreatic islets.* Transplant Proc, 1990. **22**(2): p. 797-9.
352. Kurian, P., et al., *Synthesis, permeability and biocompatibility of tricomponent membranes containing polyethylene glycol, polydimethylsiloxane and polypentamethylcyclopentasiloxane domains.* Biomaterials, 2003. **24**(20): p. 3493-503.
353. Cruise, G.M., et al., *In vitro and in vivo performance of porcine islets encapsulated in interfacially photopolymerized poly(ethylene glycol) diacrylate membranes.* Cell Transplant, 1999. **8**(3): p. 293-306.
354. Barker, T.H., *The role of ECM proteins and protein fragments in guiding cell behavior in regenerative medicine.* Biomaterials, 2011. **32**(18): p. 4211-4.
355. Giger, K., et al., *Suppression of insulin aggregation by heparin.* Biomacromolecules, 2008. **9**(9): p. 2338-44.
356. Xu, Y., et al., *Effect of heparin on protein aggregation: Inhibition versus promotion.* Biomacromolecules, 2012. **13**(5): p. 1642-1651.
357. Kawai, M., et al., *The heparin-binding domain of IGFBP-2 has insulin-like growth factor binding-independent biologic activity in the growing skeleton.* J Biol Chem, 2011. **286**(16): p. 14670-80.
358. Yaoi, Y., et al., *Insulin binds to type V collagen with retention of mitogenic activity.* Exp Cell Res, 1991. **194**(2): p. 180-5.
359. Dawson, T.P., et al., *The MTS vs. the ATP assay for in vitro chemosensitivity testing of primary glioma tumour culture.* Neuropathol Appl Neurobiol, 2010. **36**(6): p. 564-7.
360. Ulukaya, E., et al., *The MTT assay yields a relatively lower result of growth inhibition than the ATP assay depending on the chemotherapeutic drugs tested.* Toxicol In Vitro, 2008. **22**(1): p. 232-9.
361. Petty, R.D., et al., *Comparison of MTT and ATP-based assays for the measurement of viable cell number.* J Biolumin Chemilumin, 1995. **10**(1): p. 29-34.
362. Young, T.H., et al., *Evaluation of asymmetric poly(vinyl alcohol) membranes for use in artificial islets.* Biomaterials, 1996. **17**(22): p. 2139-45.
363. Tun, T., et al., *A newly developed three-layer agarose microcapsule for a promising biohybrid artificial pancreas: rat to mouse xenotransplantation.* Cell Transplant, 1996. **5**(5 Suppl 1): p. S59-63.
364. Orive, G., et al., *Biocompatibility of alginate-poly-L-lysine microcapsules for cell therapy.* Biomaterials, 2006. **27**(20): p. 3691-700.
365. Blasiak, J., et al., *Perspectives on the use of melatonin to reduce cytotoxic and genotoxic effects of methacrylate-based dental materials.* J Pineal Res, 2011. **51**(2): p. 157-162.
366. Wang, Y.Q., et al., *Poly(methyl methacrylate)-graft-oligoamines as low cytotoxic and efficient nonviral gene vectors.* Mol BioSyst, 2009. **6**(1): p. 256-263.

367. Taira, M., et al., *Cytotoxic Effect of Methyl Methacrylate on 4 Cultured Fibroblasts.* Int J Prosthodont, 2000. **13**(4): p. 311-315.
368. Yoshii, E., *Cytotoxic effects of acrylates and methacrylates: Relationships of monomer structures and cytotoxicity.* J Biomed Mater Res, 1997. **37**(4): p. 517-524.
369. Geisler, B., D.G. Weiss, and T. Lindl, *Video-microscopic analysis of the cytotoxic effects of hydroxyethyl methacrylate on diploid human fibroblasts.* In Vitro Mol Toxicol, 1995. **8**(4): p. 369-375.
370. Danilewicz-Stysiak, Z., *Experimental investigations on the cytotoxic nature of methyl methacrylate.* J Prosthet Dent, 1980. **44**(1): p. 13-16.
371. Reers, C., et al., *Downregulation of proliferation does not affect the secretory function of transformed β-cell lines regardless of their anatomical configuration.* Islets, 2011. **3**(3): p. 80-88.
372. Lin, C.C., A. Raza, and H. Shih, *PEG hydrogels formed by thiol-ene photo-click chemistry and their effect on the formation and recovery of insulin-secreting cell spheroids.* Biomaterials, 2011. **32**(36): p. 9685-95.
373. Su, J., et al., *Anti-inflammatory peptide-functionalized hydrogels for insulin-secreting cell encapsulation.* Biomaterials, 2010. **31**(2): p. 308-14.
374. Ziolkowski, A.F., et al., *Heparan sulfate and heparanase play key roles in mouse beta cell survival and autoimmune diabetes.* J Clin Invest, 2012. **122**(1): p. 132-41.
375. Takahashi, I., et al., *Important role of heparan sulfate in postnatal islet growth and insulin secretion.* Biochem Bioph Res Co, 2009. **383**(1): p. 113-118.
376. Lin, C.C. and K.S. Anseth, *Glucagon-like peptide-1 functionalized PEG hydrogels promote survival and function of encapsulated pancreatic Î²-cells.* Biomacromolecules, 2009. **10**(9): p. 2460-2467.
377. Rogers, G.J., M.N. Hodgkin, and P.E. Squires, *E-cadherin and cell adhesion: A role in architecture and function in the pancreatic islet.* Cell Physiol Biochem, 2007. **20**(6): p. 987-994.
378. Bosco, D., D.G. Rouiller, and P.A. Halban, *Differential expression of E-cadherin at the surface of rat β-cells as a marker of functional heterogeneity.* J Endocrinol, 2007. **194**(1): p. 21-29.
379. Kaido, T., et al., *Impact of defined matrix interactions on insulin production by cultured human β-cells: Effect on insulin content, secretion, and gene transcription.* Diabetes, 2006. **55**(10): p. 2723-2729.
380. Edamura, K., et al., *Effect of adhesion or collagen molecules on cell attachment, insulin secretion, and glucose responsiveness in the cultured adult porcine endocrine pancreas: a preliminary study.* Cell Transplant, 2003. **12**(4): p. 439-46.
381. Daoud, J., et al., *The effect of extracellular matrix components on the preservation of human islet function in vitro.* Biomaterials, 2010. **31**(7): p. 1676-82.
382. de Groot, M., et al., *Microcapsules and their ability to protect islets against cytokine-mediated dysfunction.* Transplant Proc, 2001. **33**(1-2): p. 1711-1712.
383. de Haan, B.J., M.M. Faas, and P. de Vos, *Factors influencing insulin secretion from encapsulated islets.* Cell Transplant, 2003. **12**(6): p. 617-625.
384. Wiegand, F., K.D. Kroncke, and V. Kolb-Bachofen, *Macrophage-generated nitric oxide as cytotoxic factor in destruction of alginate-encapsulated islets. Protection by arginine analogs and/or coencapsulated erythrocytes.* Transplantation, 1993. **56**(5): p. 1206-12.

385. Doyle, T.J., et al., *Immunoprotective properties of primary Sertoli cells in mice: potential functional pathways that confer immune privilege.* Biol Reprod, 2012. **86**(1): p. 1-14.
386. Zhou, M., et al., *Microencapsulation of rat islets prolongs xenograft survival in diabetic mice.* Chin Med J (Engl), 1998. **111**(5): p. 394-7.
387. Murakami, Y., et al., *Interaction of poly(styrene sulfonic acid) with the classical pathway of the serum complement system.* J Biomater Sci, Polym Ed, 2005. **16**(6): p. 685-697.
388. Mukaida, N., A. Harada, and K. Matsushima, *Interleukin-8 (IL-8) and monocyte chemotactic and activating factor (MCAF/MCP-1), chemokines essentially involved in inflammatory and immune reactions.* Cytokine Growth Factor Rev, 1998. **9**(1): p. 9-23.
389. Bizzarri, C., et al., *Selective inhibition of interleukin-8-induced neutrophil chemotaxis by ketoprofen isomers.* Biochem Pharmacol, 2001. **61**(11): p. 1429-37.
390. Blasi, P., et al., *Preparation and in vitro and in vivo characterization of composite microcapsules for cell encapsulation.* Int J Pharm, 2006. **324**(1): p. 27-36.
391. Lin, C.C., A.T. Metters, and K.S. Anseth, *Functional PEG-peptide hydrogels to modulate local inflammation induced by the pro-inflammatory cytokine TNFalpha.* Biomaterials, 2009. **30**(28): p. 4907-14.
392. Cheung, C.Y. and K.S. Anseth, *Synthesis of immunoisolation barriers that provide localized immunosuppression for encapsulated pancreatic islets.* Bioconjugate Chemistry, 2006. **17**(4): p. 1036-1042.